

BIOSYNTHESIS AND CHARACTERIZATION OF METAL NANOPARTICLES

**Thesis submitted to BHARATHIDASAN UNIVERSITY
for the award of the Degree of**

**DOCTOR OF PHILOSOPHY
IN
PHYSICS**

By

M. SIVAKAMI

(Ref. No. 05838 / Ph.D. K2 / Physics / Part-Time / July 2017)

RESEARCH ADVISOR

**Dr. K. RENUKA DEVI M.Sc., M.Phil., Ph.D., PGDCA
Associate Professor and Head**



**PG & RESEARCH DEPARTMENT OF PHYSICS
KALAINAR KARUNANIDHI GOVERNMENT ARTS
COLLEGE FOR WOMEN**

(Autonomous with B++ Grade by NAAC)

PUDUKKOTTAI - 622 001

TAMIL NADU, INDIA

JUNE– 2022



KALAINGAR KARUNANIDHI GOVERNMENT ARTS COLLEGE FOR WOMEN

(Autonomous with B++ Grade by NAAC)
PUDUKKOTTAI, TAMIL NADU, INDIA

Dr. K. Renuka Devi, M.Sc., M. Phil., PGDCA., Ph.D.,

Associate Professor, Head & Research Advisor

PG & Research Department of Physics

Kalaignar Karunanidhi Government Arts College for Women (A)

Pudukkottai-622 001

CERTIFICATE

This is to certify that the thesis entitled **“BIOSYNTHESIS AND CHARACTERIZATION OF METAL NANOPARTICLES”** is a bonafide record of research work done by **Ms. M. SIVAKAMI**, a part-time Research Scholar, PG and Research Department of Physics, Kalaignar Karunanidhi Government Arts College for Women (Autonomous), Pudukkottai, during the period July 2017 to June 2022 under my guidance at Bharathidasan University, Tiruchirappalli, for the award of the Degree of Doctor of Philosophy in Physics and the thesis has not previously formed the basis for the award of any Degree, Diploma, Associateship, Fellowship or other similar titles. I further certify that the thesis represents the original and independent work on the part of the candidate.

Place: Pudukkottai

Date:

Dr. K. Renuka Devi

Research Advisor

M. SIVAKAMI

Part-Time Ph.D., Research Scholar

(Ref. No. 05838 / Ph.D. K2 / Physics / Part-Time / July 2017)

Date: 28.06.2017

PG & Research Department of Physics
Kalaingar Karunanidhi Government Arts
College for Women (A)
Pudukkottai -622 001

DECLARATION

I, **Ms. M. Sivakami** hereby declare that the thesis entitled, “**BIOSYNTHESIS AND CHARACTERIZATION OF METAL NANOPARTICLES**” submitted to Bharathidasan University, Tiruchirappalli, for the award of the degree of **DOCTOR OF PHILOSOPHY IN PHYSICS** is a record of original research work done by me under the supervision and guidance of **Dr. K. RENUKA DEVI**, Associate Professor and Head, PG & Research Department of Physics, Kalaingar Karunanidhi Government Arts College for women (Autonomous), Pudukkottai, during the period July 2017 to June 2022. This work has not previously formed the basis for the award of any Degree, Diploma, Associateship, Fellowship or other similar titles in any institution or University to my knowledge.

Place: Pudukkottai












Date:








Signature of the Candidate
(M. Sivakami)

Document Information

Analyzed document	M. SIVAKAMI - PHYSICS - FINAL THESIS.pdf (D140068544)
Submitted	2022-06-12T06:34:00.0000000
Submitted by	Dr.S.Vanitha
Submitter email	vanitha@bdu.ac.in
Similarity	5%
Analysis address	vanitha.bdu@analysis.orkund.com

Sources included in the report

W	URL: https://core.ac.uk/download/pdf/53188005.pdf Fetched: 2020-06-20T05:53:16.3770000	 2
W	URL: https://www.researchgate.net/publication/326861754_Green_synthesis_and_characterization_of_silver_nanoparticles_using_Enicostemma_axillare_Lam_leaf_extract Fetched: 2022-04-25T14:49:26.6600000	 2
W	URL: https://www.iosrjournals.org/iosr-jbb/papers/Volume%204,%20Issue%203/N0403017883.pdf Fetched: 2019-12-03T08:17:33.8030000	 1
W	URL: https://pubmed.ncbi.nlm.nih.gov/24784347/ Fetched: 2022-06-12T06:34:56.4400000	 2
W	URL: https://www.researchgate.net/publication/342898466_Biosynthesis_and_characterization_of_iron_nanoparticles_produced_by_Thymus_vulgaris_L_and_their_antimicrobial_activity Fetched: 2021-09-12T07:01:46.7770000	 3
W	URL: https://www.researchgate.net/publication/342029446_Green_Synthesis_and_characterization_of_iron_oxide_nanoparticles_by_Phoenix_Dactylifera_leaf_extract_and_evaluation_of_their_antioxidant_activity Fetched: 2022-06-12T06:32:46.8230000	 6
W	URL: https://www.sciencedirect.com/science/article/pii/S2405844021002644 Fetched: 2021-12-08T08:37:51.0870000	 1
W	URL: https://www.sciencedirect.com/science/article/abs/pii/S2352554120302205 Fetched: 2021-10-16T07:42:38.5870000	 1
W	URL: https://www.hindawi.com/journals/jchem/2021/1581444/ Fetched: 2022-02-09T06:37:00.1100000	 1
W	URL: https://www.researchgate.net/publication/277944432_Green_Synthesis_of_Nanoparticles_Current_Prospectus Fetched: 2019-12-08T19:01:02.6970000	 3
W	URL: https://www.researchgate.net/publication/356150509_Biologically_synthesized_iron_nanoparticles_FeNPs_from_Phoenix_dactylifera_have_anti-bacterial_activities Fetched: 2022-06-12T06:32:45.7370000	 1

W	URL: http://www.ijcrar.com/4-8-2016/M.%20Srvanathi,%20et%20al.pdf Fetched: 2021-09-16T12:59:08.4430000	 3
W	URL: https://www.sciencedirect.com/science/article/pii/S2213343720307697 Fetched: 2020-10-16T01:35:31.0130000	 5
W	URL: https://www.researchgate.net/publication/330935209_Terminalia_belerica_Mediated_Green_Synthesis_of_Nanoparticles_of_Copper_Iron_and_Zinc_Metal_Oxides_as_the_Alternate_Antibacterial_Agents_Against_some_Common_Pathogens Fetched: 2020-01-30T06:49:52.8900000	 3
W	URL: https://www.degruyter.com/document/doi/10.1515/gps-2016-0133/pdf Fetched: 2021-08-05T15:09:41.5570000	 1
W	URL: https://www.researchgate.net/publication/279802829_Synthesis_and_characterization_of_silver_nanoparticles_using_fruit_extract_of_Momordica_cymbalaria_and_assessment_of_their_in_vitro_antimicrobial_antioxidant_and_cytotoxicity_activities Fetched: 2021-05-14T07:09:24.0830000	 4
W	URL: http://irphouse.com/ijnn/ijnnv6n1_06.pdf Fetched: 2021-11-17T17:55:15.1430000	 1
W	URL: https://journaljpri.com/index.php/JPRI/article/download/30866/57925/ Fetched: 2022-05-20T10:30:05.8100000	 1

CONTENTS

Preface

Acknowledgement

List of Tables

List of Figures

Abbreviation of symbols

Chapter No.	Title	Page No.
I.	General Introduction, Review of Literature, and Scope of the Work	1 - 41
1.1.	The world of nano regime	2
1.2	Nanotechnology	4
1.2.1	Nanobiotechnology	6
1.3	Methodology for nanoparticle synthesis	7
1.3.1	Bottom-Up Techniques	7
1.3.2	Top-down Fabrication Techniques	8
1.4	Nanoparticles	9
1.4.1	Dimensions of nanoparticles	10
1.5	Classifications of nanoparticles	11
1.5.1	Organic nanoparticles	11
1.5.2	Inorganic nanoparticles	12
1.5.3	Metal nanoparticles	12
1.5.4	Iron nanoparticles	13
1.6	Green synthesis of iron nanoparticles	14
1.7	Applications	16

1.7.1	Biological Applications	16
1.7.1.1	Antibacterial activity	16
1.7.1.2	Anti-inflammatory activity	17
1.7.1.3	Anti-oxidant activity	17
1.7.1.4	Anti-diabetic activity	18
1.8	Review of Literature	19
1.9	Scope of the work	36
	References	39

II. Materials, Experimental Work, and Characterization Techniques 42 - 65

2.1	Materials utilized	42
2.2	Experimental work	43
2.2.1	Plant mediated synthesis	43
2.2.2	Mechanism of plant mediated synthesis of iron nanoparticles	43
2.2.3	Preparation of plant extracts	44
2.2.4	Biosynthesis of iron nanoparticles	44
2.3	Characterization techniques	46
2.3.1	Phase and morphology characterization techniques	47
2.3.1.1	X-ray diffractometer	47
2.3.1.2	Scanning electron microscope (SEM)	48
2.3.1.3	Energy Dispersive X-ray Spectroscopy (EDS)	50
2.3.1.4	High Resolution-Transmission Electron Microscope (HR-TEM)	51
2.3.2	Magnetic characterization techniques	53
2.3.2.1	Vibrating Sample Magnetometer (VSM)	53
2.3.3	Optical characterization techniques	55
2.3.3.1	UV-Visible spectrometer	55
2.3.3.2	Fourier Transform Infrared Spectroscopy (FTIR)	57
2.3.3.3	Dynamic Light Scattering (DLS)	58
2.4	Analysis of biological activities	61

2.4.1	Anti-bacterial activity assay	61
2.4.1.1	Disc preparation	61
2.4.1.2	Collection of test bacterial species	61
2.4.1.3	Assay of antibacterial activity	61
2.4.2	Anti-oxidant assay	62
2.4.3	Anti-inflammatory activity	62
2.4.4	Anti-diabetic assay	63
	References	64
III.	Green Synthesis of Magnetic Nanoparticles via <i>Cinnamomum verum</i> Bark Extract for Biological Application	66 - 91
3.1	Introduction	66
3.2	Experimental Section	69
3.2.1	Chemicals	69
3.2.2	Preparation of <i>Cinnamomum verum</i> bark extract	70
3.2.3	Synthesis of iron nanoparticles	70
3.2.4	Characterization of iron nanoparticles	70
3.2.5	Biological activities	71
3.2.5.1	Antibacterial assay	71
3.2.5.2	Antioxidant assay	72
3.2.5.3	Anti-inflammatory assay	72
3.2.5.4	Anti-diabetic assay	72
3.3	Results and Discussion	73
3.3.1	UV-Vis spectroscopy analysis	73
3.3.2	XRD analysis	73
3.3.3	FTIR analysis	74
3.3.4	SEM and EDS analysis	75
3.3.5	HR-TEM analysis	79
3.3.6	Phytochemical analysis	80
3.3.6.1	Antibacterial Assay	80

3.3.6.2	Antioxidant assay	83
3.3.6.3	Anti-inflammatory assay	84
3.3.6.4	Anti-diabetic assay	86
3.3.7	Vibrating Sample Magnetometer (VSM) analysis	87
3.4	Conclusion	88

References

IV. Phytomediated Synthesis of Magnetic Nanoparticles by *Murraya koenigii* Leaves Extract and its Biomedical Applications 92 - 117

4.1	Introduction	92
4.2	Experimental section	95
4.2.1	Chemicals used	95
4.2.2	<i>Murraya koenigii</i> leaves extract preparation	95
4.2.3	Synthesis of iron NPs by <i>Murraya koenigii</i> leaves extract	96
4.2.4	Characterization of magnetic nanoparticles	96
4.2.5	Antimicrobial assay	97
4.2.6	Antioxidant assay	98
4.2.7	Anti-inflammatory assay	98
4.2.8	Anti-diabetic assay	99
4.3	Results and Discussion	99
4.3.1	UV, XRD, FT-IR, DLS and VSM analysis	100
4.3.2	HR-TEM analysis	103
4.3.3	EDS analysis	105
4.3.4	Antimicrobial assay	106
4.3.5	Antioxidant assay	108
4.3.6	Anti-inflammatory assay	110
4.3.7	Anti-diabetic assay	111
4.4	Conclusion	113
	References	114

V.	Biosynthesized Magnetic Nanoparticles using <i>Rosa Gallica</i> Petals Extract and its Antibacterial Activities against selected Pathogens for Biomedical Applications	118 -137
5.1	Introduction	118
5.2	Materials and methods	120
5.2.1	Materials	120
5.2.2	Methods	121
	5.2.2.1 Preparation and synthesis of magnetic nanoparticles using <i>Rosa Gallica</i> petals extract	121
5.2.3	Characterization of magnetic nanoparticles	121
5.2.4	Antimicrobial activity of iron nanoparticles	123
5.3	Results and Discussion	123
5.3.1	UV- visible analysis	123
5.3.2	Fourier Transform-InfraRed (FT-IR) Analysis	125
5.3.3	X-ray diffraction analysis	127
5.3.4	SEM and EDAX spectral analysis	128
5.3.5	TEM Analysis	129
5.3.7	Antibacterial properties of synthesized FeNPs	131
5.4	Conclusion	134
	References	135
VI.	Antimicrobial Efficacy of Iron Nanoparticles (INPs) using <i>Camellia sinensis</i> Leaves Extract an Alternate Approach	138 - 155
6.1	Introduction	138
6.2	Materials and methods	140
6.2.1	Plant collection	140
6.2.2	Preparation of extract and synthesis of INPs using <i>C. sinensis</i> leaves	140
6.2.3	Characterization methods	142
6.2.4	Microorganisms	141
6.2.5	Antibacterial activity	141

6.3	Results and Discussion	142
6.3.1	UV-Vis analysis	143
6.3.2	FTIR analysis	144
6.3.3	XRD-analysis	145
6.3.4	SEM and EDX analysis	147
6.3.5	VSM Analysis	148
6.3.6	Antibacterial activity	149
6.4	Conclusion	151
	References	152

VII. A Comparative Study of Antibacterial Activities of Plant Mediated Iron Nanoparticles 156 - 163

7.1.	Highlights	156
7.2.	Introduction	156
7.3.	Plants chosen for the comparative analysis	158
7.4.	Nomenclature	159
7.5.	Comparison of antibacterial activities	160
7.6.	Conclusion	163

SUMMARY 164 - 168

LIST OF PUBLICATIONS 169 - 170

Preface

The thesis comprised of seven chapters and the results of all the works were comprehensively discussed with suitable illustrations.

Chapter-I focuses the evolution of nanotechnology and their significance. The fundamentals of nanoparticles, classifications of nanoparticles and their importance were highlighted. An ephemeral summary on synthesis methods, the need of biological method for synthesizing nanoparticles and the cause for searching an alternative low-cost method have been explained in detail. The reviews and the scope of the work and the major objectives of this research have been elaborated.

Chapter-II enlightens the details about materials used in this research work and the experimental section to prepare iron nanoparticles.

Chapter-III emphasizes the green synthesis of magnetic nanoparticles via *Cinnamomum verum* bark extract for biological application.

Chapter-IV demonstrates the phytomediated synthesis of magnetic nanoparticles by using *Murraya Koenigii* leaves extract and its optical, spectral, morphological, magnetic and biomedical characterizations.

Chapter-V illustrates the biosynthesized magnetic nanoparticles using *rosa gallica* extract. It also discusses the antibacterial activities of iron nanoparticles against selected human pathogens for biomedical applications.

Chapter-VI gives an account on an alternate approach of antimicrobial efficacy of iron nanoparticles using camellia sinensis leaves extract. It also confers the role of camellia sinensis in the reduction and stabilization of nanoparticles.

Chapter-VII provides the comparative analysis of antibacterial activities of plant mediated iron nanoparticles.

Summary of all the chapters present as an overview of significant findings in a simple way.

The list of publications, seminars, conferences, workshops, training programme attended were summarized in appendix in this thesis.



*“I dedicate my Research works
to the Almighty of God,
My beloved parents,
My adorable Sister and My
Brother*

ACKNOWLEDGEMENT

First and foremost, praises and thanks to **God, the Almighty**, for his showers of blessings throughout my life and specially thank him for giving me the wisdom, strength, support and knowledge in exploring things, for the guidance in helping surpass all the trials that I encountered and for giving determination to pursue my study, and to make this study successful.

I express my sincere thanks to our Principal **Dr. B. Buvaneswari**, Kalaingar Karunanidhi Government Arts College for Women (Autonomous), Pudukkottai for granting me the permission to do this research work in the Department of Physics with all the necessary facilities.

With deepest from the core of my heart, I take this opportunity to thank my highly honorable teacher and my guide **Dr. K. Renuka Devi**, Associate Professor and Head, PG & Research Department of Physics, for giving me the opportunity to do research and providing invaluable guidance throughout this research. Her dynamism, sincerity, vision and provocation have really inspired me. It was my great privilege and honor to work and study under her guidance.

I would like to thank my doctoral committee members: **Dr. T. V. Sundar**, Associate Professor, Department of Physics, National College (A), Tiruchirappalli, and **Dr. T. Thilagavathi**, Assistant Professor, Department of Physics, Government Arts College for Women (Autonomous), Kumbakonam, for their insightful comments, encouragement, and for the hard questions that incited me to widen my research from various perspectives.

I thank my friends **Dr. R. Renuka** and **Dr. A. Dhanalakshmi** for their support and co-operation.

It is indeed a pleasure to thank my well-wishers as well as my sisters, **Dr. J. Benazir Jiya, Dr. R. Seema, and Dr. R. Seethalakshmi** for their stimulating discussions and support throughout my research.

My heartfelt thanks to **Dr. V. S. Rajakrishnan**, Associate Professor of Commerce, **Dr. S. Karpagam**, Vice Principal, EGS Pillay Arts and Science College, Nagapattinam, **Dr. M. Kouthaman, Mr. K. Velshankar, Mr. Tony** and **Mr. Bairav** for their encouragement and support for the completion of my research work successfully.

I also extend my acknowledgement to all the faculty members and non-teaching staff in the Department of Physics, Kalaignar Karunanidhi Government Arts College for Women (Autonomous), Pudukkottai, for their constant encouragement during the tenure.

I wish to express my gratitude to all the people involved in this work who were generous in sharing their time and knowledge with me.

There are many people who have selflessly enriched me and this work in ways beyond measure, I thank them all.

Last but not the least, I would like to thank my family: my parents **Mr. A. Muthu** and **Mrs. M. Ariyamala Muthu**, my sister **Dr. M. Sridevi** and my brother **Er. M. Balathandayuthabani** for supporting me spiritually throughout this research work and my life.

LIST OF TABLES

Table No.	Title	Page No.
1.1	Size and name of the particles	4
2.1	The details of materials utilized in this work	42
3.1	Elemental composition of synthesized iron NPs using <i>Cinnamomum verum</i> extract	78
3.2	Inhibition zone of biosynthesized iron NPs against various human pathogenic bacteria	80
3.3	Antioxidant assay of synthesized FeNPs via <i>Cinnamomum verum</i> bark extract	83
3.4	Anti-inflammatory assay of synthesized Fe NPs via <i>Cinnamomum verum</i> bark extract	85
3.5	Anti-diabetic assay of synthesized Fe NPs via <i>Cinnamomum verum</i> bark extract	87
4.1	Phytochemical analysis of <i>Murraya koenigii</i> leaf extract	100
4.2	Percentage of inhibition in antioxidant assay of green synthesized iron NPs by <i>Murraya koenigii</i> leaf extract	109
4.3	Percentage of inhibition in anti-inflammatory and anti-diabetic assays of green synthesized iron NPs by <i>Murraya koenigii</i> leaf extract	112
5.1	Change in color of the solution during synthesis of magnetic nanoparticles	124
5.2	Assay of antibacterial activity	132
6.1	XRD pattern of <i>C. sinensis</i> leaf extract iron nanoparticles	146
6.2	Assay of antibacterial activity	149
7.1	Summarized Characterization results of Biosynthesized iron nanoparticles	161

LIST OF FIGURES

Figure No.	Title	Page No.
1.1	Richard Feynman	1
1.2	Eric Drexler	2
1.3	Different entities representing the nano length scale	3
1.4	Schematic representation of 'top-down' and 'bottom-up' approaches used in Nanotechnology	7
1.5	Organic nanoparticles (a) Dendrimers (b) Liposomes and Micelles c) Ferritin	12
1.6	Applications of iron nanoparticles	14
2.1	Schematic diagram of green technique for the synthesis of iron nanoparticles	45
2.2	Synthesis mechanisms of FeNPs	45
2.3	(a) Schematic representation of X-ray diffractometer b) Photograph of X'pert PRO -PANalytical model	48
2.4	a) Schematic representation of SEM, b) Photograph of CARL ZEISS, EVO 18	49
2.5	Photograph of EDS (Quantax 200 with X Flash ® 6130)	51
2.6	a) Schematic diagram of HR-TEM b) Photograph of HR-TEM (JEOL 2100+)	52
2.7	a) Block diagram of a vibrating sample magnetometer (VSM). b) Pictorial representation of VSM (Model ADE – EV9)	54
2.8	a) Schematic diagram of a UV-visible spectrometer b) Pictorial representation of a UV-visible spectrometer (Shimadzu 2600)	56
2.9	a) Schematic diagram of Michelson Interferometer configured for FTIR b) Pictorial representation of FT-IR (Thermo Nicolet 380)	58
2.10	Schematic diagram of DLS	59
3.1	UV spectra of a) Extract and b) Synthesized iron NPs	73
3.2	XRD pattern of FeNPs synthesized using <i>Cinnamomum verum</i> extract	74

3.3	FT-IR spectrum of FeNPs synthesized using <i>Cinnamomum verum</i> extract	75
3.4	SEM images of synthesized iron NPs using <i>Cinnamomum verum</i> extract at 300 nm, and 200 nm magnification	76
3.5	EDS Spectrum of synthesized iron NPs using <i>Cinnamomum verum</i> extract	77
3.6	Mapping of a) Oxygen b) Carbon c) Fe elements in synthesized iron NPs using <i>Cinnamomum verum</i> extract at 20 μm magnification	78
3.7	HR-TEM images in the magnification of 100 nm, 100 nm, 10 nm, 5 nm and 2 nm respectively and f) SAED pattern of synthesized Fe NPs	79
3.8	Antibacterial assay of synthesized iron NPs using <i>Cinnamomum verum</i> extract against a) <i>Bacillus subtilis</i> b) <i>Staphylococcus aureus</i> c) <i>Escherichia coli</i> d) <i>Klebsiella pneumonia</i>	81
3.9	Inhibition zone of biosynthesized FeNPs against various bacteria	82
3.10	Antioxidant assay of synthesized Fe NPs using <i>Cinnamomum verum</i> extract	84
3.11	Anti-inflammatory assay of synthesized Fe NPs using <i>Cinnamomum verum</i> extract	85
3.12	Anti-diabetic assay of synthesized Fe NPs using <i>Cinnamomum verum</i> extract	86
3.13	Magnetization curve of synthesized Fe NPs using <i>Cinnamomum verum</i> extract	87
4.1	Synthesis scheme of iron NPs green synthesized by <i>Murraya koenigii</i> leaf extract	96
4.2	a) UV-visible, b) X-ray diffraction (XRD) pattern, c) Fourier Transform Infra-Red spectrum (FT-IR), d) Particle size distribution (dynamic light scattering-DLS) graph and e) Magnetization curve (vibrating sample magnetometer-VSM) of green synthesized iron NPs by <i>Murraya koenigii</i> leaf extract	102
4.3	(a-b) High resolution-transmission electron micrographs (HR-TEM) at 20nm, 50nm scale and (c) selected area electron diffraction pattern at 1/10nm scale of green synthesized iron NPs by <i>Murraya koenigii</i> leaf extract	106

4.4	Energy dispersive X-ray spectrum (EDX) of green synthesized iron NPs by <i>Murraya koenigii</i> leaf extract	105
4.5	Energy dispersive X-ray spectrum (EDX) mapping of green synthesized iron NPs by <i>Murraya koenigii</i> leaf extract	106
4.6	Antimicrobial assay of green synthesized iron NPs by <i>Murraya koenigii</i> leaf extract on <i>Pseudomonas aeruginosa</i> , <i>Acinetobacter baumannii</i> , <i>Serratia marcescens</i> , <i>Chromobacterium violaceum</i> , <i>Enterobacter aerogenes</i> , <i>Klebsiella pneumonia</i> (Gram-negative bacterial cells), <i>Enterococcus faecalis</i> , <i>Staphylococcus aureus</i> (Gram-positive bacterial cells), <i>Candida albicans</i> , <i>Candida tropicalis</i> , <i>Aspergillus niger</i> , and <i>Aspergillus flavus</i> (fungi cells).	108
4.7	Antioxidant assays of green synthesized iron NPs by <i>Murraya koenigii</i> leaf extract	109
4.8	Anti-inflammatory assays of green synthesized iron NPs by <i>Murraya koenigii</i> leaf extract	110
4.9	Anti-diabetic assays of green synthesized iron NPs by <i>Murraya koenigii</i> leaf	112
5.1	Rosa Gallica images	121
5.2	UV-vis spectrum of <i>Rosa gallica</i> extract in green synthesis nanoparticles	124
5.3	FT-IR spectrum of biosynthesized iron nanoparticles using <i>Rosa gallica</i> extract	126
5.4	XRD pattern of biosynthesized iron nanoparticles using <i>Rosa gallica</i> extract	127
5.5	(a-b) SEM images of biosynthesized iron nanoparticles using <i>Rosa gallica petals</i> extract	128
5.6	EDAX images of biosynthesized iron nanoparticles using <i>Rosa gallica petals</i> extract	129
5.7	TEM micrographs of biosynthesized iron nanoparticles using <i>Rosa gallica</i> Extract	130
5.8	Magnetization curve of biosynthesized iron nanoparticles using <i>Rosa gallica</i> extract	130
5.9	Antibacterial activity of iron nanoparticles using <i>Rosa gallica petals</i> extract a) <i>Escherichia coli</i> b) <i>Klebsiella pneumoniae</i> c) <i>Staphylococcus aureus</i> d) <i>Bacillus subtilis</i>	132

5.10	Inhibition zone of biosynthesized FeNPs against various bacteria	133
6.1	Color changes of iron nanoparticles fabrication a) FeCl ₃ b) Green tea leaves extract c) After plant extract added with FeCl ₃ solution	142
6.2	UV-vis spectrum of <i>C.sinensis</i> leaf extract in green synthesis iron nanoparticles	143
6.3	FTIR spectrum of <i>C.sinensis</i> leaf extract and iron nanoparticles	145
6.4	XRD pattern of <i>C. sinensis</i> leaf extract iron nanoparticles	146
6.5	SEM images synthesized iron nanoparticles of <i>C.sinensis</i> leaf extract	147
6.6	EDX images of biosynthesized iron nanoparticles of <i>C.sinensis</i> . leaf extract	148
6.7	Hysteresis curve of biosynthesized iron nanoparticles using <i>C. sinensis</i> leaf extract	149
6.8	Antibacterial activity of iron nanoparticle a) <i>Bacillus subtilis</i> b) <i>Escherichia coli</i> c) <i>Klebsiella pneumoniae</i> d) <i>Staphylococcus aureus</i>	150
6.9	Graphical representation of zone of inhibition of INPs versus standard value	151
7.1	Pictorial representation of <i>Camellia sinensis</i> , <i>Cinnamomum verum</i> , <i>Murraya koenigii</i> and Rosa Gallica	159
7.2	Comparison of antibacterial capacity of biosynthesized iron nanoparticles	160

LIST OF SYMBOLS, ABBREVIATIONS AND NOMENCLATURE

Å	-	Angstrom
FeCl ₃	-	Iron III Chloride
cm	-	Centimeter
°C	-	Degree Celsius
EDX	-	Energy dispersive X-ray spectroscopy
<i>E.coli</i>	-	<i>Escherichia coli</i>
FT-IR	-	Fourier Transform - Infrared spectroscopy
(G+)	-	Gram-positive +
(G-)	-	Gram-negative -
h	-	Hour
JCPDS	-	Joint Committee on Powder Diffraction Standards
ml	-	millilitre
mg	-	milligram
mm	-	millimeter
µl	-	microlitre
NPs	-	Nanoparticles
nm	-	Nanometer
ROS	-	Reactive oxygen species
rpm	-	Rotation Per Minute
s	-	second (time)
SAED	-	Selected Area Electron Diffraction
<i>S. aureus</i>	-	<i>Staphylococcus aureus</i>
SEM	-	Scanning Electron Microscopy
TEM	-	Transmission Electron Microscopy
UV-Vis	-	Ultra Violet-Visible
XRD	-	X-ray diffraction

XPS	- X-ray photoelectron spectroscopy
DLS	- Dynamic Light Scattering
ZI	- Zone of Inhibition
VSM	- Vibrating Sample Magnetometer
EDS	- Energy Dispersive X-ray Spectroscopy
nZVI	- Nano scaled Zero Valent Iron
C ₃ H ₆ O	- Acetone
INPs	- Iron nanoparticles
PT INPs	- <i>Cinnamomum verum</i> (Pattai) bark extract-based iron nanoparticles
CL INPs	- <i>Murraya koenigii</i> (Curry leaves) extract -based iron nanoparticles
RP INPs	- <i>Rosa gallica</i> (Rose petals) extract -based iron nanoparticles
GT INPs	- <i>Camellia sinensis</i> (Green tea) extract -based iron nanoparticles
MRI	- Magnetic Resonance Imaging
Fe NPs	- Iron nanoparticles

Chapter I

General Introduction, Review of Literature, and Scope of the Work

Introduction

Nanoscience and nanotechnology, expiate a lot to two personalities. First is physicist Richard Feynman. The power of nanotechnology was a spark conceived by Nobel Laureate physicist Richard P. Feymann (Fig.1.1). In 1959, in his presentation at California Institute of Technology, he has unveiled the unlimited potentials of nanotechnology [1]. He could envision the benefits of manipulating matter at the atomic level by breaking them into smaller basic units ranging from the atom, nuclei, nucleons, quarks and much beyond. His presentation on the title “There is plenty of room at the bottom” has motivated the researchers to concentrate on top-down methods to manipulate matter.



Fig.1.1 Richard Feynman

The second one is Dr. K. Eric Drexler (Fig.1.2), who by writing the book titled Nano systems: Molecular Machinery, Manufacturing and computation, created the basis of molecular manufacturing which is an important component of nanoscience. He promoted the technological significance of nanoscale phenomena and devices through speeches. In 1986, Dr. Drexler, who envisioned a future in which the molecular machines, smaller than

dust motes could construct everything ranging from chair to rocket engine and could treat human illness cell by cell. This idea was reflected in his publication titled “Engines of creation”. This motivated the scientists to work on bottom-up approaches to understand, how complex systems are built from simple atomic level constituents. The long vision of these scientists has revolutionized the basic sciences and has given rise to a new discipline called Nanoscience which has gradually become the nucleus around which all existing sciences are prospering.



Fig.1.2 K. Eric Drexler

In this chapter, a brief review on nanotechnology, the methodology of nanoparticle synthesis, uniqueness and applications of iron nanoparticles, need for greener methods for synthesizing iron nanoparticles, the scope of the research, the effect of medicinal plants in synthesis and its biomedical applications such as anti-bacterial, anti-oxidant, anti-inflammatory, and anti-diabetic activities, review of literature, and the scenario of research on biosynthesized iron nanoparticle were discussed.

1.1 The world of nano regime

Nowadays, people live in the world of meters. It is quite hard for us to imagine a world where extremely small things do wonders and take control over macroscopic things. Many substances behave very differently when their sizes were reduced to a new level. Copper, which is a brown metal at the normal condition, appears transparent and gold,

which is a highly unreactive solid at the normal state, becomes a chemically reactive liquid metal, when its size is reduced to nanoscale. Similarly, carbon, which is quite soft in its naturally occurring graphite form, becomes incredibly hard Carbon Nano Tube (CNT) in its nanoscopic arrangement. Platinum, which is best known for its inertness, acts as the best catalyst in the nanoscale and the stable material like aluminium turns combustible at the nano regime. The physiochemical properties of a substance become entirely different when it is shrunken down to nanosize.

Size of nano

The word “Nano” is a Greek word, meaning dwarf or small. To the scientist, nano does not just mean small, it means almost unimaginably small equivalent to a factor of one billionth of a meter. One nanometer is 1000 times smaller than the world of a microscopic scale and a billion times smaller than the world of meters that people live in. To have a feel of its size, it is 1/10,000 times thin of a human hair, 1/1000 times smaller than that of a red blood cell. If five atoms of carbon would occupy a space of about 1nm, five million carbon atoms would be accommodated in a dot representing a full stop. One can appreciate the size of nano, if it is compared with various biological components as given in figure (Fig.1.3).

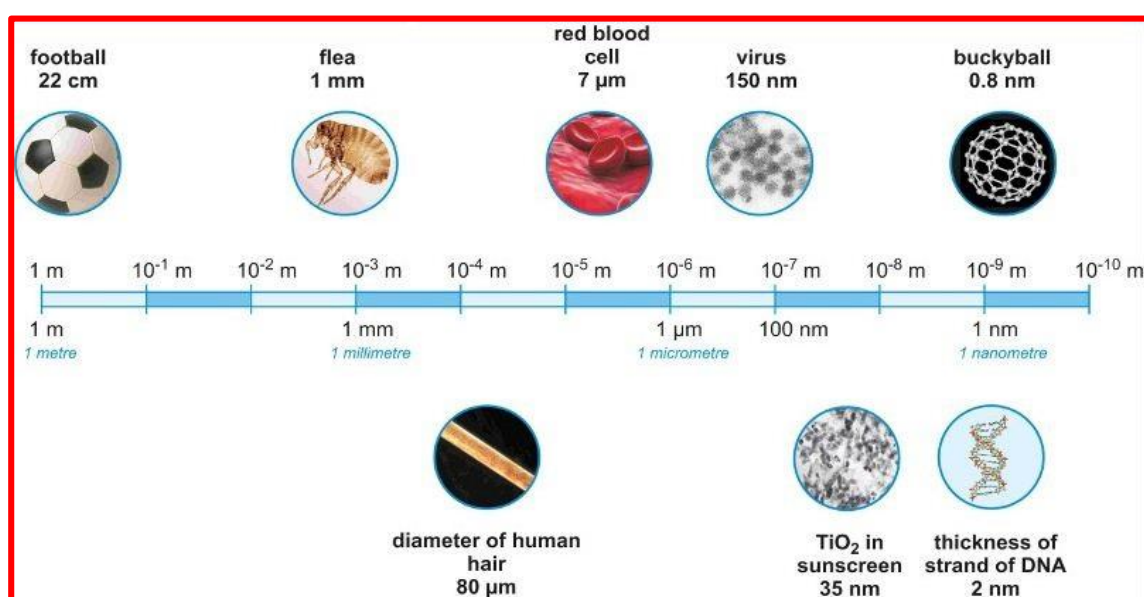


Fig.1.3 Different entities representing the nano length scale

In general, nano-range is the margin where the materials start showing distinct properties. This is usually observed in the range of 1-100nm. Most of the materials including metals and semiconductors exhibit distinct size and shape dependent properties in this range [2]. Hence, nanomaterials can be defined as those materials in which atleast one of the dimensions of the structural components is in the range of 1- 100nm.

$$1\text{nm} = 10^{-3}\mu\text{m} = 10^{-6}\text{mm} = 10^{-9}\text{m}$$

Some examples of sizes from the macro to the molecular level are provided in the table (table 1.1).

Table 1.1 Size and name of the particles

Size (nm)	Examples	Terminology
0.1-0.5	Individual chemical bonds	Molecular/ atomic
0.5-1.0	Small molecules, pores in zeolites	Molecular
1-1000	Proteins, DNA, Inorganic nanoparticles	Nano
10^3-10^4	Microfluidic channels, MEMS, devices on a silicon chip, living cells (bacteria: 1 μm ; yeast: 5 μm ; Human hair 50 μm)	Micro
$>10^4$	Normal bulk matter	Macro

1.2 Nanotechnology

Nanotechnology is a broad-based science and multidisciplinary involving manipulation of atoms, electrons, protons and neutrons in a variety of ways to generate new understanding of how materials can be developed to solve many problems in medicine, engineering, agriculture, biology, chemistry, material science, space exploration, ocean and

marine science, geography and geology. Nanotechnology is the function of science to organize matter at the molecular level. Nanotechnology consists all of the following:

- i) development of bulk material into at the atomic, molecular or macromolecular levels in the range of about 1-100nm.
- ii) development of structure, devices and system and its use in such a ways that they have innovative properties and functions because of their small size.
- iii) ability to arrange, stabilize or manipulate at atomic level (USPEA,2007). In modern research, a dominant field is “Nanotechnology” can be termed as the synthesis, characterization, exploration and application of nanosized materials for the development of science.

In recent years, the term Nanotechnology has been overblown and has become synonyms for the things that are innovative and highly promising. Working with many active fields in nanotechnology research demand and understanding of diverse areas of science to make new challenges and share a common scientific and management and regulatory language so as to maximize effective interdisciplinary interaction [3]. The eventual goal is to produce new materials, devices, and systems modified to meet the essentials of a growing range of commercial, scientific, engineering, and medical applications and yielding dramatic benefits. Its practical applications based on a scientific knowledge would change the world that people live in (Balzani,2005). The nanotechnology has extraordinary prospects for exploitation across the medical, biotechnology, engineering, manufacturing, telecommunications, and information technology. Its impact in these areas will be broad and far reaching, not only in terms of cost effectiveness and improvements in performance compared to current products and processes but also in the longer term, yielding new approaches to address health and societal problems.

1.2.1 Nanobiotechnology

Technological applications in nano are highly suitable for biological molecules because of their size compatibility and because of the ability of the nano particulates to cross some of the biological barriers. Remarkable advancement in engineering technologies has opened up tremendous opportunities to explore biological systems for both health care problems and also for biomedical applications, leading to the establishment of a separate branch of nanotechnology called Nanobiotechnology [4]. Nanobiotechnology is a fertile interdisciplinary research area of nano science which extends the horizons of nanosized systems for various newer applications, both in the field of biotechnology as well as in the field of nanomedicine. Use of nano medicines provide several advantages such as increased bio-based drug availability at the systematic level due to the high relative surface area of nanoparticles and better targeted delivery due to their enhanced permeability and retention effect at the tissue level. Nanoparticles enabled targeted drug delivery is found to be efficient for treating the dreadful diseases. Use of nanomedicines is a good old traditional medical practice. Combining it with the technology would definitely unravel the mysteries of many unsolved problems and would revolutionize the medical field.

Nanotechnology also made a remarkable contribution in the field of optical imaging, diagnosis, implantable materials, tissue engineering etc. The great promise of Nano biotechnology lies in our ability to design and fabricate nanomaterials with unique characteristics and to create devices of unique features that could improve the quality of life of people like differently abled and by large could benefit the whole society. Among nanomaterials, majority of the research has mainly focused on the synthesis, properties and applications of nanoparticles, as they are the building blocks of all nanomaterials.

1.3 Methodology for nanoparticle synthesis

Two main techniques are used in nanotechnology: one is a bottom-up technique where materials and devices are built up atom by atom, the other a top-down technique (Fig.1.4) where they are synthesized or constructed by taking away the existing material from larger entities.

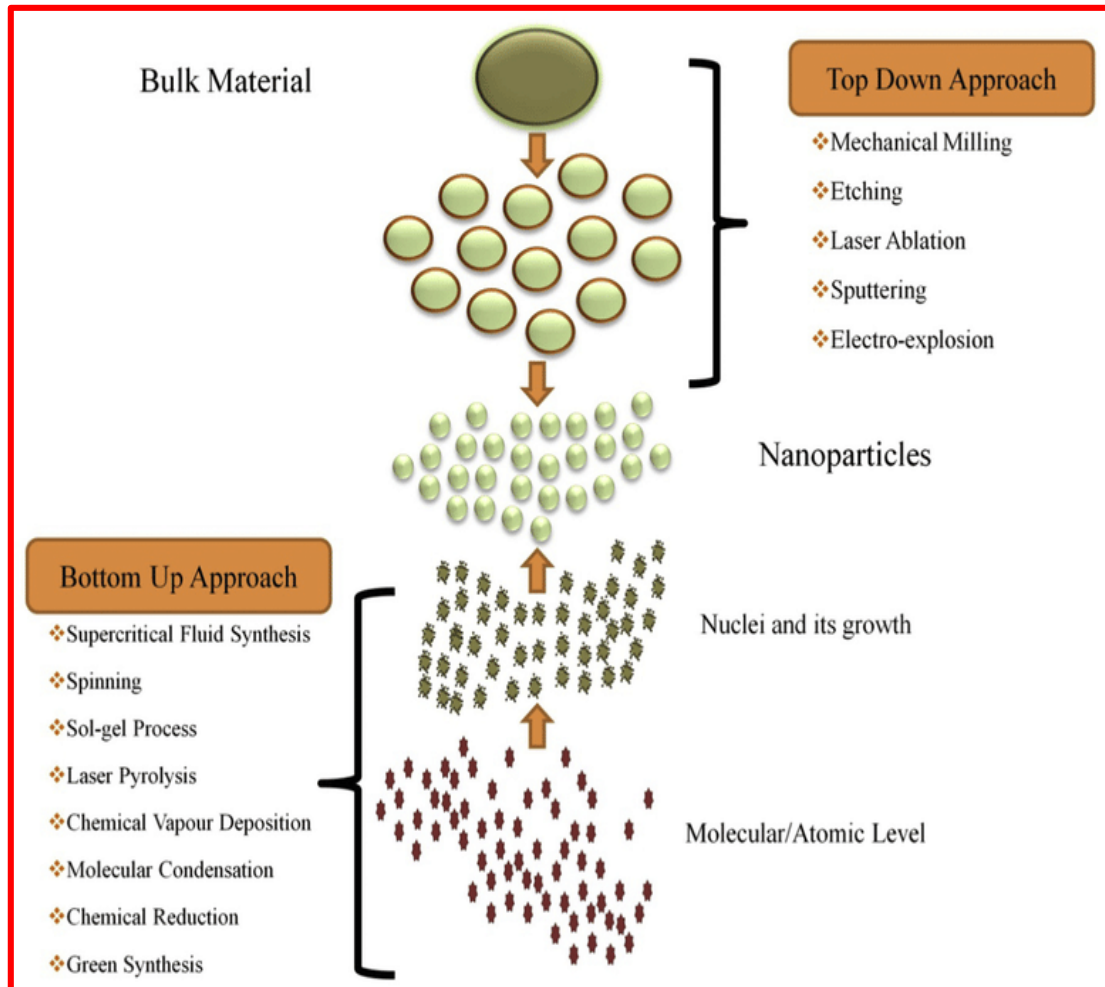


Fig.1.4 Schematic representation of ‘top-down’ and ‘bottom-up’ approaches used in Nanotechnology

1.3.1 Bottom-Up Techniques

The bottom-up techniques are used to grow larger structures atom by atom or molecule by molecule. These techniques include

- Chemical synthesis
- Self-assembly
- Positional assembly

Self-assembly is the fundamental principle, which creates structural organization on all scales from molecules to galaxies. It is defined as reversible processes in which disordered components of a pre-existing system form structures of patterns. It can occur spontaneously in nature, e.g., in cells and other biological systems, as well as in human engineered systems as a Langmuir monolayer. It gives more results in internal organization of the system. Biological self-assembling systems, including synthetically engineered self-assembling peptides and other biomaterials, shown superior handling, biocompatibility and functionality. It is used to construct things at the microscale, which is comprised of structures with at least one dimension that is less than 100 microns. Numerous biological systems could use self-assembly to assemble various molecules and structures. Simulating these strategies and generating novel molecules with the ability to self-assemble into supramolecular assemblies is a significant technique in nanotechnology.

1.3.2 Top-down Fabrication Techniques

In top-down fabrication, a bulk material can be reduced into nanoscale pattern. These look for creating smaller devices by using larger ones to direct their assembly.

- Many technologies climb down from conventional solid-state silicon methods for manufacturing microprocessors are now possible of creating features smaller than 100 nm, falling under the definition of nanotechnology. Giant magnetoresistance based hard drives already on the market fit this description, as atomic layer deposition (ALD) techniques.

- Solid-state techniques can also be used to fabricate devices known as nanoelectromechanical systems or NEMS, which are related to microelectromechanical systems or MEMS.
- Electron beam lithography (EBL) uses a beam of electrons to generate patterns on the surface which is used in creating integrated circuits at nanolevel.
- Atomic force microscope (AFM) daps can be used as a nanoscale “wire head” to deposit a chemical on a surface in a desired pattern in a process called dip pen nanolithography. This is suitable for the larger subfield of nanolithography.

1.4 Nanoparticles

Nanoparticles have offered significant attention from the materials science community. Nanoparticles, which are particles of the material with diameter in nanometer range, promise to play a significant role in developing technologies. They exhibit solitary physical properties that give rise to many potential applications in areas such as nonlinear optics, luminescence, electronics, catalyst, solar energy conversion, and optoelectronics. Researchers are interested in nanoparticles because of their properties unlike from those at a larger scale. At nano scale, particles often possess novel size-dependent properties different from their large counterparts, many of which have been explored for applications [5]. Once materials are reduced to nanometer size (below 100nm), its components demonstrate unusual features based on quantum mechanics, rather than macroscopic Newtonian mechanics, which influence a variety of material properties such as conductivity, heat transfer, melting temperature, optical properties, and magnetization [6]. Taking the advantages of these singular properties in order to develop new products is the main purpose of technology, and that is why it is regarded as “the next industrial revolution”.

Due to their generis active surface area, nanoparticles can provide a wide range of applications such as catalytic membranes, nano sorbents, bioactive nanoparticles and metal nanoparticles such as iron, silver, titanium oxide and many others. One among them is application of nanomaterials to detect, prevent and remove pollutants, or using nanotechnology to design eco-friendly products. It has the power to develop the life of people in general and especially of those with severe health problems [7].

1.4.1 Dimensions of nanoparticles

Based on the number of dimensions in the nano range materials are classified as Zero-dimension (0-D), one-dimension (1-D), two-dimension (2-D), and three-dimension (3-D) - Materials wherein all the dimensions are measured within the nanoscale. ($x, y, z < 100\text{nm}$). No dimension is more than 100nm. Zero dimensional materials include Quantum dots, nanoparticles, and fullerene.

One-dimension (1-D) - Materials in which, one dimension is out of nano range (macroscopic dimension) and two of the three dimensions is $< 100\text{nm}$. 1-D materials include nanotubes, nanorods, and nanowires.

Two-dimension (2-D) - Materials in which two of the three dimensions are not confined to nanoscale. Either x, y or y, z or x, z will be above 100nm and one is in nanoregime. 2-D nanomaterials include nanofilms, nanolayers, and nano coatings.

Three-dimension (3-D) - Bulk nanomaterials are materials which are not defined to the nanolevel in any dimension. All the dimensions of materials are around 100 nm. 3-D nanomaterials may contain scattered nanoparticles, bundles of nanowires, and nanotubes as well as multi mono layers.

When the length scale of the materials is in the range of 1-100nm, many physical properties such as optical, mechanical, magnetic and surface phenomena becomes comparable with the critical length scales giving rise to size and shape dependent effects to nanomaterials. This makes nanomaterials to exhibit unique properties and provides the opportunity to use such nanostructured materials in novel applications and devices.

1.5 Classifications of nanoparticles

The nanoparticles may be classified into various types on the basis of morphology, size and shape. Some of the important classes of nanoparticles are following:

1.5.1 Organic nanoparticles

The organic nanoparticles consist of ferritin, micelles, dendrimers and liposomes shown in figure (Fig.1.5). The organic nanoparticles are non- toxic, biodegradable and some organic nanoparticles have a hollow sphere i.e. micelles and liposomes. It is also known with the name of nano capsules which have thermal and optical sensitivity. Organic nanoparticles are an optimal choice for drugs delivery due to these characteristics. Nanoparticles are also extensively applied in target drug delivery system. The organic nanoparticles are also called as polymeric nanoparticles. The most familiar shape of organic or polymeric nanoparticles is nanosphere or nano capsule. The matrix particles are former overall mass of which is solid and outer limits of spherical surface adsorb other molecules. In other case, particles encapsulated the solid mass.

- ❖ Carbon nanomaterials (e.g., fullerenes, nanotubes, nano cones etc.)
- ❖ Organic polymers (dendrimers, polystyrene, etc.)

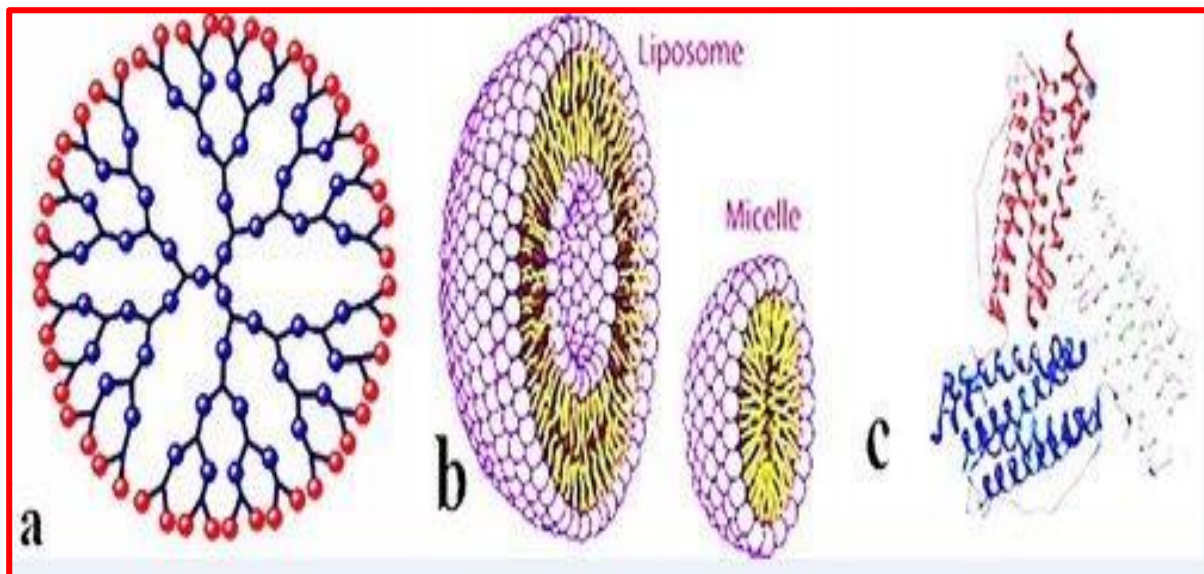


Fig. 1.5 Organic nanoparticles (a) Dendrimers (b) Liposomes and Micelles (c) Ferritin

1.5.2 Inorganic nanoparticles

Carbon is not present in inorganic nanoparticles. The inorganic nanoparticles are not toxic. They are biocompatible and hydrophilic. The inorganic nanoparticles are highly stable when compared to organic. They are classified into metal and metal oxide nanoparticles.

- ❖ Noble metal nanoparticles (e.g., iron, silver and gold nanoparticles).
- ❖ Semiconductor nanoparticles (or binary compounds when including carbides, nitrides, etc.), e.g., TiO_2 and Fe oxides
- ❖ Complex compounds (alloys, composites, nanofluids, etc., contain two or more molecules), e.g., cobalt and zinc iron oxide.
- ❖ Quantum dots (or q-dots), e.g., cadmium telluride and cadmium selenide.

1.5.3 Metal nanoparticles

Metals are used to synthesize metallic nanoparticles by using destructive or constructive methods. The metal precursors are used to fabricate the pure metal nanoparticles. The metal nanoparticles possess unique optoelectrical properties due to

plasma resonance characteristics. The synthesis of metal nanoparticles has been controlled by shape, face and size. All metals can be synthesized and fabricated into nanoparticles. The nanoparticles of aluminium, gold, iron, lead, silver, cobalt, zinc, cadmium and copper are well-known metal nanoparticles. Metal nanoparticles have unique properties because of its smaller size (10–100 nm), surface characteristics such as surface area to volume ratio, surface charge, pore size, surface charge density, structure (crystalline and amorphous), shapes (spherical, rod, hexagonal, tetragonal, cylindrical and irregular), color and environmental factors (sunlight, moisture, air and heat).

1.5.4 Iron nanoparticles

Iron is one of the most widespread transition metals and the fourth most plentiful element in the Earth's crust, and is the structural backbone of our modern infrastructure. Iron has a grand deal to offer at the nanoscale, including very potent magnetic and catalytic properties. Among all the metal nanoparticles, iron nanoparticles have always been attracted the researchers due to their distinct physiochemical properties.

Owing to their remarkable optical, electrical and biological properties, they find extensive applications in various fields and more particularly iron nanoparticles have a promising future in biomedical field due to their therapeutic potentialities and multifunctional activities. Hence, they provide a significant contribution to Nation's economy, as depicted in figure (Fig.1.6).

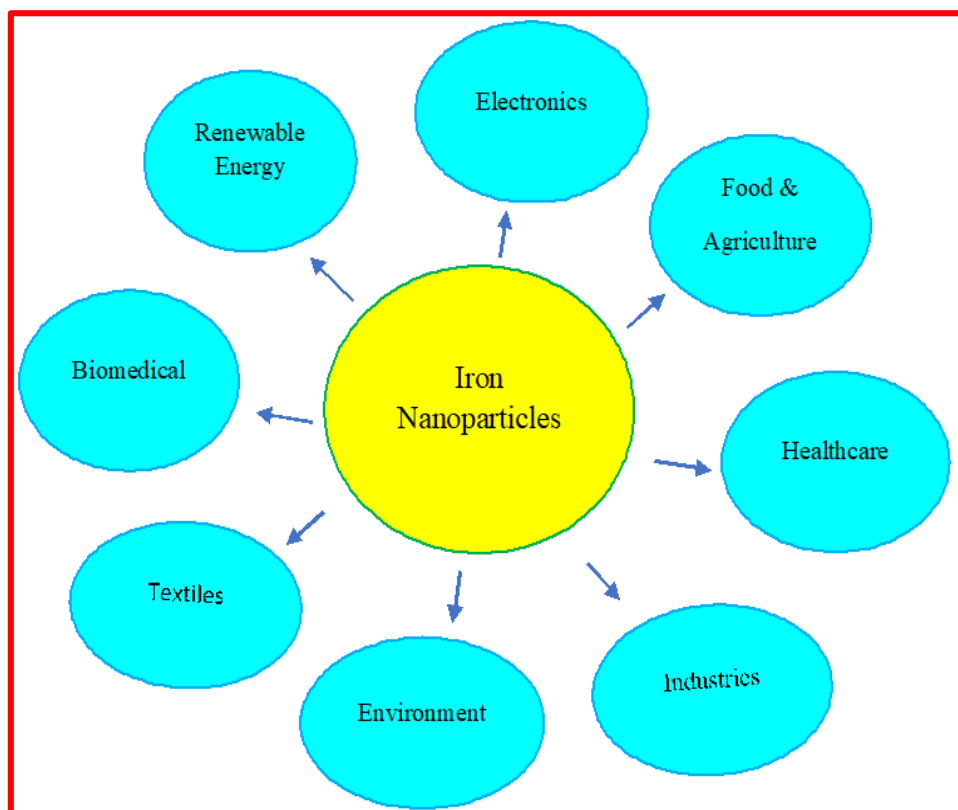


Fig.1.6 Applications of iron nanoparticles

1.6 Green synthesis of iron nanoparticles

Green synthesis of nanoparticles refers to the synthesis of different iron nanoparticles using bioactive agents such as plant extracts, microorganisms, and various bio-wastes including vegetable waste, fruit peel waste, eggshell, agricultural waste, and so on. The growing need to develop “green” and economical synthesis systems for iron nanoparticles has prompted researchers to explore the use of microorganisms, plant extracts, and other biomaterials [10]. The involvement of natural bioactive elements in the synthesis of iron nanoparticles greatly reduces the risk of environmental pollution. Green synthesized nanoparticles and their applications provide an insight into the synthesis of nanoparticles utilizing natural ways.

Green synthesis of iron nanoparticles is an advance method when compared to other methods because it is easy, cost-effective, and relatively reproducible, and often results in

more stable materials [11]. Microorganisms can also be used in nanoparticles synthesis, but the rate of synthesis is very slow and only a limited number of sizes and shapes are manageable to the method which compared to synthesis of plant-based materials. In green synthesis method, there is no requirement for high pressure, energy, temperature, or hazardous chemicals. Hence, nowadays, a lot of researchers are diverting themselves from using chemical methods. Plants provides more stable due to their biomolecules present in them and it is very straightforward to scale up. The contamination in this process is also very low.

Soon, a lot of new extracts from plants, bacteria, and other green elements are expected to be used to fabricate, stabilize, and synthesize metal nanoparticles. These include green components that have not been previously used for these purposes, especially those elements that have potential medicational applications, bactericides, fungicides, and others, as well as green components that include sugar, ascorbic acid, starch, and so on. In the same way, researchers would progressively expect results that, besides focusing on synthesis, achieve adequate control of particle size by controlling macroscopic parameters in the experimental process [12]. This is achieving the fine-tuning of optical, morphological, and structural properties, in order to obtain target applications, in the different areas where green synthesis has been active such as: sensing, fluorescent cell imaging, drug delivery, cancer theragnostic, etc. In the future, this growth can be extended to obtain semiconductor nanoparticles where green synthesis has exhibited less growth, to achieve acceptable progress in fields such as solar cells, fuel cells, load carriers, ferromagnetic studies, single-photon source, and others.

1.7 Applications

The key applications of iron nanoparticles are listed below:

- For treating industrial sites contaminated with chlorinated organic compounds
- To treat many types of ground contamination such as grounds contaminated by polychlorinated biphenyls (PCBs), organochlorine pesticides, and chlorinated organic solvents
- As a primary colorant in glass and ceramics and as a catalyst
- The magnetic properties of the nanoparticles allow them to be used in memory tape
- In medical and laboratory applications
- In magnetic data storage and resonance imaging (MRI)
- In plastics, nanowires, coatings, nanofibers and textiles
- In certain alloy and catalyst applications.

1.7.1 Biological Applications

1.7.1.1 Antibacterial activity

Antibacterial is completely associated with the compounds that provincially kill bacteria and slow down their rate of growth, without being extensively toxic to nearby tissues. A variety of laboratory methods can be used to screen the antibacterial activity of an extract or a pure sample. The well-known and basic methods are the disk-diffusion and agar dilution methods. Other methods are used especially for antifungal testing, such as poisoned food technique. Dilution method is used to measure the minimum inhibitory concentration (MIC) and minimum bactericidal concentrations (MBC) of the antibacterial agent. MIC is the lowest concentration of an antibacterial agent which inhibits the growth of the tested organisms whereas MBC is the lowest concentration of any agent which kills the majority of bacterial inoculums. Agar disk-Diffusion method is a well-known method

used for routine antibacterial susceptibility testing. The bacterial cell wall is designed to confer strength, rigidity, and shape, and to protect the cell from osmotic rupture and mechanical damage. According to their shape, elements, and actions, the bacteria cell wall can be classified into two main groups: Gram positive (+) and Gram negative (-).

1.7.1.2 Anti-inflammatory activity

Inflammation is caused by the release of chemicals from tissues and migrating cells that creates redness, swelling, and pain in the body. Anti-inflammatory agents obstruct particular substances in the human body that produce inflammation. They have been used to heal many different diseases. In this occasion, medicinal plants and their compounds have been employed worldwide in traditional medicine to cure different inflammatory conditions, such as lung and skin inflammations. Inflammation may be separated into two categories: Stringent and immedicable. Stringent inflammation is a low duration process, persisting during minutes, hours, or few days, with the prime characteristics of exudation of fluids and emigration of leukocytes, mainly neutrophils. In contradictory, immedicable inflammation duration is longer and is linked histologically to the existence of lymphocytes, macrophages, fibrosis, and tissue necrosis. Cultured mammalian cell systems produce low cost, quick, and reproducible assays for the analysis and validation of different food peptides having anti-inflammatory properties. Most of the recent insight to biologically active peptides exhibiting anti-inflammatory properties which have been identified through mammalian cell culture studies.

1.7.1.3 Anti-oxidant activity

Antioxidants are ginormous important substances which possess the ability to secure the body from damage due to free radical induced oxidative stress. Substantial evidences have been accumulated and indicated lead roles for reactive oxygen species (ROS) and other oxidants for causing several disorders and diseases. The substantiation has brought the

observation of researchers to an appreciation of antioxidants for prevention and treatment of diseases, and maintenance of human health. Human bodies have an inherent antioxidative mechanism and numerous biological functions such as the antimutagenic, anti-carcinogenic, and anti-aging responses originate from this attribute. Antioxidants affirmate or deactivate free radicals, often before they assault targets in biological cells. lately attraction in naturally arising antioxidants has considerably increased for use in food, cosmetic and pharmaceutical products, because they exhibit multifaceted in their multitude and magnitude of activity and give enormous scope in correcting imbalance. The part of free radical reactions in disease pathology is well developed and is involved in many acute and chronic disorders in human bodies, such as diabetes, atherosclerosis, aging, immunosuppression and neurodegeneration. An imbalance between ROS and the inherent antioxidant capacity of the body, directed the use of medicinal supplements particularly during the disease attack. Studies on medicinal plants, vegetables, and fruits have represented the presence of antioxidants such as phenolics, flavonoids, and tannins.

The antioxidant elements of medicinal plants may contribute to the protection they offer from diseases. The ingestion of naturally occurred antioxidants has been inversely associated with morbidity and mortality from degenerative disorders. Liver diseases remain a severe health problem. Antioxidant agents of natural origin have attracted special interest due to their free radical scavenging abilities. The use of herbals with high level of antioxidant components has been proposed as an effective therapeutic approach for hepatic damages.

1.7.1.4 Anti-diabetic activity

Diabetes is not at all a disease. It is the deficiency in the pancreatic system. So far there is no curative medication in all fields for diabetes. But it is controllable by way of taking up the medicine continuously apart from doing physical exercises daily. Chemical

based medicines only reduce the causes and the suffering temporarily whereas plant-based medicines are excellent in controlling and curing the diabetes. This will not produce any adverse effects like other medications.

Plants have always been an excellent source for drugs fabrication and a lot of present time available drugs which have been derived directly or indirectly from them. The hypoglycaemic effect of many plants used as antidiabetic medicines which has been confirmed, and the mechanisms of hypoglycaemic activity of these plants are being studied. Natural products like plants having antidiabetic potential activity which acts through either insulin mimetic or secretagogues properties. Anti-hyperglycaemic properties of the plants are due to their restoring ability of the function of pancreatic tissues by causing propagation of insulin level or resist the intestinal absorption of glucose or simplification of metabolites in insulin related processes. More than 400 plant species having hypoglycaemic nature which have been available in literature, however, plants derived new antidiabetic drugs searching increases day by day because of the biological substances like glycosides, alkaloids, terpenoids, flavonoids, carbohydrates, glycopeptides, terpenoids, amino acids and carotenoids, etc., which possess antidiabetic effect.

1.8 Review of Literature

Recently, many studies have proven that the plant extracts act as a potential precursor for the synthesis of the nanomaterials in non-hazardous ways. The plants are used successfully in the synthesis of several metal nanoparticles such as cobalt, copper, silver, gold, palladium, platinum, zinc oxide and magnetite. During the past decade, it has been demonstrated that many biological systems, including plants, algae, bacteria, yeast, fungi and human cells can transform inorganic metal ions into metal nanoparticles by the reductive capacities of the proteins and metabolites present in these organisms. Synthesis of

metallic nanoparticles using biological entities has great interest due to their unusual optical and chemical properties.

The synthesis of metallic nanoparticles would benefit from the development of clean, nontoxic and environmentally acceptable green chemistry procedures, probably involving organism ranging from bacteria to fungi and even plants.

Iron nanoparticles were successfully synthesized in an easy and less time-consuming way using *Camellia sinensis* leaves extract by **Gottimukkala et al.** [13]. The iron nanoparticles were prepared by green synthesis method through ferric (III) chloride as a precursor. As a result, the polyphenols in *Camellia sinensis* may possess the properties of reducing the ferric cations and also act as capping agents. The polyphenols consist of flavonoids and catechins. The catechin mainly the Epigallocatechin Gallate (EGCG) was the active catechin that take part in reduction process because it had a standard potential of 0.57V that can reduce the Fe^{3+} to Fe^0 as the standard potential of the iron is -0.036V. The morphology and size of iron nanoparticles were verified by characterizing the sample by FTIR and SEM analysis for studying the functional groups. The average size of iron nanoparticles was also found to be about 116nm.

Makarov et al. [14] reported that the synthesis and characterization of amorphous iron oxide nanoparticles from iron salts in aqueous extracts of *Hordeum vulgare* and *Rumex acetosa* plants. The synthesized nanoparticles were characterized by TEM, absorbance spectroscopy, XPS, EELS, SAED, and DLS methods and were shown to contain mainly iron oxide and iron oxohydroxide. *H. vulgare* extracts produced amorphous iron oxide nanoparticles with diameters of up to 30nm. These iron nanoparticles were intrinsically unstable and prone to aggregation. This study revealed that the presence of organic acids

played a vital role in the stabilization of iron nanoparticles, and that plants contained such constituents may be more efficacious for the green synthesis of iron nanoparticles.

Iron nanoparticles were prepared and synthesized using a rapid, single step, and completely biosynthetic method employing aqueous sorghum extracts as both the reducing and capping agent by **Njagi et al.** [15]. Iron ions were reduced by the aqueous *Sorghum bran* extracts, leading to the formation of amorphous iron nanoparticles with an average diameter of 50nm. The reactivity of iron nanoparticles was tested by the H₂O₂- catalyzed degradation of bromothymol blue as a model organic contaminant.

S. P. Dubey et al. [16] explored that the green synthesis is a low-cost method for nanoparticles synthesis. The synthesized gold and silver nanoparticles using leaf extract of *Rosa rugosa* were examined by UV-vis, TEM, XRD, FTIR, Zetasizer and EDX. The concentration of leaves extract had played an important role in the green synthesis of AgNPs and AuNPs. These nanoparticles were mostly spherical with some triangular and hexagonal in shapes with an average size of 12 and 11 nm, respectively.

Yosmery Vitta et al. [17] obtained iron nanoparticles from the aqueous extract of the leaves of *E. robusta*. In this work, the antimicrobial activity of iron nanoparticles on different pathogenic microorganisms such as *Pseudomonas aeruginosa*, *Escherichia coli*, *Staphylococcus aureus* and *Bacillus subtilis* were evaluated. The results had revealed that the increase or decrease of the antimicrobial activity depended on the particle size of FeNP and synthesis conditions. Finally, the quantification of flavonoids and total polyphenols was carried out and the antioxidant activity of the *E.robusta* extract was evaluated, which allowed associating the antimicrobial activity found in the FeNPs with the components present in the extract.

N Beheshtkhoo et al. [18] synthesized iron oxide nanoparticles by a simple bio-reduction method. Aqueous leaf extract of *Daphne mezereum* was used as a reducing and stabilizing agent. IONPS were characterized by transmission electron microscopy (TEM), particle size analysis (PSA), Fourier transform Infrared (FT-IR) spectroscopy, X-ray diffractometer (XRD), Vibrating sample magnetometer (VSM), and thermo gravimetric analysis (TGA). The average diameter of the prepared NPs ranged from 6.5 to 14.9 nm with a mean particle size of 9.2nm. In addition, the synthesized nanoparticles were tested for dye removing activities. Thus, it could be concluded that *D.mezereum* aqueous leaf extract can be used efficiently in the production of iron oxide NPs for commercial applications in environmental fields.

Green tea extract was used to synthesize iron nanoparticles (GT-Fe NPs) and degrade malachite green (MG) in aqueous solution by **X. Weng et al.** [19]. The results showed that the damage to morphology and increase in size of GT-Fe NPs after reaction with MG were observed by SEM and EDS. XRD had showed that there were few changes in the characteristic peaks of GT-Fe NPs before and after reaction. UV–vis spectroscopy showed that the absorption peak of MG decreased, while FTIR showing that the band at 1585 cm^{-1} corresponded to the phenyl group after reaction. The factors impacting on the removal efficiency of MG, including the initial solution pH, the initial concentration of MG, the dosage of GT-Fe NPs, and the reaction temperature, was also investigated. It emerged that 96% of MG was removed with a 50 mg/L at 298K. Kinetics studies showed that the removal of MG fitted well to the pseudo first-order mode.

Synthesis of iron nanoparticles using *Azadirachta Indica* leaf extract is performed by **C.P. Devatha et al** [20]. Different proportions of precursor (ferrous sulphate) to leaf extract were prepared by varying the volume quantity of leaf extract from 1:1 to 1:5. Their

morphology, structure and size distribution was confirmed by Scanning Electron Microscope along with X-ray energy dispersive spectroscopy and Fourier Transform Infrared spectroscopy analysis. Presence of accountable polyphenols such as total phenolic content by Folin-Ciocalteu (FC) method (20 mg per gram of leaf extract) and gallic acid (0.280 mg/g), caffeic acid (0.278 mg/g) & catechin (0.532 mg/g) for synthesis conciliation and were quantified by High Performance Liquid Chromatography. Its performance was evaluated on treatment of petrochemical refinery waste water to assess Chemical Oxygen Demand (COD) and nitrate removal for different proportions. The performance of COD removal (77%) and nitrate removal (74%) for 1:5 on 5th day was observed to be efficient. Antibacterial activity of synthesized iron nanoparticles from *Azadirachta Indica* leaf extract on bacteria (*Escherichia Coli*, *Pseudomonas Aeruginosa*, and *Staphylococcus Aureus*) was accomplished by well diffusion method. Size of FeNPs achieved for 1:2 ratio was 98–200 nm and for all proportions varying between 120 and 600 nm due to agglomeration enhanced bacterial decay. It was portrayed that there was an increase in the inhibition zone as the proportions increased from 1:2 to 1:5. Hence for the contact time of 48 h, 1:5 found to be effective in inhibiting a greater number of bacterial cells compared to other proportions.

R A Ismail et al. [21] (50 - 110nm) synthesized magnetic iron oxide (α - Fe₂O₃) nanoparticles were by pulsed laser ablation of iron target in dimethylformamide (DMF) and sodium dodecyl sulfate (SDS) solutions. The structural properties of the synthesised nanoparticles were investigated by using Fourier transform infrared spectroscopy (FT-IR), UV-VIS absorption, scanning electron microscopy (SEM), atomic force microscopy (AFM), and x-ray diffraction (XRD). The effect of laser fleunce on the characteristics of these nanoparticles was studied. Antibacterial activities of iron oxides nanoparticles were tested against gram-positive; *Staphylococcus aureus* and gram-negative; *Escherichia coli*,

Pseudomonas aeruginosa and *Serratia marcescens*. The results showed that a noteworthy inhibition on both bacterial strains. The preparation conditions were found to affect significantly the antibacterial activity of these nanoparticles. The synthesised magnetic nanoparticles were used to capture rapidly *staphylococcus aureus* bacteria under the magnetic field effect.

S. Das et al. [22] focused on the huge importance associated in developing functional materials, this research study describes the synthesis, characterization of morphology, bactericidal activity and cytotoxic effect of iron oxide nanoparticles (IONPs). IONPs had been successfully fabricated through thermal decomposition of a diiron (III) complex precursor. The morphology of the nanoparticles had been delineated with different spectroscopic and analytic methods. Scanning and transmission electron microscopy (FE-SEM and HR-TEM) analysed the cross-linked porous structure of IONPs with an average size ~97 nm. Dynamic light scattering (DLS) study of IONPs determined the hydrodynamic diameter as 104 nm. The cytotoxic behavior of IONPs had been examined against human lung cancer cell line (A549) through different fluorescence staining studies which ensure the mode of apoptosis for cell death of A549. Furthermore, measurement of reactive oxygen species suggested that the destruction of mitochondrial membrane of *Staphylococcus aureus*, leading to effective bactericidal propensity which holds a good promise for IONPs to become a clinically approved antibacterial agent.

The chemical synthesis of iron oxide nanoparticles (IO-NPs) followed by characterization and evaluation of antibacterial activity after treating with *Argemone mexicana L.* leaf extract was analysed **S. Arokiyaraj et al.** [23]. The formation of IO-NPs was confirmed by the colour change and further examined by UV–vis spectroscopy. The morphology was characterized by using SEM and TEM, which showed spherical particles

of uniform size ranged between 10 and 30 nm and the crystallites were determined through XRD. The peaks in XRD pattern were in good agreement with that of face-centered cubic form of iron oxide nanoparticles. FT-IR spectroscopy confirmed the attachment of bioactive molecules of plant on the IONPs surfaces. Furthermore, the antibacterial efficacy of IO-NPs, plant extract and IO-NPs treated with plant extract was screened against *Escherichia coli* MTCC 443, *Proteus mirabilis* MTCC 425 and *Bacillus subtilis* MTCC 441. The results showed a noteworthy inhibition on *P. mirabilis* and *E. coli* with IO-NPs treated plant extract. This outcome might pave a way for using the magnetic nanoparticles as a drug carrier system to cure bacterial diseases.

The antibacterial activity of Fe₃O₄ nanoparticles synthesized by **Y.T Prabhu et al.** [24] through chemical combustion method where ferric nitrate was used as precursor material and urea as fuel with the assistant of Tween 80, a non-ionic surfactant. The obtained Fe₃O₄ nanoparticles were characterized by X-ray diffraction, differential thermal analysis/thermo gravimetric analysis (DTA/TGA), particle size analyzer, SEM with EDAX and TEM. Various parameters such as dislocation density, micro strain, analysis of weight loss and surface morphological studies were calculated. The particle size was calculated from XRD and it was found to be 33–40 nm. Using well diffusion method antibacterial activity of Fe₃O₄ nanoparticles was tested against gram-positive and gram negative *Staphylococcus aureus*, *Xanthomonas*, *Escherichia coli* and *Proteus vulgaris*. Fe₃O₄ nanoparticles exhibited strong antibacterial activity against bacterial species.

Kumar V G et al. [25] studied the green method of synthesizing iron oxide nanoparticles from *Phyllanthus niruri* leaf extract. Furthermore, the green synthesized iron oxide nanoparticles were characterized and its antimicrobial activity was investigated. A characteristic comparison with chemical method of synthesis was also done, for iron

nanoparticles. The characterization of nanoparticle included that the IR, UV-Vis, surface morphology and size determination using TEM, SEM, and XRD. The analytical studies revealed that the synthesized iron oxide nanoparticles from these two different methods have almost identical size and morphology. The synthesized iron oxide nanoparticles showed that the significant antimicrobial activity against the microbes, *E. coli* and *P. aeruginosa*. The studies concluded that the synthesis of iron oxide nanoparticles using plant extracts was more beneficial as it is an economical, energy efficient, low cost and environment-friendly process than the bio-hazardous chemical synthesis.

For the first time, the aqueous extract of *Rosemary* was applied in green iron nanoparticle platform by **H.K. Farshchi et al.** [26] (*Rosemary*-FeNPs). Various methods, including dynamic light scattering (DLS), field emission scanning electron microscopy (FESEM), X-ray diffraction (XRD), Transmission electron microscopy (TEM), and Raman spectroscopy and Fourier Transform Infrared Spectroscopy (FTIR) were employed to characterize *Rosemary*-FeNPs. The mean size of the *Rosemary*-FeNPs were at about 100nm with PDI of less than 0.12, which indicated that the homogeneous size distribution of the nanoparticles. The cytotoxicity of *Rosemary*-FeNPs and total extract of rosemary was determined using MTT cytotoxic test on 4T1 and C26 cancer cell lines. The results showed that *Rosemary*-FeNPs could exerted more cytotoxic effect than total extract on both cancer cell lines.

Devatha, C.P et al. [27] explored that the synthesis of iron nanoparticles for treating domestic waste water. Synthesis of iron nanoparticles was done by using various leaf extracts viz. *Mangifera indica*, *Murraya Koenigii*, *Azadiracta indica*, *Magnolia champaca*, and to check its potential for treating domestic waste water. Characterization of the synthesized iron nanoparticles was done by UV-Visible spectrophotometer, Scanning

Electron Microscopy equipped with X-ray energy dispersive spectroscopy and Fourier Transform Infrared spectroscopy. The characterization results confirmed that the formation and presence of iron nanoparticles and biomolecules which could help in capping the nanoparticles. Among the different plant mediated synthesized iron nanoparticles, *Azadiracta indica* showed that 98.08% of phosphate, 84.32% of ammonia nitrogen and 82.35% of chemical oxygen demand removal. Overall performance of synthesized iron nanoparticles using *Azadiracta indica* showed that the satisfactory results compared to other leaf extracts for treating domestic waste water.

Spinacia oleracea (spinach) and *Musa acuminata* (banana) were chosen by **Pankaj Kumar Tyagi et al.** [28] for the study, and aqueous extracts of *spinach* leaf extract (SLE) and banana peel extract (BPE) were prepared for the synthesis of iron nanoparticles (FeNPs), and their antibacterial potential against pathogenic bacteria *Bacillus subtilis* (MTTC 1133) and *Escherichia coli* (MTTC 62) was evaluated. The XRD analysis revealed amorphism, with a weak iron characteristic peak, indicating non crystallinity. The antibacterial potential of BPE- and SLE-FeNPs was investigated, and inhibition zones (mm) against *B. subtilis* and *E. coli* were observed, as well as SLE-FeNPs against *B. subtilis* and *E. coli*. The findings suggest that FeNPs have a high antibacterial potential and could be used as antibacterial agents against pathogenic bacteria while being nontoxic in nature.

Iron oxide nanoparticles have been successfully synthesized by **Elvan Üstün et al.** [29] from various plant species using green synthesis pathways and analysed for different bioactivity properties. Iron oxide nanoparticles were synthesized using a completely non-hazardous method using *Ficus carica* leaf extract. The synthesized product was characterized by SEM, EDX, XRD crystallography, FT-IR, and UV-Vis spectroscopy. Characterization methods have shown that the product was synthesized in mixed form with

43-57 nm size. In addition, the antioxidant activity of the product was analysed, and it was recorded that the nanoparticle has remarkable antioxidant activity.

The aqueous extract of *Chlorophytum comosum* leaf was applied by **Shaker Ardakani et al.** [30] for the preparation of iron nanoparticles (INPs). The synthesized INPs managed to eliminate methyl orange (MO) from the aqueous solution. The concentration of MO could be easily checked via ultraviolet-visible (UV-Vis) spectroscopy throughout the usage of INPs at the presence of H₂O₂. The synthesized INPs exhibited MO degradation efficiency of 77% after 6 h. Furthermore, the synthesized INPs exhibited antibacterial activity against both Gram-negative and Gram-positive bacteria. The prepared INPs had an impressive effect on *Staphylococcus aureus* at concentrations below 6 µg/ml. Overall, the synthesized INPs could considerably contribute to our combat against organic dyes and bacteria.

Silver and iron nanoparticles were synthesized, characterized and investigated by **RR Chavan et al.** [31] for biological screening using *alcoholic blumea eriantha DC* plant extract. Formation of silver and iron nanoparticles was confirmed by using UV, FT-IR spectroscopy, SEM, X-ray diffraction, and TEM. The anti-oxidant, antimicrobial, cytotoxic activities of the synthesized nanoparticles were determined by using standard protocols. The results of the studies revealed that the synthesized nanoparticles exhibited effective antioxidant, antibacterial and cytotoxic activity. Therefore, it may open up a new avenue for anticancer therapies that needs further research.

The biosynthesis of stable iron nanoparticles was carried out by **J.A.A. Abdullah et al.** [32] using *Phoenix dactylifera L.* extract which was able to reduce iron ions to iron nanoparticles. The process comprises maceration extraction overnight and heat treatment of

the extract with iron chloride (FeCl_3) at 70°C for 1 h. X-ray diffraction (XRD), scanning electron microscope (SEM), and Fourier transform infrared spectroscopy (FTIR) were used for nanoparticles characterization. The stability of the bio-reduced iron nanoparticle was analysed using UV-VIS absorption spectra, and their antioxidant and anti-radical activities were measured against PhosPhoMolybdate (PPM) and 2,2-diphenyl-1-picryl-hydrazyl (DPPH), respectively. The results demonstrated that ecological biosynthesis of 2–30 nm stable iron nanoparticles of size with antioxidant activity could be achieved suggesting their possible applications.

CM Sangode et al. [33] worked on green synthesis of nanoparticles utilizing plant extract which shown enormous advantages over the methods of synthesis. Green nanoparticles were generally synthesized using metal atoms like silver, iron, copper, zinc, and plant extract containing reducible phytoconstituents like alkaloids, flavonoids, tannins, etc. Several iron nanoparticles were reported using plant extracts. Iron nanoparticles had a greater advantage of small size, affordable cost stability, or having some biomedical application. The results suggested the new pathway to synthesize iron nanoparticles by using the various plant extracts which exhibited high antimicrobial activity.

The anti-cancer, anti-aging, anti-inflammatory, antioxidant, and anti-diabetic effects of zinc oxide nanoparticles (ZnO-NPs) produced from aqueous leaf extract of *Aquilegia pubiflora* were evaluated by **H Jan et al.** [34]. Several methods were used to characterize ZnO-NPs, including SEM, FTIR, XRD, DLS, PL, Raman, and HPLC. The nanoparticles that had a size of 34.23 nm as well as a strong aqueous dispersion potential were highly pure, spherical or elliptical in form, and had a mean size of 34.23 nm. According to FTIR and HPLC studies, the flavonoids and hydroxycinnamic acid derivatives were successfully capped. Synthesized ZnO-NPs in water have a zeta potential of -18.4 mV , showed that they

are stable solutions. The ZnO-NPs proved to be highly toxic for the HepG2 cell line and showed a reduced cell viability of after 24 hours of ZnO-NP treatment. ZnO-NPs also showed an excellent inhibitory potential against the enzyme's acetylcholinesterase (IC_{50} : $102 \mu\text{g/mL}$) and butyrylcholinesterase (IC_{50} : $125 \mu\text{g/mL}$). Overall, the enzymes involved in aging, diabetes, and inflammation showed a moderate inhibitory response to ZnO-NPs. Given these findings, these biosynthesized ZnO-NPs could be a good option for the cure of deadly diseases such as cancer, diabetes, Alzheimer's, and other inflammatory diseases due to their strong anticancer potential and efficient antioxidant properties.

A Bouafia et al. [35] described that the green synthesis of Fe_3O_4 nanoparticles (NPs) using plant extract was safe for humans and the environment. Magnetite Fe_3O_4 NPs were greenly prepared using *Punica granatum L.* fruit peel extract as a reducing and capping agent. The effect of iron precursor contraction ($0.01\text{--}0.1 \text{ M}$, FeCl_3) was studied. The Fe_3O_4 crystalline with an average crystallite size range from 21 to 23 nm was proven by X-ray powder diffraction. Scanning electron microscopy images showed that the synthesized Fe_3O_4 NPs were mostly cubical. Ultraviolet-visible spectra showed that the prepared Fe_3O_4 NPs exhibit absorption at 270 nm related to the Fe_3O_4 NPs with a direct bandgap ranging from 1.87 to 2.26 eV and indirect bandgap of 2.16–2.48 eV. Fourier transform infrared spectroscopy analysis showed two characteristic absorption bands at 515 and 567 cm^{-1} , which proved the successful formation of Fe_3O_4 . The proposed method using *Punica granatum L.* fruit peel extract offers an economical and environmentally friendly route for synthesizing many other types of metal oxides.

In this work, six medicinal plants were used by **B Khanzada et al.** [36] for the synthesis of gold nanoparticles (AuNPs) and iron nanoparticles (FeNPs). The synthesized nanoparticles were characterized by different techniques including UV-visible

spectrophotometry, scanning electron microscopy (SEM), and Fourier transform infrared spectroscopy (FTIR). Furthermore, the activities of green synthesized nanoparticles were screened *in vitro* using, for example, antibacterial, antioxidant, cytotoxic, and DNA protection assays. Both FeNPs and AuNPs had spherical shapes with an average size less than 50 nm and were found to have good antimicrobial and nontoxic effects. Furthermore, FeNPs from *Ficus microcarpa* demonstrated high drug loading efficiency (65%) as compared to an anti-inflammatory drug (diclofenac potassium, DFP). This study explained that the drug delivery potential, as well as anti-inflammatory and anticoagulant properties, of nanoparticles *in vivo*. Interestingly, AuNPs of *Syzygium cumini* exhibited strong anti-inflammatory potential as compared to DFP and diclofenac-loaded FeNPs of *Ficus microcarpa*. The results suggested the potential pharmacological applications of biogenic synthesized AuNPs and FeNPs which could be explored further. The study revealed that the green synthesized AuNPs and FeNPs provide a promising approach for the synthesis of drug-loaded nanoparticles and consequently in the field of targeted drug delivery.

The fresh green and yellow *banana peel* of (Musa, cv. Cavendish) fruits were treated by **M.S Mokbel et al.** [37] with 70% acetone, which were partitioned with chloroform (CHCl₃) and ethyl acetate (EtOAc), sequentially. The antioxidant activities of the extracts were evaluated by using the thiocyanate method, β -carotene bleaching method and 1,1-diphenyl-2-picrylhydrazyl (DPPH) free radical elimination. While, antimicrobial activities of the extracts and isolated components were evaluated using paper disc methods and Minimum Inhibition Concentration (MIC). The EtOAc and water-soluble fractions of green peel displayed high antimicrobial and antioxidant activity, respectively. Antioxidant activity of water extracts was comparable to those of synthetic antioxidants such as butylated hydroxyanisole and butylated hydroxytoluene. Among all isolated components β -sitosterol,

malic acid, succinic acid, palmitic acid, 12-hydroxystearic acid, glycoside, the d-malic and 12-hydroxystearic acid were the most active against all the gram-negative and positive bacterial species tested.

In the present work, nano scaled zero valent irons (nZVI) were synthesized by **Monalisa Pattanayak et al.** [38] from the plant extract of under atmospheric conditions. The obtained iron nanoparticles were mainly in zero valent oxidation state. A systematic characterization of nZVI was performed using UV, XRD and SEM studies. The diameter of iron nanoparticles was predominantly found within the range 50-100 nm. It has been demonstrated that extract was capable of producing iron nanoparticles that showed the good stability in solution, under the UV-Visible wavelength nanoparticles shown quiet good surface plasmon resonance behavior. Ferric chloride with reducing agent i.e. *Neem plant* leaves extract has shown a remarkable color change with concerned change in pH of solution. Success of such a rapid time scale for synthesis of metallic nanoparticles was an alternative to chemical synthesis protocols and low-cost reductant for synthesizing iron nanoparticles.

This study explored the potential use of *apple peel* extract (APE) for the biosynthesis of iron nanoparticles (FeNPs) by **A. S. Y. Ting et al.** [39]. The synthesized APE-FeNPs were characterized by UV-Vis spectroscopy, Fourier-transform infrared spectroscopy (FTIR), field emission scanning electron microscopy (FE-SEM), energy-dispersive X-ray spectroscopy (EDX), and transmission scanning electron microscopy (TEM). The biosynthesis of APE based FeNPs was confirmed with polyphenol peaks (237 nm, 272 nm) which detected as biological components integrated into APE-FeNPs, and FTIR analysis profiled the presence of primary functional groups (OH-, NH-, CH bending vibrations). The formed APE-FeNPs were elliptical and spherical shapes, measuring 50 nm. Treatment of

malachite green dye with APE-FeNPs showed 71.51% dye decolorization within the first 1 min. This study has shown that apple peel extract could be used to synthesize FeNPs that are useful for removal for malachite green dye.

Water extracts from different bio-based products of plant origins were studied by **Martínez-Cabanas et al.** [40] to evaluate their antioxidant capacity and their potential to fabricate the metal nanoparticles from aqueous solutions. Two traditional tests, the Folin–Ciocalteu assay and the DPPH radical scavenging capacity method were compared with a more recent one, SNPAC, based on the formation of silver nanoparticles. The silver nanoparticle antioxidant capacity method (SNPAC) was optimized for its application in the characterization of the extracts selected in this work; kinetic studies and extract concentration were also evaluated. The extracts were obtained from leaves of *oak*, *eucalyptus*, *green tea*, *white and common thyme*, *white cedar*, *mint*, *rosemary*, *bay*, *lemon*, and *the seaweed sargassum muticum*. The results demonstrated that any of these three methods could be used as a quick test to identify an extract to be employed for nanoparticle formation. Additionally, the synthesis of Cu, Fe, Pb, Ni, and Ag nanoparticles using *eucalyptus extracts* were studied for demonstrating the efficiency of this plant extract to form metallic nanoparticles from aqueous metal salt solutions.

The gold nanoparticles (Au-NPs) using aqueous extract of *Sumac* were synthesized by **H Shabestarian et al.** [41]. The bio-synthesized Au-NPs were characterized by the UV-visible spectroscopy, FTIR, TEM, and zeta-potential measurements. The surface plasmon resonance band centred at 520 nm for Au-NPs was characterized by UV-visible spectrophotometer. The probable bio-molecules are polyphenols might be responsible for reduction of gold ions were recognized through FT-IR. The TEM result showed that the bio-formed Au-NPs are spherical in shapes with the mean size of 20.83 ± 4.4 nm. The

capping of anionic bio-molecules on the surface of Au-NPs was confirmed by zeta potential assessment (-25.3 mV) and was responsible for the electrostatic stability. In vitro antioxidant activity studies showed that DPPH (2, 2-diphenyl-1-picrylhydrazyl) and ABTS (2, 2'-azino-bis 3-ethylbenzthiazoline-6-sulfonic acid) activities increased in a dose dependent manner. This study not only unveils the roles of *sumac extract* but also presented some insights into designing the gold nanoparticles with both high reducing capability and high stability through the green synthesis route and explained that these nanoparticles could potentially be useful in pharmaceutical and biomedical applications.

Green synthesis of iron nanoparticles (FeNPs) using leaf and seed extracts of *Moringa oleifera* (*M. oleifera*) were prepared by **L Katata-Seru et al.** [42] mixing different ratios of plant extracts with iron chloride solution. They were characterized by using the characterization techniques such as dynamic light scattering, UV-Visible spectroscopy (UV-Vis), X-ray diffraction (XRD), Fourier transform infrared spectroscopy (FTIR) and transmission electron microscopy (TEM). The UV-Vis spectrum of *M. oleifera* leaf (MOL) and seed (MOS) based on FeNPs showed the absorption at 210 and 240 nm, respectively. In addition, the green application of synthesized nanoparticles for the removal of nitrate ion (NO_3^-) from surface and ground water was also investigated. The batch adsorption results showed that the enhanced removal of NO_3^- by 85 % and 26 % MOS-FeNPs and MOL-FeNPs respectively as compared to *M. oleifera* extracts. Furthermore, the antibacterial activity illustrated that the maximum zone of inhibition against *Escherichia coli* was observed by MOS-FeNPs (6 mm), followed by MOL-FeNPs (5 mm). The results confirmed that MOL and MOS extracts could play an important role in the bio-reduction of Fe ions to FeNPs. Nitrate removal from aqueous solutions using *M. oleifera* extracts and FeNPs, exhibited better effects in water purification.

Houng et al. [43] synthesized the silver nanoparticles (AgNPs) using *Sapindus mukorossi* fruit pericarp extract as the excellent reducing as well as capping agent. The synthesized AgNPs had spherical shaped morphology with the unimodal size distribution and the average particle size was found to be 17.3 nm. The green synthesized AgNPs exhibited the excellent antibacterial activities against the *Staphylococcus aureus* (gram +ve) with the maximum zone of inhibition of 27.3 ± 0.28 mm and *Pseudomonas aeruginosa* (gram -ve) with the maximum zone of inhibition of 12.0 ± 0.49 mm.

Bhuiyan et al. [44]. reported that the formation of iron oxide nanoparticles (α -Fe₂O₃ NPs) in a eco-friendly greener approach by the addition of *Carica papaya* leaf extract as the reducing agent. The as-prepared α -Fe₂O₃ NPs were tested for antibacterial activities against the three gram negative bacterial pathogens like *Klebsiella spp.*, *E.Coli*, *Pseudomonas spp.* and a gram positive bacteria like *S.aureus*. The α -Fe₂O₃ NPs showed the higher activity for *S.aureus* with the zone of inhibition of 7 ± 1 mm at 5 μ g/ml and 12.5 ± 0.5 mm at 30 μ g/ml. In contrast, the *Klebsiella pneumoniae* exhibited the resistance at 5 μ g/ml concentration but it showed the zone of inhibition of about 9 ± 1 mm at the concentration dose of 30 μ g/ml.

David et al. [45] developed the rapid, eco-friendly, and extracellular biosynthesis of silver nanoparticles (AgNPs) using *Sambucus nigra* (European black elderberry) fruit extract. The anti-inflammatory activity of AgNPs was studied in vitro on HaCaT cells that exposed to UVB radiation and in vivo on acute inflammatory model and in humans on psoriasis lesions. In vitro anti-inflammatory studies of AgNPs demonstrated that the decrease of cytokines production on UVB radiation exposure. Similarly, in vivo anti-inflammatory study of AgNPs showed the reduced levels of edema and cytokines in paw tissues. The local treatment of psoriasis vulgaris skin lesions exhibited the superior anti-

inflammatory activity of AgNPs, which confirms the better anti-inflammatory activity compared with hydrocortisone.

Torres et al. [46]. demonstrated the biosynthesis of selenium nanoparticles (Se NPs) using the bacterial pathogen of *Pantoea agglomerans* strain UC-32 under aerobic conditions to form the bioactive Se NPs with the particle size ranging between 30-300 nm. The synthesized Se NPs showed the superior anti-oxidant activity by trapping the free radicals in the induction of seleno enzymes with potential biologic activity by producing the reactive oxygen species via the human umbilical vein endothelial cells.

1.9 Scope of the work

Conventional nanoparticle synthesis methods like physical and chemical synthesis methods involve the usage of toxic chemicals, formation of hazardous byproducts, and contamination from precursor chemicals M Herlekar et al. [47]. Hence, there is a growing need to develop clean, nontoxic, and environment-friendly procedures for nanoparticle synthesis. Some of the distinct advantages that biological synthesis protocols have over the conventionally used physical and chemical methods are clean and eco-friendly method, as toxic chemicals are not used the active biological component like enzyme itself acts as a reducing and capping agent, thereby reducing the overall cost of the synthesis process.

Recently, a very wide range of biological resources like microorganisms (bacteria, yeast, fungi, algae, and viruses) and plants can be used for nanoparticles synthesis. While microbe-based protocols have been developed from the cumulative research efforts of several authors, plant-mediated biological synthesis of nanoparticles has gained importance only in the recent years (Bedlovicova et al.) [48]. Plant extracts reduce the metal ions in a shorter time as compared to microbes. Depending upon plant types and concentration of

phytochemicals, nanoparticles are synthesized within a few minutes or hours, whereas microorganism-based methods require a longer time [49]. All these reasons, along with the easy availability of plants in nature, make them more preferred biological resources than microbes. Among the metal nanoparticles, magnetic nanoparticles have been emerged as a new class of important nanoparticles as they possess many exceptional properties like super paramagnetism, high coercivity, and so forth.

The major objectives of the work are as follows:

- To extract the bio-active components from the various plants, by using biosynthesis method.
- To examine the nature of chemical compounds which present in the plants by standard methods such as UV-Vis and FT-IR spectrophotometric analysis.
- To evaluate the antioxidant, antibacterial, antifungal and anti-inflammatory activities of iron nanoparticles samples by well diffusion methods.
- To characterize the plants - mediated iron nanoparticles by the following sophisticated techniques.
- To confirm the formation of iron nanoparticles by UV-Vis analysis.
- To investigate the bio-components involved in the interaction and stabilization of the synthesized iron nanoparticles by Fourier Transform-InfraRed (FT-IR) spectroscopic analysis.
- To determine their crystalline nature of synthesized iron nanoparticles by X-Ray Diffraction (XRD) Analysis.

- To study the size and shape of the biosynthesized iron nanoparticles by Scanning Electron Microscopy (SEM) technique.
- To confirm the presence of elemental iron nanoparticles by Energy Dispersive X-ray Diffraction Spectroscopy Analysis (EDS).
- To create high magnification images of the internal structure of the iron nanoparticles by High-resolution-transmission electron microscope (HR-TEM).
- To study the size of particles in solution by Dynamic Light Scattering– Particle Size Analysis.

References

- [1] R.P. Feynman, There's Plenty of Room at the Bottom. *Engineering and Science*, 23 (5) (1960) 22-36.
- [2] J.N. Tiwari, R.N. Tiwari, K.S. Kim, *Prog. Mater. Sci.*, 57(4) (2012) 724-803.
- [3] S. A. T. O. S. H. I. Horikoshi, N. I. C. K. Serpone, *Microwaves Nanoparticles Synthesis Fundamental Applications*, (2013) 1–24.
- [4] S. Laurent, D. Forge, M. Port, A. Roch, C. Robic, L. Vander Elst, R.N. Muller, *Chem. Rev.* 108(6) (2008) 2064-2110.
- [5] E. Abbasi, M. Milani, S. Fekri Aval, M. Kouhi, A. Akbarzadeh, H. Tayefi Nasrabadi, P. Nikasa, S.W. Joo, Y. Hanifehpour, K. Nejati-Koshki, M. Samiei, *Crit. Rev. Microbiol.*, 42(2) (2016) 173-180.
- [6] I. Khan, K. Saeed, I. Khan, *Arab. J. Chem.*, 12(7) (2019) 908-931.
- [7] <http://eprints.um.edu.my/id/eprint/13180>
- [8] P.K. Jain, X. Huang, I.H. El-Sayed, M.A. El-Sayed, *Acc. Chem. Res.*, 41(12) (2008) 1578-1586.
- [9] L. Marchiol, *Ital. J. Agron.*, 7(3) (2012) e37-e37.
- [10] S.C. Kumari, V. Dhand, P.N. Padma, *Nanomaterials*, (2021) 259-281.
- [11] C.P. Devatha, A.K. Thalla, *Synthesis of inorganic nanomaterials*, (2018) 169-184. <https://doi.org/10.1016/B978-0-08-101975-7.00007-5>.
- [12] R. Britto-Hurtado, M. Cortez-Valadez, *Green Functionalized Nanomaterials for Environmental Applications*, (2022) 83-127. <https://doi.org/10.1016/B978-0-12-823137-1.00002-6>.
- [13] K.S.V. Gottimukkala, *Journal of Nanomedicine & Biotherapeutic Discovery*, Volume (2017), 7:151.
- [14] V.V. Makarov, S.S. Makarova, A.J. Love, O.V. Sinitsyna, A.O. Dudnik, I.V. Yaminsky, M.E. Taliany, N.O. Kalinina, *Langmuir*, 30(20) (2014) 5982-5988.
- [15] E.C. Njagi, H. Huang, L. Stafford, H. Genuino, H.M. Galindo, J.B. Collins, G.E. Hoag, S.L. Suib, *Langmuir*, 27(1) (2011) 264-271.
- [16] S.P. Dubey, M. Lahtinen, M. Sillanpää, *Colloids Surf. A: Physicochem. Eng. Asp.*, 364(1-3) (2010) 34-41.
- [17] Yosmery Vitta, Calos Ciangherotti, *Materials Science for Energy Technologies*, Volume 3 (2020) 97-103.

- [18] N. Beheshtkhoo, M.A.J. Kouhbanani, A. Savardashtaki, A.M. Amani, and S Taghizadeh, *Applied Physics A*, 124(5) (2018) 1-7.
- [19] Xiulan Weng, Lanlan Huang, Zuliang Chen, Mallavarapu Megharaj, Ravendra Naidu, *Industrial Crops and Products*, Volume 51 (2013) 342-347.
- [20] C.P. Devatha, K.Jagadeesh, M. Patil, *Environmental Nanotechnology, Monitoring & Management*, 9 (2018) 85-94.
- [21] R.A. Ismail, G.M. Sulaiman, S.A. Abdulrahman, T.R. Marzoog, *Materials Science and Engineering,C*, 53 (2015) 286-297.
- [22] S. Das, S. Diyali, G. Vinothini, B. Perumalsamy, G. Balakrishnan, T. Ramasamy, D. Dharumadurai, B. Biswas. *Heliyon*, 6(9) (2020) 04953.
- [23] S. Arokiyaraj, M. Saravanan, N.K. Udaya Prakash, M. Valan Arasu, B. Vijayakumar, S. Vincent, *Materials Research Bulletin*, 48(9) (2013) 3323–3327.
- [24] Y.T. Prabhu, K.V. Rao, B.S. Kumari, V.S.S. Kumar, T. Pavani, *International Nano Letters*, 5(2) (2015) 85-92.
- [25] V.G.V. Kumar, A.A. Prem, *Oriental Journal of Chemistry*, 34(5) (2018) 2583.
- [26] H.K. Farshchi, M. Azizi, M.R. Jaafari, S.H. Nemati, A. Fotovat, *Biocatalysis and agricultural biotechnology*, 16 (2018) 54-62.
- [27] C.P. Devatha, A.K. Thalla, S.Y. Katte, *Journal of cleaner production*, 139 (2016) 1425-1435.
- [28] P.K. Tyagi, S. Gupta, S. Tyagi, M. Kumar, R. Pandiselvam, S.D. Daştan, J.Sharifi-Rad, D. Gola, A. Arya, *Journal of Nanomaterials*, Volume 2021, <https://doi.org/10.1155/2021/4871453>.
- [29] E. Üstün, S.C. Önbaş, S.K. Çelik, M.Ç. Ayvaz, N. Şahin, *Biointerface Research in Applied Chemistry*, (12) (2021) 2108-2116.
- [30] L.S. Ardakani, V. Alimardani, A.M. Tamaddon, A.M. Amani, S. Taghizadeh, *Heliyon*, 7(2) (2021) 06159.
- [31] R.R. Chavan, S.D. Bhinge, M.A. Bhutkar, D.S. Randive, G.H. Wadkar, S.S. Todkar, M.N. Urade, *Materials Today Communications*, 24 (2020) 101320.
- [32] J.A.A. Abdullah, L.S. Eddine, B. Abderrhmane, M. Alonso-González, A. Guerrero, A. Romero, *Sustainable Chemistry and Pharmacy*, 17 (2020) 100280.
- [33] C.M. Sangode, S.A. Mahant, P.C. Tidke, M.J. Umekar, R.T. Lohiya, *Biological and Pharmaceutical Sciences*, 15(2) (2021) 117-127.

- [34] H. Jan, M. Shah, A. Andleeb, S. Faisal, A. Khattak, M. Rizwan, S. Drouet, C. Hano, B.H. Abbasi, *Oxidative medicine and cellular longevity*, volume 2021 <https://doi.org/10.1155/2021/4786227> (2021).
- [35] A. Bouafia, S.E. Laouini, M.L. Tedjani, G.A. Ali, A. Barhoum, *Textile Research Journal*, volume 6 (2) (2021).
- [36] B. Khanzada, N. Akthar, M.Z. Bhatti, H. Ismail, M. Alqarni, B. Mirza, G. Mostafa-Hedeab, G.E.S. Batiha, *Journal of Chemistry*, Volume 2021 (2021) <https://doi.org/10.1155/2021/1581444>.
- [37] M.S. Mokbel, F. Hashinaga, *American journal of Biochemistry and Biotechnology*, 1(3) (2005) 125-131.
- [38] M. Pattanayak, P.L. Nayak, *World Journal of Nano Science & Technology*, 2(1) (2013) 06-09.
- [39] A.S.Y. Ting, J.E. Chin, *Water Air and Soil Pollution*, 231 (2020) 1-10.
- [40] M. Martínez-Cabanas, M. López-García, P. Rodríguez-Barro, T. Vilariño, P. Lodeiro, R. Herrero, J.L. Barriada, M.E. Sastre de Vicente, *Nanomaterials*, 11(7) (2021) 1679.
- [41] H. Shabestarian, M. Homayouni-Tabrizi, M. Soltani, F. Namvar, S. Azizi, R. Mohamad, H. Shabestarian, *Materials Research*, 20 (2016) 264-270.
- [42] L. Katata-Seru, T. Moremedi, O.S. Aremu, and I. Bahadur, *Journal of Molecular Liquids*, 256 (2018) 296-304.
- [43] V.T.L. Huong, N.T. Nguyen, *Mater. Today*, volume 42, (2021) 88-93.
- [44] M.S.H. Bhuiyan, M.Y. Miah, S.C. Paul, T.D. Aka, O. Saha, M.M. Rahaman, M.J.I. Sharif, O. Habiba, M. Ashaduzzaman, *Heliyon*, 6(8) 2020, e04603.
- [45] L. David, B. Moldovan, A. Vulcu, L. Olenic, M. Perde-Schrepler, E. Fischer-Fodor, A. Florea, M. Crisan, I. Chiorean, S. Clichici, G.A. Filip, *Colloids Surf. B: Biointerfaces*, 122, (2014)767-777.
- [46] S.K. Torres, V. L Campos, C.G. León, S.M. Rodríguez-Llamazares, S.M. Rojas, M. Gonzalez, C. Smith, M.A. Mondaca, *J. Nanoparticle Res.*, 14(11) (2012) 1-9.
- [47] M. Herlekar, S. Barve, R. Kumar, *Journal of Nanoparticles*, Volume 2014 (2014) <https://doi.org/10.1155/2014/140614>.
- [48] Z. Bedlovicova, I. Strapac, M. Balaz, A. Salayova, *Molecules*, 25 (14) (2020) 3191.
- [49] A.A. Bunaciu, A.F. Danet, Ş. Fleschin, H.Y. Aboul-Enein, *Crit. Rev. Anal. Chem.*, 46 (5) (2016) 389-399.

Chapter II

Materials, Experimental Work, and Characterization Techniques

2.1 Materials utilized

Materials chosen for this research work was iron to synthesize nanoparticles among all metals because of its magnificent properties towards biomedical applications. Iron (III) chloride was used as a metal precursor. Biosynthesis approach has been used for the synthesis of iron nanoparticles by using plant extracts.

- (i) Metal Precursor : Iron (III) Chloride
- (ii) Solvent : De-ionized Water
- (iii) Plant Extracts : *Cinnamomum verum* (Cinnamon Bark)
Murraya koenigii (Curry Leaves)
Rosa gallica (Rose Petals)
Camellia sinensis (Green Tea Leaves)

Table 2.1 The details of materials utilized in this work

S. No.	Materials utilized	Chemical formula	Company name
1	Iron (III) chloride	FeCl ₃	Alfa Aesar
2	Deionized water	H ₂ O	Sigma Aldrich
3	Acetone	C ₃ H ₆ O	Alfa Aesar
4	Separator (GF/D)	-	Whatmann

Using the above materials, the following different combinations of iron nanoparticles were synthesized and their properties were carried out in aqueous media (table 2.1).

The four different systems given below were taken for this research work.

- 0.01M of FeCl₃+30 ml of *Cinnamomum verum* bark extract
- 0.01M of FeCl₃+30 ml of *Murraya koenigii* leaves extract
- 0.01M of FeCl₃+30 ml of *Rosa gallica* petals extract
- 0.01M of FeCl₃+30 ml of *Camellia sinensis* leaves extract

2.2 Experimental work

The iron nanoparticles were successfully prepared by biosynthesis method by using plant extracts for biomedical applications.

2.2.1 Plant mediated synthesis

Plant mediated synthesis is the best platform as its being free from toxic chemicals and providing natural capping agents for the stabilization of iron nanoparticles. Hence, green synthesis of iron nanoparticles that provide advancement over physical and chemical methods are eco-friendly, cost effective. The adaptability in use for medicinal, surgical, pharmaceutical applications and as bactericidal compounds is being accepted [1].

The plants have medicinal values and are environmental benign, yet chemically complex structures. This medicinal properties of plants due to presence of bioactive compounds or phytochemicals such as alkaloids, flavones, ketones, phenolic acids, polyphenols, organic acids, and quinines, saponins ,enzyme , proteins, sugars, terpenoids, and vitamins. These bioactive compounds have an important role in reduction followed by stabilization of metallic ions. However, plant mediated synthesis is quite straightforward process at room temperature [2].

2.2.2 Mechanism of plant mediated synthesis of iron nanoparticles

Four different plant extracts were used to synthesize iron nanoparticles (FeNPs). FeNPs were prepared by varying the plant extract concentration and keeping the concentration of iron (III) chloride constant. 0.01M of iron (III) chloride was added to plant extract to prepare a solution.

2.2.3 Preparation of plant extracts

The various parts of several plant species such as *Cinnamomum verum* bark, *Murraya koenigii* leaves, *Camellia sinensis* leaves, and *Rosa Gallica* petals have been collected and thoroughly cleansed with tap water and followed by deionized water. The purified plants were dried at room temperature. About 5g of each plant was weighed and transferred to the glass kettle with 100ml of deionized water and heated up to 70° C for 20 minutes in a heater mantel under reflux. This mixture put in undisturbed condition to attain room temperature and then it was filtered through a Whatmann No.1 paper. The extract solution was stored at 4°C for further use. The obtained extracts of various plants were subjected separately for the synthesis within two to three days.

2.2.4 Biosynthesis of iron nanoparticles

In the 0.01 M of FeCl₃ solution, the 30 ml extract from the solution of each plant species such as *Cinnamomum verum* bark, *Murraya koenigii* leaves, *Rosa gallica* petals, and *Camellia sinensis* leaves was added in four different beakers in dropwise by a burette at room temperature. The reaction mixture solution was converted from pale brown into black color right away. It was indicated the formation of iron nanoparticles, which absorbed the radiation in the visible region (Fig.2.1). After 24 hours, the reaction mixture was centrifuged at 10,000 rpm for 15 min. The resultant black pellet was purified with deionized water and ethanol. Then, it was dehydrated at 60°C in a hot air oven for removing residual

impurities and moisture. The attained black powder of iron nanoparticles was deposited in a dried dark place for further analyses.

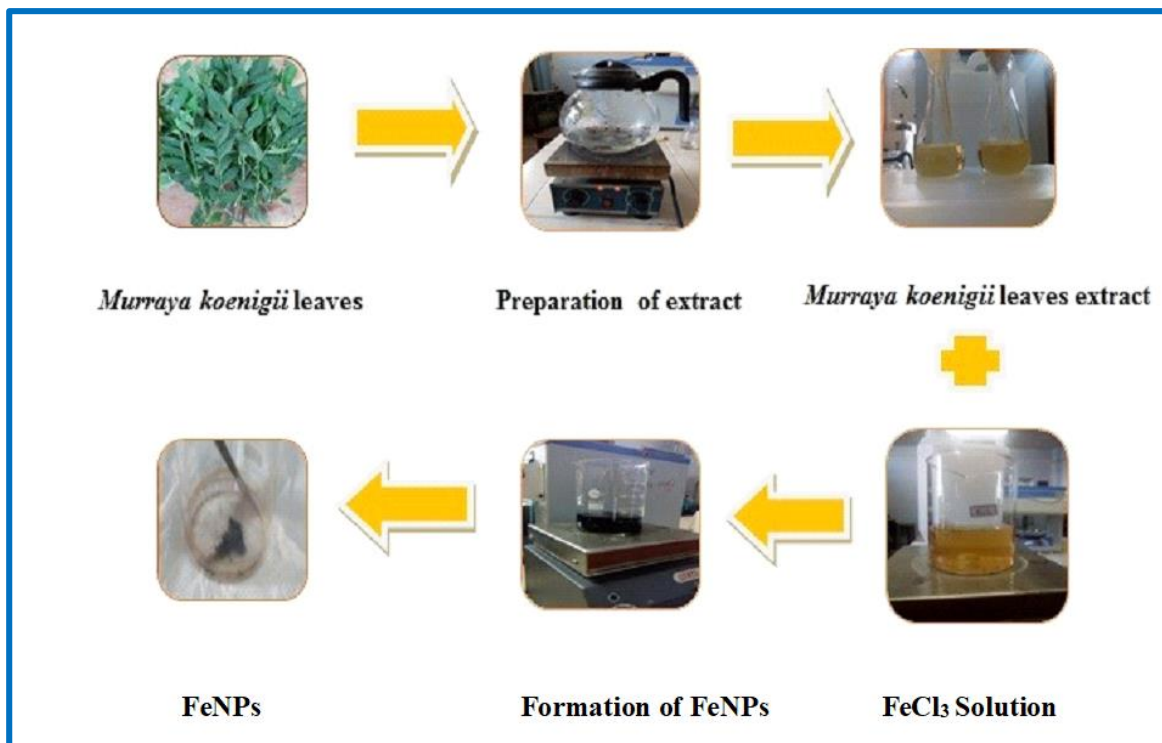


Fig.2.1 Schematic diagram of green technique for the synthesis of iron nanoparticles

At the end of synthesis, plant extracts have the ability to stabilize the nanoparticle (NPs) eventually determines the most energetically favourable and stable morphology (Fig.2.2). The nature of the plant extract, its concentration, the concentration of the metal salt, the pH, temperature and contact time significantly influencing the rate of production of the nanoparticles, their quantity and other characteristics [3].

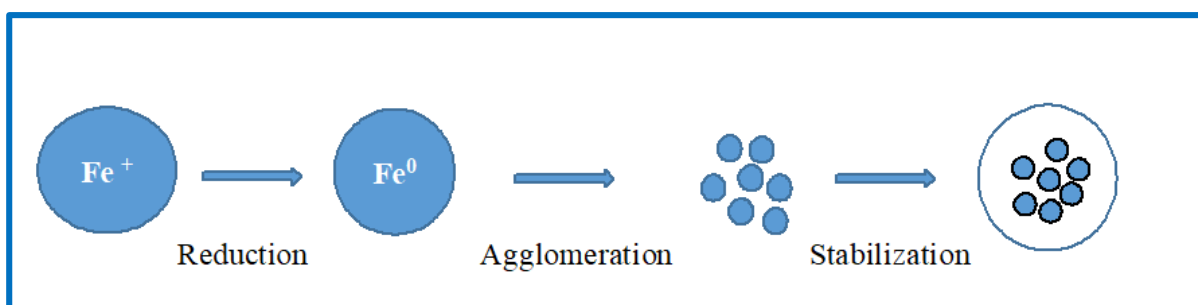


Fig.2.2 Synthesis mechanisms of FeNPs

2.3 Characterization techniques

The biosynthesized nanoparticles were subjected to various characterization techniques which are listed below for their respective analysis.

❖ Phase and morphology characterization techniques

- XRD - X-Ray Diffraction ((X'pert PRO -PANalytical model) using CuK α radiation ($\lambda = 0.15406 \text{ \AA}$) between $2\theta = 10^\circ$ and 80°)
- SEM - Scanning Electron Microscopy (CARL ZEISS, EVO 18)
- EDS-Energy Dispersive Spectroscopy (Quantax 200 with X Flash ® 6130)
- HR-TEM - High Resolution-Transmission Electron Microscope (JEOL 2100+)

❖ Magnetic characterization technique

- VSM-Vibrating Sample Magnetometer (magnetic field up to 2.2 T Microsense, Model ADE – EV9)

❖ Optical characterization techniques

- UV-Visible absorption spectrometer (Shimadzu 2600)
- FT-IR - Fourier Transform-Infrared spectroscopy (Thermo Nicolet 380 FT-IR spectrometer)
- DLS-Dynamic Light Scattering

❖ Analysis of Biological Activities

- Anti-bacterial activity
- Anti-oxidant activity
- Anti –inflammatory activity
- Anti-diabetic activity

2.3.1 Phase and morphology characterization techniques

2.3.1.1 X-ray diffractometer

X-ray diffraction is a popular analytical technique that provides information about crystallinity, crystallite size, orientation of the crystallites and phase composition and aid in molecular modelling to determine the structure of the material [4]. The X-ray diffraction patterns are obtained by measurement of the angles at which an X-ray beam is diffracted by the crystalline phases in the specimen (Fig 2.3a).

X-ray crystallography has been used for determining atomic and molecular structure of our crystalline materials. Here, the atomic planes of the material diffract the X-rays in different specific directions depending on their atomic orientations [5]. The angle and intensity of the diffracted beams give us a three dimensional idea about the density of electrons within the measured crystal. A pictorial representation of a typical X-ray diffractometer is shown in figure (Fig. 2.3b). When high energy electron beam is incident on a target, it tears out the inner shell electrons [6]. The electrons from the next excited states fill up the vacancy and as a result, X-ray is generated. The monochromatic beam of X-rays of wavelength λ from the source is made to fall on a crystalline sample where the X-rays are scattered elastically by the electrons within the crystal planes and interfere constructively in few specific directions that are determined by Bragg's law as:

$$2d \sin\theta = n\lambda \quad (2.1)$$

where, d is the spacing between two consecutive parallel crystallographic planes aligned in the same direction, θ is the angle of diffraction and n is an integer. The detector moves accordingly with the sample or source's movement and records the angles and intensities of the diffracted beams. The intensity is plotted against the angle 2θ which gives us standard X-ray diffraction pattern [7]. It is possible to estimate the grain size (D) of the

sample from the width of the diffraction peaks following the Debye-Scherrer formula as given below:

$$D = k\lambda/\beta \cos\theta \quad (2.2)$$

where, K is a Scherrer constant that depends on the particles shape, λ is the wavelength of X-ray, β is the full width at the half maxima of the diffraction peak at angle 2θ [8].

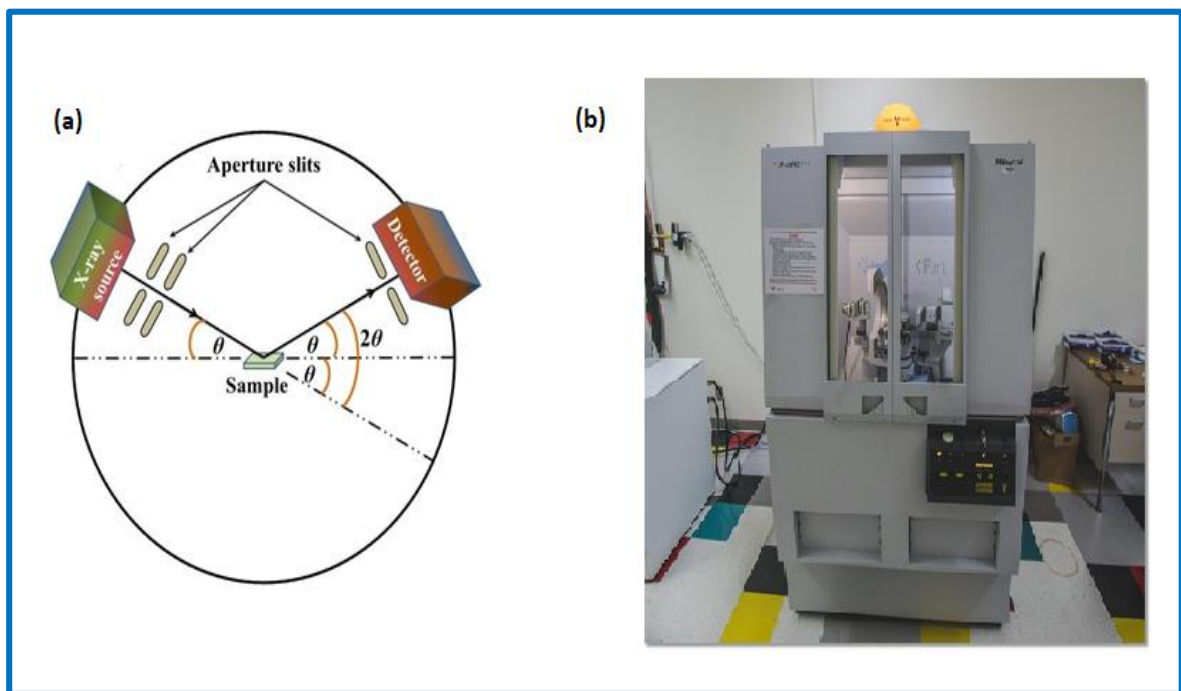


Fig.2.3 (a) Schematic representation of X-ray diffractometer b) Photograph of X'pert PRO -PANalytical model

2.3.1.2 Scanning electron microscope (SEM)

Electron microscope is a type of microscope where a beam of highly energetic electrons illuminates a specimen to produce its magnified image. There are two types of electron microscopes which have been used to analyze the samples [9].

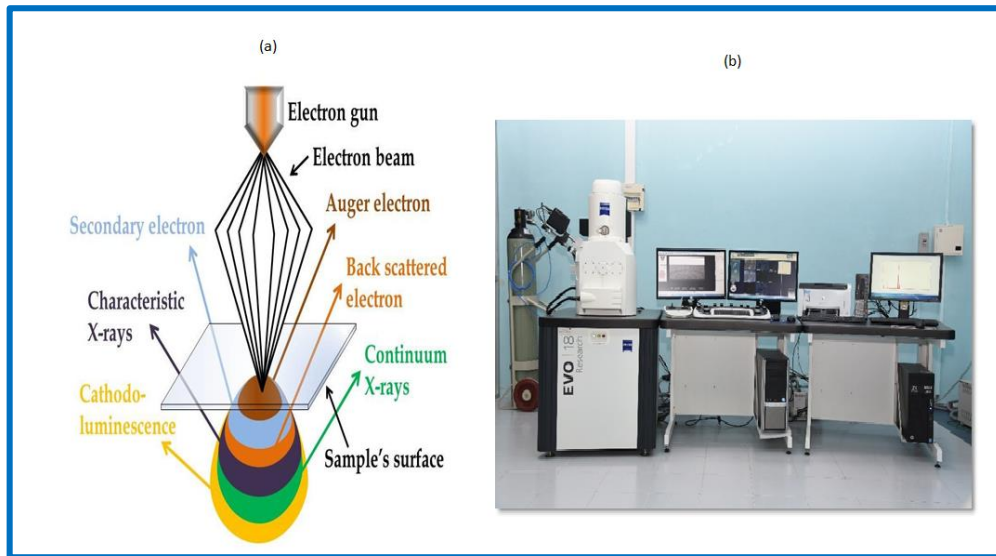


Fig.2.4 a) Schematic representation of SEM, b) Photograph of CARL ZEISS, EVO 18

In electron microscopes, a highly energetic beam of focused electrons is allowed to interact with the sample is shown in figure (Fig.2.4a). The signals that come out from the sample, give us various important information about the material. The figure (Fig. 2.4b) represents a photograph of scanning electron microscope (SEM). The thermally ionized or field emitted beam of electrons from the electron gun is focused in vacuum to incident on the sample.

The beam of electrons passes through positively charged electrodes, condenser lenses, scan coils and objective lens. The final focusing of the beam is done by the objective lens to scan the sample's surface. The lenses are magnetic in nature which deflect the electrons and focus them. The typical voltage range for SEM is 2 to 50 kV. The diameter of the beam can be varied from 5nm to 2 μ m. Highly energetic electrons interact with the material's surface and loss most of their energy due to inelastic collision at the surface of the sample and also via other various mechanisms that produce different types of signals [10]. Such signals contain low energy secondary electrons (produced during inelastic scattering of incident electrons with the outer shells' electrons of the atoms of the sample), high energy backscattered electrons, diffracted backscattered electrons, characteristic X-

rays (produced after the inelastic collisions of the incident electrons with the inner shells' electrons) and visible light (cathodo-luminescence) (Fig. 2.7). The secondary electrons can easily be separated from the backscattered electrons by considering their energies using a detector.

The displayed image in SEM is a visualization of the mapped intensities of signals as produced by the secondary electrons. A three dimensional SEM micrograph may be visualized due to the large depth of field in the narrow electron beam. The characteristic X-rays that come out from the inner shells of the atoms of the specimen are used for elemental analysis.

2.3.1.3 Energy Dispersive X-ray Spectroscopy (EDS)

Energy dispersive X-ray diffraction analysis is used for identifying the elemental composition of the testing sample (Fig.2.5). During EDX analysis, a beam of electrons ejects some of the electrons out from the nanoparticles creating a vacancy position in the atomic structure. This is immediately filled up by electrons from other energy levels [11]. Depending on from which energy level the electrons are transferred that much excess energy is given out in the form of X-rays, which is characteristic and unique for a particular element. Peaks in the EDX spectrum corresponds to energy levels for which the most X-rays had been received. Each of these peaks is unique to an atom, and therefore corresponds to a single element. The higher peak in a spectrum represents the more concentrated the element is in the specimen. In the present study, the elemental composition of the synthesized iron nanoparticles was determined using SUPRA 55 EDX equipment. EDX analysis also provides information on contaminants and their relative concentrations present in the sample.



Fig.2.5 Photograph of EDS (Quantax 200 with X Flash ® 6130)

2.3.1.4 High Resolution-Transmission Electron Microscope (HR-TEM)

HR-TEM is a microscopy technique whereby a beam of electrons is transmitted through an ultra-thin specimen, thereby interacting with the specimen as it passes through. When the electron beam passes through the sample, get transmitted and refracted beams are shown in figure (Fig.2.6a). An image is formed by the interference between transmitted and diffracted beams; the image is magnified and focused onto an imaging device, such as a fluorescent screen, on a layer of photographic film, or to be detected by a sensor such as a CCD camera [12]. Using HR-TEM (Fig.2.6.b), the size and morphology of the particles are determined. Image of the particles were taken at 300kV accelerating voltage. Transmission electron microscopic techniques are capable of imaging at a significantly higher resolution than light microscopes, owing to the small de Broglie wavelength of electrons. This enables the instrument's user to examine fine detail-even as small as a single column of atoms, which is tens of thousands times smaller than the smallest resolvable object in a light microscope.

HR-TEM forms a major analysis method in a range of scientific fields in both the physical and the biological sciences. At smaller magnifications, HR-TEM image contrast is due to absorption of electrons in the material, due to the thickness and composition of the material. At higher magnifications, complex wave interactions modulate the intensity of the image, requiring expert analysis of observed images. Electrons are usually generated in an electron microscope by a process known as thermionic emission from a filament, usually tungsten, in the same manner as a light bulb, or alternatively by field electron emission [13]. The electrons are then accelerated by an electric potential (measured in volts) and focused by electrostatic and electromagnetic lenses onto the sample. The transmitted beam contains information about electron density, phase and periodicity; this beam is used to form an image.

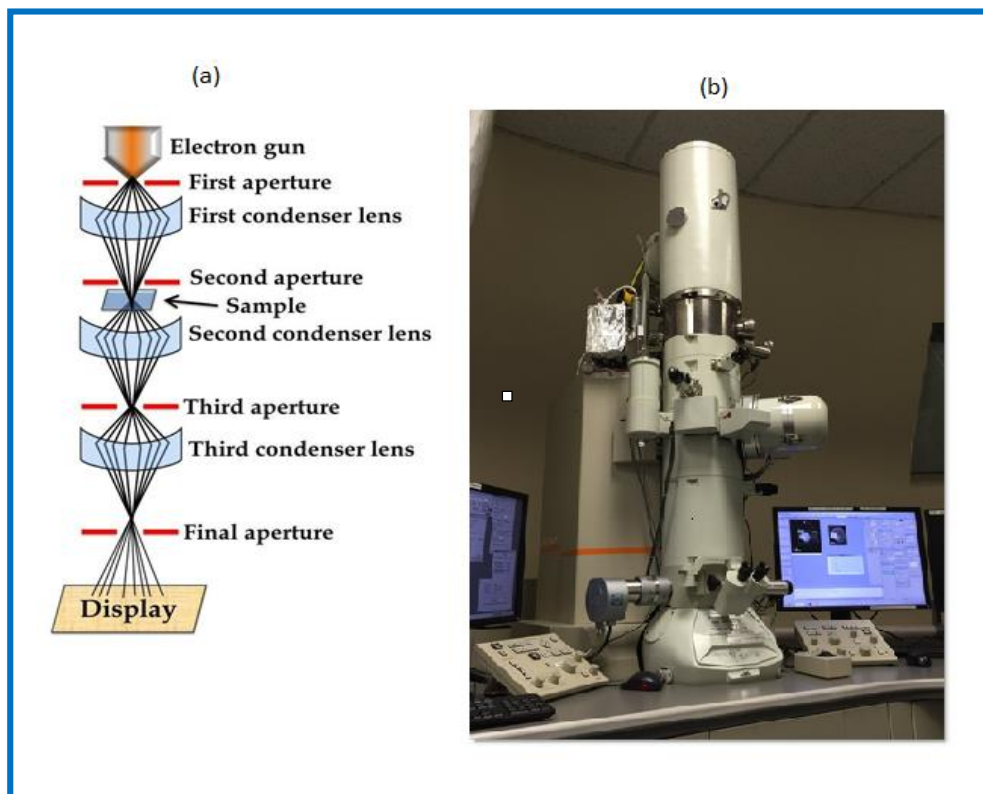


Fig.2.6 a) Schematic diagram of HR-TEM b) Photograph of HR-TEM (JEOL 2100+)

From HR-TEM, firstly the particles were dispersed well in suitable solvent, preferably water or ethanol. Now a very small amount (~5mL) of this dispersion solution was taken and placed gently on a coated copper grid. The grid was kept under ambient conditions so that the solvent evaporates and the particles get struck to the grid. The dry grid was then examined under the HRTEM (TECNAI G² – 30 U- Twin) instrument to see the size and morphology of the particles.

2.3.2 Magnetic characterization techniques

2.3.2.1 Vibrating Sample Magnetometer (VSM)

In a vibrating sample magnetometer (VSM) (Fig.2.7.a), an electromagnet is used to apply the magnetic field to the sample. Two identical but oppositely wound pickup coils are placed near the sample space. The sample is placed in between the two pick up coils and oscillated sinusoidally in a particular frequency [14]. The figure (Fig. 2.7b) shows a pictorial representation of VSM. An applied DC field magnetizes the sample and its mechanical vibration result in a change in special density of magnetic flux that links with the pickup coils and thus induces a voltage (V) according to the Faraday's law:

$$V = NA \frac{dB}{dt} \quad (2.3)$$

where, N is the number of turns in a pickup coil, A is its cross-sectional area, B is the magnetic flux density and t is the time. Now, if M be the magnetization of the sample then the change in B can be written as

$$\Delta B = \mu_0 M \quad (2.4)$$

Therefore, the signal becomes:

$$\Delta dt = -\mu_0 NAM \quad (2.5)$$

The pickup voltage is feed to the input of a lock in amplifier. The mechanical vibrator's frequency is given to the lock in as reference which estimates the magnetization of the sample. The basic principle of the measurement for the AC and DC magnetic properties is very similar. In the case of AC measurements, the applied time varying field causes an oscillating response from the sample which induce signal to the secondary coils. But here, as the applied field is DC and therefore, the sample is vibrated in order to generate a spatial and temporal oscillation of flux. However, the induced signal is proportional to the magnitude of the sample's moment, it also depends on the frequency and amplitude of the vibration. This can add an error. In order to resolve the problem, a vibrating capacitor is used to generate the reference signal which varies with the moment, vibrational frequency and amplitude of the sample in the similar way as the pickup coils' signal.

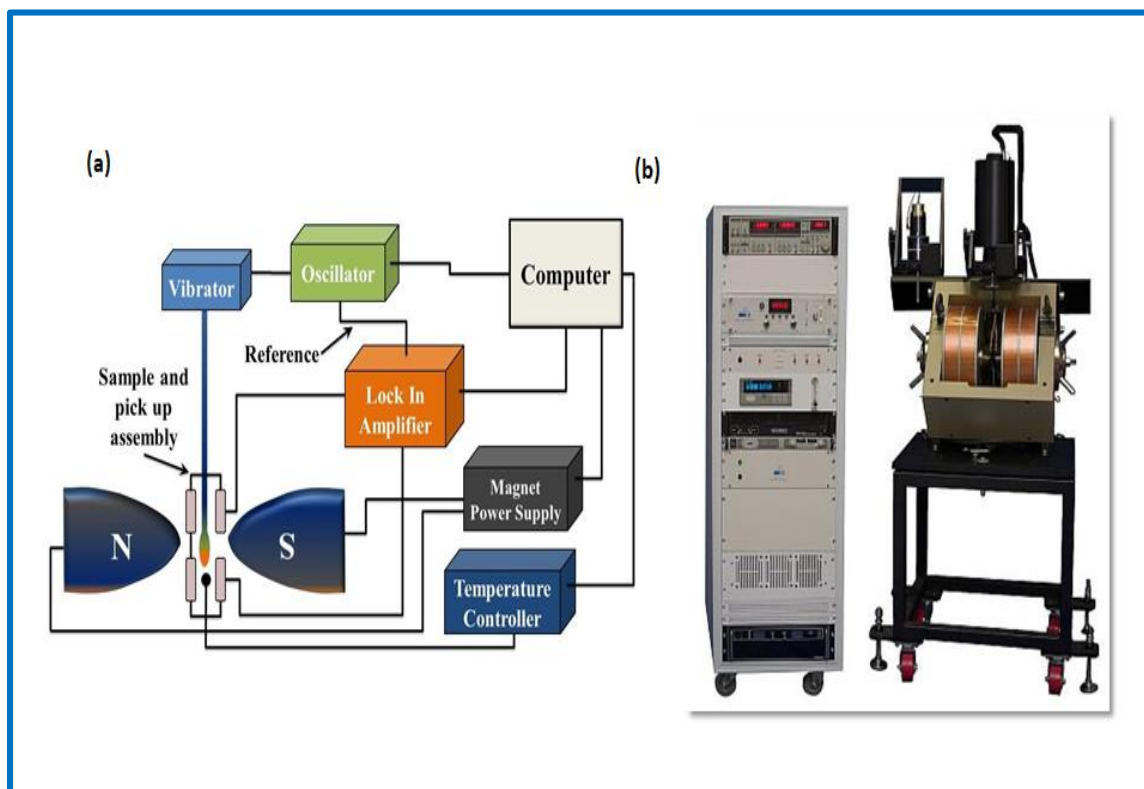


Fig.2.7 a) Block diagram of a vibrating sample magnetometer (VSM). b) Pictorial representation of VSM (Model ADE – EV9)

2.3.3 Optical characterization techniques

2.3.3.1 UV-Visible spectrometer

Ultraviolet–visible spectroscopy refers to absorption spectroscopy or reflectance spectroscopy in the ultraviolet-visible spectral region (Fig.2.8a). This means it uses light in the visible and adjacent (near-UV and near-infrared (NIR)) ranges. The absorption or reflectance in the visible range directly affects the perceived color of the chemicals involved. In this region of the electromagnetic spectrum, molecules undergo electronic transitions. This technique is complementary to fluorescence spectroscopy, in that fluorescence deals with transitions from the excited state to the ground state, while absorption measures transitions from the ground state to the excited state [15]. Molecules containing π -electrons or non-bonding electrons (n-electrons) can absorb the energy in the form of ultraviolet or visible light to excite these electrons to higher anti-bonding molecular orbitals. The more easily excited the electrons (i.e. lower energy gap between the HOMO and the LUMO), the longer the wavelength of light it can absorb.

UV-Vis spectrophotometer measures the intensity of light passing through a sample (I), and compares it to the intensity of light before it passes through the sample (I_0). The ratio I / I_0 is called the *transmittance*, and is usually expressed as a percentage (%T). The absorbance, A is based on the transmittance:

$$A = -\log (\%T/100) \quad (2.6)$$

The Beer-Lambert law states that the absorbance of a solution is directly proportional to the concentration of the absorbing species in the solution and the path length. Thus, for a fixed path length, UV/Vis spectroscopy can be used to determine the concentration of the absorbing species in the solution. It is necessary to know how quickly the absorbance changes with concentration. The wavelengths of absorption peaks can be correlated with the types of bonds in a given molecule and are valuable in determining the

functional groups within a molecule. The spectrum alone is not, however, a specific test for any given sample. The nature of the solvent, the pH of the solution, temperature, high electrolyte concentrations, and the presence of interfering substances can influence the absorption spectrum. Experimental variations such as the slit width (effective bandwidth) of the spectrophotometer will also alter the spectrum. To apply UV/Vis spectroscopy to analysis, these variables must be controlled or accounted for in order to identify the substances present. The method is most often used in a quantitative way to determine concentrations of an absorbing species in solution, using the Beer-Lambert law

$$A = \log_{10} (I_0 / I) = \epsilon cl \quad (2.7)$$

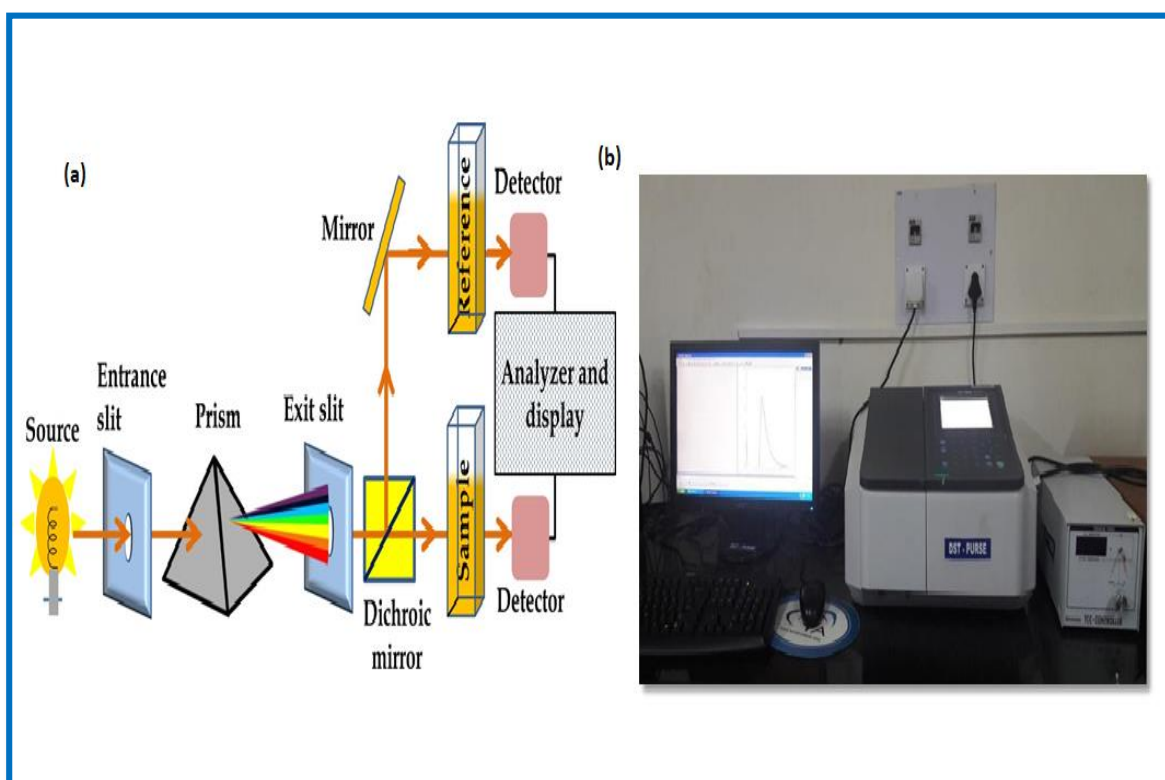


Fig.2.8 a) Schematic diagram of a UV-visible spectrometer b) Pictorial representation of a UV-visible spectrometer (Shimadzu 2600)

where, A is the measured absorbance of the sample, I_0 is the intensity of the incident light at a given wavelength, I is that for the transmitted light, l is the path length of light through

the sample, c is the concentration of the absorbing species and ε is the molar absorptivity or molar extinction coefficient that is constant for a particular absorber. The pictorial diagram of the UV-visible spectrometer is shown in figure (Fig. 2.8b). The UV-visible absorbance spectra of our samples were measured using Shimadzu UV-2600 spectrophotometer.

2.3.3.2 Fourier Transform Infrared Spectroscopy (FTIR)

FTIR is an instrument for identifying the functional groups which present in a molecule (2.9.a). It works by generating infrared absorption spectrum like a molecular fingerprint. The two beams of Michelson interferometer are the main key of the FTIR. The parallel IR beam is partly reflected and transmitted across the beam splitter and shift towards the stationary and moving mirrors, respectively. The transmitted beam from the fixed mirror and reflected beam from the moving mirror may interfere constructively or destructively at the behind of the beam splitter [16]. It mainly depends on the wavelengths of the lights and the optical path difference introduced by the moving mirror. This resulting signal is named as interferogram [17].

Finally, Fourier transformation of this interferogram is carried out to get a frequency spectrum. For the FTIR measurements, powdered samples were mixed with KBr powder and pelletized in a hydraulic press [18]. Before measurement, the background correction was done using a fresh reference KBr pellet. Fourier-Transform Infrared (FT-IR) spectroscopy (Fig.2.9.b) is an important technique in organic chemistry. It is an easy way to identify the presence of certain functional groups in a molecule. Analysis by infrared spectroscopy is based on the fact that molecules have specific frequencies of internal vibrations. These frequencies occur in the infrared region of the electromagnetic spectrum: $\sim 4000\text{ cm}^{-1}$ to $\sim 400\text{ cm}^{-1}$. When a sample is placed in a beam of infrared radiation, the sample will absorb radiation at frequencies corresponding to molecular vibrational frequencies, but will transmit all other frequencies. The frequencies of radiation absorbed

are measured by an infrared spectrometer, and the resulting plot of absorbed energy versus frequency is called infrared spectrum of the material.

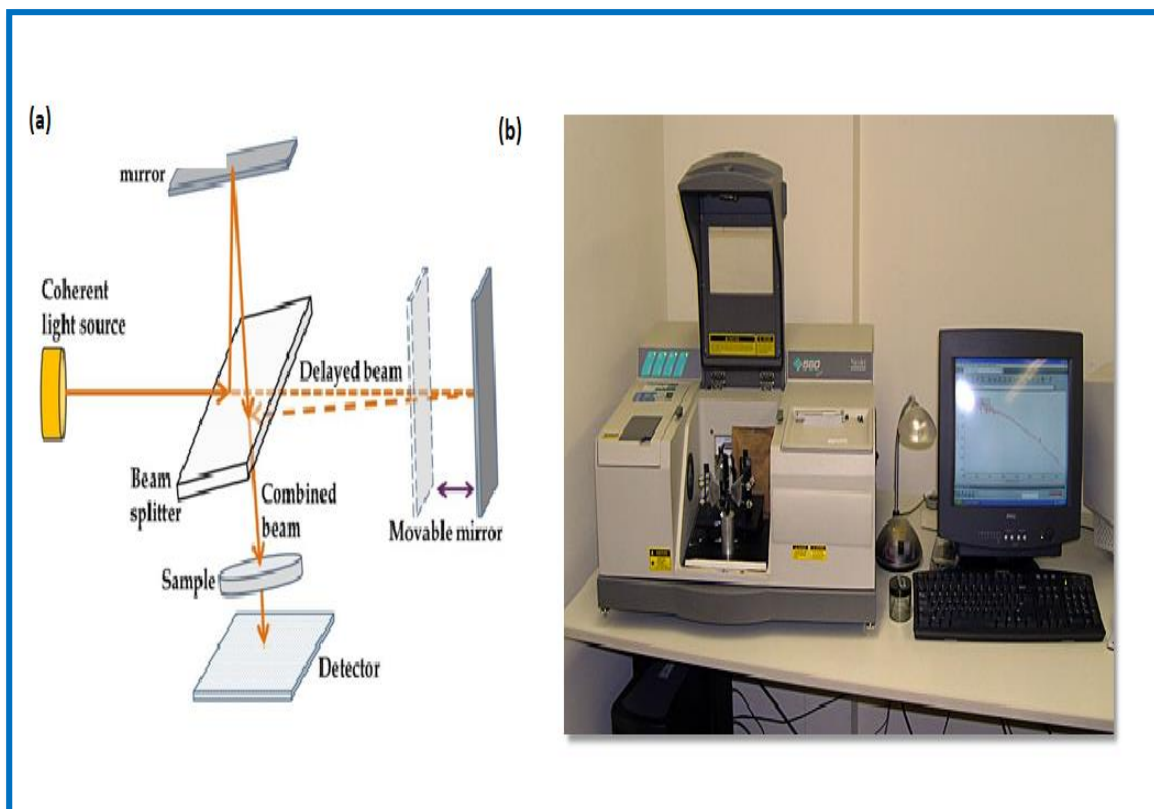


**Fig.2.9 a) Schematic diagram of Michelson Interferometer configured for FTIR
b) Pictorial representation of FT-IR (Thermo Nicolet 380)**

2.3.3.3 Dynamic Light Scattering (DLS)

Dynamic light scattering (also known as photon correlation spectroscopy or quasi-elastic light scattering) is a technique that can be used to determine the size and size distribution profile of small particles in suspension and polymers in solution [19]. In recent years, this technique (DLS) has proven to be an invaluable - analytical tool for characterizing the size distribution of particles (Fig.2.10). The useful size range for the DLS technique is quite large - from below 5 nm (0.005 micron) to several microns. DLS- based sizing instruments have been used extensively to characterize a wide range of particulate systems including synthetic polymers (e.g. latexes, PVCs etc.), oil-in-water and water-in-

oil emulsions, vesicles, micelles, biological macromolecules, pigments, dyes, Silicas, metallic sols, ceramics and numerous other colloidal suspensions and dispersions.

When light hits small particles, the light scatters in all directions (Rayleigh scattering) as long as the particles are small compared to the wavelength (below 250 nm). If the light source is a laser, and thus is monochromatic and coherent, then one observes a time-dependent fluctuation in the scattering intensity. This fluctuation is due to the fact that the small particles in solutions are undergoing Brownian motion, and the distance between the particles in the solution is constantly changing with time. The dynamic information of the particles is derived from an autocorrelation of the intensity trace recorded during the experiment [20].

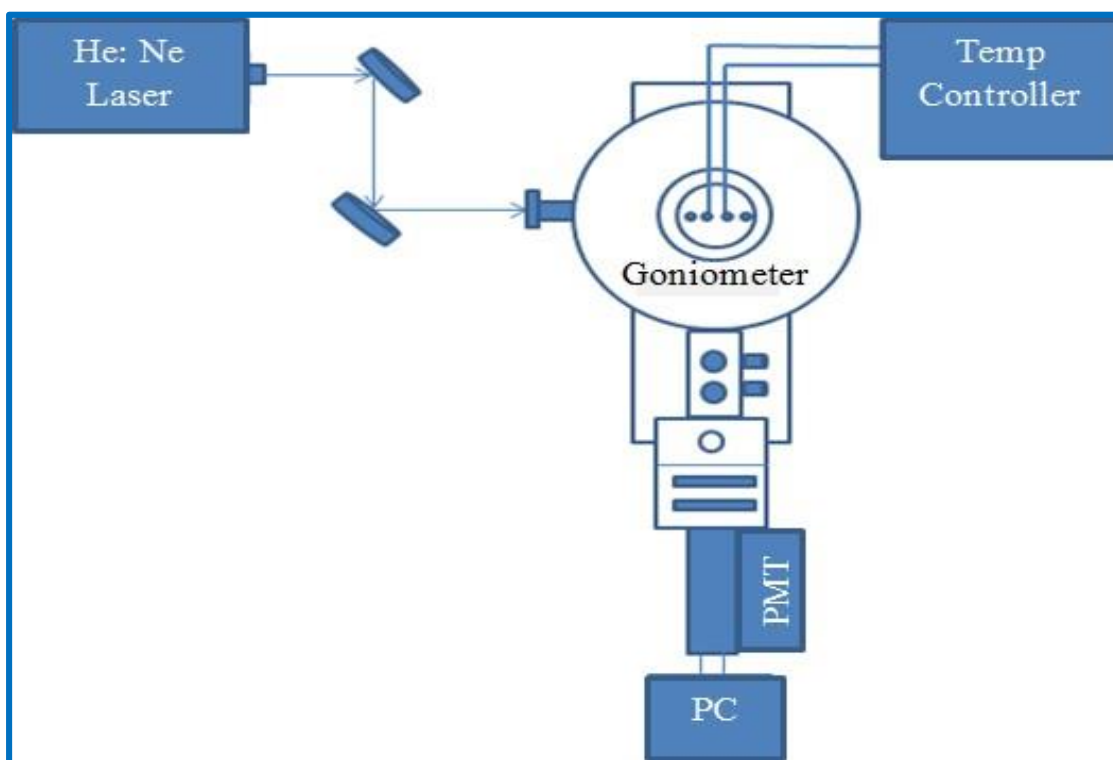


Fig.2.10 Schematic diagram of DLS

Once the autocorrelation data have been generated, different mathematical approaches are employed to determine from it. The simplest approach is to treat the first

order autocorrelation function as a single exponential decay. This is appropriate for a monodisperse population.

$$g^1(q:r) = \exp(-\Gamma\tau) \quad (2.8)$$

Where Γ is the decay rate. The translational diffusion coefficient D_t may be derived at a single angle or at a range of angles depending on the wave vector q .

$$\Gamma = q^2 D_t \quad (2.9)$$

With

$$q = \frac{4\pi n_0}{\lambda} \left(\frac{\theta}{2}\right) \quad (2.10)$$

Where λ is the incident laser wavelength, n_0 is the refractive index of the sample and θ is angle at which the detector is located with respect to the sample cell. In the absence of interparticle interaction, the hydrodynamic radius (RH) is then calculated from the diffusion coefficient using the Stokes-Einstein equation,

$$q = \frac{KT}{f} = \frac{KT}{6\pi\eta RH} \quad (2.11)$$

Where k is the Boltzmann constant, T is the temperature, η is the medium viscosity, and $f = 6\pi\eta RH$ is the frictional coefficient.

D is often used to calculate the hydrodynamic radius of a sphere through the Stokes–Einstein equation. It is important to note that the size determined by dynamic light scattering is the size of a sphere that moves in the same manner as the scatterer for example, if the scatterer is a random coil polymer, the determined size is not the same as the radius of gyration determined by static light scattering. It is also useful to point out that the obtained size will include any other molecules or solvent molecules that move with the particle. So colloidal gold, for example, with a layer of surfactant will appear larger by

dynamic light scattering (which includes the surfactant layer) than by transmission electron microscopy (which does not “see” the layer due to poor contrast).

2.4 Analysis of biological activities

2.4.1 Anti-bacterial activity assay

2.4.1.1 Disc preparation

The 6 mm (diameter) discs were made from Whatmann No. 1 filter paper. The discs were sterilized by autoclave at 121°C. After the sterilization, the moisture discs were dried on a hot air oven at 50°C. Then various solvent extract discs and control discs have prepared [21].

2.4.1.2 Collection of test bacterial species

The bacterial strains of *Bacillus subtilis*, *Escherichia coli*, *Klebsiella pneumonia* and *Staphylococcus aureus* were obtained from Microbial Type Culture Collection Centre (MTCC), Chandigarh.

2.4.1.3 Assay of antibacterial activity

The antibacterial activity test was carried out following the modification of the method originally defined by Bauer et al. (1966). Muller Hinton agar was ready and autoclaved at 15 fifteen lbs pressure for twenty minutes and cooled to 45°C. The medium was permitted to cool and poured on to sterile petri plates and left for solidification. The plates with media were seeded with their corresponding microbial suspension by utilizing a sterile swab [22]. The various solvents extract were made as discs individually set on each petri plates and also placed control and standard (Nitrofurantoin (300 µg) for Bacteria) discs. The plates were incubated at 37°C for one day. After the incubation period, the diameter of the zone formed around the paper disc was measured and expressed in mm.

2.4.2 Anti-oxidant assay

1, 1-diphenyl-2-picryl hydrazyl radical (DPPH) assay was employed for the determination of free radical scavenging activity [23]. BHT (Butyl Hydroxyl Toluene) was used as the standard. Absolute methanol is used as the blank. 100 μ l of different concentration of the samples were taken in separate test tubes containing 3.7ml of absolute methanol. 200 μ l of DPPH reagent was added to all the test tubes including blank [24]. The reaction mixture was incubated at room temperature under dark conditions for 30 minutes. The absorbance of the reaction mixture was recorded at 517nm using an UV-Visible spectrophotometer [25]. The same procedure was done for the standard BHT and its absorbance was also measured.

$$\text{Scavenging behavior (\%)} = 100 - [(A_c - A_s) / A_c] \times 100 \quad (2.12)$$

Where A_c = Control absorbance, A_s = Sample absorbance.

2.4.3 Anti-inflammatory activity

The anti-inflammatory assay was investigated by the method stated and followed as in the previous report [26]. At first, 2.8 mL of phosphate-buffered saline (PBS) (pH 6.4) and 0.2 mL of bovine serum albumin were taken and mixed with prepared NPs sample solution of 2 mL in varied concentration, viz. 100, 200, 300, 400 and 500 μ g/mL. After that, the reaction mixture solution was incubated at 37 ± 2 °C. The procedure was completed in 15 min, and after completing it, it was heated to 70 °C. The solution was allowed to attain room temperature, and then, the absorbance was recorded from a UV-visible spectrophotometer. Similarly, positive control diclofenac sodium was treated. The assay was performed in triplicates

$$\text{Anti-inflammatory assay (\%)} = 100 - [(V_c - V_t) / V_c] \times 100 \quad (2.13)$$

Where, V_t = Sample absorbance, V_c = Control absorbance.

2.4.4 Anti-diabetic assay

The anti-diabetic assay was investigated by the method as stated in the earlier report [27]. At first, 0.5 mg/mL of α -Amylase was maintained at 25 °C for 10 min. The prepared NPs solution of 2 mL was taken in varied concentrations, viz. 100, 200, 300, 400 and 500 μ g/ mL, and was added to the starch solution. 20 mM of sodium phosphate (pH 6.9) and 6 mM of sodium chloride were also added to the sample solution, and then, it was mixed with the α -Amylase solution. The reaction mixture solution was maintained at 25 °C for 30 min. In this solution, di-nitrosalicylic acid was blended to view the color change. Further, the reaction mixture solution was heated to 70 °C for 5 min. Then, the absorbance was recorded from a UV–visible spectrophotometer to calculate the percentage of inhibition. Similarly, positive control acarbose was treated. The assay was performed thrice.

$$\text{Anti-diabetic assay (\%)} = 100 - \left[\frac{V_c - V_t}{V_c} \right] \times 100 \quad (2.14)$$

Where, V_c = Control absorbance, and V_t = Sample absorbance.

References

- [1] A. Gendaken, *Curr. Sci.*, 85(12), (2003)1720-1722.
- [2] A.S. Howard, R.H. William, Wiley Interscience, 1973.
- [3] P. Heera, S. Shanmugam, *Int. J. Curr. Microbiol. App. Sci.* 4(8), (2015) 379-386.
- [4] M. Shah, D. Fawcett, S. Sharma, S.K. Tripathy, G.E.J. Poinern, *Mater.* , 8(11), (2015) 7278-7308.
- [5] A.D. Dwivedi, K. Gopal, *Colloids Surf. A: Physicochem. Eng. Asp.* 369(1-3), (2010) 27-33.
- [6] J. H. Bang, K. S Suslick, *Adv. Mater.*, 22(10), (2010)1039-1059.
- [7] I. Hussain, N.B. Singh, A. Singh, H. Singh, S.C. Singh, *Biotechnol. Lett.* 38(4), (2016) 545-560.
- [8] Y.K. Rao, G. Vimalamma, C.V. Rao, and Y.M. Tzeng, *Phytochemistry*, 65(16), (2004) 2317-2321.
- [9] T.J.I. Edison, M.G. Sethuraman, *Process Biochem*, 47(9), (2012) 1351-1357.
- [10] R.F. Egerton, *Physical principles of electron microscopy: an introduction to TEM, SEM, and AFM.* Springer: New York, 2005.
- [11] R.E. Lee, *Scanning Electron Microscopy and X-ray Microanalysis.* PTR Prentice Hall: Englewood Cliffs, New Jersey, 1993.
- [12] R.F. Egerton, *Physical principles of electron microscopy: an introduction to TEM, SEM, and AFM.* Springer: New York, 2005.
- [13] J.H. Spence, *High-Resolution Electron Microscopy.* 4th edition; Oxford press, 1980.
- [14] A. Mishra, R. Ahmad, M. Sardar, *J. Nanosci. Nanotechnol.*, 5(1), (2015) 37-42.
- [15] K.L. Kelly, E. Coronado, L.L. Zhao, G.C. Schatz, *J. Phys. Chem. B*, 107(3), (2003) 668-677.
- [16] K. Krishnan, S.L. Hill, J.R. Ferraro, *FT-IR microsampling techniques*, *Calif.* (1990)103-165.
- [17] L.El Fels, M. Zamama, M. Hafidi, *InTech*, (2015) 127-144.
- [18] <https://www.newport.com/n/introduction-to-ftir-spectroscopy>.

- [19] K.S.W. Sing, Particle Size Analysis, R. Soc. Chem., (1992)13-32.
- [20] B.J. Berne, R. Pecora, Dynamic light scattering: with applications to chemistry, biology, and physics. Courier Corporation, 2000.
- [21] S. Prabhu, E.K. Poullose, Int. Nano Lett. 2(1), (2012) 1-10.
- [22] M.M. Almoudi, A.S. Hussein, M.I.A. Hassan, N.M. Zain, The Saudi dental journal, 30(4), (2018) 283-291.
- [23] A.A. Bunaciu, A.F. Danet, Ş. Fleschin, H.Y. Aboul-Enein, Crit Rev Anal Chem, 46 (5) (2016) 389-399.
- [24] A.M. Pisoschi, G.P. Negulescu, Anal. Biochem, 1(1), (2011)106.
- [25] S. Sanpa, K. Sutjarittangtham, T. Tunkasiri, S. Eitssayeam, P. Chantawannakul, J. Adv. Mater. Res, 506, (2012) 371-374.
- [26] R. de Cássia da Silveira e Sá, L.N. Andrade, D.P. de Sousa, Molecules, 18(1), (2013)1227-1254.
- [27] A. Alkaladi, A.M. Abdelazim, M. Afifi, Int. J. Mol. Sci., 15(2), (2014) 2015-2023.

Green Synthesis of Magnetic Nanoparticles via *Cinnamomum verum* Bark Extract for Biological Application

Abstract

The green synthesis of magnetic Fe nanoparticles (NPs) was prepared via *Cinnamomum verum* bark extract. The UV-visible analysis explained the formation of Fe NPs with SPR band at 288 nm. The powder X-ray diffraction analysis (XRD) explicated the mean crystallite size was at 36 nm. The fourier transform infra-red analysis (FTIR) revealed the functional groups in the prepared FeNPs. The scanning electron microscope (SEM) and high resolution transmission electron microscope (HR-TEM) analyses notified the circular and spherical shaped FeNPs with the size at 20-50 nm. The energy dispersive X-ray spectroscopy (EDS) and mapping analyses validated the formation of FeNPs with purity. The vibrating sample magnetometer (VSM) revealed the paramagnetic behavior of prepared FeNPs. The phytochemical analysis described the phytochemicals compounds which present in *Cinnamomum verum* bark extract. The antibacterial assay described the much higher inhibition zone of prepared FeNPs upon human pathogenic bacteria. The Antioxidant (DPPH) assay described the efficient scavenging behavior of Fe NPs with 89 % at 80 µg/mL concentration. The anti-inflammatory assay explicated the potential protein denaturation behavior of Fe NPs with 87 % at 500 µg/mL concentration. The anti-diabetic assay reported the much higher potential efficiency of prepared Fe NPs with 84 % at 500 µg/mL concentration.

3.1 Introduction

In recent decades, nanotechnology has gained more recognition due to its unique properties associated with the size distribution and morphology of nanoparticles.

Nanotechnology was an umbrella term that covers many research areas dealing with objects that are covered in nanometers such as chemistry, physics, biology, engineering and other scientific aspects of nanotechnology [1, 2]. Nanoparticles having 1 to 100 nm possess great impact in the field of chemistry, optics, batteries, physics, environmental remediation, drug delivery and medicine. Nanoparticles exhibit enormous structures which create a different approach in catalytic, physical, chemical and medicinal properties of materials than bulk [3-5]. Nowadays, the researchers concentrate on the metal nanoparticles due to the large surface area, low melting point, and good optical, catalytic, electrical and thermal properties. These distinctive properties of metal nanoparticles create exploitation in the industrial area such as food, agriculture, space, cosmetics, medical and chemical aspects of use in day-to-day life [6-9].

Recent research in the synthesis of nanoparticles opened a new era in the fast-growing method for the production of nanoparticles. Physical and chemical methods were usually used for the synthesis of nanoparticles, however, based on the toxicity of these methods; the objective of the research has latterly moved towards the biosynthetic method [10-12]. Nanoparticles of magnetic materials have attracted much consideration due to their properties deviate from those of bulk materials and they can be used to make materials and devices with new properties [1]. Magnetic nanoparticles have important applications in magnetic storage devices, in ferrofluids, i.e. stable suspensions of magnetic nanoparticles, in magnetic beads that are applied in biotechnology, for contrast enhancement in magnetic resonance imaging (MRI), and targeted drug delivery, bioelectrochemical sensing, environmental remediation and as an electrode for supercapacitors and lithium-ion batteries [2]. The magnetic nanoparticles received from the green synthesis method using plants applied in many fields such as semiconductors [13], catalysts [14], optics, chemistry [15] and medicine [16].

Metal nanoparticles can be synthesized by adopting several methods such as physical, chemical or photochemical reactions, thermal decomposition, electrochemical and sonication. However, most of the methods are related to certain disadvantages such as using hazardous chemicals and high energy requirements which extended the environmental toxicity and cost ineffectiveness [17-20]. The biosynthetic method has recognized as an environment-friendly, low-cost, and safer alternative to chemical and physical methods. Nanoparticles can be synthesized from a variety of biological entities such as actinomycetes, algae, bacteria, fungi, plants, viruses, and yeast. Mainly, Fe nanoparticles were used in industrial sites. More focusly, iron nanoparticles used in textile industry [21], plastic industry [22] with nanowire and nanofibre structure for coatings. In medical field, Fe nanoparticles are used in tissue repair, drug delivery and detoxification of biological fluids, hyperthermia, and immunoassay in cell separation. Iron nanoparticles contribution extended in sunscreen products [23], leather industry [24] and food industry [25]. The antibacterial effect of Fe nanoparticles creates distinctive position for it among other metal nanoparticles. The magnetic property of Fe nanoparticles exhibited a specific approach in drug delivery on targeted cancer cells [26-30]. Plants are particularly assuring for bioreduction since they are easily available, inexpensive and scalable [31-33]. Plant extracts containing bioactive alkaloids, phenolic acids, polyphenols, proteins, sugars, and terpenoids which can reduce the metal ions and then stabilizing them.

Medicinal plants are of most importance in traditional medicine, in which in most part, the antioxidant activity of the plant-derived compounds deemed responsible for curing numerous diseases. *Cinnamomum verum* consists of many polyphenolic compounds with antioxidant activity. The purpose of this research was to reduce iron III chlorides to iron nanoparticles by biosynthesis method using *Cinnamomum verum* extracts which contain phenolic compounds that act as reducing and capping agents. *Cinnamomum verum* plant was used as a spice to flavor cooking, stewed fruit, and tea. Traditionally, it was used as one

of the Ayurvedic medicinal herbs in Asia. It required warm climate. *Cinnamomum verum* was native to Sri Lanka and favors free-draining soils in a humid position. *Cinnamomum verum* was rich in polyphenols and its biomolecules act as reducing and capping agents during the synthesis of iron nanoparticles. *Cinnamomum verum* was a spice that has ancient origins and popularly used as flavorings, condiment in cooking. *Cinnamomum verum* was also known to provide various medicinal benefits that include lowering of blood cholesterol, for diabetes. *Cinnamomum verum* was widely believed to be high in anti-oxidants. Regular drinking of *Cinnamomum verum* tea could be beneficial to oxidative stress-related illness in humans. *Cinnamomum verum* barks received from the *Cinnamomum verum* tree. It has a polyphenolic compound which diminished the iron chloride to iron nanoparticles [34,35].

There are many plants based reports to synthesize silver and gold nanoparticles. A few pieces of literature were available on the biosynthesis of metals like iron and palladium. The present study of biosynthesized nanoparticles was the first report which narrated the synthesis of iron nanoparticles using *Cinnamomum verum* extracts. Comparing with recent literatures, we prepared iron nanoparticles with cost effectiveness and high antibacterial effect. The phytochemicals in *Cinnamomum verum* bark extract provide much higher rapid capping and stabilizing action for Fe nanoparticles. Therefore, the present work was carried out to synthesize and characterize the iron nanoparticles using *Cinnamomum verum* extract.

3.2 Experimental Section

3.2.1 Chemicals

Ferric III chloride (FeCl_3) ($\geq 98.97\%$), ethanol ($\text{C}_2\text{H}_5\text{OH}$) ($\geq 98.02\%$), acetone ($\text{C}_3\text{H}_6\text{O}$) ($\geq 99.20\%$) and Deionized water ($\geq 99.58\%$) were obtained from Sigma-Aldrich chemicals. All glass wares was cleaned with distilled water and acetone as well as dried well before use. The raw *Cinnamomum verum* barks were used.

3.2.2 Preparation of *Cinnamomum verum* bark extract

The barks of *Cinnamomum verum* were purified with deionized water for three times for eliminating mud and dust. After, it was dehydrated at room temperature for three weeks. 5 g of *Cinnamomum verum* strands put in 100 mL of distilled water and the solution heated up to 70°C for 20 min in a heater mantel under reflux. This mixture put in undisturbed condition to attain room temperature and then it was filtered through a Whatmann No.1 paper. The extract solution was stored at 4°C for further use.

3.2.3 Synthesis of iron nanoparticles

0.01M of FeCl₃ solution and *Cinnamomum verum* bark extract was taken as precursor in 1:1 proportion for synthesizing iron nanoparticles. In the 0.01M of FeCl₃ solution, the extract solution was added in dropwise by a burette. The reaction mixture solution was converted into black color instantly. It was indicated the formation of iron nanoparticles, which absorb radiation in the visible region. After 24 h, the reaction mixture was centrifuged at 10000 rpm for 15 min. The resultant black pellet was purified with deionized water and ethanol. Then, it was dehydrated at 60°C in a hot air oven for removing residual impurities and moisture. The attained black powder of iron nanoparticles was deposited in a dried dark place for further analyses.

3.2.4 Characterization of iron nanoparticles

The synthesized iron NPs characterized with the help of a UV-Vis Spectrophotometer. X-ray powder diffraction (XRD) data was taken with a Ni filter and Cu K α radiation ($\lambda=0.15406$ nm), on the PANalytical X'pert PRO powder X-Ray diffractometer. The FTIR spectra of extracts were taken before and after synthesis of iron NPs by using Thermo Nicolet 380 FTIR spectrometer in attenuated total reflection mode and using a spectral range of 4000-400 cm⁻¹. To identify the average particle size and morphology of iron NPs, SEM and HR-TEM analyses have performed using CARL ZEISS,

EVO 18 SEM machine and JEOL-2100+ High-Resolution Transmission Electron Microscope. The presence of the elemental composition of magnetic NPs was determined employing EDX analysis. The magnetic measurements were taken utilizing vibrating sample magnetometer (VSM) at room temperature with a magnetic field up to 2.2 Tesla using Microsense, Model ADE – EV9.

3.2.5 Biological activities

3.2.5.1 Antibacterial assay

Disc preparation

The 6 mm (diameter) discs were made from Whatmann No. 1 filter paper. The discs were sterilized by autoclave at 121°C. After the sterilization, the moisture discs were dried on a hot air oven at 50°C. Then various solvent extract discs and control discs have prepared [36].

Collection of test bacterial Species

The bacterial strains of *Bacillus subtilis*, *Escherichia coli*, *Klebsiella pneumonia* and *Staphylococcus aureus* were obtained from Microbial Type Culture Collection Centre (MTCC), Chandigarh.

Assay of antibacterial activity

The antibacterial activity test was carried out the following modification of the method originally defined by Bauer *et al.*, (1966). Muller Hinton agar was ready and autoclaved at 15 fifteen lbs pressure for twenty minutes and cooled to 45°C. The medium was permitted to cool and poured on to sterile Petri plates and left for solidification. The plates with media were seeded with their corresponding microbial suspension by utilizing a sterile swab. The various solvents extract were made as discs individually set on each petri plates and also placed control and standard (*Nitrofurantoin* (300 µg) for Bacteria) discs. The

plates were incubated at 37°C for one day. After the incubation period, the diameter of the zone formed around the paper disc was measured and expressed in mm [36].

3.2.5.2 Antioxidant assay

Aliquot of DPPH methanol solution (2 ml) was added with a sample solution in various concentrations. For a few min, this solution was stirred. After this, it was allowed to stand in dark at room temperature for 30min. After, the inhibition percentage was viewed with the help of spectrophotometer [37]. The inhibition percentage by,

$$\text{Scavenging behavior (\%)} = 100 - [(A_c - A_s) / A_c] \times 100 \quad (3.1)$$

Where A_c = Control absorbance, A_s = Sample absorbance.

3.2.5.3 Anti-inflammatory assay

0.2 ml of *egg albumin*, 2.8 ml phosphate-buffered saline at pH 6.4 and 2 ml of analyzed sample with different concentrations were mixed. Then, this solution was put in an incubator at $37 \pm 2^\circ\text{C}$ for 15 min. After, the reaction mixture was dehydrated at 70°C for 5 min. After, the inhibition percentage was viewed with the help of spectrophotometer [37]. The inhibition percentage by,

$$\text{Inhibition \%} = 100 - [\{V_c - V_t\} / V_c] \times 100 \quad (3.2)$$

Where, V_t = Sample absorbance, V_c = Control absorbance.

3.2.5.4 Anti-diabetic assay

For 10 min, 0.5 mg/ml of α -amylase was placed at 25°C . After, it was mixed with the starch solution, 20 mM of sodium phosphate buffer at pH 6.9 and 6mM of sodium chloride. Then, this solution was placed at 25°C for 30 min. For 5min, the medium was dehydrated at 70°C . After, the inhibition percentage was viewed with the help of spectrophotometer [37]. The inhibition percentage by,

$$\text{Inhibition \%} = 100 - [\{V_c - V_t\} / V_c] \times 100 \quad (3.3)$$

Where, V_t = Sample absorbance, V_c = Control absorbance.

3.3 Results and Discussion

3.3.1 UV-Vis spectroscopy analysis

The UV-Vis spectrum of synthesized iron NPs showed (Fig.3.1) a maximum absorbance at about 288nm which may be assigned to the surface plasmon absorption of iron NPs [35]. The peak at 220 nm in UV-Vis spectra for the extract assigned to $\pi \rightarrow \pi^*$ or $n \leftarrow \pi^*$ transitions confined in the polyphenolic compounds. After the addition of the FeCl_3 solution to an aqueous *Cinnamomum verum* extract, the brown color solution was transferred into black color which intimated the form of Fe^0 from Fe^+ [20].

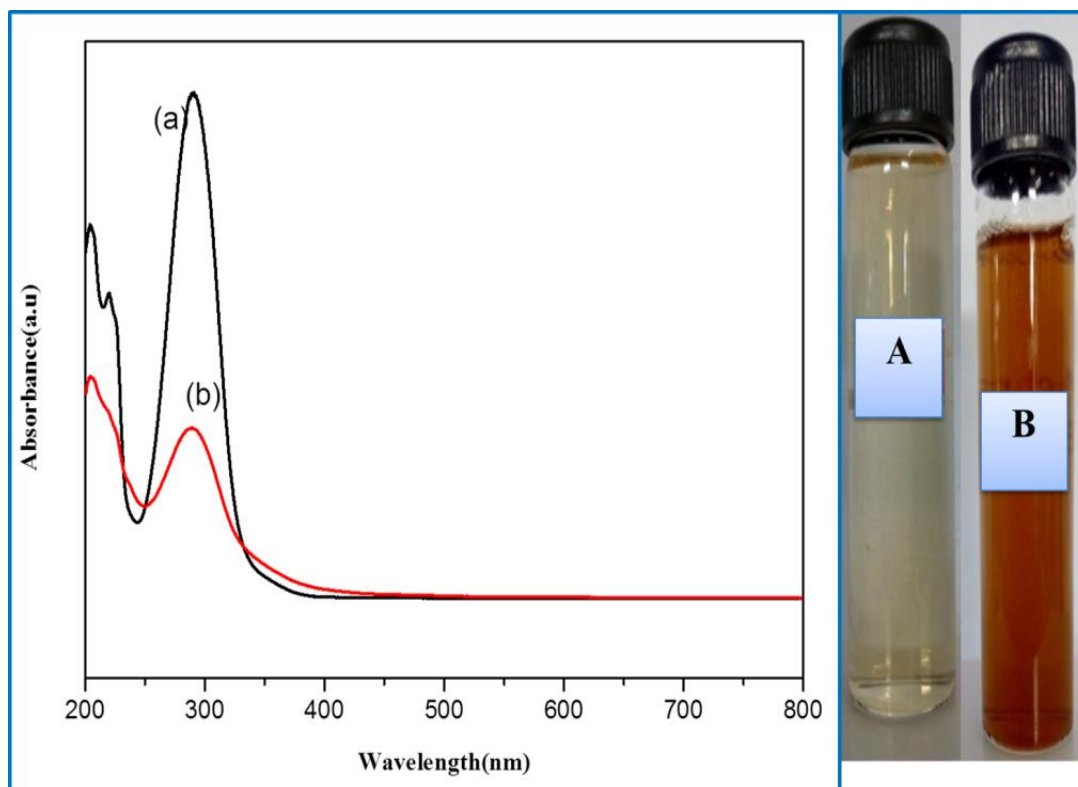


Fig. 3.1 UV spectra of a) Extract and b) Synthesized iron NPs

3.3.2 XRD analysis

The structure and formation of iron NPs was further supported by X-ray diffraction (XRD) analysis. The sample was scanned from 5° to $80^\circ 2\theta$ at a scanning rate of $3^\circ 2\theta$ per minute. It was observed that the pattern has deficient in distinctive diffraction peaks and

suggested that iron NPs exist in amorphous. The reflections in the figure (Fig.3.2) realized the elemental iron (Fe). The characteristics peak at 32.23° corresponded to iron NPs, (JCPDS no.89-7047) [20]. In the XRD pattern of iron NPs, another peak appeared at $2\theta = 22^\circ$ which could be enclosed to organic materials adsorbed from extract as a capping or stabilizing agent [19,20]. The average crystallite size determined with Schererr's formula was at 36 nm. This pattern coincides with a similar type of XRD pattern for iron NPs synthesized using T. Chebula extract [20].

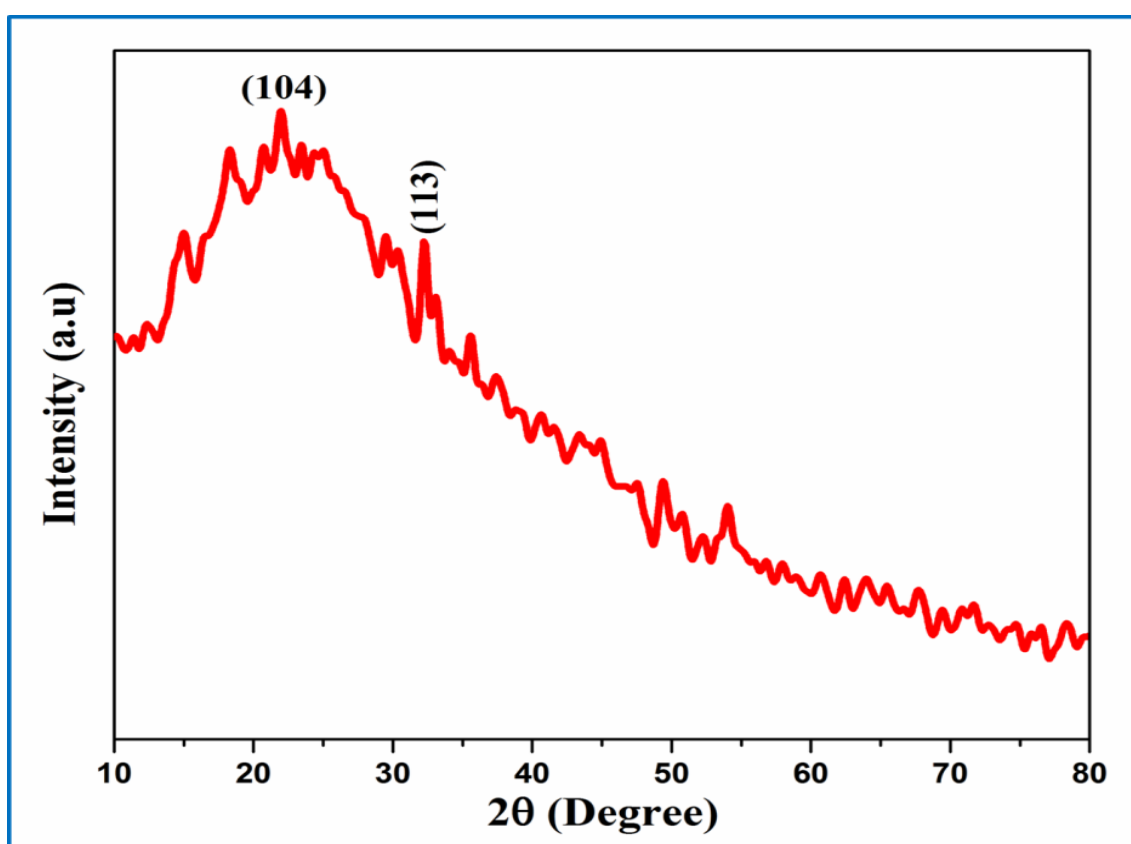


Fig. 3.2 XRD pattern of FeNPs synthesized using *Cinnamomum verum* extract

3.3.3 FTIR analysis

The FTIR of synthesized iron NPs was carried out to demonstrate the presence of polyphenols as antioxidant sources for green synthesis of iron NPs. The FT-IR spectrum of *Cinnamomum verum* (Fig.3.3) revealed the peaks at 3428 cm^{-1} , 2924 cm^{-1} and 1026 cm^{-1} which was related to C-H and C-OH stretching vibrations due to hydroxyl groups [38]. The

strong absorption band at 1618cm^{-1} was due to C=O stretching of the carbonyl group and the peak at about 1442cm^{-1} which intimated C=C stretching vibrations because of aromatic hydrocarbon groups. The FT-IR of synthesized iron NPs by *Cinnamomum verum* peaks which were slightly modified from the FT-IR spectrum of *Cinnamomum verum* extract. This observation confirmed that the organic compounds in the extract which absorbed on the surface of magnetic NPs by π -electrons interaction. Hence, the constituents of extract not only act as reducing agents but also played the role of capping agents for the stabilization on the surface of prepared iron NPs [39].

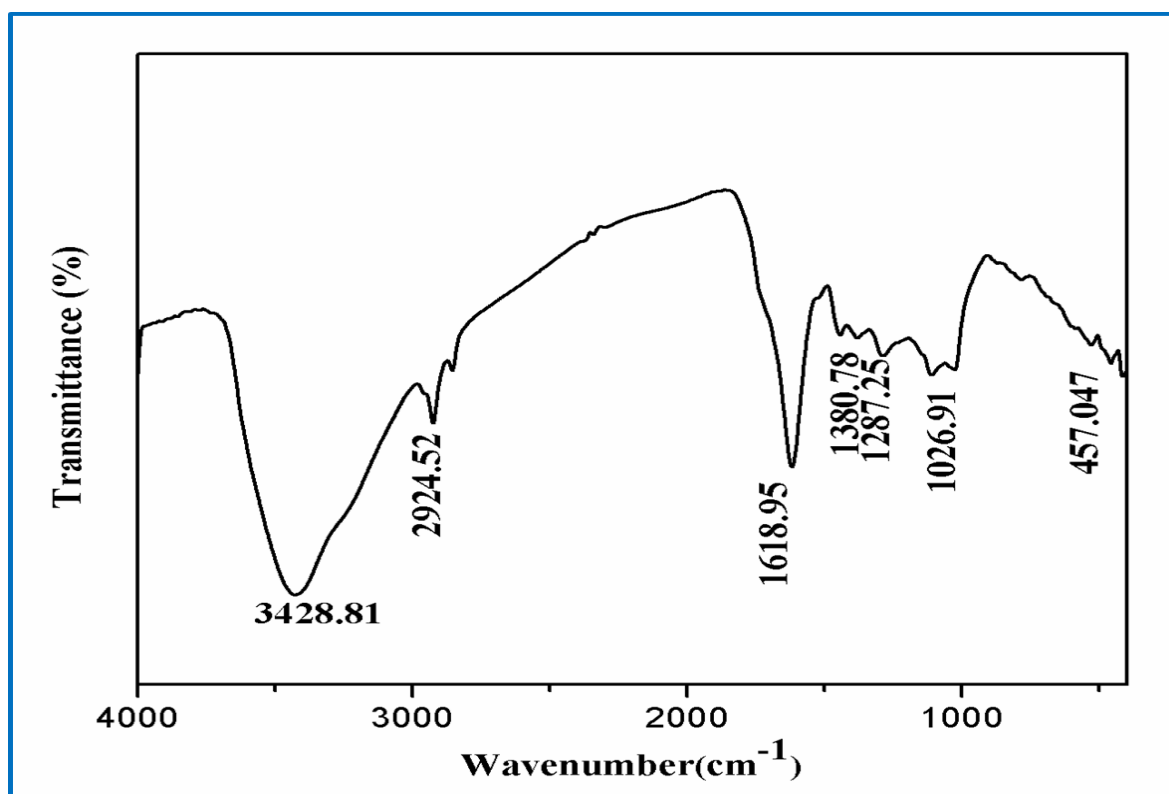


Fig. 3.3 FT-IR spectrum of FeNPs synthesized using *Cinnamomum verum* extract

3.3.4 SEM and EDS analysis

The SEM images (Fig.3.4) of iron NPs exposed that the synthesis of nano-sized particles. It has simply revealed that the particles varied from 20 to 80 nm with spherical morphology. It was varied from those iron NPs synthesized using chemicals as reducing

agents, which tend to have a more homogeneous size distribution [40]. The different shapes of NPs lead to the different distinctive applications [39]. The spherical shaped NPs were mainly contributing its efficient application in biomedical field. The hexagonal and rectangular shaped NPs contributed its tendency mainly in biomedical imaging application [39]. The circular shaped NPs contributed its potential in electrical, optical and biomedical applications [37]. It was most surely since the *Cinnamomum verum* extract was a combination of various naturally occurred compounds with different reducing properties [41]. Polyphenols or antioxidants in the *Cinnamomum verum* bark played an indispensable role in controlling the agglomeration of the NPs and developed their dispersion by operating as a capping agent [42]. To furthermore understanding the elements in the synthesized NPs, the elemental composition of biosynthesized NPs was determined with EDS analysis which was given in figure 3.5. From that, a strong intense peak of C, O, and Fe in the spectrum was observed.

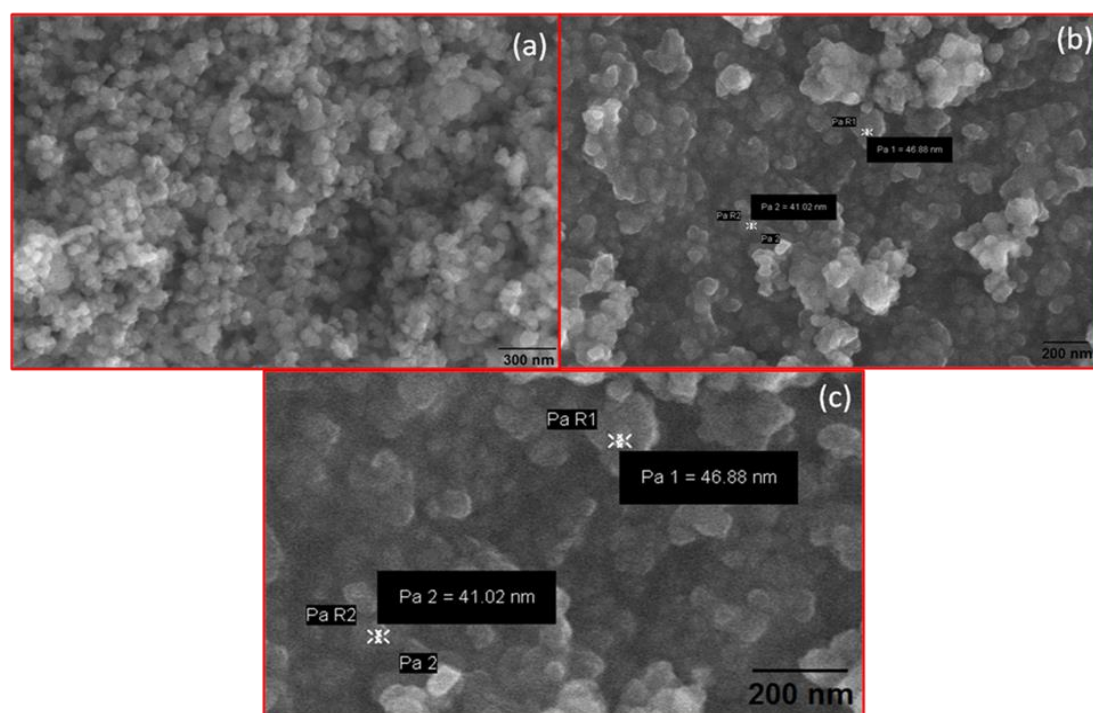


Fig. 3.4 SEM images of synthesized iron NPs using *Cinnamomum verum* extract at 300 nm, and 200 nm magnification

This spectrum established the existence of Fe in nanoparticles. The C and O peaks were attributed mainly to the polyphenol groups and other C, O-containing molecules in the *Cinnamomum verum* [43, 44]. The weight percentage of molecules present in FeNPs was registered in the table (table.3.1). This weight percentage was 27 % weight of O, 71% weight of C and 2% weight of Fe. The EDS spectrum could further be signified with EDS mapping. EDS mapping designed in different colors (Green, yellow and Red) showed the oxygen, carbon and iron elements in the FeNPs which bestowed in figure (Fig.3.6). Fe was originated from FeCl_3 as a precursor in the synthesis of iron NPs. O_2 may be from high flavonoids content in *Cinnamomum verum* extract. The mentioned values would be useful in atomic content on the surface regions of iron NPs [45, 46].

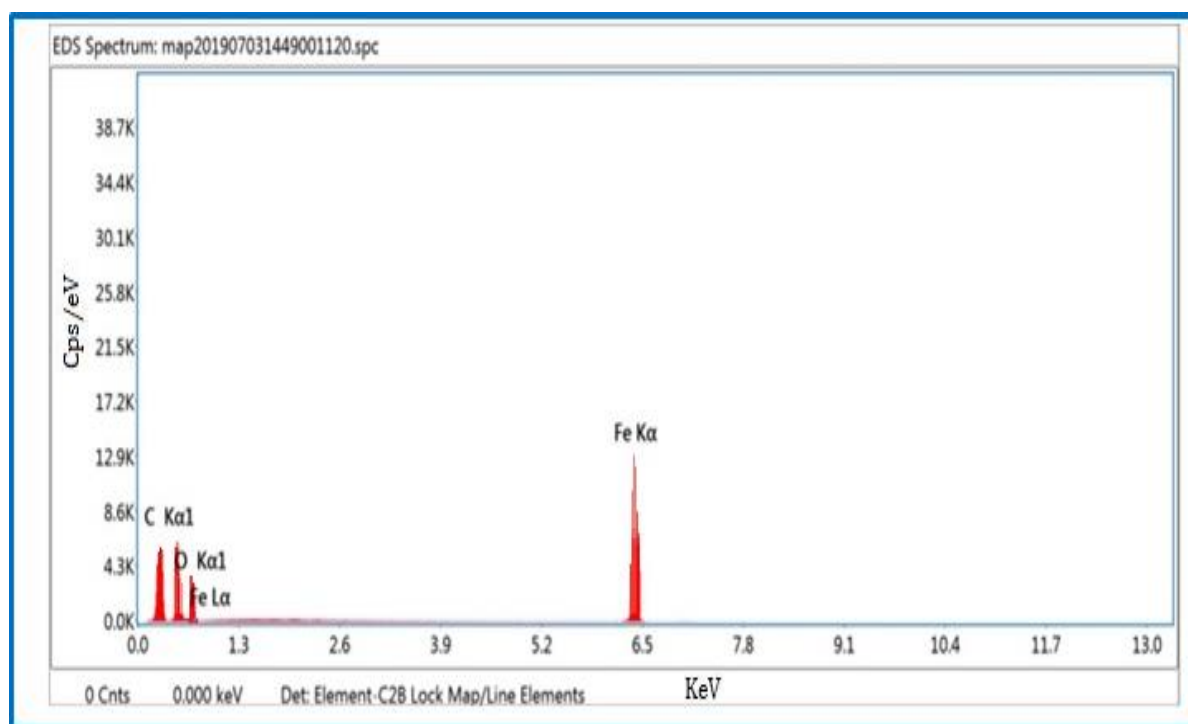


Fig. 3.5 EDS Spectrum of synthesized iron NPs using *Cinnamomum verum* extract

Table 3.1 Elemental composition of synthesized iron NPs using *Cinnamomum verum* extract

Elements	Weight (%)
C K	3
O K	3
Fe K	94

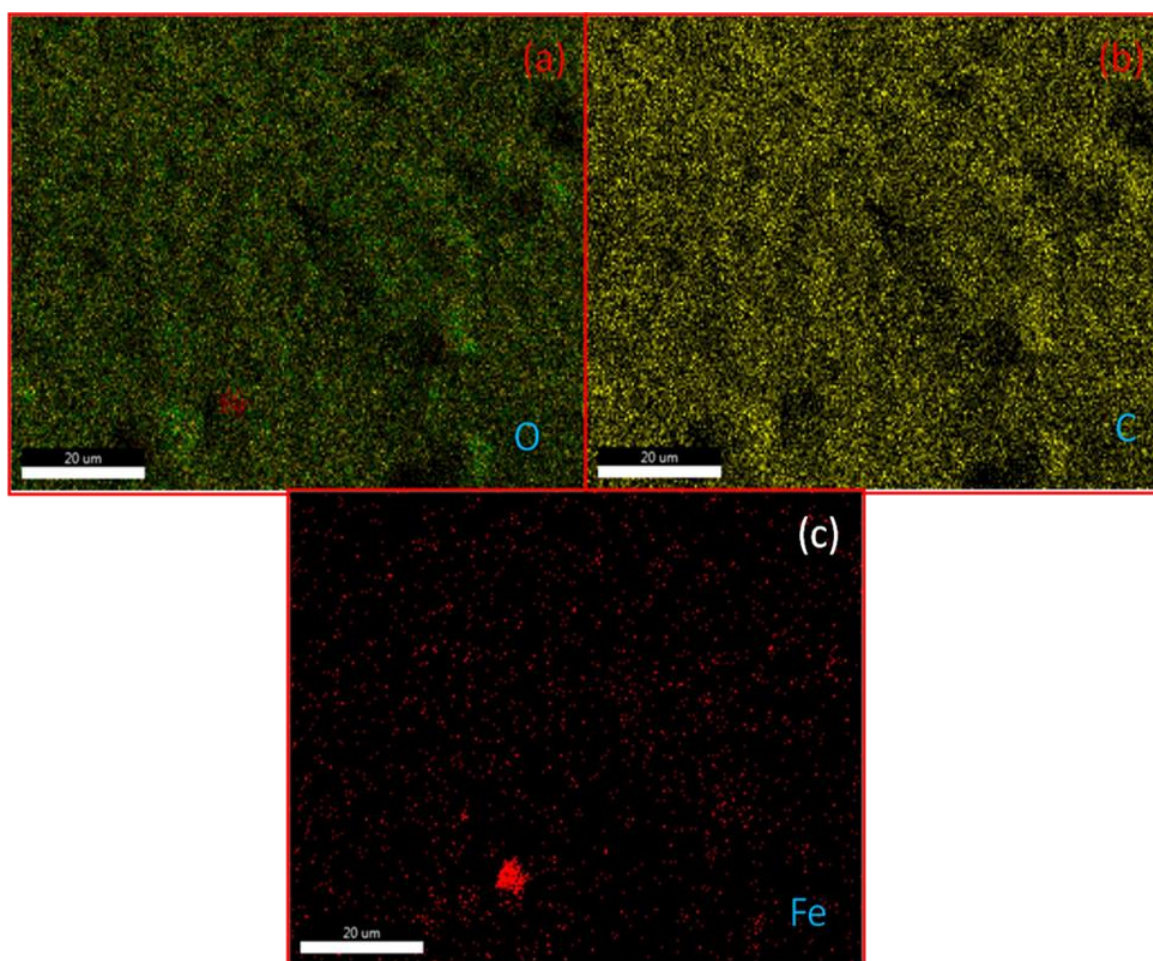


Fig. 3.6 Mapping of a) Oxygen b) Carbon c) Fe elements in synthesized iron NPs using *Cinnamomum verum* extract at 20 μm magnification

3.3.5 HR-TEM analysis

The HR-TEM analysis (Fig.3.7) of prepared Fe NPs explicated the circular, spherical shaped NPs with size at 20 to 50nm. The large agglomeration of NPs was eliminated by extract usage in synthesis. Some agglomeration of NPs was viewed with the high surface energy of Fe NPs. Further, it was reasoned by the Fe NPs synthesis was carried out in water medium. The hydrophilic and hydrophobic behavior of prepared Fe NPs was understood by the black and white regions viewed in the images. The viewed fringes denoted the regular arrangement of lattice planes in prepared Fe NPs [37, 39]. The fringes and SAED pattern was merged with the XRD d-spacings of (113) plane.

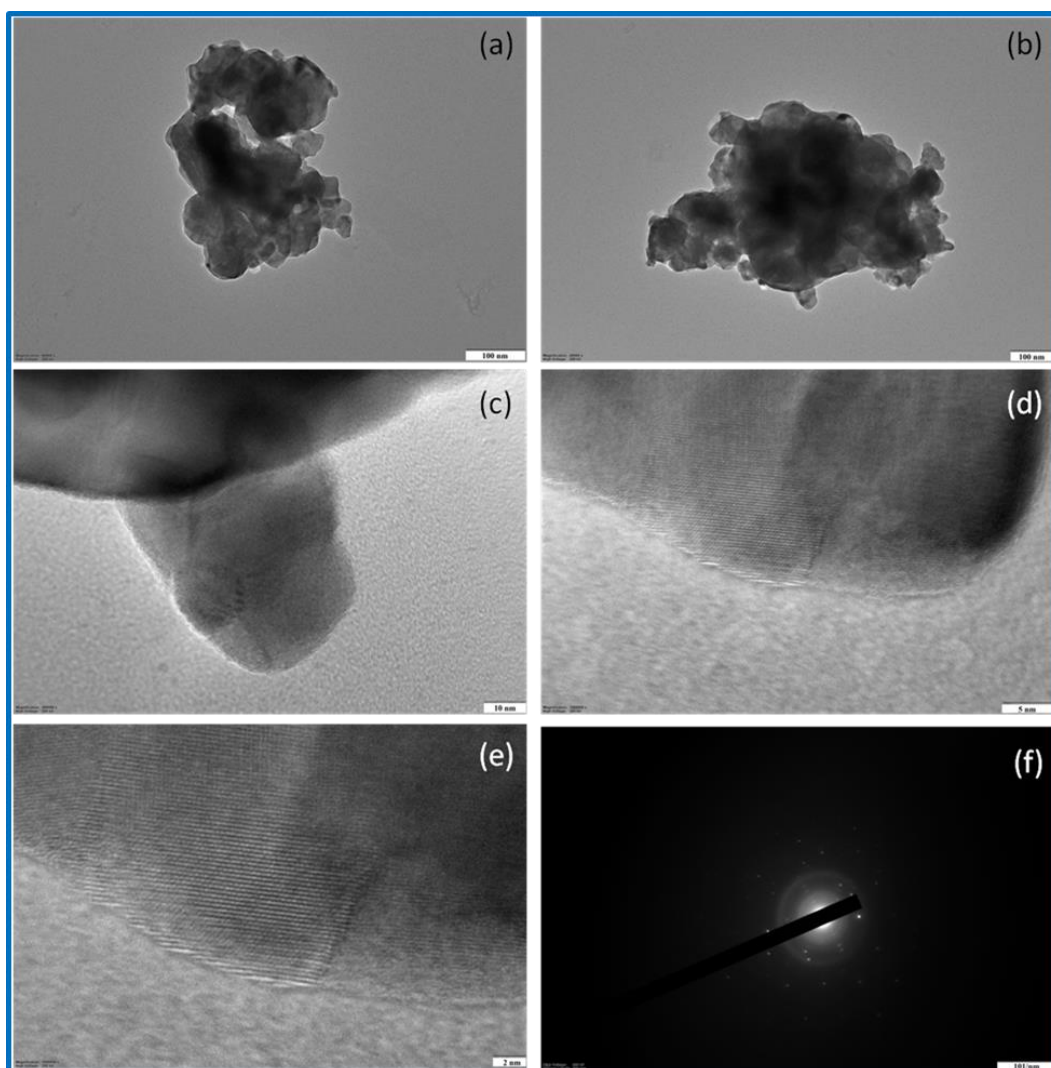


Fig. 3.7 (a-e) HR-TEM images in the magnification of 100 nm, 100 nm, 10 nm, 5 nm and 2 nm respectively and f) SAED pattern of synthesized Fe NPs

3.3.6 Phytochemical analysis

The phytochemical analysis listed the phytochemicals in *Cinnamomum verum* bark extract which were responsible for capping and stabilizing action of prepared Fe NPs [39]. In the aqueous extractive value, polyphenols, alkaloids, tannin, steroids, terpenoids, and glycoside were present in high concentration. These phytochemicals were the reason for the reduction of iron chloride to iron NPs. Further, it reasoned for the capping and stabilizing action of prepared Fe NPs. This phytochemicals diminished the size of NPs. It has represented the *Cinnamomum verum* bark were rich in antioxidants agents. This further improved the biomedical application of prepared Fe NPs.

3.3.6.1 Antibacterial Assay

Table 3.2 Inhibition zone of biosynthesized iron NPs against various human pathogenic bacteria

Bacterial Species	Zone of Inhibition (mm) against human pathogenic bacteria	
	Standard*	Fe
<i>Escherichia coli</i>	18	18
<i>Klebsiella pneumoniae</i>	17	25
<i>Staphylococcus aureus</i>	16	20
<i>Bacillus subtilis</i>	18	19

**Nitrofurantoin (300µg)*

The antibacterial activity of synthesized iron NPs from *Cinnamomum verum* extract was investigated against various pathogenic organisms such as *Escherichia coli*, *Klebsiella pneumoniae*, *Staphylococcus aureus* and *Bacillus subtilis* using disc diffusion method was shown in figure (Fig.3.8). The diameter of inhibition zones (mm) of iron NPs was reported in the table (table 3.2).

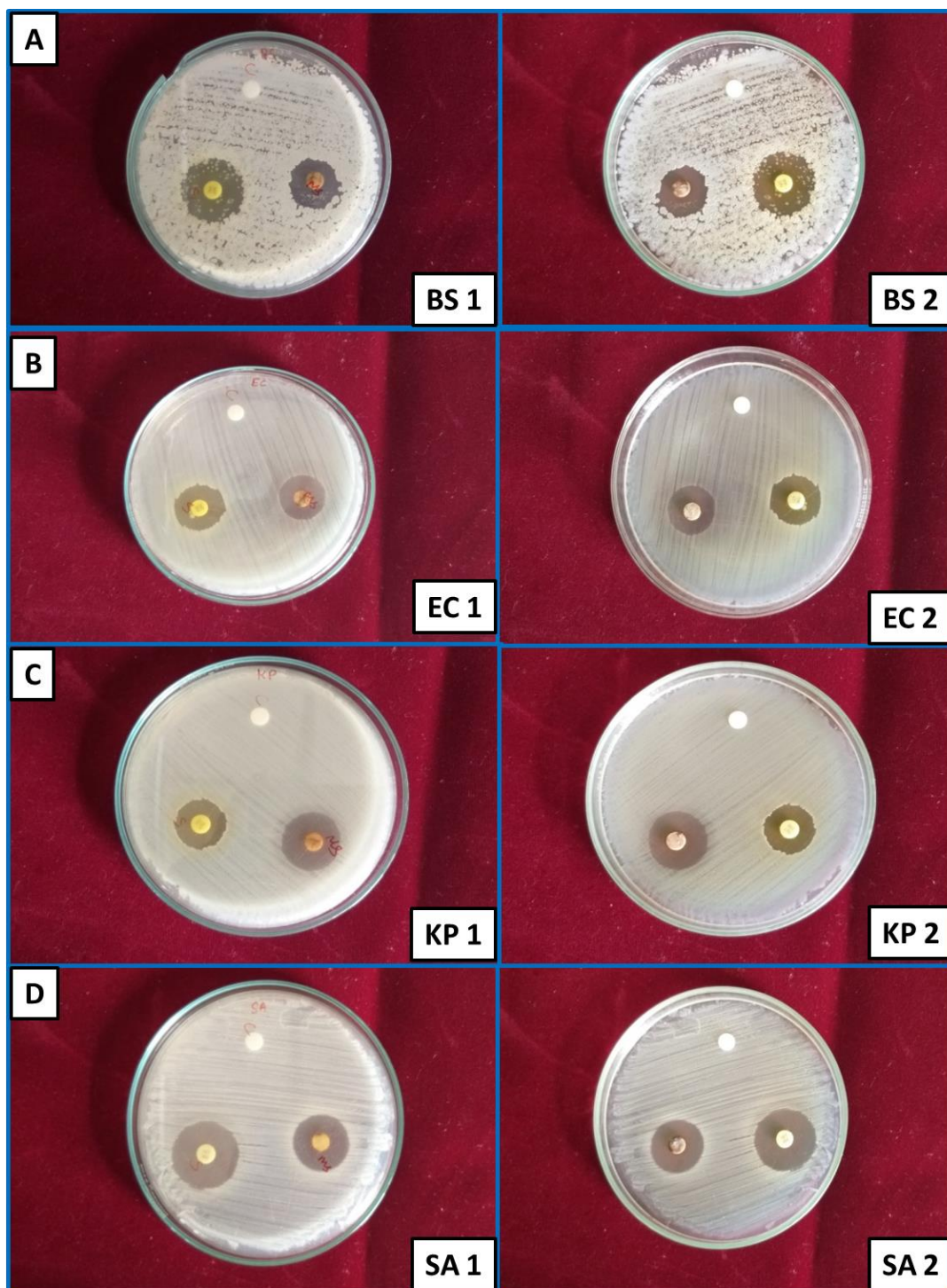


Fig. 3.8 Antibacterial assay of synthesized iron NPs using *Cinnamomum verum* extract against a) *Bacillus subtilis* b) *Staphylococcus aureus* c) *Escherichia coli* d) *Klebsiella pneumoniae*

Cinnamomum verum functionalized iron NPs displayed higher inhibition activity against *Klebsiella pneumonia* (25mm), *Staphylococcus aureus* (20mm) and *Bacillus subtilis* (19mm) bacterial strains. Therefore, we can conclude that the biosynthesized iron NPs were shown efficient antibacterial property because of plant extract when compared to a standard value. This inhibition values were also shown in figure 3.9.

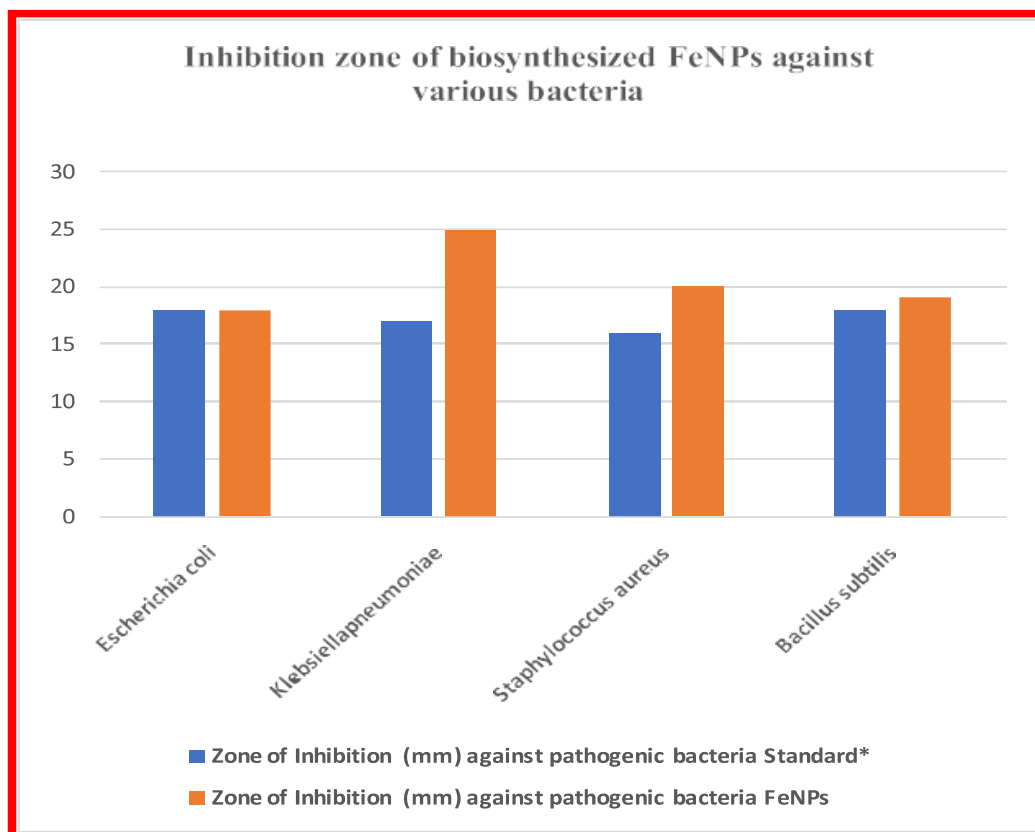


Fig. 3.9 Inhibition zone of biosynthesized FeNPs against various bacteria

The inhibition of applied bacteria with synthesized iron NPs was demonstrated in the following ways.

- The release of reactive oxygen species such as H_2O_2 , Fe^{2+} ions, O_2^{2-} ions bind with the cell wall of bacteria.
- These species penetrate and perforated the cell membrane. This leads to cell wall damage.

- This action released the interior components of the cell and attacks the DNA of bacteria.
- Moreover, all actions lead to cell damage and death [47]. This result has comparable with the earlier literatures [37,47].

3.3.6.2 Antioxidant assay

The DPPH antioxidant assay analyzed the scavenging behavior of Fe NPs and which was showed in figure 3.10. The table 3.3 provided the percentage of inhibition values and which showed the high concentration of Fe NPs applied have high inhibition. The concentrations used for analyzing the scavenging behavior of Fe NPs were 20, 40, 60 and 80 $\mu\text{g/mL}$. Moreover the positive control of *ascorbic acid* as standard was used in analysis.

The inhibition values of Fe NPs were 20%, 42%, 75% and 89% and for *ascorbic acid* were 16%, 36%, 70% and 83% with 20, 40, 60 and 80 $\mu\text{g/mL}$ concentrations respectively.

Table 3.3 Antioxidant assay of synthesized FeNPs via *Cinnamomum verum* bark extract

Samples	% of inhibitions (%)				
	Concentration ($\mu\text{g/mL}$)				
	20	40	60	80	IC ₅₀ value
<i>Fe</i>	20.19 \pm 0.70	42.07 \pm 0.14	75.43 \pm 1.10	89.24 \pm 0.18	47.50
<i>Ascorbic acid</i> (Standard)	16.73 \pm 0.32	36.45 \pm 0.71	70.81 \pm 1.01	83.18 \pm 0.10	50.02

\pm indicated the triplicate experimental results.

Further, the IC₅₀ value measurement described the 50% of inhibition. The low value of IC₅₀ value expressed the efficient inhibition. The IC₅₀ value measured for FeNPs was at 47.50 $\mu\text{g/mL}$ and for ascorbic acid measured was at 50.02 $\mu\text{g/mL}$. The phytochemicals in *Cinnamomum verum* bark extract may also reasoned for the high scavenging behavior of

prepared Fe NPs [37]. Overall, the synthesized Fe NPs expressed the efficient scavenging assay than *ascorbic acid*. This result has comparable with earlier reports [37,48].

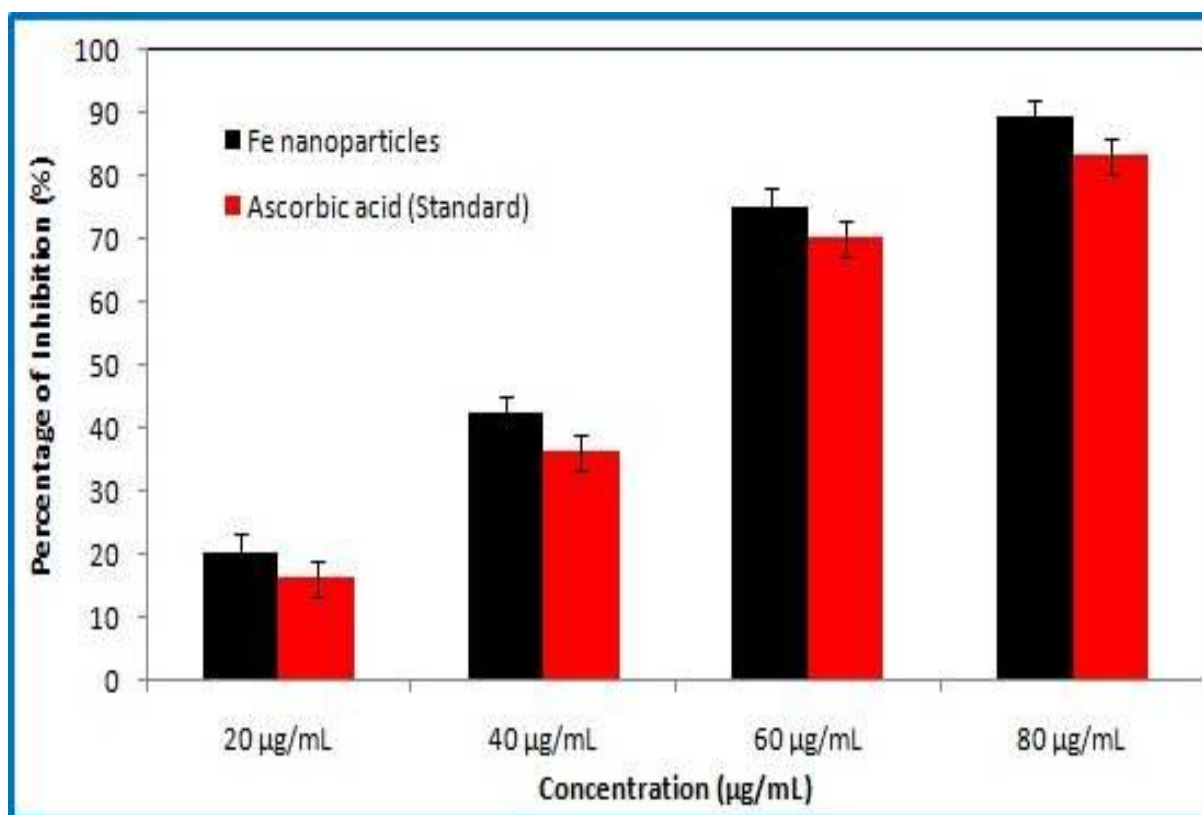


Fig. 3.10 Antioxidant assay of synthesized Fe NPs using *Cinnamomum verum* extract

3.3.6.3 Anti-inflammatory assay

The usual process of breaking the proteins as secondary and tertiary structures provided the loss of biological function. It was an interesting assay for analyzing the protective action than destroying action as antibacterial assay. With this, the anti-inflammatory assay was evaluated for synthesized FeNPs and which was showed in figure (Fig.3.11). The table (table 3.4) has showed the values of inhibition percentage measured in the analysis. These values expressed the high concentration applied in analysis have high inhibition percentage value. The concentrations used in analysis were 100, 200, 300, 400 and 500 µg/mL and the positive control of *Diclofenac sodium* as standard have also deployed.

The inhibition percentage of Fe NPs were at 21%, 44%, 70%, 79% and 87% and for *Diclofenac sodium* were at 17%, 38%, 63%, 73% and 83% with 100, 200, 300, 400 and 500 $\mu\text{g/mL}$ concentrations respectively.

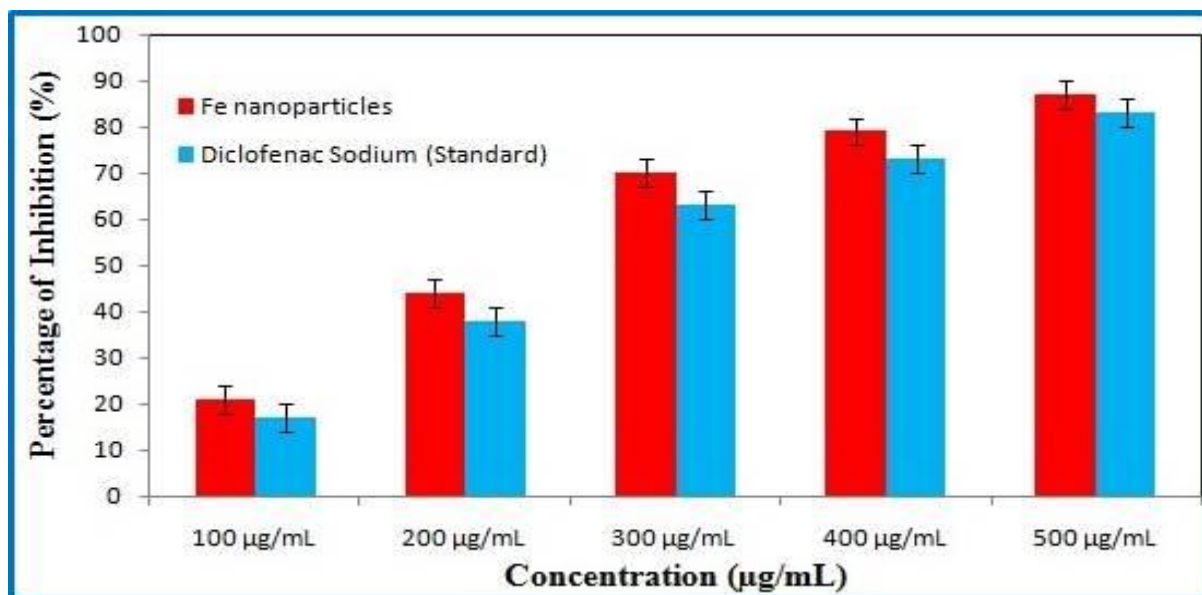


Fig. 3.11 Anti-inflammatory assay of synthesized Fe NPs using *Cinnamomum verum* extract

Table 3.4 Anti-inflammatory assay of synthesized Fe NPs via *Cinnamomum verum* bark extract

Samples	% of inhibitions (%)					
	Concentration ($\mu\text{g/mL}$)					
	100	200	300	400	500	IC ₅₀ value
<i>Fe</i>	21.10 \pm 0.15	44.10 \pm 0.13	70.19 \pm 1.05	79.45 \pm 0.90	87.35 \pm 0.10	212.10
<i>Diclofenac sodium</i> (Standard)	17.20 \pm 0.40	38.15 \pm 0.12	63.15 \pm 0.20	73.06 \pm 0.70	83.03 \pm 0.81	250.06

\pm indicated the triplicate experimental results.

The IC₅₀ value measured for Fe NPs was at 212 $\mu\text{g/mL}$ and for *Diclofenac sodium* was at 250 $\mu\text{g/mL}$. These values reported the synthesized Fe NPs have efficient action than *Diclofenac sodium*. This result has comparable with the earlier reports [37,49].

3.3.6.4 Anti-diabetic assay

The biomedical behavior of synthesized Fe NPs was understood via analyzing it in anti-diabetic assay. The figure (Fig.3.12) described the anti-diabetic assay and the measured values of inhibition percentages were grouped in the table (table 3.5). The concentrations used in analysis were 100, 200, 300, 400 and 500 $\mu\text{g/mL}$ and the positive control of *Acarbose* as standard have also deployed.

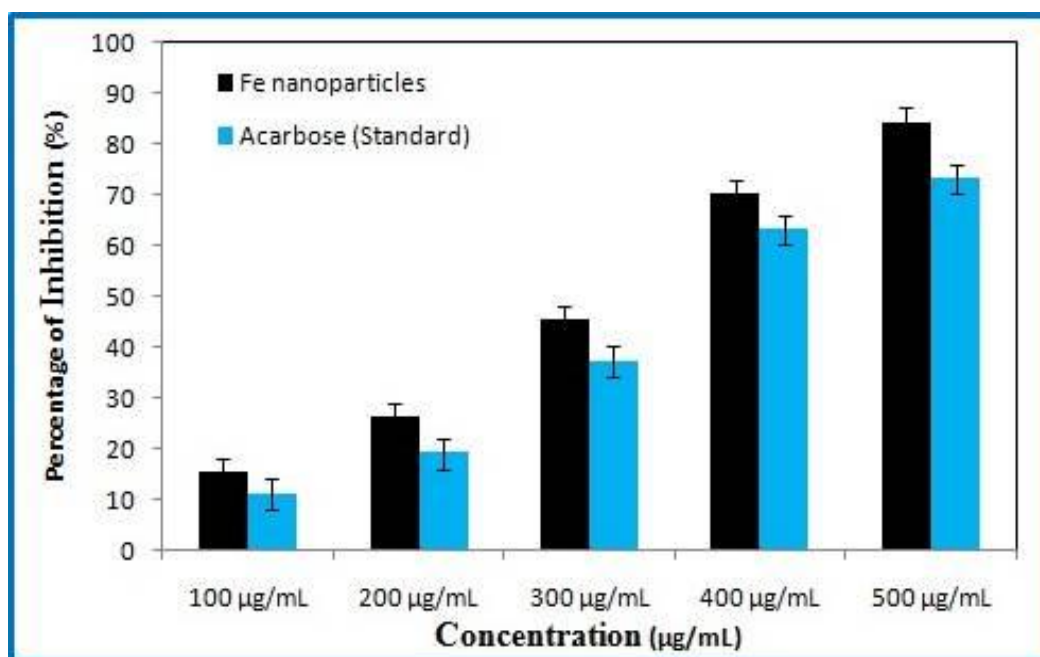


Fig. 3.12 Anti-diabetic assay of synthesized Fe NPs using *Cinnamomum verum* extract

The inhibition percentage for Fe NPs were at 15%, 26%, 45%, 70%, 84% and for *acarbose* were at 11%, 19%, 37%, 63%, 73% with 100, 200, 300, 400 and 500 $\mu\text{g/mL}$ concentrations respectively. These values described the high concentration applied in analysis have high inhibition percentage value.

Table 3.5 Anti-diabetic assay of synthesized Fe NPs via *Cinnamomum verum* bark extract

Samples	% of inhibitions (%)					
	Concentration ($\mu\text{g/mL}$)					
	100	200	300	400	500	IC ₅₀ value
<i>Fe</i>	15.19 \pm 0.15	26.20 \pm 0.13	45.09 \pm 0.45	70.19 \pm 1.17	84.15 \pm 0.170	312.17
<i>Acarbose (Standard)</i>	11.19 \pm 0.19	19.17 \pm 0.05	37.26 \pm 0.15	63.15 \pm 0.17	73.15 \pm 0.19	370.13

\pm indicated the triplicate experimental results.

The IC₅₀ value measured for Fe NPs was at 312 $\mu\text{g/mL}$ and for *acarbose* was at 370 $\mu\text{g/mL}$. These values proved the effective behavior of Fe NPs than *acarbose*. This result has comparable with earlier reports [48,49].

3.3.7 Vibrating Sample Magnetometer (VSM) analysis

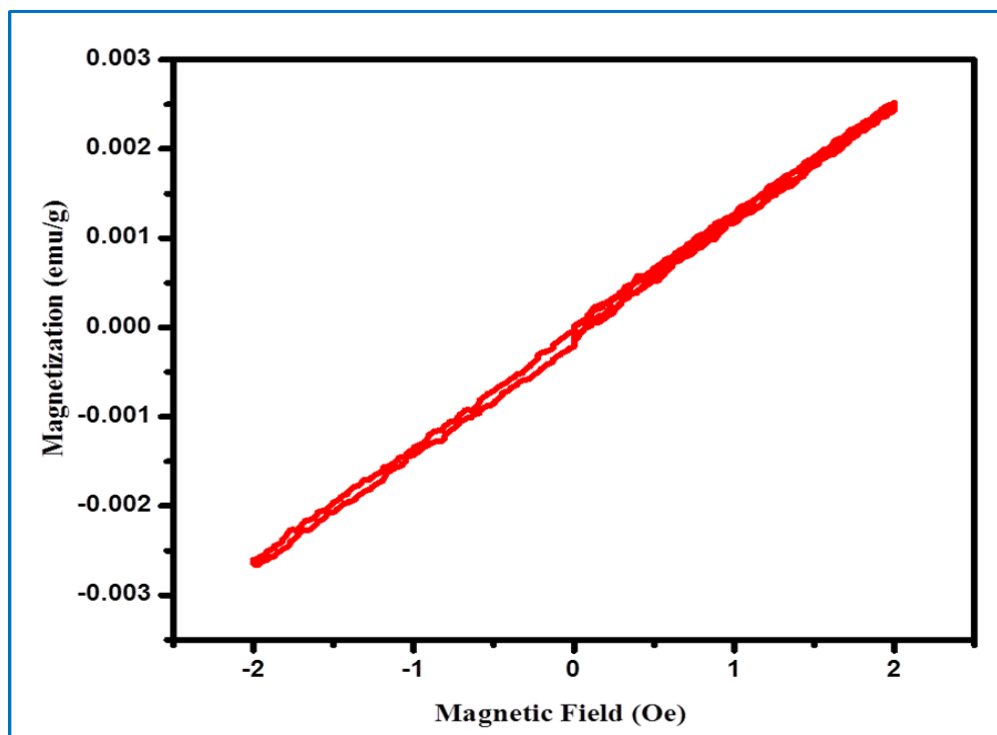


Fig.3.13 Magnetization curve of synthesized Fe NPs using *Cinnamomum verum* extract

To investigate the magnetic behavior of biosynthesized iron NPs, magnetization measurements were made using a vibrating sample magnetometer (VSM) at room temperature. Figure 3.13 showed the magnetization curve of synthesized FeNPs. A linear Magnetization-Applied magnetic field (M-H) graph with no hysteresis loop was achieved, which indicated that the synthesized iron NPs have paramagnetic properties. Therefore, the biosynthesized iron NPs were weakly attracted by a strong externally applied magnetic field, and form internal induced magnetic fields in the direction of the applied magnetic field [50].

3.4 Conclusion

The present study compiled the impact of iron NPs and *Cinnamomum verum* extract plays an essential role in the reduction and stabilization of iron NPs. The synthesized magnetic Fe NPs have confirmed by UV-Vis analysis with SPR band at 288 nm. XRD analysis revealed the mean crystallite size of iron NPs was at 36 nm. SEM and HRTEM images revealed that iron NPs were compatible, stable in circular and spherical shaped with size at 20-50 nm. The EDAX and mapping analysis validated the formation of FeNPs. The VSM analysis explicated the paramagnetic behavior of prepared NPs. The inhibition zones that appeared in the antibacterial assay designated the synthesized FeNPs has an efficient higher inhibition of antibacterial effect against human pathogenic bacteria. The antioxidant, anti-inflammatory and anti-diabetic assay showed the efficient behavior of FeNPs with low concentration value in biomedical applications. These studies revealed that green synthesis of iron NPs has potential as an easy, economical and beneficial process for most scientific and technical applications in the future, including treatment of wastewater, pesticides in agriculture and screening of drugs to hasten the natural drug discovery against promising chemicals.

References

- [1] S.P. Dubey, M. Lahtinen, M. Sillanpää, *Colloid Surface A.*, 364(1-3) (2010) 34-41.
- [2] N. Beheshtkhoo, M.A.J. Kouhbanani, A. Savardashtaki, A.M. Amani, S. Taghizadeh, *Applied Physics A-Matter*, 124(5) (2018) 363.
- [3] M. Sabet, M. Salavati-Niasari, O. Amiri, *Electrochimica Acta*, 117 (2014) 504-520.
- [4] M. Salavati-Niasari, *Chemical Letters*, 34(10) (2005) 1444-1445.
- [5] M. Salavati-Niasari, D. Ghanbari, M.R. Loghman-Estarki, *Polyhedron*, 35(1) (2012) 149-153.
- [6] F. Davar, M. Salavati-Niasari, *Journal of Alloys and Compounds*, 509(5) (2011) 2487-2492.
- [7] F. Mohandes, F. Davar, M. Salavati-Niasari, *Journal of Physics and Chemistry of Solids*, 71(12) (2010) 1623-1628.
- [8] M. Salavati-Niasari, M.R. Loghman-Estarki, F. Davar, *Chemical Engineering Journal*, 145(2) (2008) 346-350.
- [9] M. Salavati-Niasari, *Microporous and Mesoporous Materials*, 95(1-3) (2006) 248-256.
- [10] M. Salavati-Niasari, *Inorganic Chemistry Communications*, 8(2) (2005) 174-177.
- [11] E. Esmaili, M. Salavati-Niasari, F. Mohandes, F. Davar, H. Seyghalkar, *Chemical Engineering Journal*, 170(1) (2011) 278-285.
- [12] M. Salavati-Niasari, A. Sobhani, F. Davar, *Journal of Alloys and Compounds*, 507(1) (2010) 77-83.
- [13] S. Mortazavi-Derazkola, S. Zinatloo-Ajabshir, M. Salavati-Niasari, *Ceramics International*, 41(8) (2015) 9593-9601.
- [14] M. Yousefi, F. Gholamian, D. Ghanbari, M. Salavati-Niasari, *Polyhedron*, 30(6) (2011) 1055-1060.
- [15] M. Masjedi-Arani, M. Salavati-Niasari, *Ultrasonics sonochemistry*, 29 (2016) 226-235.
- [16] S. Zinatloo-Ajabshir, M.S. Morassaei, O. Amiri, M. Salavati-Niasari, *Ceramics International*, 46(5) (2020) 6095-6107.
- [17] T. Meenatchi, A. Palanimurugan, A. Dhanalakshmi, V. Maheshkumar, B. Natarajan, *Chemical Physics Letters*, (2020) 137429.
- [18] V.V. Makarov, S.S. Makarova, A.J. Love, O.V. Sinitsyna, A.O. Dudnik, I.V. Yaminsky, N.O. Kalinina, *Langmuir*, 30(20) (2014) 5982-5988.

- [19] S. Arokiyaraj, M. Saravanan, N.U. Prakash, M.V. Arasu, B. Vijayakumar, S. Vincent, *Materials Research*, 48(9) (2013) 3323-3327.
- [20] K.M. Kumar, B.K. Mandal, K.S. Kumar, P.S. Reddy, B. Sreedhar, *Spectrochimica Acta A*, 102 (2013) 128-133.
- [21] P. Mehdizadeh, Y. Orooji, O. Amiri, M. Salavati-Niasari, H. Moayedi, *Journal of Cleaner Production*, 252 (2020) 119765.
- [22] Y. Orooji, R. Mohassel, O. Amiri, A. Sobhani, M. Salavati-Niasari, *Journal of Alloys and Compounds*, 835 (2020) 155240.
- [23] Y. Orooji, A.A. Alizadeh, E. Ghasali, M.R. Derakhshandeh, M. Alizadeh, M.S. Asl, T. Ebadzadeh, *Ceramics International*, 45(16) (2019) 20844-20854.
- [24] M. Ghasemi, A. Khataee, P. Gholami, R.D.C. Soltani, A. Hassani, Y. Orooji, *Journal of Environmental Management*, 267 (2020) 110629.
- [25] A.J. Sisi, M. Fathinia, A. Khataee, Y. Orooji, *Journal of Molecular Liquids*, 308 (2020) 113018.
- [26] Y. Orooji, M. Ghanbari, O. Amiri, M. Salavati-Niasari, *Journal of Hazardous Materials*, 389 (2020) 122079.
- [27] M. Bordbar, N. Negahdar, M. Nasrollahzadeh, L. Melissa Officinalis, *Separation and Purification Technology*, 191 (2018) 295-300.
- [28] M. Nasrollahzadeh, S.M. Sajadi, *RSC Advances*, 5(57) (2015) 46240-46246.
- [29] M. Nasrollahzadeh, S.M. Sajadi, A. Rostami-Vartooni, *Journal of Colloid and Interface Science*, 459 (2015) 183-188.
- [30] B. Khodadadi, M. Bordbar, M. Nasrollahzadeh, *Journal of Colloid and Interface Science*, 493 (2017) 85-93.
- [31] A. Rostami-Vartooni, M. Nasrollahzadeh, M. Alizadeh, *Journal of Colloid and Interface Science*, 470 (2016) 268-275.
- [32] M. Nasrollahzadeh, S.M. Sajadi, A. Rostami-Vartooni, S.M. Hussin, *Journal of Colloid and Interface Science*, 466 (2016) 113-119.
- [33] S. Mathew, T.E. Abraham, *Food Chemistry*, 94(4) (2006) 520-528.
- [34] P.S. Yap, T. Krishnan, K.G. Chan, S.H. Lim, *Journal of Microbiology and Biotechnology*, 25(8) (2015) 1299-1306.
- [35] L. Huang, X. Weng, Z. Chen, M. Megharaj, *Spectrochimica Acta A*, 117 (2014) 801-804.
- [36] D. Li, T. Yang, Y. Li, Z. Liu, W. Jiao, *Journal of Cleaner Production*, 246 (2020) 119033.

- [37] K. Velsankar, R. Preethi, P.S. Jeevan Ram, M. Ramesh, S. Sudhahar, *Applied Nanoscience*, 10(9) (2020) 3675-3691.
- [38] A. Rostami-Vartooni, M. Alizadeh, M. Bagherzadeh, *Beilstein Journal of Nanotechnology*, 6(1) (2015) 2300-2309.
- [39] K. Velsankar, S. Sudhahar, G. Parvathy, R. Kaliasammal, *Materials Chemistry and Physics*, 239 (2020) 121976.
- [40] M. Mahdavi, F. Namvar, M. Ahmad, R. Mohamad, *Molecules*, 18(5) (2013) 5954-5964.
- [41] T. Wang, X. Jin, Z. Chen, M. Megharaj, R. Naidu, *Science of the Total Environment*, 466 (2014) 210-213.
- [42] S. Venkateswarlu, Y.S. Rao, T. Balaji, B. Prathima, N.V.V. Jyothi, *Material Letters*, 100 (2013) 241-244.
- [43] B. Kumar, K. Smita, L. Cumbal, A. Debut, *Journal of Saudi Chemical Society*, 18(4) (2014) 364-369.
- [44] M. Senthil, C. Ramesh, *Digest Journal of Nanomaterials and Biostructures*, 4 (2012) 7.
- [45] E.C. Njagi, H. Huang, L. Stafford, H. Genuino, H.M. Galindo, J.B. Collins, S.L. Suib, *Langmuir*, 27(1) (2010) 264-271.
- [46] H. Muthukumar, M. Matheswaran, *ACS Sustainable Chemistry and Engineering*, 3(12) (2015) 3149-3156.
- [47] K. Velsankar, S. Sudhahar, G. Maheswaran, M. Krishna Kumar, *Journal of Photochemistry and Photobiology B*, 200 (2019) 111650.
- [48] K. Velsankar, R.M. Aswin Kumar, R. Preethi, V. Muthulakshmi, S. Sudhahar, *Journal of Environmental Chemical Engineering*, 8(5) (2020) 104123.
- [49] K. Velsankar, V. Vinothini, S. Sudhahar, M. Krishna Kumar, S. Mohandoss, *Applied Nanoscience*, 10(10) (2020) 3953-3971.
- [50] B. Desalegn, M. Megharaj, Z. Chen, R. Naidu, *Heliyon*, 5 (2019) e01750.

Phytomediated Synthesis of Magnetic Nanoparticles by *Murraya koenigii* Leaves Extract and Its Biomedical Applications

Abstract

Green synthesis of nanoparticles is a facile method as they are eco-friendly, cost-effective and also the resources are easily available. Nowadays, the demand for magnetic nanoparticles has increased around 13 % and they are used in magnetic sensing, medical imaging, waste water treatment, and antibiotic drugs. In this report, the eco-friendly green synthesis of magnetic iron nanoparticles was efficiently synthesized by using *Murraya koenigii* leaves extract. The UV-visible spectrum revealed the presence of a surface plasmon resonance band at 240 nm and analyzed the formation of iron nanoparticles. X-ray diffraction pattern determined the crystallinity of nanoparticles. Fourier-Transform Infrared spectrum illustrated the functional groups of iron nanoparticles. The particle size distribution graph showed that the formed particles were in the range of nanometer. High resolution-transmission electron microscopy spectrum realized the spherical shaped iron nanoparticles were ranging between 4-9 nm in size. The energy dispersive X-ray spectrum and mapping revealed the iron, oxygen and carbon elements in the prepared nanoparticles. The vibrating sample magnetometer analysis showed the paramagnetic behavior of the prepared magnetic iron nanoparticles. The inhibition potent of magnetic nanoparticles on various human pathogens was revealed through antimicrobial assay. The antioxidant, anti-inflammatory and anti-diabetic assays revealed the biomedical behavior of the iron nanoparticles.

4.1 Introduction

Nanoparticles (NPs) with a dimension of 1 to 100nm have specific physical, chemical, magnetic and biological properties. Nanotechnology has shown tremendous

growth in all the fields such as optical, electronic, textile, agricultural, environmental, biomedical etc., [1-5]. Nanoparticles have enormous applications with a particularly large surface to volume ratio property and enhanced efficiency in all the fields in the form of catalysts, batteries, solar cells, gas sensors, LEDs, semiconductors, glasses, sunscreen products, cosmetics, building materials, leathers, food packaging, batteries, clothes and drugs etc., [6-10]. The manipulation of nanoparticles is one of the interesting research areas for researchers as it creates a demand for the existence of living organisms in the world. Because, it solves the simple and difficult issues which are imperative in materials science [11,12]. Nowadays, treating nutrition deficiency diseases and bacterial infections has become a challenge to the clinical field. The infectious strains are easily spread and cause huge health crisis problems to humans and animals. Some pathogenic strains are not responding to antimicrobial agents and create huge damage to the human health system [13]. Bio-nanotechnology involves the production, operation and implementation process of drugs to several human and animal diseases and hence it aids. It can able to create antibiotic drugs against human pathogens without producing any side effects. In clinical fields, bio-nanotechnology plays a vital role in finding drugs to cure life-threatening diseases [13-17].

In nanotechnology, particles were synthesized by various physical, chemical and biological methods [6,7,15-19]. The synthesis of nanoparticles in some chemical methods require toxic reducing agents which may produce harmful by-products, that pollute the environment and affect the living organisms [13,15,16]. But, in green synthesis method, it can be reduced by substituting the chemicals with plant materials, bacteria or fungi, yeasts and agricultural wastes. Also, it is inexpensive comparatively and does not require high energy, pressure and hazardous chemicals. It does not produce any hazards to the environment [15,16]. Furthermore, green synthesis of nanoparticles using plant extracts is an easy large productive approach compared to other biological methods and is a cost-effective method, which utilizes easily available resources. The chemicals and by-products

in green synthesis of NPs is comparably low hazardous to environment than other methods [13,16]. The eco-friendly synthesis of nanoparticles has practical applications in clinical, biomedical, agricultural, and drug delivery fields as drugs without producing any adverse effects [20,21].

Among the green synthesized nanoparticles, researchers have a specific interest in inorganic nanoparticles since they are easily available and necessary [11] as they have many practical applications viz., sunscreen glasses and products [22], cosmetics [23], sensors [24], catalysts [25], food packaging [26], paints [27], ceramics [28], batteries [29], and drugs [30]. The magnetic NPs attain interest in research with their high catalytic, intrinsic, and versatile properties. It is used in vast field's viz., food, bio-sensing, medical and magnetic separation, degradation of organic pollutants, and waste-water treatment [31]. Iron NPs are mostly used as dye removers for conserving a pollution-free environment [12]. Mostly, iron NPs are clinically used as biosensors in a magnetic field-assisted drug delivery therapy [32]. Reports of green synthesis of magnetic NPs using different plant extracts have gained attention and some of them are; *Cymbopogon citratus* [33], *Carica papaya* [34], *Laurus nobilis* [35], *Platanus orientalis* [36], *Amaranthus spinosus* [37], *Pinus pinaster* [38], *Moringa oleifera* [39], Eucalyptus [40], Rosemary [41], *Mangifera indica* [42], *Camellia sinensis* [43], *Daphne mezereum* [12], *Vitex negundo* [44], *Terminalia bellirica* [39], and *Psoralea corylifolia* [45].

Murraya koenigii is native to India, and they are used in both medicinal and culinary applications. They are highly aromatic and have a unique citrus flavor. Aside from being a versatile culinary herb, they offer an abundance of health benefits due to the presence of powerful phytochemicals. Curry leaves are rich in alkaloids, glycosides, and phenolic compounds that give potent health benefits and most of them possess antioxidant properties. Antioxidants play an indispensable role in maintaining our body healthy also; they help us

to stay away from diseases. Curry leaves are good sources of iron and calcium, and hence they are used to treat calcium deficiency. Also, it reduces blood glucose levels effectively. They shield the insulin-producing cells and protect them from the harms caused by free radicals [46]. Traditionally, curry leaves are assumed to have favorable effect for good-eyesight, so they can be used to prevent the early onset of cataract problems. Most of the illnesses caused in our body are initiated by infections or oxidative damage in the body. Curry leaves can be used as an alternative to treat certain infections. Curry leaves contains The carbazole alkaloids that are present in the curry leaves possess antibacterial, anti-inflammatory, antioxidant and anticancer properties [46,47].

In this study, the eco-friendly synthesis of iron NPs by *Murraya koenigii* leaves extract from the literature survey were reported for the first time. The prepared magnetic NPs were studied using various analytical techniques for realizing their spectral, optical, morphological, electrical, magnetic and biological properties.

4.2 Experimental section

4.2.1 Chemicals used

Ferric chloride (FeCl_3 ($\geq 98.99\%$)), ethanol ($\geq 99.92\%$), deionized water and *Murraya koenigii* leaves collected from Pudukkottai was used. All the chemicals used for this study were purchased from Sigma Aldrich, India.

4.2.2 *Murraya koenigii* leaves extract preparation

5 g of fresh healthy *Murraya koenigii* leaves were taken and thoroughly cleaned with tap water and deionized water. The leaves were immersed in 100 ml of deionized water and heated on a magnetic stirrer to 80°C for 30 min. The solution was allowed to cool once it reaches room temperature, the solution was filtered with Whatmann No.1 filter paper to remove the residual impurities. The filtered *Murraya koenigii* leaves extract solution was preserved at 4°C in a refrigerator for further use.

4.2.3 Synthesis of iron NPs by *Murraya koenigii* leaves extract

About 0.01M of FeCl_3 was dissolved in 90 ml of deionized water by continuous stirring on a magnetic stirrer. Then, a 10ml of *Murraya koenigii* leaves extract was taken in a burette and mixed with ferric chloride solution which was added drop by drop. The solution was heated to 70°C for 2h and stirred continuously. The brown color solution turned into black color immediately, which indicated the formation of iron NPs. The dark brownish-black precipitate was washed with deionized water and dried at 80°C in a hot air oven. Then, the magnetic NPs were preserved and analyzed by various analytical techniques. The synthesis scheme was revealed in figure (Fig. 4.1).

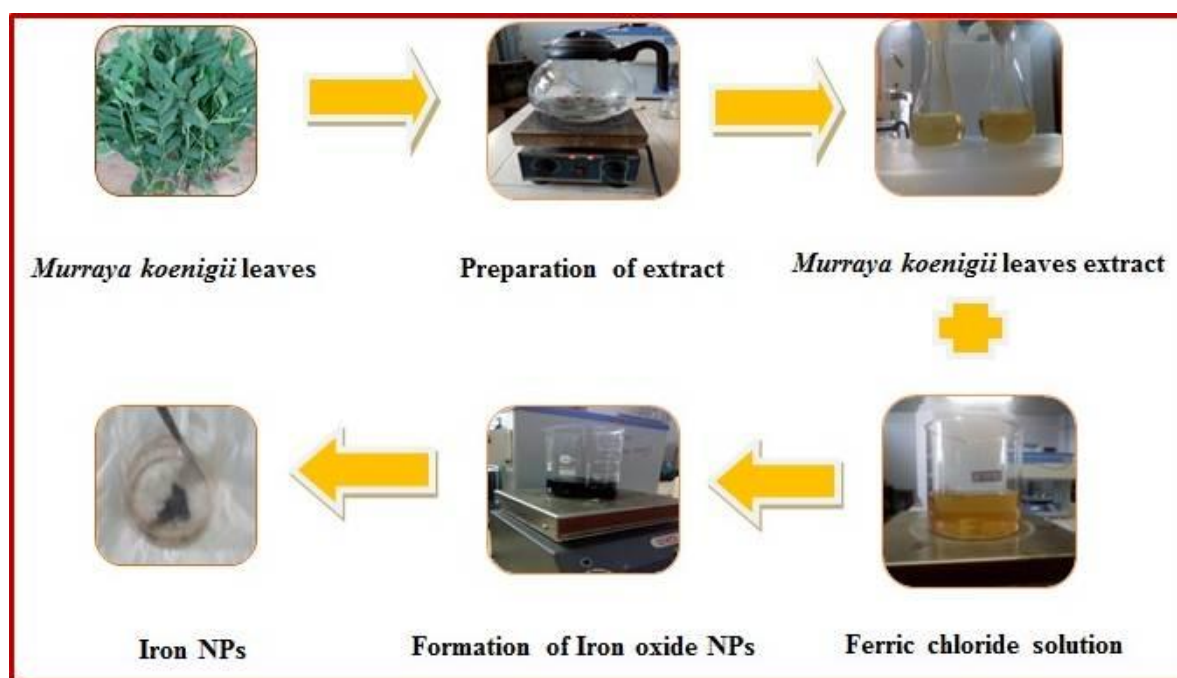


Fig. 4.1 Synthesis scheme of iron NPs green synthesized by *Murraya koenigii* leaf extract

4.2.4 Characterization of magnetic nanoparticles

The prepared NPs were characterized by using various analytical techniques. UV-visible analysis was completed by UV-DRS spectrophotometer Thermofisher Evaluation 220. X-ray powder diffraction (XRD) analysis was recorded with the help of PANalytical

X'Pert PRO powder X-ray diffractometer at 10° to 80° scan rate using CuK α radiation ($\lambda=1.5406$ Å). Fourier Transform Infra-Red spectrum was recorded using Thermo Nicolet 380 FT-IR spectrometer at 4000-400 cm⁻¹. The particle size distribution analysis (Dynamic Light Scattering-DLS) was studied by a particle size analyzer. The morphology of the prepared sample was analyzed using JEOL-2100+ High-Resolution Transmission Electron Microscope. The elemental and mapping analyses were taken from Energy Dispersive X-ray Spectrometer Quantax 200 with X Flash® 6130. The phytochemical analysis was carried out by the procedure described as in the earlier reports [48-50,30]. The magnetic property of the prepared sample was studied by Microsense model ADE-EV9 vibrating sample magnetometer at room temperature in -2 to 2 T magnetic fields.

4.2.5 Antimicrobial assay

The antimicrobial assay was completed through well plate method using microtitre plate [48]. LB broth and the chosen microbial cells such as *Pseudomonas aeruginosa*, *Acinetobacter baumannii*, *Serratia marcescens*, *Chromobacterium violaceum*, *Enterobacter aerogenes*, *Klebsiella pneumonia* (Gram-negative bacterial cells), *Enterococcus faecalis*, *Staphylococcus aureus* (Gram-positive bacterial cells), *Candida albicans*, *Candida tropicalis*, *Aspergillus niger*, and *Aspergillus flavus* (fungus cells) were utilized as a growth medium. The analysis was performed by 96 microtitre plates containing fully grown microbial cells in the medium and microbial inoculums with the prepared sample in varied concentrations viz., 5, 10, 25, 50, 100, and 150 $\mu\text{g/ml}$. Similarly, positive control chloramphenicol was treated. Then, the plates were put at 37°C for 24h. The analysis was performed and studied in triplicates. Later, it was analyzed with UV-spectrophotometer. The changes in absorbance were noted for calculating percentage of inhibition by,

$$\text{Antimicrobial assay (\%)} = [(A_c - A_s) / A_c] \times 100 \quad (4.1)$$

Where, A_c = Control absorbance, A_s = Sample absorbance.

4.2.6 Antioxidant assay

The antioxidant assay was completed as stated in the earlier report [49]. 0.5 ml of prepared NPs solution was taken and separated into varied concentrations viz., 20, 40, 60, 80 and 100 $\mu\text{g/ml}$. It was then mixed with 2 ml of DPPH methanol solution. The reaction mixture solution was continuously stirred for 30 min. Then, it was kept in a dark place at room temperature. After 30 min, it was analyzed by UV-visible spectrophotometer and the absorbance was recorded. Similarly, the positive control ascorbic acid was treated. The assay was performed thrice.

$$\text{Antioxidant assay (\%)} = 100 - [(A_c - A_s) / A_c] \times 100 \quad (4.2)$$

Where, A_c = Control absorbance, A_s = Sample absorbance.

4.2.7 Anti-inflammatory assay

The anti-inflammatory assay was investigated by the method stated and followed as in the previous report [49]. At first, 2.8 ml of phosphate-buffered saline (PBS) (pH 6.4), 0.2 mL of bovine serum albumin was taken and mixed with prepared NPs sample solution of 2 mL in varied concentration viz., 100, 200, 300, 400, and 500 $\mu\text{g/ml}$. After that the reaction mixture solution was incubated at $37 \pm 2^\circ\text{C}$. The procedure was completed in 15min and after completing it, it was heated to 70°C . The solution was allowed to attain room temperature and then the absorbance was recorded from a UV-visible spectrophotometer. Similarly, positive control diclofenac sodium was treated. The assay was performed in triplicates.

$$\text{Anti-inflammatory assay (\%)} = 100 - [\{V_c - V_t\} / V_c] \times 100 \quad (4.3)$$

Where, V_c = Control absorbance, V_t = Sample absorbance.

4.2.8 Anti-diabetic assay

The anti-diabetic assay was investigated by the method as stated in the earlier report [49]. At first, 0.5 mg/ml of α -Amylase was maintained at 25°C for 10min. The prepared NPs solution of 2 ml was taken in varied concentrations viz., 100, 200, 300, 400, and 500 μ g/ ml and was added to the starch solution. 20mM of sodium phosphate (pH 6.9) and 6mM of sodium chloride were also added to the sample solution then, it was mixed with the α -Amylase solution. The reaction mixture solution was maintained at 25°C for 30min. In this solution, di-nitrosalicylic acid was blended to view the color change. Further, the reaction mixture solution was heated to 70°C for 5min. Then, the absorbance was recorded from a UV-visible spectrophotometer to calculate the percentage of inhibition. Similarly, the positive control acarbose was treated. The assay was performed thrice.

$$\text{Anti-diabetic assay (\%)} = 100 - [\{V_c - V_t\} / V_c] \times 100 \quad (4.4)$$

Where, V_c = Control absorbance, V_t = Sample absorbance.

4.3 Results and Discussion

In this report, the iron NPs were green synthesized with *Murraya koenigii* leaves extract. Green synthesis is a method that is eco-friendly, cost-effective and also avoids the production of hazardous by-products. The formation of iron NPs was confirmed when the solution turns to brownish-black color change during the synthesis. The phytochemicals in *Murraya koenigii* leaves extract played the role of capping and stabilizing agents in the formation of iron NPs [15,16]. The phytochemicals are the most important agents in capping and stabilizing action of NPs. They interacted and attached to the precursor ions and which stabilized the NPs [13,15,16]. The phytochemicals in *Murraya koenigii* leaves extract were analyzed via two ways viz., alcoholic and aqueous extractive method, among these, aqueous extracts provided favorable phytochemicals. Then, the synthesis was done in an aqueous extractive method. The phytochemicals in *Murraya koenigii* leaves extract were listed in

Table 4.1. The *Murraya koenigii* aqueous leaf extract contains flavonoids, alkaloids and triterpenoids in high concentration, whereas tannin, terpenoids, steroids and polyphenol are in low concentration. The greener way mediated iron NPs were characterized by various analytical techniques for perceiving their properties.

Table 4.1 Phytochemical analysis of *Murraya koenigii* leaf extract

Phytochemicals analysis		
Phytochemicals	Aqueous extract	Ethanollic extract
Tannin	+	+
Flavonoids	++	+
Steroids	+	-
Saponin	-	-
Alkaloids	++	+
Terpenoids	+	+
Triterpenoids	++	+
Polyphenol	+	++
Anthraquinone	-	-
Glycoside	-	+
Coumarins	-	-

(-) Absent, (+) Present, (++) High concentration.

4.3.1 UV, XRD, FT-IR, DLS and VSM analysis

The UV-visible spectrum of prepared iron NPs was exposed in figure (Fig.4.2a). The surface plasmon resonance band was observed at 240nm. It has confirmed the formation of iron NPs and has compared with the inference recorded in the earlier report [51]. Rajendran et al. [51] reported that the magnetic NPs synthesized using *Sesbania grandiflora* leaf extract had its SPR band at 220 nm.

XRD pattern of prepared iron NPs is shown in figure (Fig.4.2b). The strong and intense peaks at 36.09°, 41.87°, 60.72°, 72.74°, and 76.54° and their corresponding planes

(111), (200), (220), (311), and (222) represent the high crystalline formation of iron NPs. The pattern was matched with JCPDS no. 654150 and indicated the face centered cubic phase formation of iron NPs. Certain amorphous behavior of noise signal is observed due to the use of leaf extract in synthesis of NPs [13, 16]. The extra peaks are witnessed due to the oxidation of iron NPs [52]. The average crystallite size was calculated at 14nm from Scherrer's formula,

$$D = K\lambda/\beta\cos\theta \quad (4.5)$$

Where, K - Scherrer's constant (0.94), λ - 1.5406 Å, β - Full width at half maximum (FWHM), θ – Bragg angle. Here, β - 0.635 and θ - 41.87°

Kanagasubbulakshmi et al. has reported that the magnetic NPs synthesized using *Lagenaria Siceraria* had its crystallite size between 14-18 nm [53]. The lattice strain was calculated at 0.0039 by [54],

$$\Delta L = L-L_0 \quad (4.6)$$

The dislocation density was calculated at $7.815 \times 10^{15} \text{ m}^{-2}$ by [55],

$$\delta = 1/D^2 \quad (4.7)$$

The microstrain was found at 5.030×10^{-3} by [54],

$$\varepsilon = \beta \cos\theta/4 \quad (4.8)$$

The high crystalline and small size of iron NPs were attained by using *Murraya koenigii* leaves extract.

FT-IR spectrum of the prepared iron NPs has revealed in figure (Fig.4.2c). The bands were recorded at 3454, 2427, 1767, 1637, 1384, 1112, 831, 537, and 459 cm^{-1} . The band at 3454 cm^{-1} may be due to the OH stretching vibration of hydroxyl or phenolic group [55]. The band at 2427 cm^{-1} corresponds to the aromatic aldehyde group of C-H stretching vibration whereas the band at 1767 cm^{-1} may be due to the ester group of C=O stretching

vibration [56]. The band at 1637 cm^{-1} denotes the amino acid stretching vibration whereas the band at 1384 cm^{-1} represents the germinal methyl group stretching vibration [48].

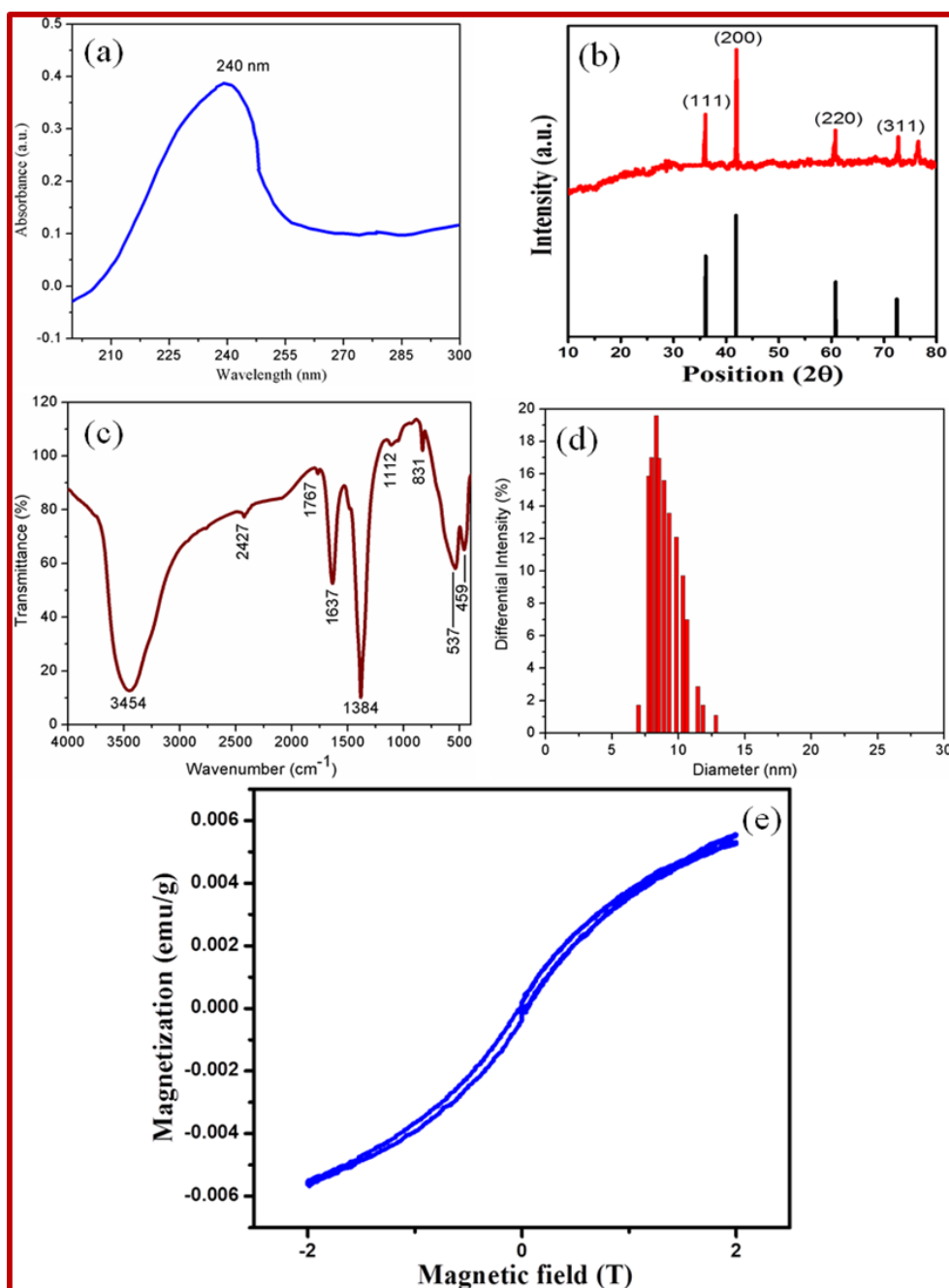


Fig. 4.2 a) UV-visible, b) X-ray diffraction (XRD) pattern, c) Fourier Transform Infra-Red spectrum (FT-IR), d) Particle size distribution (dynamic light scattering-DLS) graph and e) Magnetization curve (vibrating sample magnetometer-VSM) of green synthesized iron NPs by *Murraya koenigii* leaf extract

The band at 1112 cm^{-1} corresponds to carboxylic group stretching vibration [49,54]. The bands at 831 , 537 , and 459 cm^{-1} represent the metal and oxygen stretching vibration.

The appearance of oxygen functional group is mainly due to the oxidation of iron NPs [30]. It was clearly understood from the presence of various vibrations than oxygen functional groups and they were due to the use of leaf extract in synthesis of NPs [13,16].

DLS analysis was carried out to observe the particle size distribution and it is shown in figure (Fig. 4.2d). The particle size of the prepared iron NPs was at 7-15 nm. It was further confirmed by TEM particle size measurement. Compared with TEM analysis, the particle size observed in DLS was greater; it was appeared to be greater due to the measurement in hydrodynamic size. The polydispersity index (PDI) was obtained at 0.298 which indicates the potential application of NPs in drug delivery and bio-medical fields [55].

The magnetization curve of prepared iron NPs is revealed in figure (Fig.4.2e). The paramagnetic behavior of the prepared iron NPs was found to have no hysteresis loop that contains magnetization versus applied magnetic field (M-H) curve. The green synthesized magnetic NPs were weakly attracted by the strong magnetic field (B) and formed an internal induced magnetic field in that applied direction [42,57].

4.3.2 HR-TEM analysis

HR-TEM analysis was carried out to view the morphology of the prepared iron NPs and its graphs are displayed in figure (Fig.4.3 (a-b)). The spherical shaped [58] iron NPs was observed and their size ranged from 4-9 nm. Some regions seem to be agglomerated due to the usage of *Murraya koenigii* leaves extract in synthesis (plant extract). Aarsalani et al. synthesized magnetic NPs using natural rubber latex and reported that the size ranged from 7-15 nm and were spherical in shape [59]. Jamzad et al. [35] prepared magnetic NPs using *Laurus nobilis* leaf extract and mentioned that they were spherical in shape and the sizes ranged from 8-10 nm. Figure 4.3c illustrated the selected area electron diffraction (SAED) pattern of NPs. The polycrystalline formation of NPs was understood from the

white spots in the black area (SAED pattern). The d-spacing of (200) lattice plane in XRD was well-matched with SAED d-spacings measurement.

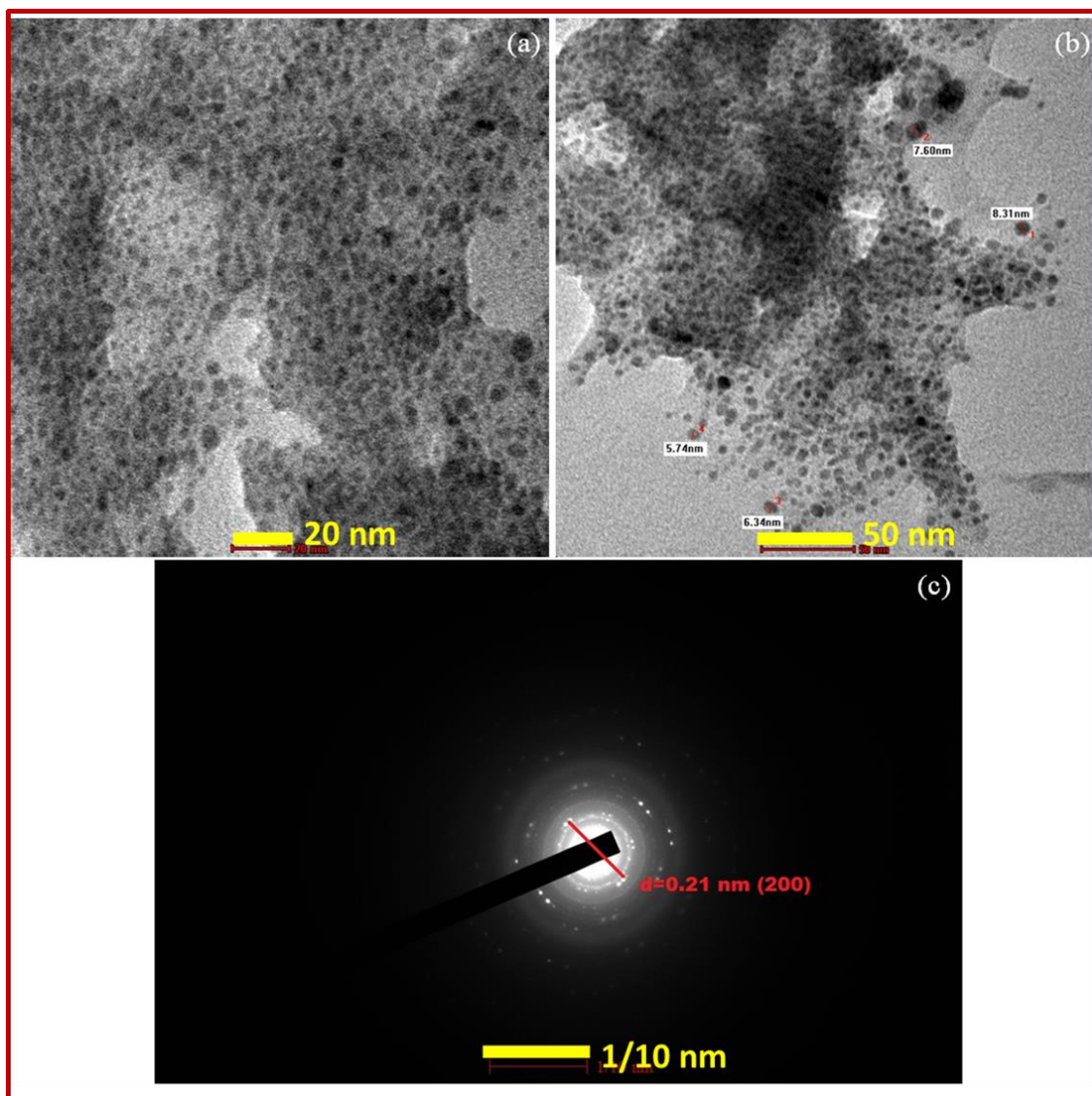


Fig.4.3 (a-b) High resolution-transmission electron micrographs (HR-TEM) at 20nm, 50nm scale and (c) selected area electron diffraction pattern at 1/10nm scale of green synthesized iron NPs by *Murraya koenigii* leaf extract

4.3.3 EDS analysis

The EDS spectrum of iron NPs was shown in figure (Fig.4.4). It has confirmed the presence of iron (Fe) and oxygen (O) in the synthesized NPs. The low carbon (C) signal was present due to the use of leaf extract in synthesis of iron NPs [48,54]. The presence of O represents the oxidation of prepared NPs [30]. The atomic and weight percentages of Fe, O and C are displayed in the table (Fig.4.4).

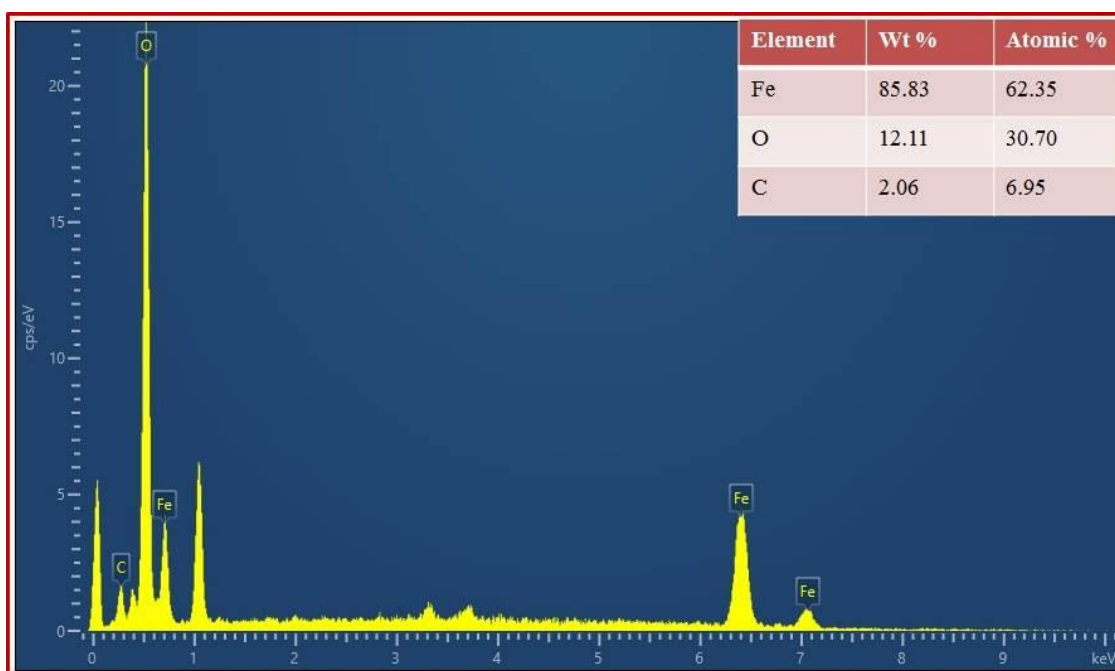


Fig.4.4 Energy dispersive X-ray spectrum (EDX) of green synthesized iron NPs by *Murraya koenigii* leaf extract

The EDS spectrum was further analyzed with mapping analysis which is revealed in figure (Fig.4.5). It has also showed the presence of iron, oxygen and carbon in NPs with red, green and blue spots.

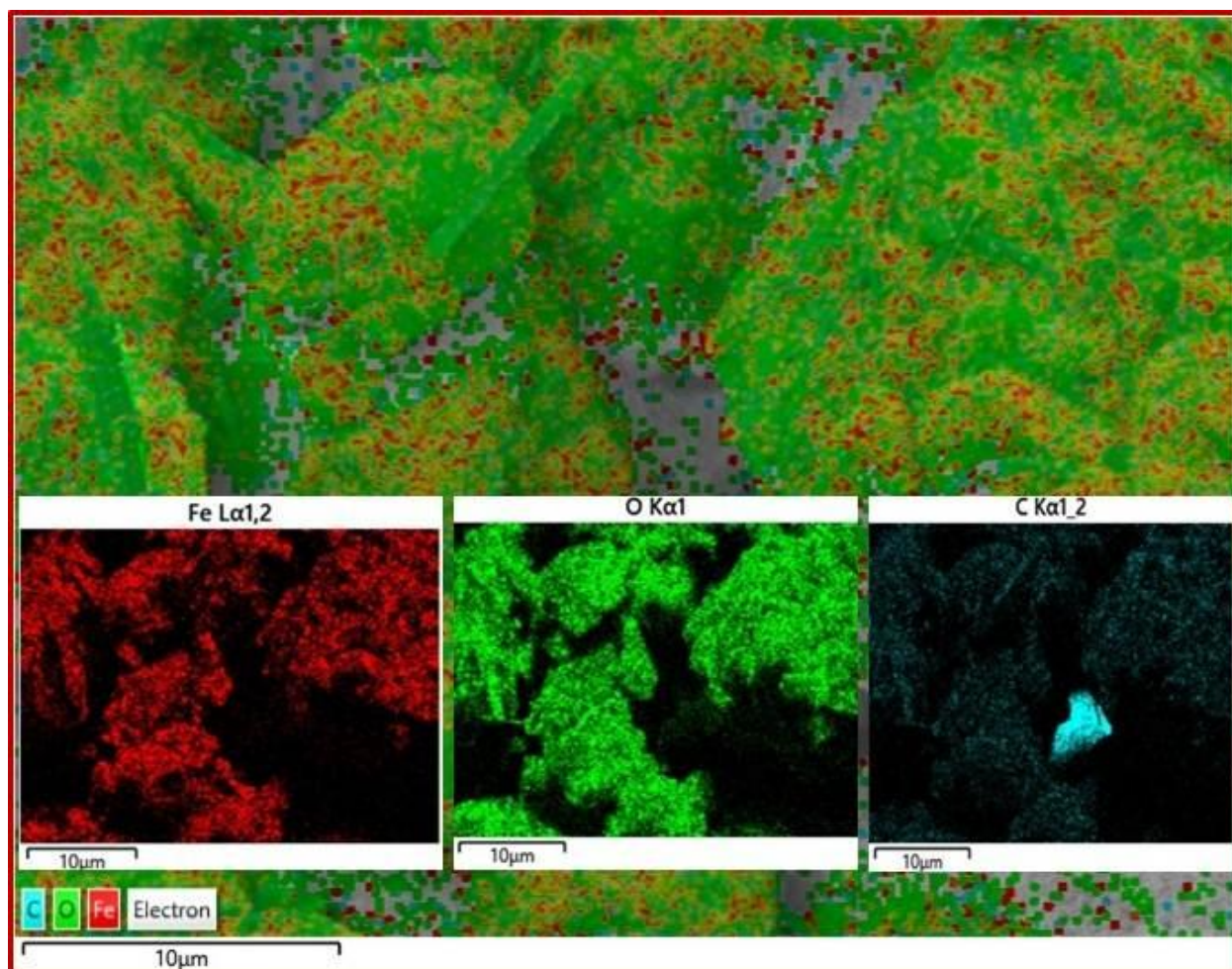


Fig.4.5 Energy dispersive X-ray spectrum (EDX) mapping of green synthesized iron NPs by *Murraya koenigii* leaf extract

4.3.4 Antimicrobial assay

The antimicrobial analysis is a preliminary investigation in the bio-medical field to understand the antibiotic behavior against human pathogens as the microbial pathogens cause huge health crisis in the world. In this analysis, the prepared NPs was tested on various human pathogens such as *Pseudomonas aeruginosa*, *Acinetobacter baumannii*, *Serratia marcescens*, *Chromobacterium violaceum*, *Enterobacter aerogenes*, *Klebsiella pneumonia* (Gram-negative bacterial cells), *Enterococcus faecalis*, *Staphylococcus aureus* (Gram-positive bacterial cells), *Candida albicans*, *Candida tropicalis*, *Aspergillus niger*, and *Aspergillus flavus* (fungus cells). The analysis was studied through Agar well diffusion method. The various concentrations such as 5, 10, 25, 50, 100, and 150 $\mu\text{g/ml}$ were applied

for finding antibacterial potency of prepared NPs. Chloramphenicol was set as a positive control. The gram-negative bacterium was more pathogenic than the gram-positive bacterium [60]. Then, the analysis was studied mostly on gram-negative bacterial cells. Further, the fungi cell has much stronger cell wall structure than bacteria. Therefore, analysis was also investigated in fungi cells to know the NPs potency. The tested microbes which were present in the soil, water and air medium produced many dreadful infections. The microbes that produced the dreadful diseases were the habitats of dirt, hospital, drainage and unhygienic zones [49]. The inhibition of microbial cells by NPs were expressed as a percentage in figure (Fig.4.6) and taken in triplicate times.

Among the tested microorganisms, *Pseudomonas aeruginosa*, *Enterobacter aerogenes*, *Klebsiella pneumonia*, *Chromobacterium violaceum* were more susceptible at 100 µg/ml. *Acinetobacter baumannii*, *Serratia marcescens*, *Enterococcus faecalis*, *Staphylococcus aureus*, *Candida albicans*, *Candida tropicalis*, *Aspergillus niger*, and *Aspergillus flavus* were susceptible at 25 µg/ml. Gram-positive bacteria were more inhibited than gram-negative comparatively Premanathan et al. [61]. The high concentration of NPs used in the analysis has higher inhibition on microbial cells and it was harmonized with Sangeetha et al. [62]. These results proved the synthesized NPs have antibiotic behavior on various human pathogens.

The process of inhibition of microbial cells by prepared NPs was as follows:

The generation of reactive oxygen species such as hydrogen peroxide (H₂O₂), superoxide ions (O₂²⁻ ions), free radicals, Fe²⁺ ions and its attachment on microbial cell wall leads to rupturing of the cell wall structure. Also, the electrostatic attraction between NPs and microbial cells prompts the cell wall damage; it has led to the release of cytoplasmic ingredients from the cell then, the ROS easily penetrated it and has inhibited the DNA nuclei

of the cell. Finally, it leads to cell decay and it prompts the cell damage and death of the microbes [49,54,60].

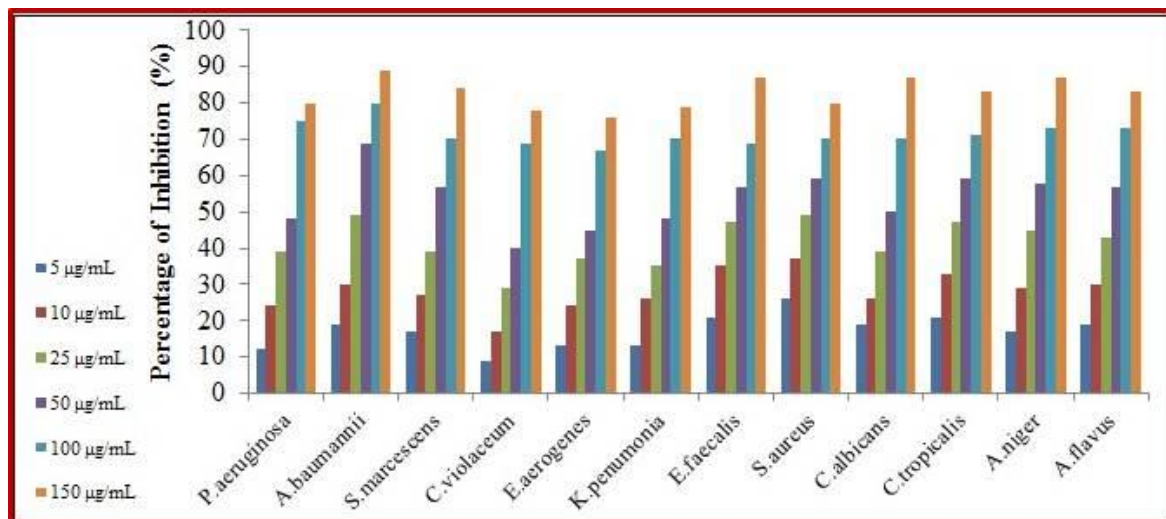


Fig.4.6 Antimicrobial assay of green synthesized iron NPs by *Murraya koenigii* leaf extract on *Pseudomonas aeruginosa*, *Acinetobacter baumannii*, *Serratia marcescens*, *Chromobacterium violaceum*, *Enterobacter aerogenes*, *Klebsiella pneumoniae* (Gram-negative bacterial cells), *Enterococcus faecalis*, *Staphylococcus aureus* (Gram-positive bacterial cells), *Candida albicans*, *Candida tropicalis*, *Aspergillus niger*, and *Aspergillus flavus* (fungi cells).

4.3.5 Antioxidant assay

The antioxidant assay of the prepared iron nanoparticles was displayed in the figure (Fig. 4.7). Antioxidants are the essential agents for the human to attain stable functioning of the health system. Antioxidants are enormously present in fruits, nuts and vegetables. Free radicals contained unpaired electrons and they are easily bound to the nearest molecules for attaining stability. They are produced in the human body to systemize immune function, chemical signaling, energy supply and detoxification [37]. An assay was carried out with various concentrations such as 20, 40, 60, 80 and 100 µg/ml. Ascorbic acid was set as a positive control. The results were expressed as a percentage in figure (Fig.4.7) and was taken in triplicate times and the values were listed in table (Table 4.2).

The percentage of inhibition by magnetic NPs and ascorbic acid were 24.04, 45.17, 67.19, 80.06, 91.17% and 20.06, 40.15, 59.12, 75.27, 85.19% with 20, 40, 60, 80 and 100 $\mu\text{g/ml}$ concentrations respectively. The high concentration of iron NPs was directly proportional to the inhibition percentage. In all concentrations, the iron NPs had a higher inhibition percentage than the positive control.

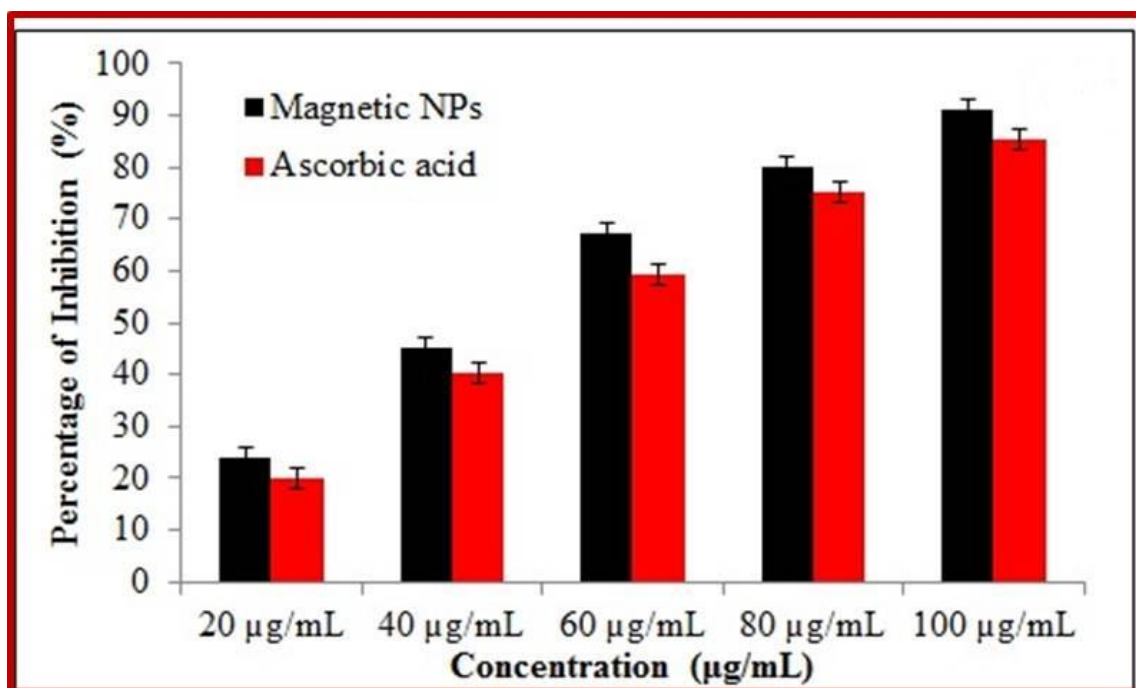


Fig.4.7 Antioxidant assays of green synthesized iron NPs by *Murraya koenigii* leaf extract

Table 4.2 Percentage of inhibition in antioxidant assay of green synthesized iron NPs by *Murraya koenigii* leaf extract

Samples	Percentage of Inhibition (%)				
	Concentration ($\mu\text{g/mL}$)				
	20	40	60	80	100
Magnetic NPs	24.04 \pm 0.19	45.17 \pm 0.97	67.19 \pm 0.93	80.06 \pm 0.06	91.17 \pm 0.04
Ascorbic acid	20.06 \pm 0.17	40.15 \pm 0.12	59.12 \pm 0.27	75.27 \pm 0.12	85.19 \pm 0.06

\pm performed in triplicate times

IC₅₀ value was represented the quantity of sample needed to attain 50 % inhibition; it denotes the potency of the sample. Low IC₅₀ value symbolizes the efficient behavior of the sample. The IC₅₀ value for NPs and ascorbic acid was at 42 and 49 µg/ml respectively. The results proved the potential behavior of prepared NPs and were compared with earlier reports [37,48].

4.3.6 Anti-inflammatory assay

The anti-inflammatory assay of synthesized iron NPs is illustrated in figure (Fig.4.8). It is an interesting analysis to show the protective behavior of the sample than other destroying analyses. The fragmentation of secondary and tertiary protein structures caused loss of biological function [50]. The assay was carried out with assorted concentrations such as 100, 200, 300, 400 and 500 µg/ml. Diclofenac sodium was set as a positive control. The results were expressed as a percentage in figure (Fig.4.8) and taken in triplicate times and the values were listed in the table (Table 4.3).

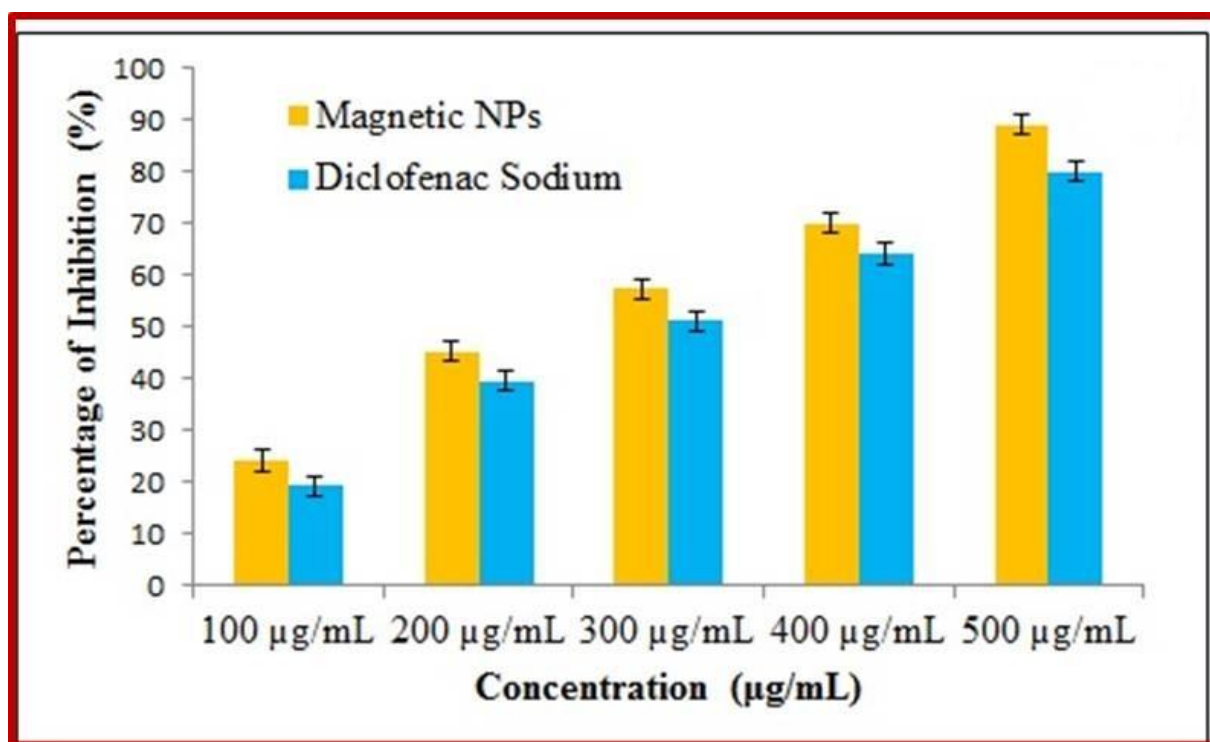


Fig.4.8 Anti-inflammatory assays of green synthesized iron NPs by *Murraya koenigii* leaf extract

The percentage of inhibition by magnetic NPs and diclofenac sodium were 24.04, 45.27, 57.30, 70.04., 89.12% and 19.04, 39.47, 51.02., 64.17, 79.99% with 100, 200, 300, 400 and 500 $\mu\text{g/mL}$ concentrations respectively. The high concentration of FeNPs is directly proportional to the inhibition percentage. In all the concentrations, FeNPs have a higher inhibition percentage than the positive control. The IC_{50} value for FeNPs and diclofenac sodium was at 247 and 293 $\mu\text{g/ml}$ respectively. The results have proved the potential behavior of prepared NPs and have compared with earlier reports [49,50].

4.3.7 Anti-diabetic assay

The anti-diabetic assay of prepared NPs has revealed in figure (Fig.4.9). It is a preliminary analysis to show the sample has anti-diabetic potency. Free radical causes the oxidative damage and resist enzyme such as α -Amylase, α -Glucosidase. These enzymes cause diabetes. In this analysis, α -Amylase was used. It is an enzyme; it is present in saliva and the pancreas. α -Amylase played a vital role in the conversion of carbohydrates, glycogen and starch. Further, it was rehabilitated into oligosaccharides from α -D(1,4) glycosidic bonds [48]. Earlier reports [63] stated that the diabetes can be efficiently healed by plant-based material. Green synthesized FeSNPs have more efficient results in curing diabetes than chemically prepared NPs without any adverse effects. The assay was carried out with various concentrations such as 100, 200, 300, 400 and 500 $\mu\text{g/ml}$ where acarbose was set as a positive control. The results were expressed as a percentage in figure (Fig. 4.9) and taken in triplicate times which values were listed in the table (Table 4.3).

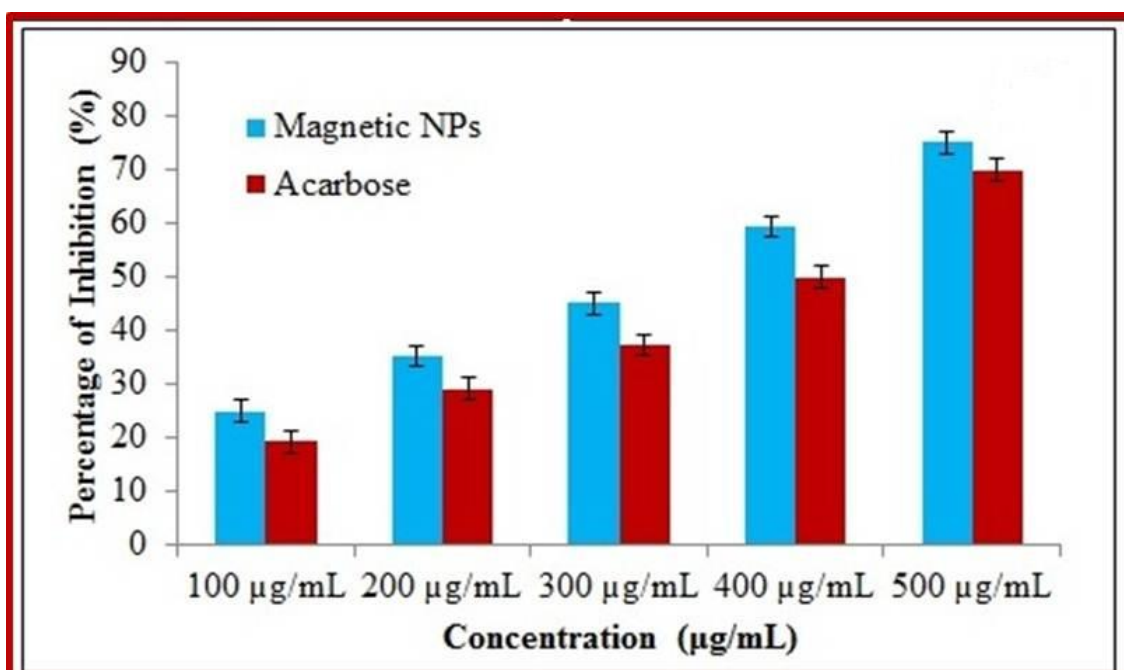


Fig. 4.9 Anti-diabetic assays of green synthesized iron NPs by *Murraya koenigii* leaf

Table 4.3 Percentage of inhibition in anti-inflammatory and anti-diabetic assays of green synthesized iron NPs by *Murraya koenigii* leaf extract

Samples	Percentage of Inhibition (%)				
	Concentration (µg/mL)				
	100	200	300	400	500
Magnetic NPs	24.04± 0.12	35.19± 0.35	45.06± 1.12	59.37± 0.39	75.06± 0.99
Diclofenac sodium	19.04± 0.19	29.04± 0.37	37.17± 0.17	49.93± 0.93	69.99± 1.04
Magnetic NPs	24.93± 0.33	35.19± 0.35	45.06± 1.12	59.37± 0.39	75.06± 0.99
Acarbose	19.12± 0.19	29.04± 0.37	37.17± 0.17	49.93± 0.93	69.99± 0.97

± performed in triplicate times

The percentage of inhibition on α -Amylase by NPs and acarbose were 24.93, 35.19, 45.06, 59.37, 75.06% and 19.12, 29.04, 37.17, 49.93, 69.99% with 100, 200, 300, 400 and

500 µg/ml concentrations respectively. The high concentration of iron NPs has the higher inhibition percentage. In all concentrations, FeNPs have a higher inhibition percentage than the positive control. The IC₅₀ value for FeNPs and diclofenac sodium was at 330 and 397 µg/ml respectively. The results proved the potency of prepared NPs and compared with earlier reports [48,63].

4.4 Conclusion

In this study, the eco-friendly green synthesis of iron NPs was efficiently performed by using *Murraya koenigii* leaves extract. The synthesized NPs were characterized by various analytical techniques such as UV, XRD, FT-IR, DLS, TEM, and EDS analyses. UV analysis has confirmed the formation of iron NPs with SPR band at 240 nm. XRD pattern has proved the high crystalline formation of iron NPs with strong and intense peaks. FT-IR analysis confirmed the functional groups of iron nanoparticles. DLS spectrum has revealed that the formed particles were in nano meter range. HR-TEM graphs illustrated that the formed NPs were spherical and the size ranged from 4-9 nm. EDS spectrum with its mapping proved the presence of iron in the formed NPs. VSM analysis has revealed the paramagnetic behavior of nanoparticles. The biomedical applications-based characterizations such as antimicrobial, antioxidant, anti-inflammatory and anti-diabetic assays were performed. The antimicrobial assay has proved the potency inhibition of iron NPs on various human pathogens. The antioxidant, anti-inflammatory and anti-diabetic assays have proved the iron NPs have biomedical behavior. With these results, the prepared iron NPs will be employed as antibiotic, anti-diabetic and anti-inflammatory drugs in biomedical field in future.

References

- [1] S. Arokiyaraj, M. Saravanan, N.U. Prakash, M.V. Arasu, B. Vijayakumar, S. Vincent, *Materials Research*, 48(9) (2013) 3323-3327.
- [2] S. Li, M. Meng Lin, M.S. Toprak, D.K. Kim, M. Muhammed, *Nano Review*, 1(1) (2010) 5214.
- [3] A. Fouda, E.L. Saad, S.S. Salem, T.I. Shaheen, *Microbial Pathogenesis*, 125 (2018) 252-261.
- [4] B. Mughal, S.Z.J. Zaidi, X. Zhang, S.U. Hassan, *Applied Sciences*, 11(6) (2021) 2598.
- [5] R. Canaparo, F. Foglietta, T. Limongi, L. Serpe, *Mater*, 14(1) (2021) 53.
- [6] K. Mathiyalagan, A. Ponnaiah, K. Karuppiah, S. Rengapillai, S. Marimuthu, *Ionics*, 26(8) (2020) 3929-3936.
- [7] M. Kouthaman, K. Kannan, P. Arjunan, T. Meenatchi, R. Subadevi, M. Sivakumar, *Material Letters*, 276 (2020) 128181.
- [8] S. Sahani, Y.C. Sharma, *Food Chemistry*, 342 (2021) 128318.
- [9] L. Salvioni, L. Morelli, E. Ochoa, M. Labra, L. Fiandra, L. Palugan, M. Colombo, *Advances in Colloid and Interface Science*, 293 (2021) 102437.
- [10] S. Prabha, D. Durgalakshmi, S. Rajendran, E. Lichtfouse, *Environmental Chemistry Letters*, 19(2) (2021) 1667-1691.
- [11] K.M. Kumar, B.K. Mandal, K.S. Kumar, P.S. Reddy, B. Sreedhar, *Spectrochimica Acta A*, 102 (2013) 128-133.
- [12] N. Beheshtkhoo, M.A.J. Kouhbanani, A. Savardashtaki, A.M. Amani, S. Taghizadeh, *Applied Physics A*, 124(5) (2018) 1-7.
- [13] K. Velsankar, G. Parvathy, S. Mohandoss, M. Krishna Kumar, S. Sudhahar, *Journal of Nanostructure in Chemistry*, (2021) 1-16.
- [14] V.V. Makarov, S.S. Makarova, A.J. Love, O.V. Sinitsyna, A.O. Dudnik, I.V. Yaminsky, N.O. Kalinina, *Langmuir*, 30(20) (2014) 5982-5988.
- [15] K. Velsankar, S. Suganya, P. Muthumari, S. Mohandoss, S. Sudhahar, *Journal of Environmental Chemical Engineering*, 9(5) (2021) 106299.
- [16] K. Velsankar, A. Venkatesan, P. Muthumari, S. Suganya, S. Mohandoss, S. Sudhahar, *Journal of Molecular Structure*, 1255 (2022) 132420.

- [17] R. Kaliammal, G. Parvathy, G. Maheshwaran, K. Velsankar, V.K. Devi, M. Krishnakumar, S. Sudhakar, *Advanced Powder Technology*, 32(11) (2021) 4408-4419.
- [18] Y. Orooji, R. Mohassel, O. Amiri, A. Sobhani, M. Salavati-Niasari, *Journal of Alloys Compound*, 835 (2020) 155240.
- [19] M. Nasrollahzadeh, S.M. Sajadi, A. Rostami-Vartooni, *Journal of Colloid and Interface Science*, 459 (2015) 183-188.
- [20] B. Khodadadi, M. Bordbar, M. Nasrollahzadeh, *Journal of Colloid and Interface Science*, 493 (2017) 85-93.
- [21] M. Nasrollahzadeh, S.M. Sajadi, A. Rostami-Vartooni, S.M. Hussin, *Journal of Colloid and Interface Science*, 466 (2016) 113-119.
- [22] W.D.H. Schneider, A.J.P. Dillon, M. Camassola, *Biotechnology Advances*, 47 (2021) 107685.
- [23] A.C. Paiva-Santos, A.M. Herdade, C. Guerra, D. Peixoto, M. Pereira-Silva, M. Zeinali, F. Veiga, *International Journal of Pharmaceutics*, 597 (2021) 120311.
- [24] K.S. Kumar, T. Ramakrishnappa, *Journal of Environmental Chemical Engineering*, 9(4) (2021) 105365.
- [25] S.N. Naidi, M.H. Harunsani, A.L. Tan, M.M. Khan, *Journal of Material Chemistry B*, 9(28) (2021) 5599-5620.
- [26] N. Omerović, M. Djisalov, K. Živojević, M. Mladenović, J. Vunduk, I. Milenković, J. Vidić, *Comprehensive Reviews in Food Science and Food Safety*, 20(3) (2021) 2428-2454.
- [27] A. Roy, A. Elzaki, V. Tirth, S. Kajoak, H. Osman, A. Algahtani, M. Bilal, *Catalysts*, 11(12) (2021) 1494.
- [28] F. Elmusa, A. Aygun, F. Gulbagca, A. Seyrankaya, F. Göl, C. Yenikaya, F. Sen, *International Journal of Environmental Science and Technology*, 18(4) (2021) 849-860.
- [29] M. Kheradmandfard, H. Minouei, N. Tsvetkov, A.K. Vayghan, S.F. Kashani-Bozorg, G. Kim, D.E. Kim, *Materials Chemistry and Physics*, 262 (2021) 124265.
- [30] M. Sivakami, R. Renuka, T. Thilagavathi, *Journal of Environmental Chemical Engineering*, 8(5) (2020) 104420.
- [31] S. Venkateswarlu, Y.S. Rao, T. Balaji, B. Prathima, N.V.V. Jyothi, *Material Letters*, 100 (2013) 241-244.

- [32] L. Gu, V. Vardarajan, A.R. Koymen, S.K. Mohanty, *Journal of Biomedical Optics*, 17(1) (2012) 018003.
- [33] D. Patiño-Ruiz, L. Sánchez-Botero, L. Tejeda-Benitez, J. Hinestroza, A. Herrera, *Environmental Nanotechnology Monitoring and Management*, 14 (2020) 100377.
- [34] M.S.H. Bhuiyan, M.Y. Miah, S.C. Paul, T.D. Aka, O. Saha, M.M. Rahaman, M. Ashaduzzaman, *Heliyon*, 6(8) (2020) e04603.
- [35] M. Jamzad, M.K. Bidkorpeh, *Journal of Nanostructure in Chemistry*, 10(3) (2020) 193-201.
- [36] H.S. Devi, M.A. Boda, M.A. Shah, S. Parveen, A.H. Wani, *Green Processing and Synthesis*, 8(1) (2019) 38-45.
- [37] H. Muthukumar, M. Matheswaran, *ACS Sustainable Chemistry Engineering*, 3(12) (2015) 3149-3156.
- [38] M. Martínez-Cabanas, M. López-García, J.L. Barriada, R. Herrero, M.E.S. de Vicente, *Chemical Engineering Journal*, 301 (2016) 83-91.
- [39] G.B. Jegadeesan, K. Srimathi, N.S. Srinivas, S. Manishkanna, D. Vignesh, *Biocatalysis and Agricultural Biotechnology*, 21 (2019) 101354.
- [40] T. Wang, X. Jin, Z. Chen, M. Megharaj, R. Naidu, *Science of the Total Environment*, 466 (2014) 210-213.
- [41] H.K. Farshchi, M. Azizi, M.R. Jaafari, S.H. Nemati, A. Fotovat, *Biocatalysis and Agricultural Biotechnology*, 16 (2018) 54-62.
- [42] B. Desalegn, M. Megharaj, Z. Chen, R. Naidu, *Heliyon*, 5(5) (2019) e01750.
- [43] K.S.V. Gottimukkala, R.P. Harika, D. Zamare, *Journal of Nanomedicine and Biotherapeutic Discovery*, 7 (2017) 151.
- [44] P. Karnan, A. Anbarasu, N. Deepa, R. Usha, *International Journal of Current Pharmaceutical Research*, 10(3) (2018) 11-14.
- [45] P.C. Nagajyothi, M. Pandurangan, D.H. Kim, T.V.M. Sreekanth, J. Shim, *Journal of Cluster Science*, 28(1) (2017) 245-257.
- [46] H.K. Handral, A. Pandith, S.D. Shruthi, *Asian Journal of Pharmaceutical and Clinical Research*, 5(4) (2012) 5-14.
- [47] Y. Tachibana, H. Kikuzaki, N.H. Lajis, N. Nakatani, *Journal of Agricultural and Food Chemistry*, 49(11) (2001) 5589-5594.
- [48] K. Velsankar, R. Preethi, P.S. Jeevan Ram, M. Ramesh, S. Sudhahar, *Applied Nanoscience*, 10 (2020) 3675-3691.

- [49] K. Velsankar, V. Vinothini, S. Sudhahar, M. Krishna Kumar, S. Mohandoss, *Applied Nanoscience*, 10(10) (2020) 3953-3971.
- [50] K. Velsankar, R.M. Aswin Kumar, R. Preethi, V. Muthulakshmi, S. Sudhahar, *Journal of Environmental Chemical Engineering*, 8(5) (2020) 104123.
- [51] S.P. Rajendran, K. Sengodan, *Journal of Nanoscience*, (2017) 1-7.
- [52] R. Renuka, K.R. Devi, M. Sivakami, T. Thilagavathi, R. Uthrakumar, K. Kaviyarasu, *Biocatalysis and Agricultural Biotechnology*, 24 (2020) 101567.
- [53] S. Kanagasubbulakshmi, K. Kadirvelu, *Defence Life Science Journal*, 2(4) (2017) 422-427.
- [54] K. Velsankar, S. Sudhahar, G. Parvathy, R. Kaliammal, *Material Chemistry and Physics*, 239 (2020) 121976.
- [55] K. Velsankar, S. Sudhahar, G. Maheshwaran, M. Krishna Kumar, *Journal of Photochemistry and Photobiology B*, 200 (2019) 111650.
- [56] J. Suresh, G. Pradheesh, V. Alexramani, M. Sundrarajan, S.I. Hong, *Advances in Natural Science Nanoscience and Nanotechnology*, 9(1) (2018) 015008.
- [57] Park, D.W., Kim, K.S.: *J. Nanoscience and Nanotechnology*, 11(8) (2011) 7214-7217.
- [58] H.S. Devi, M.A. Boda, M.A. Shah, S. Parveen, A.H. Wani, *Green Processing and Synthesis*, 8(1) (2019) 38-45.
- [59] S. Arsalani, E.J. Guidelli, J.F. Araujo, A.C. Bruno, O. Baffa, *ACS Sustainable Chemical Engineering*, 6(11) (2018) 13756-13765.
- [60] L. Panawala, *Epediaa*, 3 (2017) 1-13.
- [61] M. Premanathan, K. Karthikeyan, K. Jeyasubramanian, G. Manivannan, *Nanomedicine*, 7(2) (2011) 184-192.
- [62] G. Sangeetha, S. Rajeshwari, R. Venckatesh, *Material Research Bulletin*, 46(12) (2011) 2560-2566.
- [63] M. Thiruvengadam, I.M. Chung, T. Gomathi, M.A. Ansari, V.G. Khanna, V. Babu, G. Rajakumar, *Bioprocess and Biosystems Engineering*, 42(11) (2019) 1769-1777.

Biosynthesized Magnetic Nanoparticles using *Rosa gallica* Petals Extract and its Antibacterial Activities against Selected Pathogens for Biomedical Applications

Abstract

In the present work, novel iron nanoparticles (FeNPs) were successfully fabricated by a facile and green synthesis approach by using *Rosa Gallica* extract. The fabricated iron nanoparticles were extensively examined by using UV-visible spectroscopy, Fourier Transform Infrared (FTIR) techniques, powder x-ray diffraction (XRD), Energy dispersive X-ray analysis. The size was measured and found to be the range of 17nm to 45nm. Furthermore, the ability of antibacterial activity of *Rosa Gallica* extract mediated FeNPs was also described against gram positive *staphylococcus aureus* and gram negative bacteria such as *Klebsiella pneumoniae*, *E.Coli* and *Bacillus subtilis*.

5.1 Introduction

A great sustained improvement in nanotechnology is due to its diverse beneficial applications in biomedical therapeutics, drug delivery systems. Nanoparticles have proven to be the key elements used for developing biological capabilities in recent scientific research [1]. Among them, metal nanoparticles have received more attention in recent decades, attributing their usage extensively in medicine, biology and material science [2]. Nano size materials possess specific surface area to the volume ratio and exhibit excellent physico- chemical characteristics in the field of optical, electronic and magnetic and also potential in antimicrobial ability. Iron nanoparticles (FeNPs) are noble and stable materials, capable of offering unlimited benefits such as biolabeling, optical receptors, antimicrobial stuff and also used as electrical conductors [3]. FeNPs containing an efficient inhibitory

ability against several bacterial pathogens was reported and generally found in pharmaceutical industries [4].

The mode of preparation of iron nanoparticles is performed by adapting diverse methods that are enlisted as thermal ion, pyrolysis deposition, advanced microwave irradiation and laser ablation techniques [5]. Among them, chemical deposition techniques have been presently used in the majority of the investigations with sodium borohydride and sodium citrate as reducing agents. This conventional synthesis protocol explained the involvement of metal precursors such as iron nitrate, while sodium borohydride is used as a reducing agent. However, conventional methods of synthesis of metallic nanoparticles were required abundant energy inputs, toxic reagents and were highly expensive with regulated temperature and pressure, resulting in environmental contamination [6].

In contrast, green synthesis of nanoparticles route appeared to be cheap, easily achievable and considered as an alternative for conventional approaches [7, 8]. Biogenic iron nanoparticles are reportedly promising, simple and free from environmental pollutants, an affordable cost. Synthesis enabled in room temperature with sufficient pressure and no sophisticated instrument is required [9]. Moreover, presence of phytoconstituent and aqueous surrounding modify the toxic chemicals and organic solvents [10]. Therefore, green mediated synthesis of nanoparticles has been gaining a top priority in current research. Occurrence of phytochemicals significant quantities such as polyphenols, tannin, flavonoids and other amino acids have exerted therapeutics efficiencies and were extensively studied in earlier investigations [11,12].

Rosa Gallica (Rose) fresh petals (Fig 5.1) are well known for its fragrance and taste. It also exhibits therapeutic potential for human health benefits [13]. *Rosa Gallica* is a unique species, commercially known as Rose plant, possessing abundant quantities of phenolic compounds and were made use of synthesing nanoparticles [14]. Emerging databases have

demonstrated that *Rosa Gallicais* reportedly potentially anti-inflammatory, antioxidant, improved immune response and played a protective role against dietary pathogenic bacteria and related other infections [15]. These phytochemicals are quite responsible for therapeutics and cosmetics properties, that include catechins and caffeine, that are key factors in reducing metal particles, resulting formulation of capping metallic nanoparticles in the application of drug delivery system [16, 17].

By keeping in view their benefits, in the present investigation, a biogenic synthesis of iron nanoparticles using extracts of *Rosa Gallica* plant petals was reported. Such synthesized NPs were characterized carefully with UV-Vis spectrometry, XRD, EDX analysis. Interestingly, we further determined antibacterial ability of synthesized iron nanoparticles, *in-vitro* against selected bacterial pathogens in order to examine its biologically acceptable treatment [18].

5.2 Materials and methods

5.2.1 Materials

Iron (III) chloride and accessory reagents were procured from Sigma-Aldrich, Hi media Biotech, Chennai, Tamil Nadu, India. A complete experiment was used with analytical grade reagents and deionized water. Rose petals were collected from Tamil Nadu Tea Estate (TANTEA), Govt of TN, Udthagamandalam, in India. For antimicrobial assays, culture medium, antibiotics, bovine serum were purchased from High media Biotech chemical Pvt Ltd, Chennai, Tamil Nadu. Rose petals extracts are rich in polyphenols, and other reductive biomolecules containing multiple hydroxyl functional groups such as flavonoids and phenolic compounds. These biocompounds have reduction potential which are mainly cause for the bioreduction of metal ions and stabilization of the resultant nanoparticles.



Fig. 5.1 Rosa Gallica images

5.2.2 Methods

5.2.2.1 Preparation and synthesis of magnetic nanoparticles using Rosa Gallica petals extract

A quantity of 0.01M of Iron (III) chloride solution was taken, by dissolving 100ml of double distilled water and 30ml of extract of *Rosa Gallica* from petals parts were assembled. Add in a drop wise manner, for better amalgamation with solution in room temperature. There was a change in colour, from golden brown solution to black was noticed, indicating the onset of synthesis of nanoparticles. Such synthesized FeNPs scrubbed well by using centrifugation at 10,000 rpm around 15 minutes, resulting in good fabricated nanoparticles. After retrieving the pellets from the tested solution, subsequently suspended in double distilled water and dried for nano powder.

5.2.3 Characterization of magnetic nanoparticles

UV-Vis Spectroscopy

Preliminary reduction process was confirmed by measuring UV-Vis spectra of the diluted sample using deionized water. *Rosa gallica* conciliated iron nanoparticles were scanned in UV-visible spectroscopy within the wavelength range of 200nm to 800nm to detect absorption maxima by employing a shimadzu spectrometer, (Model, UV-2600). The spectra were recorded using deionized water as a reference.

FTIR Spectroscopy

Biosynthesized iron nanoparticles were subjected into FT-IR spectral measurements to investigate the occurrence of possible biomolecules which responsible for the reduction and stabilizing of iron nanoparticles. The measurements of *Rosa gallica* extract and synthesized FeNPs were carried out by JASCO FTIR 4100 measurement at resolution of 4cm^{-1} in KBr pellets [19].

X-Ray Diffraction

Iron nanoparticles were subjected to X-ray diffraction. The morphology size of the particles and profile of synthesized FeNPs was detected, using XRD diffraction pattern, by the (X' Pert Pro – PAnalytic).

SEM

The shape of the nanoparticles was determined by Scanning Electron Microscope (SEM) with Sigma HV-Quantum 200ZIOEDS, at the sophisticated laboratory of National College, Trichy, using SEM-YEGA. The qualitative and quantitative analysis of fabricated FeNPs were performed, using energy dispersive X-ray spectroscope (EDX).

TEM

The size and morphology of the biosynthesized iron nanoparticles was calibrated by Transmission Electron Microscope (TEM). The prepared sample was placed on the carbon coated copper grid, making a thin film of sample on the grid and extra sample was also removed using the cone of a blotting paper and placed in grid box. The thin film on the grid was allowed to stand for 5 minutes to dry. The fine powder of biosynthesized iron nanoparticles has been placed on coated copper grid and the morphology was obtained by using TEM (TEM-JEOL 1200EX, JAPAN).

Vibrating Sample Magnetometer

The magnetic behaviours of biosynthesized iron nanoparticles were determined by using a vibration sample magnetometer (VSM, Cryogenic, UK). The experimental work was conducted at room temperature with increasing magnetic field upto 10 kOe and field sweeping from -10 to +10 kOe.

5.2.4 Antimicrobial activity of iron nanoparticles

In the present investigation, common and popular gram negative bacteria strain, *K.pneumoniae*, *E.Coli* and *Bacillus subtilis* and from positive pathogens, *S.aureus* were used for the examination of *Rose petals* conciliated FeNPs. Efficacy on antimicrobial properties. The tested bacterial pathogens were procured from Microbial Type Culture Collection Center (MTCC), Chandigarh. Antimicrobial properties were determined the following methods described originally by Bauer et al [20], with mere changes based on their laboratory conditions. Mullar Hinton agar was used and different dilution of synthesized NPs such as 10, 20, 30, 40 and 50 μ g, solvent extracts were prepared and placed separately in each petridish, whereas, Nitrofurantoin (300/ μ g) was maintained as control/standard. Experimental plates were incubated, over a day, at 37 $^{\circ}$ C temperature. Further, zone diameter was measured using millimetre ruler and noted expressed with nm units. Minimum inhibitory concentration (MIC) was evaluated against each strain. Subsequently, microorganisms were incubated, evaluated for low inhibitory concentration and scaled up. The whole experiment was performed in triplicate with mean value (Σ) used for statistical analysis.

5.3 Results and Discussion

5.3.1 UV- visible analysis

In this section, table (Table.5.1) showed the process of colour transformation due to the fabrication of nanoparticles during period and post period while blending with extract

of *Rosa gallica*. The UV visible absorption spectra of so formed FeNPs have been depicted in figure (Fig.5.2). Usually, the reduction reaction was noticed while changes occurred in the colour of the solution, indicating golden brown to black colour.

Table 5.1 Change in color of the solution during synthesis of magnetic nanoparticles

S. No.	Solution	Color change Before reduction	Color change After Reduction	Time
1.	<i>Rosa gallica</i> Extract	Pale yellow	Black	Immediately
2.	0.01M FeCl ₃ Solution	Golden brown		

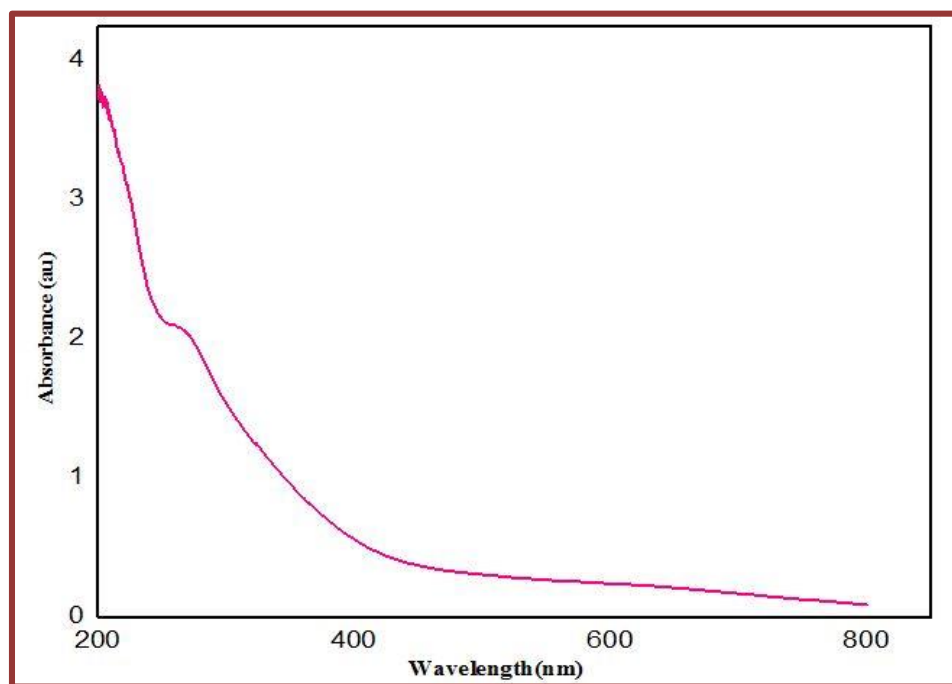


Fig.5.2 UV-vis spectrum of *Rosa gallica* extract in green synthesis nanoparticles

The UV-vis spectrum of synthesized iron nanoparticles showed (Fig.5.2) the maximum absorbance at about 263 nm which may be assigned to the surface plasmon absorption of iron nanoparticles. The peak at 205 nm in UV-Vis Spectrum for the extract

assigned to $\pi \rightarrow \pi^*$ transition confined in the phenolic compounds. After the addition of the FeCl_3 solution to *Rosa gallica* extract, the brown color solution is immediately shifted into black color which intimates the form of Fe^0 from Fe^+ . Moreover, metal nanoparticles contain unique characteristics such as prevalent free electrons to confer surface resonance absorbance that, attributed to the mutual vibrating electrons of metal NPs in waves of light energy. The obtained aspects of curve peaks denoting the surface resonance of fabricated nanoparticles. The absorption spectrum shows a decline trend of the absorbance coupled with a shift in the wavelength range from 263 to 205 nm. It has been reported that a strong association prevailing between the intensity of the plasmon resonance bands and has shown to be a decrease in the band width was observed [21]. The UV spectra results showed an increase in the intensity of absorbance. Surface plasmon peaks that elute at 263 nm and gradually declines to the lower wavelength at maximum concentration. Prevention studies were favoured to our finding that vibration in the curve might have been attributed to the indicator of shape and size of FeNPs [22, 23]. In another investigation, Absorbance of colloidal nanoparticles in the specific wavelength attributed to the vibration of surface plasmon vibration [24].

5.3.2 Fourier Transform-InfraRed (FT-IR) Analysis

The FT-IR spectrum of *Rosa gallica petals* extract is shown in figure (Fig.5.3) and was carried out to identify the functional biomolecules caused for the reduction and capping agent of the iron nanoparticles. The C-H bending of aromatic compounds absorption occurs at 819 cm^{-1} . The alkane residue is detected from C-H stretching absorptions at 1446 cm^{-1} . As C-H does not take part in hydrogen bonding, its absorption position is little effected by chemical environments. Since the most of the organic compounds possess alkanes residue, C-H absorption bands in a spectrum are of little diagnostic value [25].

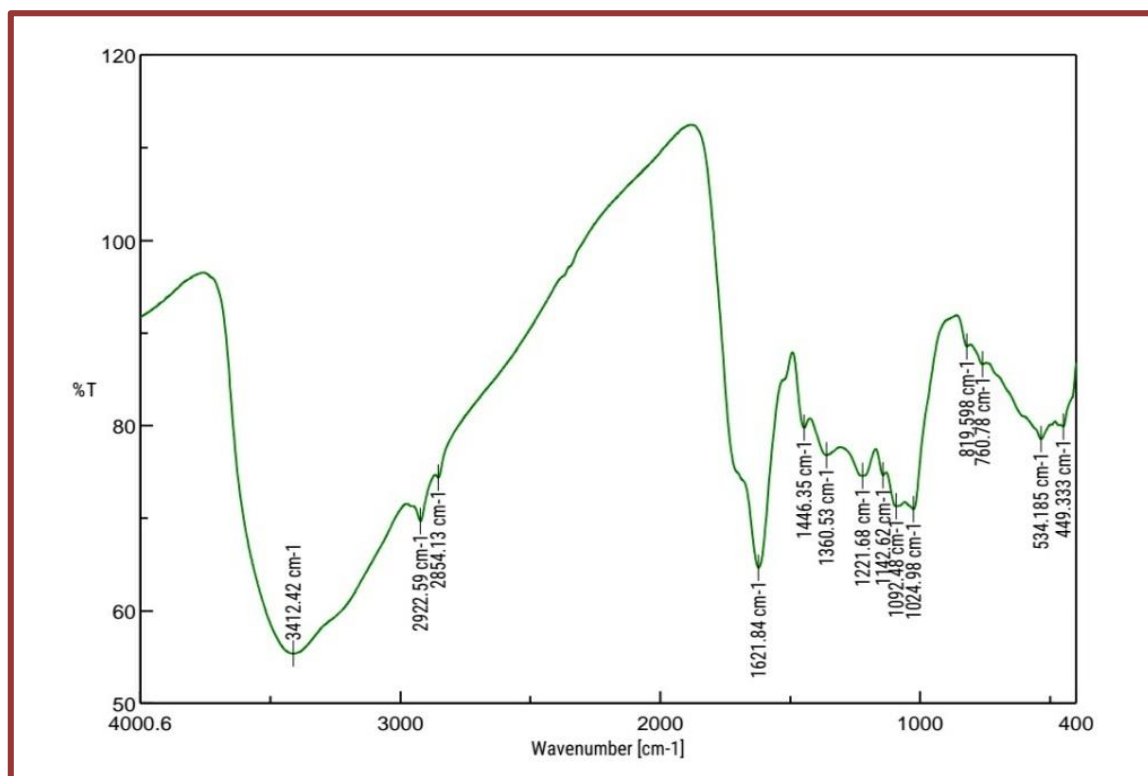


Fig.5.3 FT-IR spectrum of biosynthesized iron nanoparticles using *Rosa gallica* extract

The C=O stretching absorption in amides takes place at 1621cm^{-1} . The existence of nitrogen atom has electro-negative atom effect but a lone pair of electrons present on nitrogen atoms are involved in conjugation which tend to decrease C=O force constant. This effect is more prominent in amides groups because of the greater mobility of electron pair on nitrogen atom (less electronegative) and hence, it has greater participation in conjugation. The peak at 3412cm^{-1} indicates the O-H stretching vibrations of phenols group. Phenols form intermolecular hydrogen bonds more readily than alcohols [26]. It can be concluded that, aspects of the obtained peaks for iron nanoparticles capped with functional molecules that reduced the iron reaction in iron nanoparticles fabrication due to the presence of *Rosa gallica petals* extract [27].

5.3.3 X-ray diffraction analysis

The crystalline nature of FeNPs was further confirmed by X-Ray diffraction (XRD) analysis. The pattern of X-Ray diffraction for fabricated iron nanoparticles mediated by the petals extract of *Rosa gallica* as shown in the figure 5.4 which exhibited sharp peak including diffraction angle at 32°. The average crystallite size of the FeNPs was calculated using the peak (111) according to Debye Scherrer equation [28] and found to be in the range of 24 nm, indicating values are used for calculating unit cell dimension that enable to identify (hkl) Miller indices value, can be obtained by employing technique as depicted in table 1. According to the Debye-Scherrer formula,

$$d = k\lambda / \beta \sin\theta$$

Here, d is the particle size of the nanoparticles (nm), k is the Scherrer constant (0.9), λ is the wavelength of X-ray (0.15406 nm), β is the full width half maximum of XRD peak, and θ is Bragg diffraction angle.

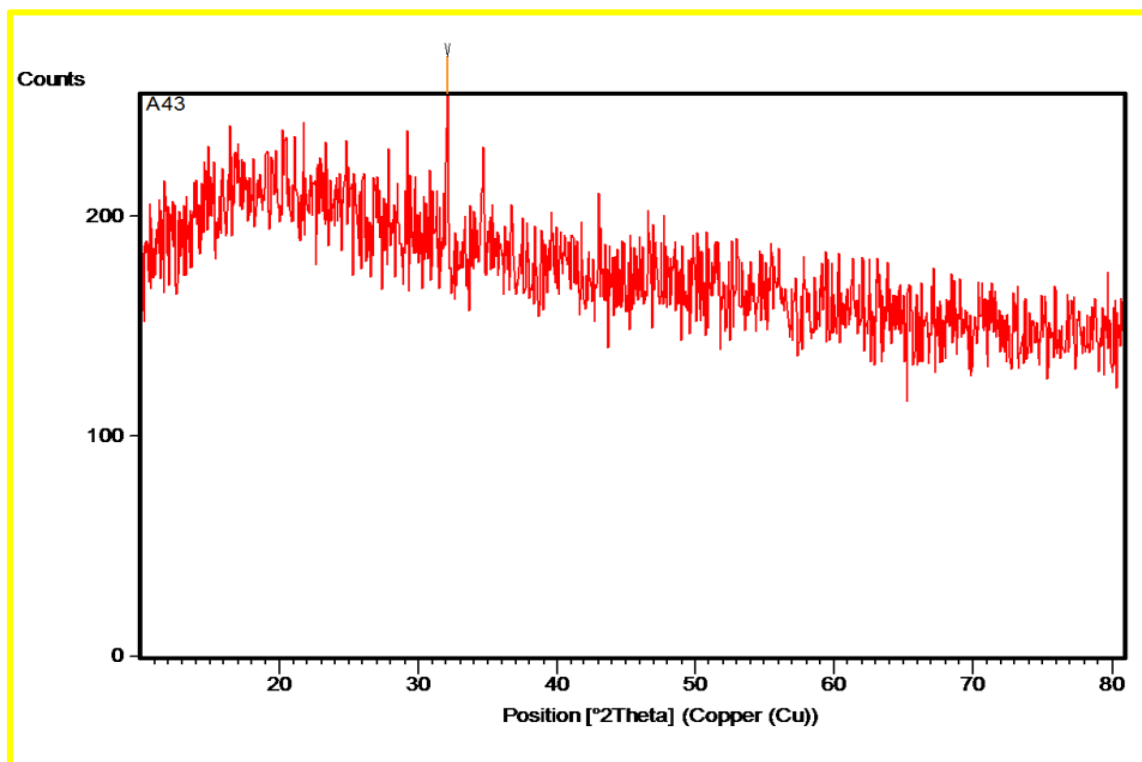


Fig.5.4 XRD pattern of biosynthesized iron nanoparticles using *Rosa gallica* extract

Outcome of our experiments of XRD were compatible with earlier investigations that evidence the preferred FeNPs is shown to be highly crystalline, with FCC crystalline structure and confirmed by lattice parameter. 2θ values for tested and control (JCPDS) values file No 04-0783 of FeNPs resulting in equal and assured synthesis of iron nanoparticles with FCC well balanced shape.

5.3.4 SEM and EDAX spectral analysis

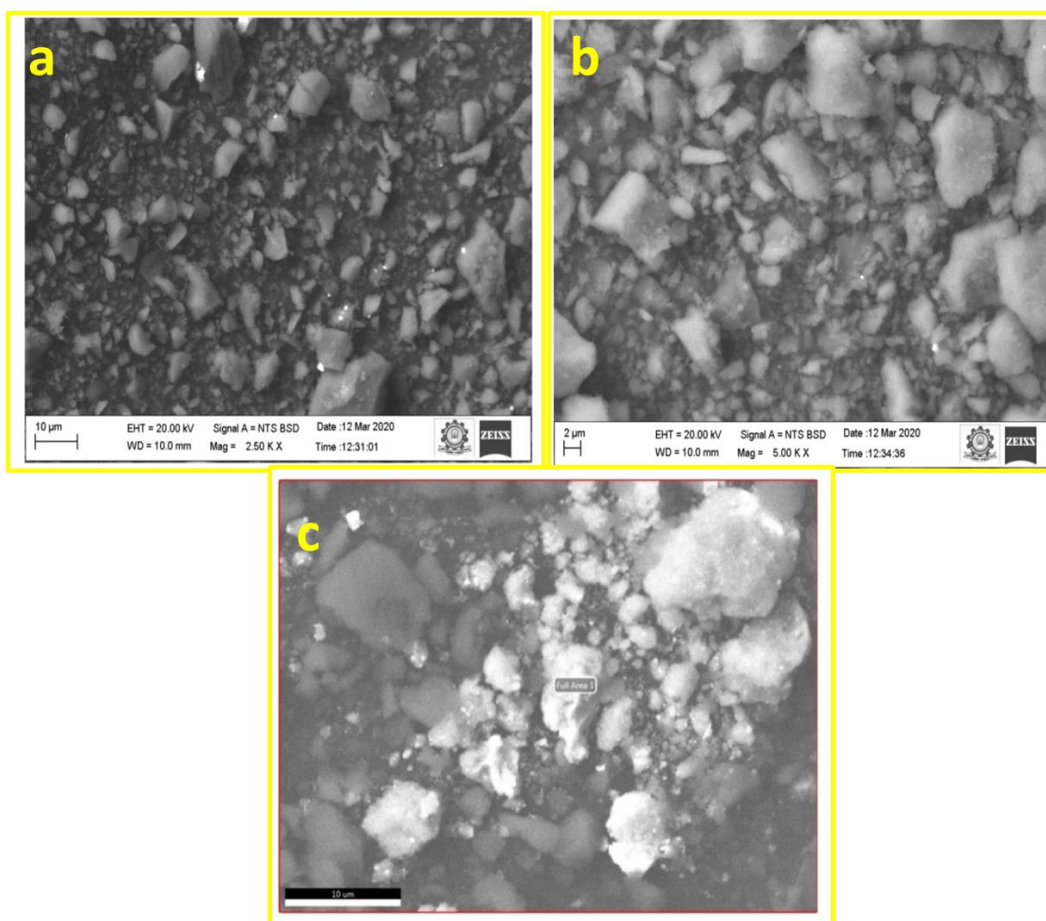


Fig.5.5 (a-b) SEM images of biosynthesized iron nanoparticles using *Rosa gallica* petals extract

External morphological structure of fractional iron nanoparticles was evaluated by scanning electron Microscope (SEM). As indicated in the figure (Fig.5.5a-b) depicted that shape of FeNPs was found to be FCC in nature. EDX was also performed to understand the chemical profile of the *Rosa gallica* petals extract (Fig.5.6). Appearance of sharp peak has

confirmed the nano sized crystalline iron, whereas the Cl indexed about 0.5V might have been derived from the extract of *Rosa gallica Petals* [29]. These findings were agreed with prior investigation as demonstrated by Wallace et al.[30].

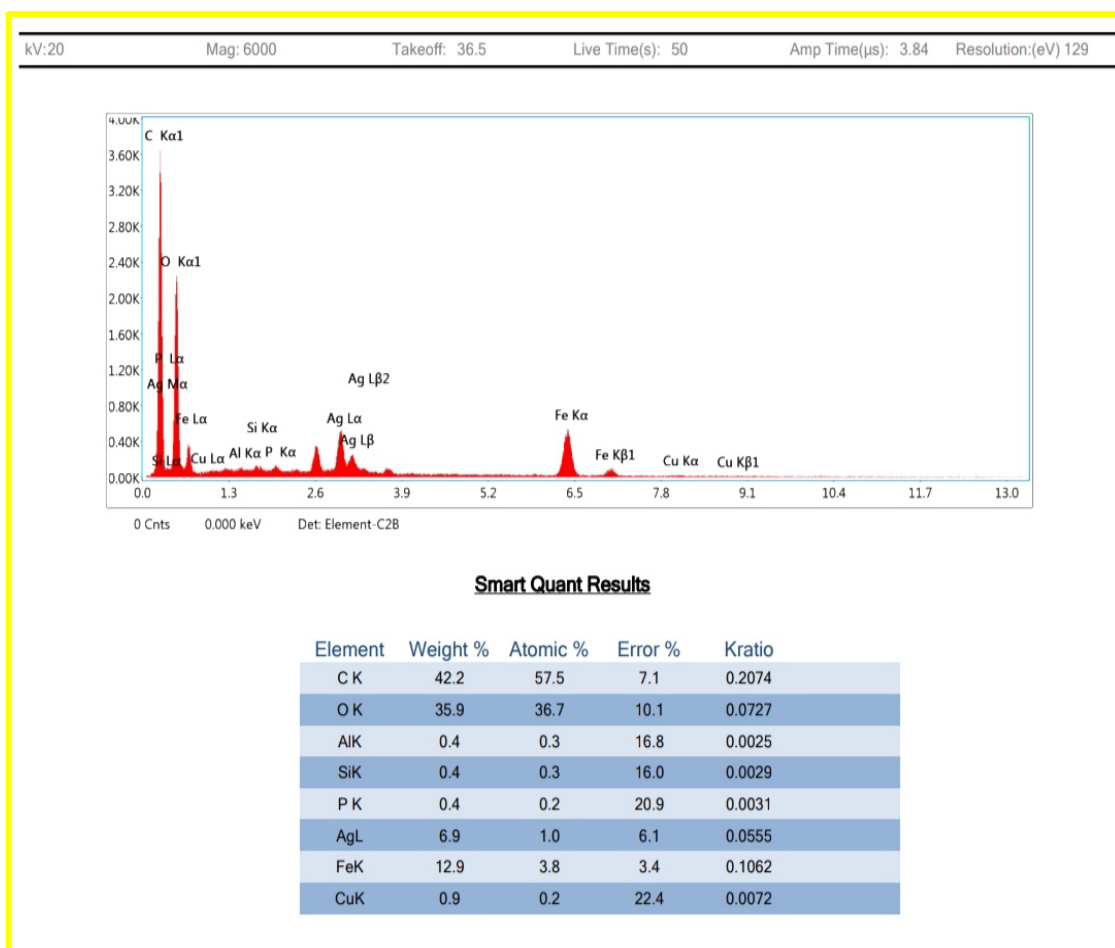


Fig.5.6 EDAX images of biosynthesized iron nanoparticles using *Rosa gallica* petals extract

5.3.5 TEM Analysis

TEM micrographs of the iron nanoparticles biosynthesized by using *Rosa gallica* extract are shown in figure (Fig.5.7). TEM images revealed that the most of the iron nanoparticles were spherical in shape with a lower degree of agglomeration [31,32,&33]. It was also noticed that these iron nanoparticles were covered by a thin layer of biological matrix showing the role of biological compounds in *Rosa gallica* extract act as agents which

are responsible for reducing the iron (III) ions to iron nanoparticles and also controlling clustering [34,35].

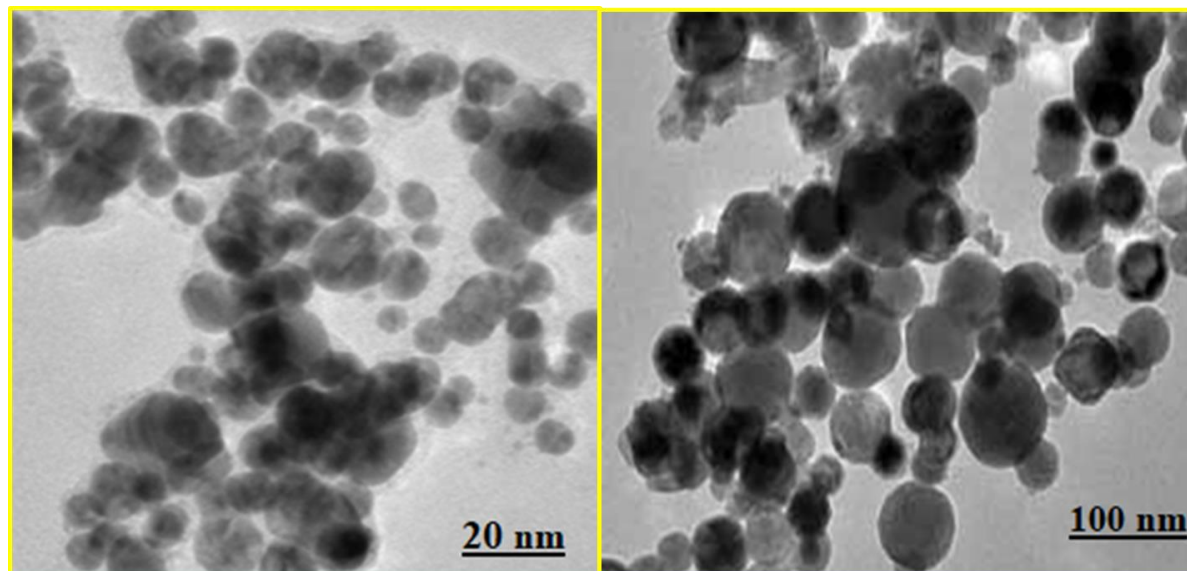


Fig.5.7 TEM micrographs of biosynthesized iron nanoparticles using *Rosa gallica* Extract

5.3.6 VSM Analysis

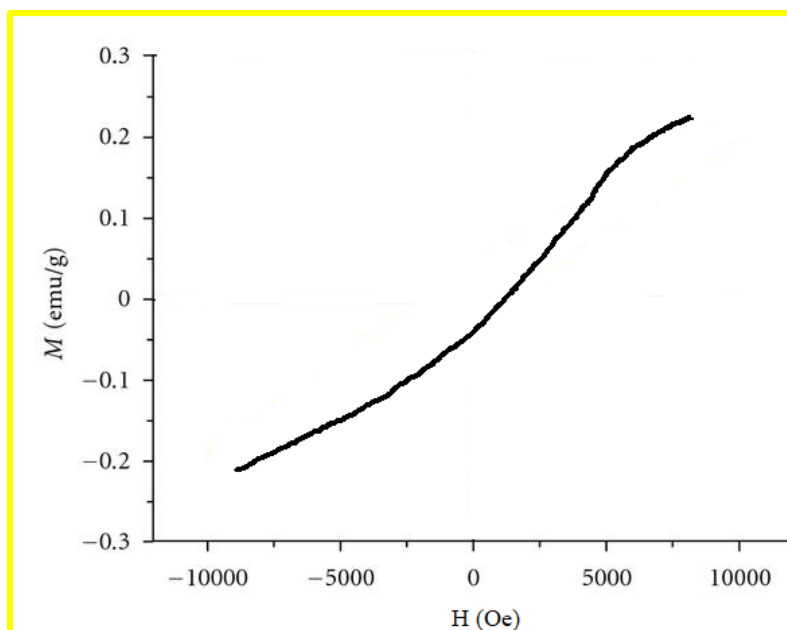


Fig.5.8 Magnetization curve of biosynthesized iron nanoparticles using *Rosa gallica* extract

Figure 5.8 showed that the magnetic behaviours of biosynthesized iron nanoparticles by using *Rosa gallica* extract examined by a vibrating sample magnetometer at room temperature. A hysteresis curve from Magnetization-Magnetic field (M-H) graph was observed which represents that the iron nanoparticles have minimum properties of ferromagnetic materials [36,37, 38 &39]. Ferromagnetic materials were attracted by a strong externally applied magnetic field and form induced magnetic fields internally in the direction of the applied magnetic field [40].

5.3.7 Antibacterial properties of synthesized FeNPs

Antibacterial potential of the Iron nanoparticles mediated by *Rosa gallica* petals extract (Fig.5.9) was determined against gram positive *S.aureus* (ID ATCC 29213) and gram negative strain, *K. pneumoniae* (ATCC 700603), *E.Coli* and *B.subtilis* with diverse concentrations (Table 5.2) denoted that the MIC values were achieved after over a period of day [41]. Incubation with fabricated nanoparticles obviously, it can be visualised, the effect of antibacterial action of synthesized FeNPs was close specificity with pathogens [42]).

Results showed that *S. aureus* exhibited strong rigidity due to its cell wall composition and forbids to invade iron nanoparticles into the cell crossing cell wall. Whereas gram negative bacterial strain, *K.pneumoniae* have lower vulnerability to the antibiotics as reported earliest by Sarkar et al [43].

The presented figure (Fig.5.10) indicated the strength of the antibacterial potential against four pathogens among them *K. pneumoniae* exerted a significant zone of inhibition when compared with *S.aureus*. Moreover, while FeNPs with standard (300µg Nitrofurantoin), it exerted effective zone of inhibition even in the least concentration (10µg) and indicated the potential of FeNPs to fight and compete against harmful pathogens [44]. The effects may be underlined by different factors such as size of FeNPs chemical profile, surface resonance and assemblage state [45]. The mechanisms involved in toxicity against

pathogens involve direct affinity with strain and surface area of NPs has played a crucial role.

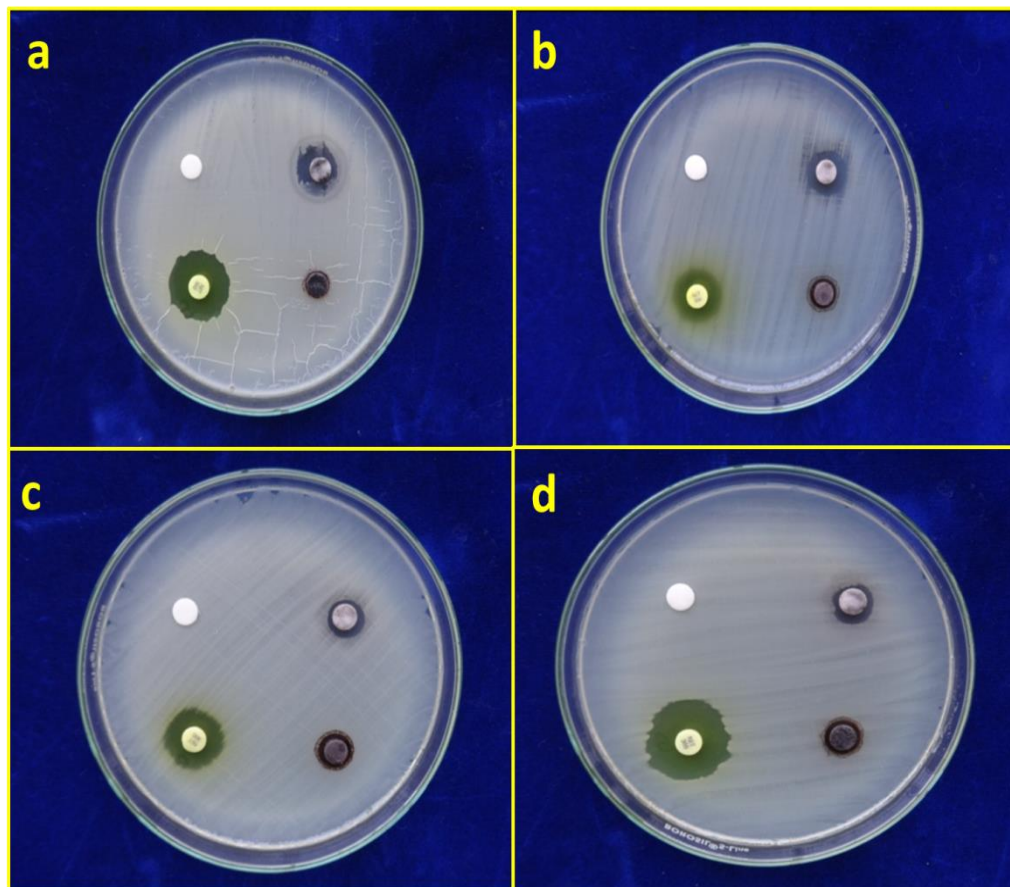


Fig. 5.9 Antibacterial activity of iron nanoparticles using *Rosa gallica* petals extract
 a) *Escherichia coli* b) *Klebsiella pneumoniae* c) *Staphylococcus aureus* d) *Bacillus subtilis*

Table 5.2 Assay of antibacterial activity

S. No.	Bacteria Name	Zone of Inhibition (mm in diameter)	
		Standard*	FeNPs
1	<i>Escherichia coli</i>	17	18
2	<i>Klebsiella pneumoniae</i>	16	20
3	<i>Staphylococcus aureus</i>	21	22
4	<i>Bacillus subtilis</i>	19	21

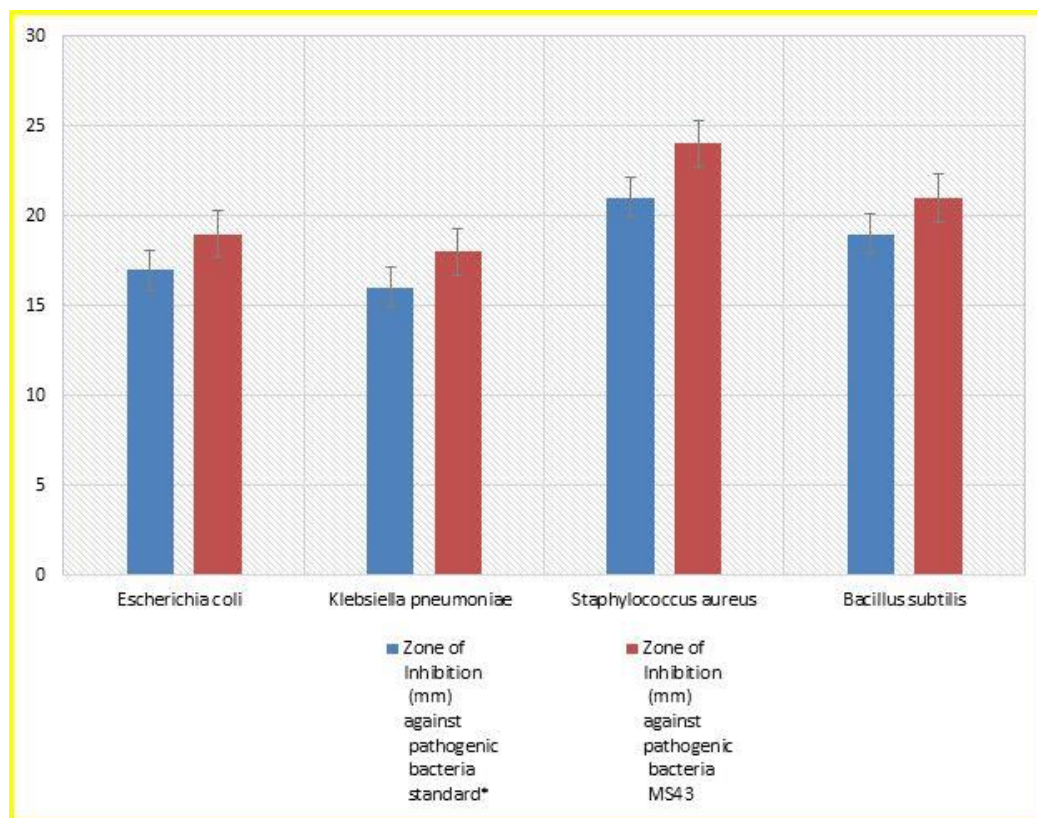


Fig. 5.10 Inhibition zone of biosynthesized FeNPs against various bacteria

Infact, Antibacterial actions remain still unclear. It has been presumed that magnetic nanoparticles directly touched the pathogen cell wall due to the affinity of proteins possessing sulphur residue [46, 47]. This action would lead to permeability distraction causing effect of intracellular content, resulting in DNA injury, ROS production and ultimately end with death of bacteria [48].

Besides, nano size of the particle might increase the invasion into the cell wall while photo constituents on the particle surface can accelerate the antimicrobial properties [49]. Studies have deciphered that the presence of phyto compound, catechin gallate in *Rose Petals* caused the injury to the cell wall and cytoplasmic membrane related function [50]. Interestingly, W. R. Rolim et al., 2019 reported that FeNPs synthesized from Rose petals have exhibited more effectiveness in antimicrobial activity than PEG-FeNPs.

5.4 Conclusion

This study has revealed the *Rosa gallica* petals extract was more compatible for the biosynthesis of iron nanoparticles. The formation of iron nanoparticles has been confirmed primarily by changing of immediate black colour while adding *Rosa gallica* petals extract to iron III chloride solution. It has been further confirmed by UV-vis spectroscopic analysis. From X-ray diffraction analysis, the average crystalline size of iron nanoparticles was calculated by using Debye Scherrer equation and was found to be in the range of 24nm. Most of the iron nanoparticles have spherical in shape was identified by TEM analysis. Moreover, iron nanoparticles have potential for antimicrobial activity against harmful bacteria strains., it can be suggested that the synthesis of iron nanoparticles from green route is an effortless, hazardless, affordable and reliable. Due to the fabricated magnetic nanoparticles exhibited highly potent antibacterial actions against *K.pneumoniae* strain and stable nature, it can also be suggested that these magnetic nanoparticles may be used for various biomedical and biotechnological applications such as biosensors, MRI, Multi Drug Resistance pathogens in clinical settings, MDR pathogens for protecting human health and environment.

References

- [1] A. Fakhri, M. Pourmand, R. Khakpour, S. Behrouz, *Journal of Photochemistry and Photobiology B: Biology*, 149 (2015) 78-83.
- [2] K. Yokohama, D.R. Welchons, *Nanotechnology*, 18 (2007) 105101–105107.
- [3] M. Zargar, S. Shameli, G. Reza Najafi, F. Farahani, *Journal of Industrial and Engineering Chemistry*, 20(6) (2014) 4169–4175.
- [4] H. Jiang, S. Manolache, A.C. Lee Wong, F.S. Denes, *Journal of Applied Polymer Sciences*, 93 (2004) 1411–1422.
- [5] K. Ranhoszek-Soliwoda, E. Tomaszewska, E. Socha, P. Krzyczmonik, A. Ignaczak, P. Orłowski, M. Krzyzowska, G. Celichowski, J. Grobelny, *Journal of Nanoparticle Research*, 19 (2017) 273.
- [6] N. Durán, A.B. Seabra, *Current Nanoscience*, 14 (2018) 82–94.
- [7] A.B. Seabra, N. Durán, *Metals*, 5 (2015) 934–975.
- [8] P. Singh, Y.J. Kim, D. Zhang, D.C. Yang, *Trends Biotechnology*, 34 (2016) 588–599.
- [9] N.M. Salem, L.S. Albanna, A.M. Awwad, *Environmental Nanotechnology, Monitoring & Management*, 6 (2016) 83–87.
- [10] A. Ebrahiminezhad, A. Zare-Hoseinabadi, A.K. Sarmah, S. Taghizadeh, Y. Ghasemi, A. Berenjian, *Molecular Biotechnology*, 60 (2018) 154–168.
- [11] N. Durán, P.D. Marcato, M. Durán, A. Yadav, A. Gade, M. Rai, *Applied Microbiology and Biotechnology*, 90 (2011) 1609–1624.
- [12] S. Ahmed, M. Ahmad, B.L. Swami, S. Ikram, *Journal of Advance Research*, 7 (2016) 17–28.
- [13] J.Y. Song, B.S. Kim, *Bioprocess and Biosystem Engineering*, 32 (2009) 79–84.
- [14] M. Flores-González, M. Talavera-Rojas, E. Soriano-Vargas, V. Rodríguez-González, *New Journal Chemistry*, 42 (2018) 2133–2139.
- [15] M. Singh, A.K. Mallick, M. Banerjee, R. Kumar, *Bulletin Material Science*, 39 (2016) 1871–1878.
- [16] B.S.O. Silva, A.B. Seabra, *Biointerface Research Applied Chemistry*, 6 (2016) 1280–1287.

- [17] D. Ramdani, A.S. Chaudhry, C.J. Seal, *Journal of Agriculture and Food Chemistry*, 61 (2013) 4961–4967.
- [18] A. Fakhri, M. Pourmand, R. Khakpour, S. Behrouz, *Journal of Photochemistry and Photobiology B: Biology*, 149 (2015) 78–83.
- [19] H. Agarwal, S.V. Kumar, S. RajeshKumar, *Resource-Efficient Technologies*, 3 (2017) 406–413.
- [20] A.W. Bauer, W.M.M. Kirby, J.C. Sherris, M. Truck, *American Journal of Clinical Pathology*, 45 (1966) 493–496.
- [21] W. Zhang, X. Qiao, J. Chen, *Chemistry and Physics*, 330 (2006) 495–500.
- [22] L. Kelly, E. Coronado, L.L. Zhao, G.C. Schatz, *Journal of Physical Chemistry B*, 107 (2003) 668–677.
- [23] K.L. Lee, M.A. El-sayed, *Journal of Physical Chemistry B*, 110 (2006) 19220–19225.
- [24] E.C. Njagi, H. Huang, L. Stafford, H. Genuino, H.M. Galindo, J.B. Collins, G.E. Hoag, S.L. Suib, *Langmuir*, 27 (2011) 264–271.
- [25] B.P. Gaire, L. Subedi, *Chinese Journal of Integrative Medicine*, 11 (2014) 1–8.
- [26] M. Sivakami, R. Renuka, T. Thilagavathi, *Journal of Environmental Chemical Engineering*, 8(5) (2020) 104420.
- [27] J.K. Patra, K. Hun Beak, *Green Chemistry letters and Reviews*. 9(2) (2016) 132–142.
- [28] N. Durán, M. Durán, M.B. de Jesus, A.B. Seabra, W.J. Fávaro, G. Nakazato, *Nanomedicine*, 12 (2016) 789–799.
- [29] N. Durán, A.B. Seabra, *Current Nanoscience*, 14 (2018) 82–94.
- [30] W.R. Rolim, M.T. Pelegriño, Bruna de Araújo Lima, L.S. Ferraz, F.N. Costa, J.S. Bernardes, T. Rodrigues, M. Brocchi, A.B. Seabra, *Applied Surface Science*, 463 (2019) 66–74.
- [31] M. Martínez-Cabanas, M. López-García, J.L. Barriada, R. Herrero, M.E.S. de Vicente, *Chemical Engineering Journal*, 301 (2016) 83–91.
- [32] M. Li, P. Zhang, M. Adeel, Z. Guo, A.J. Chetwynd, C. Ma, T. Bai, Y. Hao, Y. Rui, *Environmental Pollution*, 269 (2021) 116134.
- [33] D. Patiño-Ruiz, L. Sánchez-Botero, L. Tejeda-Benitez, J. Hinstroza, A. Herrera, *Nanotechnology Monitoring and Management*, 14 (2020) 100377.

- [34] T. Wang, X. Jin, Z. Chen, M. Megharaj, R. Naidu, *Science Total Environment*, 466 (2014) 210-213.
- [35] L.T. Kuhn, A. Bojesen, L. Timmermann, M.M. Nielsen, S. Morup, *Journal of Physics Condensed Matter*, 14 (2002) 13551–67.
- [36] X. Zhang, S. Lin, Z.L. Chen, M. Megharaj, R. Naidu, *Water Research*, 45 (2011) 3481–8.
- [37] Y. Zhao, Q. Yue, Q. Li, X. Xu, Z. Yang, X. Wang, *Chemical Engineering Journal*, 193 (2012) 161–8.
- [38] C.B. Wang, W.X. Zhang, *Environmental Science and Technology*, 31 (1997) 2154–6.
- [39] L.T. Kuhn, A. Bojesen, L. Timmermann, M.M. Nielsen, S. Morup, *Journal of Physics Condensed Matter*, 14 (2002) 13551–67.
- [40] D. Bhattacharya, G. Rajinder, *Critical Review of Biotechnology*, 25 (2005) 199-204.
- [41] D. De, M.M. Mandal, S.S. Gauri, R. Bhattacharya, S. Ram, S.K. Roy, *Journal of Biomedicine and Nanotechnology*, 6 (2010) 138-44.
- [42] M. Pattanayak, P.L. Nayak, *World Journal of Nano Science and Technology*, 2 (2013) 6-9.
- [43] B. Sarkar, S. Bhattacharjee, A. Daware, P. Tribedi, K.K. Krishnan, P.S. Minhas, *Nanoscale Research Letters*, 10 (2015) 371.
- [44] Z. Chen, T. Wang, X. Jin, Z. Chen, M. Megharaj, R. Naidu, *Journal of Colloid Interface Science*, 398 (2013) 59-66.
- [45] R.K. Das, B.B. Borthakur, U. Bora, *Material Letters*, 64 (2010) 1445-1447.
- [46] T. Wang, J. Su, X. Jin, Z. Chen, M. Megharaj, R. Naidu, *Journal of Hazardous Materials*, 262 (2013) 819-825.
- [47] T. Shahwan, S.A. Sirriah, M. Nairat, E. Boyacı, A.E. Eroglu, T.B. Scottc, K.R. Hallam, *Chemical Engineering Journal*, 172 (2011) 258-266.
- [48] P.P. Gan, S.H. Ng, Y. Huang, S.F. Li, *Bioresource and Technology*, 113 (2012) 132–135.
- [49] L. Huang, X. Weng, Z. Chen, M. Megharaj, R. Naidu, *Spectrochimica Acta A*, 130 (2014) 295–301.
- [50] X. Weng, L. Huang, Z. Chen, M. Megharaj, R. Naidu, *Industrial Crops Productions*, 51 (2013) 342–347.

Antimicrobial Efficacy of Iron Nanoparticles (INPs) using *Camellia Sinensis* Leaves Extract an Alternate Approach

Abstract

In the present investigation, a simple traditional heating process was employed to fabricate iron nanoparticles (INPs), concealed from *Camellia sinensis* leaf extract (Green tea plant), used for its medicinal properties. The formation of INPs was confirmed by the color change and further examined by UV-vis spectroscopy. The results have showed that the size of the synthesized INPs was found to be 21nm by using XRD. The morphology was characterized by SEM and EDX techniques which ensured the synthesized INPs with nano sized crystalline affirmed with Fe metal. FT-IR study confirmed the attachment of bioactive molecules of plant on the surfaces of INPs. The Vibrating Sample Magnetometer (VSM) revealed the ferromagnetic behavior of prepared INPs. Moreover, antibacterial activities of green tea leaf extract mediated INPs against both gram-positive bacterial strains such as *Staphylococcus aureus* and *Bacillus subtilis* and gram-negative bacteria such as *Klebsiella pneumoniae* and *Escherichia coli*, were examined. The results described that the much higher inhibition zone of prepared INPs upon human pathogenic bacteria.

6.1 Introduction

Metal based nanoparticles are the inorganic elements and most familiar, promising remedy, against resistance pathogens to the chemical antibiotics. They exhibited actions against bacteria targeting numerous biomolecules, arbitrating emergence of resistance strains [1]. Fabrication of metal-based NPs, has been extensively studied over the last decades and widely described its applications in the fields of cosmetics and textiles, hence forth [2]. Characterization of metal-based iron nanoparticles (INPs) has been carried out

using diverse sophisticated techniques. These offer unlimited information on its morphology, physico-chemical, electrical characteristic features of metal based INPs, and played a vital part in their *in-vivo* actions. The desirable properties of INPs are shape size, rigidity and end surface energy [3]. Their multifaceted properties confer new avenues and endless quest for comfortable synthesis route and composition. However, recent research has been targeted to other precise metals such as silver, gold, copper, zinc and iron [4,5].

The developed synthesis routes can be grouped as physical, chemical and recently emerged biological methods [6,7]. INPs have unique nanostructures used in various fields such as biomaterials and biomedical research using their most relevant properties of biocompatibility, ability to change a surface, and its high surface area to the volume ratio [8]. Their properties caused a major portion of the atom to occupy the surface to make them versatile, compared to the bulk materials. This unique feature is reportedly responsible for catalytic reactions and it has been extensively described earlier in various investigations [9,10]. Moreover, INPs applications are used in a wide spectrum of environmental cleaning technology and utilized as nanosorbents and photocatalysts [11].

Iron nanoparticles are also used in detoxification techniques [12], and waste water treatment due to its ability to clean toxic and deteriorating hazardous materials from water, that attracted considerable attention in water treatment measures [13]. INPs possess the potential to remove the pollutants with higher capability than bulk materials were reported [14]. There is an increasing demand for their bulk production with cost effective, in spite of various physical and chemical methods of preparations available for INPs [15, 16]. Nevertheless, existing methods have shown to be highly expensive, involvement of toxic reagents and tedious processing protocols. Recently, green synthesis of INPs route appeared to be cheap, easily accessible and achievable and alternative for classical approaches [17].

C.sinensis is a well-known species for its pleasant smell and possessing abundant quantities of phenolic phyto compounds and can be used for fabricating nanoparticles [18]. Emerging data evident that *C.sinensis* possesses ability in anti-inflammatory, antioxidant, improved immune response and showed protective role against dietary pathogenic bacteria and related harmful infections [19, 20]. The phytochemicals including catechins and caffeine are reportedly responsible for therapeutics and cosmetics properties and used as key factors in reducing metal particles, for the manufacturing capping metallic nanoparticle applied, in drug delivery system [21].

All taking into account, in the present investigations were reported the synthesis of INPs using leaf extract of *C.sinensis* and characterised them carefully with UV-Vis spectrometry, XRD, EDX mechanistic analyses. In order to examine the susceptibility of INPs to the biological organisms, the antibacterial ability of synthesized INPs, *in-vitro* against selected gram positive and gram-negative bacteria strains were determined.

6.2 Materials and methods

6.2.1 Plant collection

Green tea leaves were collected from Tamil Nadu Tea Estate (TANTEA), Govt of TN, Udhamandalam, in India. Ferric chloride and accessory reagents were procured from Sigma-aldrich, Hi media Biotech, Chennai, Tamil Nadu, India. A complete experiment was used with analytical grade reagents and water. For antimicrobial assays, culture medium, antibiotics, bovine serum were purchased from High Media Biotech Chemical Pvt Ltd, Chennai, Tamil Nadu.

6.2.2 Preparation of extract and synthesis of INPs using *C. sinensis* leaves

10 grams quantity of green tea was amalgamated in 100ml of deionized water and heated upto 80°C temperature for the preparation of tea extract and the extract was filtered for avoiding particles contaminant. Subsequently, the collected solution was added with

0.01M Ferric chloride (FeCl_3) in 30ml of green tea extract, a sudden black colour was noticed, indicating onset of fabrication of INPs [22]. These formed solutions were scrubbed well using centrifugation at 10,000 rpm for 15 minutes, resulting in good pallet formation and washed well with deionized water, followed by a drying at 60°C for further analysis.

6.2.3 Characterization methods

C.sinensis conciliated iron nanoparticles were scanned in UV- visible spectroscopy within the wavelength range of 200nm to 800 nm to detect absorption maxima by employing a Shimadzu spectrometer, (Model, UV-2600). To investigate the occurrence of active functional groups in *C.sinensis* leaf extract and synthesized INPs were carried out by FTIR [23]. The morphology size of the particles and profile of synthesized INPs was detected, using XRD diffraction pattern, by the XPERT-PRO. Moreover, the shape of the iron nanoparticles was determined by Scanning Electron Microscope (SEM) with Sigma HV-Quantum 200ZIOEDS, at the sophisticated laboratory of Kalasalingam university, using SEM-YEGA. The qualitative and quantitative analysis of fabricated INPs were performed, using energy dispersive X-ray spectroscope (EDX).

6.2.4 Microorganisms

Three bacterial strains chosen for studies of antibacterial assay were two gram positive bacteria and two gram negative bacteria consigned from Institute of Microbial Technology, Chandigarh, India. Bacterial cultures were prepared in Mueller Hinton Broth (Hi- Media, Pvt. Ltd., Mumbai, India) and maintained for 24 h at 37°C . The cell suspensions were diluted with sterile MHB to provide an initial cell count of about 10^6 CFU/ml.

6.2.5 Antibacterial activity

In the present investigation, common and popular gram negative bacteria strains, such as *K.pneumoniae* and *E.coli* and gram positive bacteria such as *B.subtilis* and *S.aureus* were used and examined green tea leaf conciliated INPs efficacy on antibacterial properties.

The tested bacterial pathogens were procured from Microbial Type Culture Collection Center (MTCC), Chandigarh. Antimicrobial properties were determined the following methods described by Gottimukkala et al. [24] with mere changes based on their laboratory conditions. Mullar Hinton agar was used and different dilution of synthesized INPs such as 10, 20, 30, 40 and 50 μ g, solvent extracts were prepared and placed separately in each petridish, whereas, Nitrofurantoin (300/ μ g) was maintained as control/standard. Experimental plates were incubated, over a day, at 37°C temperature. Further, zone diameter was measured using millimetre ruler and noted expressed with nanometer units. Minimum inhibitory concentration (MIC) was evaluated against each strain. Subsequently, microorganisms were incubated, evaluated for low inhibitory concentration and scaled up. The whole experiment was performed in triplicate with mean value (Σ) used for statistical analysis.

6.3 Results and Discussion

In this section, the characterization of synthesized INPs conciliated from tea extract using green synthesis routes were discussed. Furthermore, potential antimicrobial activity against selected bacterial strains were reported. The figure (Fig.6.1). Showed transformation of colour while FeCl₃ was added with green tea extract, illustrated the fabrication of INPs [25].



Fig.6.1 Color changes of iron nanoparticles fabrication a) FeCl₃ b) Green tea leaves extract c) After plant extract added with FeCl₃ solution

6.3.1 UV-Vis analysis

UV-vis spectrum has revealed the formation of dark black color was attributed to the reduction reaction and was documented with visual proof [26, 27]. Usually, INPs contain more relevant properties such as increasing free electrons to offer surface resonance absorbance, due to the vibrating electrons of INPs in light energy. The obtained aspects of peaks and curves indicated the surface resonance of synthesized INPs (Fig.6.2).

Absorbance spectra illustrated that the decline trend of absorbance coupled with a shift in the range of wavelength of 251-271nm, symptomatic that hydrolysis process to discharge iron III hydro molecules hydrolysis conferring INPs (Turner and Miles,1957), was similar to the earlier investigation in literature. However, fabricated INPs size range was recorded as 5nm to 33nm. The observed results were in good agreement with findings of Huang et al. [28].

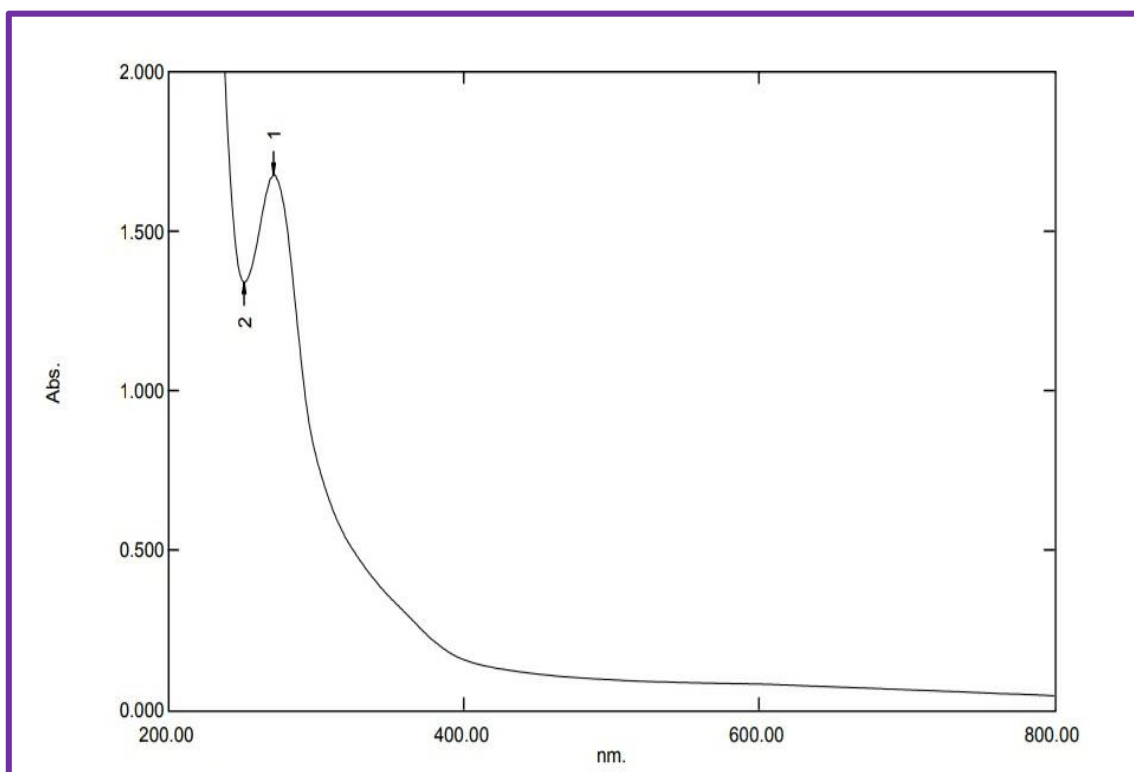


Fig.6.2 UV-vis spectrum of *C.sinensis* leaf extract in green synthesis iron nanoparticles

6.3.2 FTIR analysis

FTIR measurements were performed to know the possible functional groups of biomolecules found in the extract of *C.sinensis*, the figure (Fig.6.3) which might bind on the surface of the particles. The peaks were sharply eluted at 3412, 2922, 2854,1621 and 449 cm^{-1} and our findings were more or less similar to the earlier report of Makarov et al. [29].

Among them, high value peaks 3412 cm^{-1} indicating O-H functional groups stretching of phenol and alcohol groups. Other peaks eluted at 2854 cm^{-1} , 1621 cm^{-1} and 449 cm^{-1} indicating C-O stretching C=O corresponding to the carbonyl functional group alcohol and ester [30,31]. Moreover, 1621-449 cm^{-1} within this range of iron nanoparticles was synthesised, Pattanayak and Nayak et al.[32].

FTIR analysis revealed that carbamoyl groups derived from organic and phytochemical constituents have offered powerful stability to bind with Fe metal nanoparticles to avoid agglomeration. Therefore, it can be presumed that biological molecules execute dual targets such as formation and stableness of INPs.

FTIR analysis has confirmed, phytochemicals such as polyphenols, tanine, flavonoids and saponin present in green tea leaf have participated in the reduction of Fe^{3+} reaction [33].

It has been concluded that presence of peaks in FTIR spectra is symptomatic of functionalization of INPs with organic phytochemical [34].

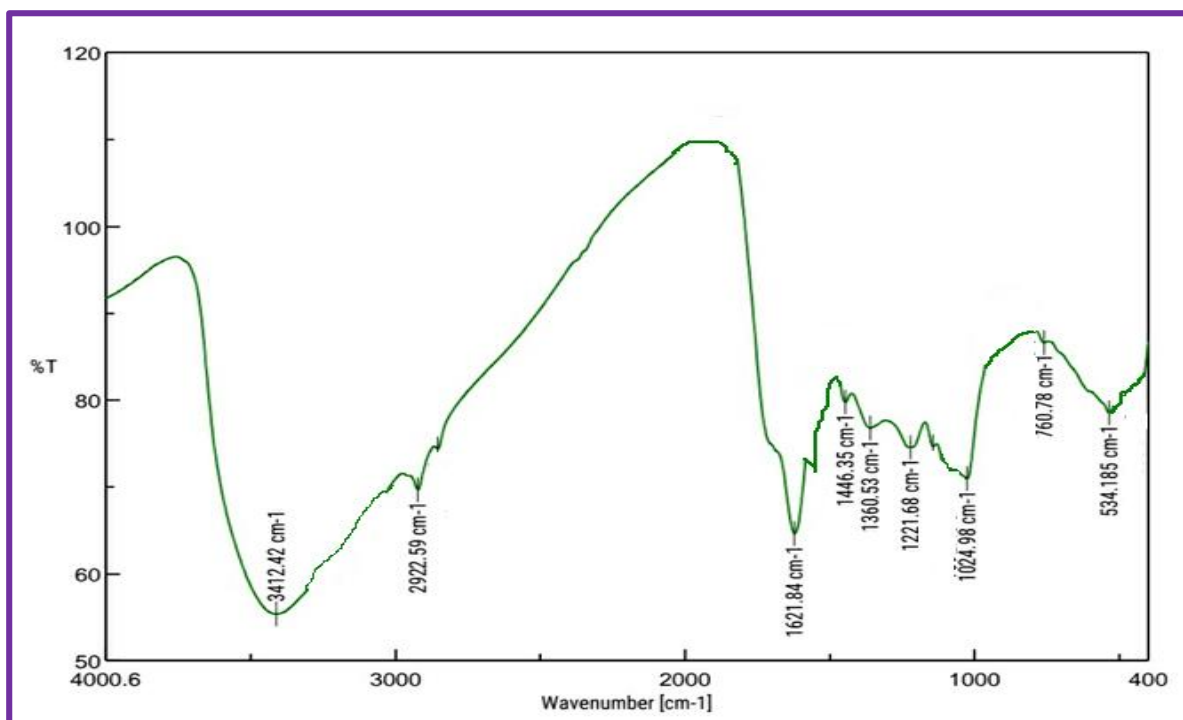


Fig.6.3 FTIR spectrum of *C.sinensis* leaf extract and iron nanoparticles

6.3.3 XRD-analysis

X-ray diffraction analysis on green synthesis INPs using green tea extract contributed amorphous INPs prediction. Previous studies reported the synthesis of amorphous INPs, using leaf extracts of various plant and waste materials of dietary industries [35]. As shown in figure (Fig.6.4), XRD pattern of synthesized INPs mediated by Green tea extract exhibited sharp peaks covering diffraction angles at 10° , 20° , 32.5° and 35° . The peak value in the range of Harelenth can be calculated using a standard Debye Scherrer's equation followed by a standard formula and illustrated in the table.6.1. The dividing constant crucial for this computation as reported by Jan et al. [36]. Our study results were agreed in the line of earlier studies reported [37, 38].

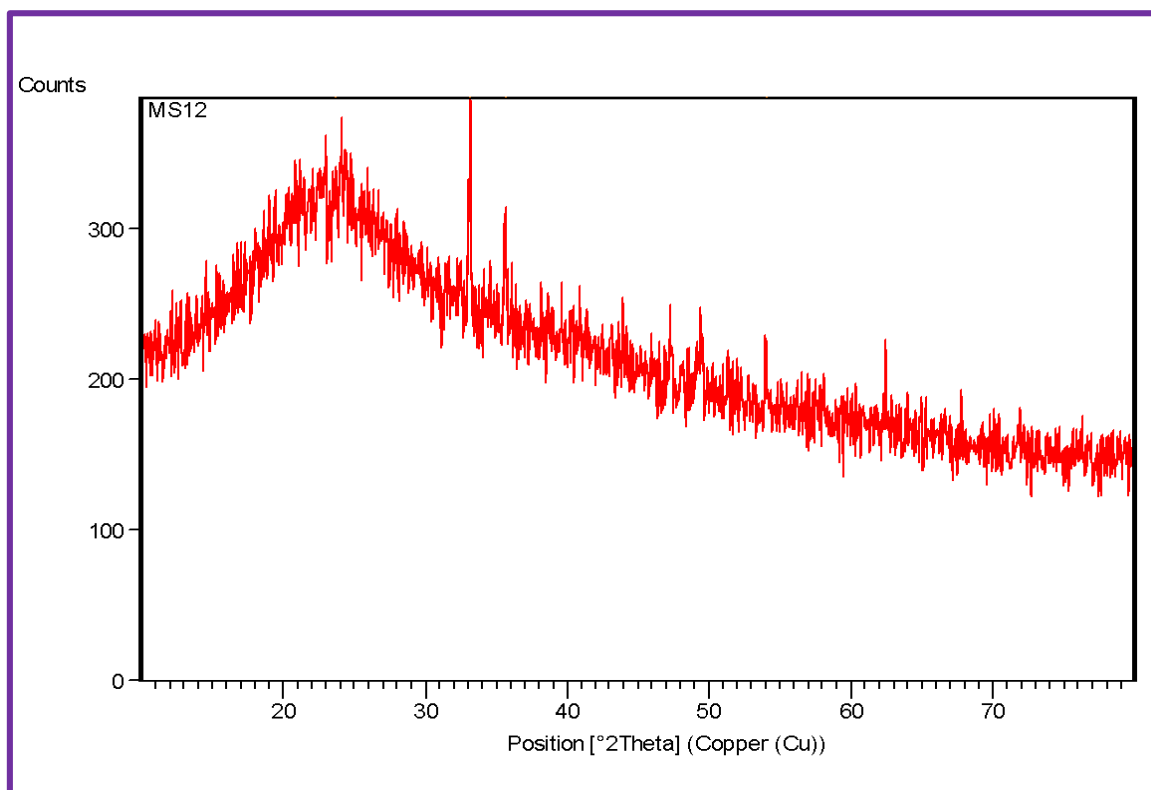


Fig.6.4 XRD pattern of *C. sinensis* leaf extract iron nanoparticles

Table 6.1 XRD pattern of *C. sinensis* leaf extract iron nanoparticles

Pos. [°2Th.]	Height [cts]	FWHM Left [°2Th.]	d-spacing [Å]	Rel. Int. [%]
23.7482	63.07	1.5587	3.74674	41.70
33.1223	151.25	0.1299	2.70468	100.00
35.5989	66.23	0.1948	2.52199	43.79
54.0647	26.28	0.3897	1.69625	17.37

Appeared small peaks were accounted for tea valent INPs and demonstrated in previous studies [39, 40]. High peaks signals ranging from 10° to 35° 2θ value was indicated occurrence of organic photo constituents present in the tea extract which are key factors for stabilizing INPs. 32.5° and 35° were associated with meghemite and was agreed with the

finding of Njagi et al. [41]. Similarly, the characteristic peaks of 16° and 20° were corresponding to iron oxyhydroxides as reported by Xio et al. [42]. It has been Confirmed that fabricated INPs have shown to be highly crystalline in nature with FCC well balanced shape.

6.3.4 SEM and EDX analysis

SEM analysis was performed to know the topology of synthesized INPs displaying external structure and shown to be in uniformed materials represented instantly the formed INPs were agglomerated due to the affinity properties resulting in irregular appearance (Fig.6.5). EDX was performed to understand the presence of elements in the fabricated INPs using green synthesis. The profile reverted that the INPs exhibited a powerful indicative of the Fe atom in the crystalline property.

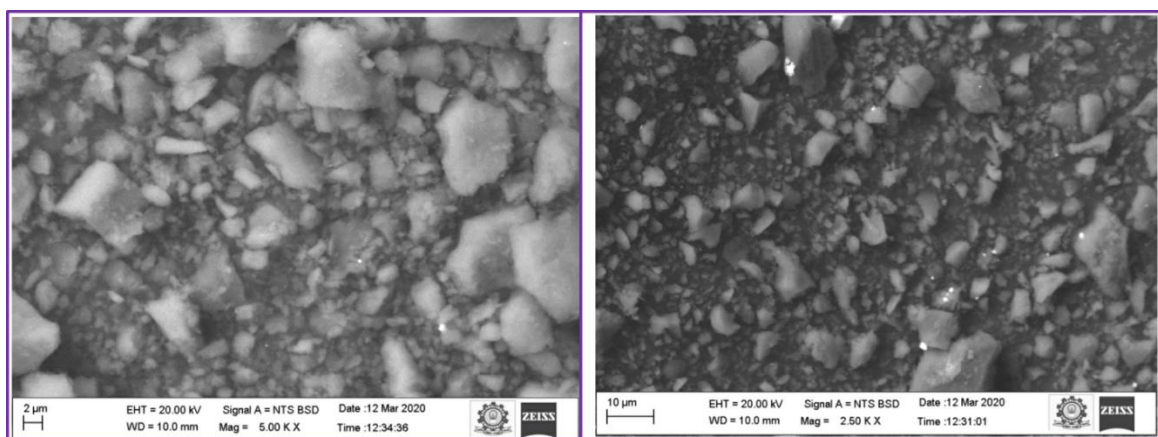


Fig.6.5 SEM images synthesized iron nanoparticles of *C.sinensis* leaf extract

As illustrated in figure (Fig.6.6) the energy KeV value fell in the range of 6 to 7 KeV indicating the value of metallic iron crystalline. Apart from Fe, C and O were recorded, would have emerged from the biomolecules on the surface of INPs due to the phytochemicals.

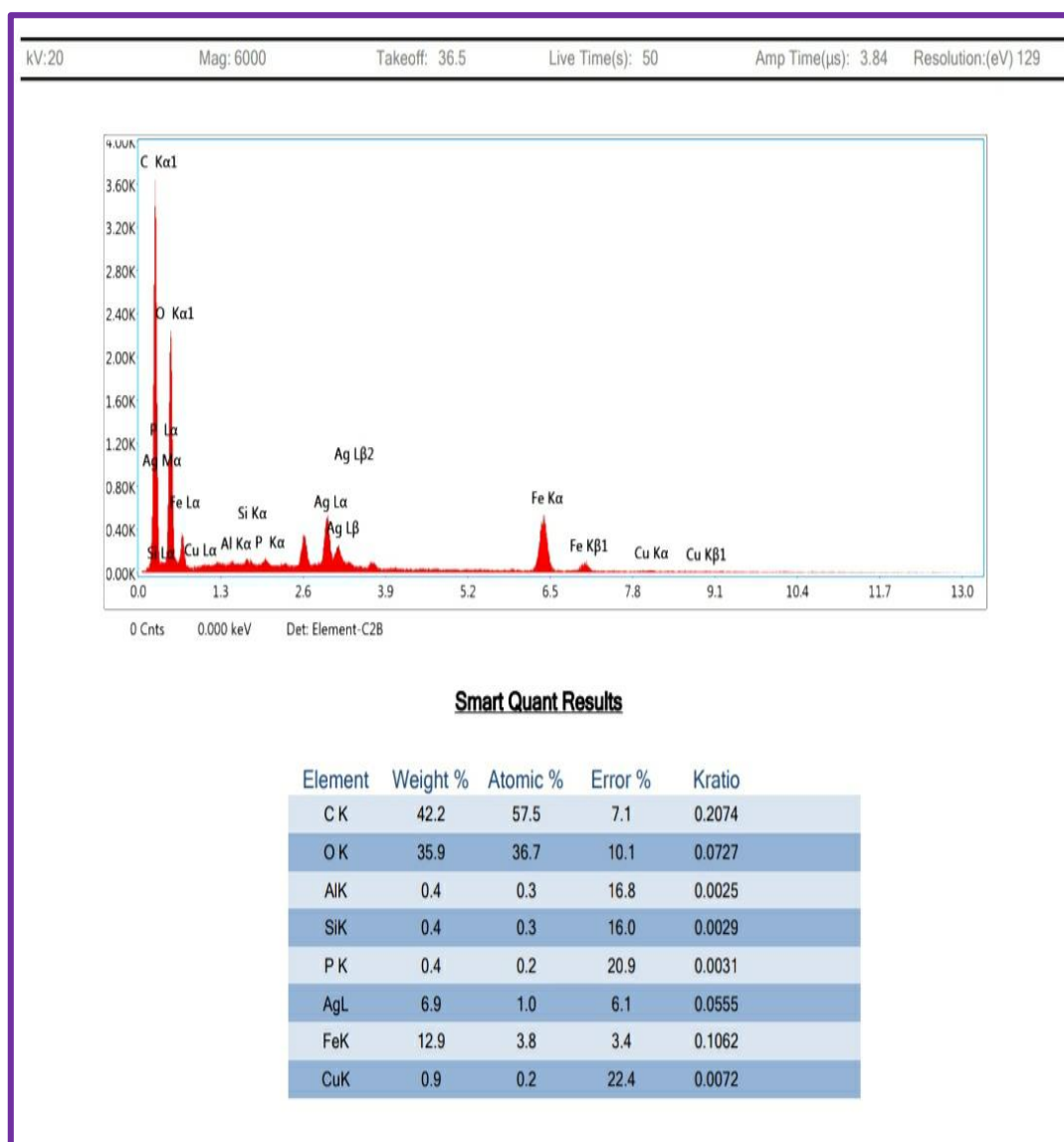


Fig.6.6 EDX images of biosynthesized iron nanoparticles of *C.sinensis*. leaf extract

6.3.5 VSM Analysis

The figure (Fig.6.7) illustrates that the magnetic behaviour of iron nanoparticles using *C. sinensis* leaf extract measured by vibrating sample magnetometer at room temperature. The M-H curve with hysteresis loop has been noticed, which represents that the synthesized iron nanoparticles have ferromagnetic properties. Ferromagnetism gives the property of nanoparticles which are strongly attracted by externally applied magnetic field and form internal induced magnetic fields in the direction of the applied magnetic field.

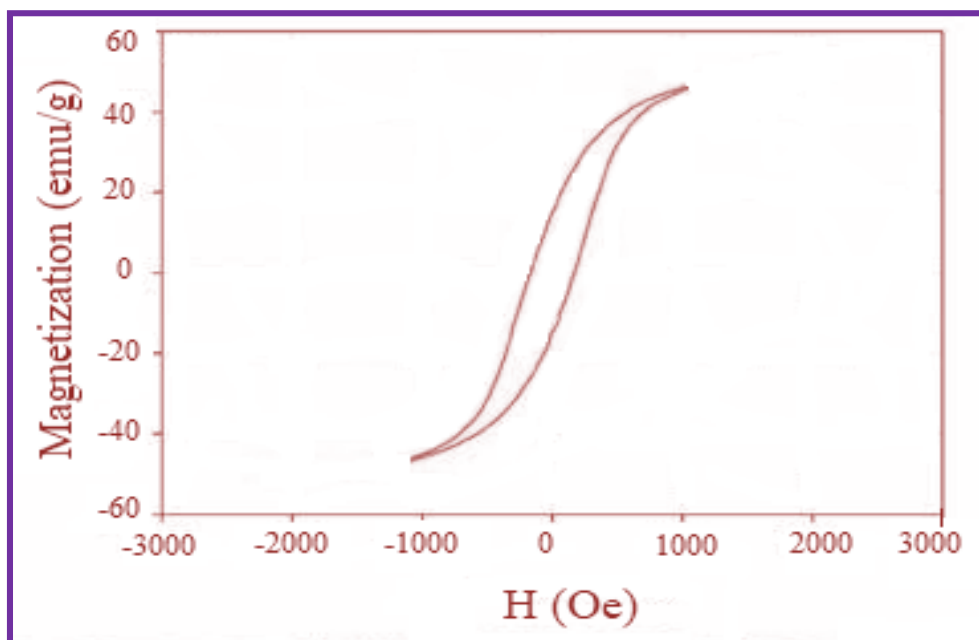


Fig.6.7 Hysteresis curve of biosynthesized iron nanoparticles using *C. sinensis* leaf extract

6.3.6 Antibacterial activity

Antibacterial potential of the INPs mediated by *C.sinensis* leaf extract was determined against gram positive *S.aureus* and *B.subtilis* and gram negative strains such as *E.coli* and *K.pneumoniae* were tested with different concentrations (Table 6.2).

Table 6.2 Assay of antibacterial activity

S.No	Bacteria Name	Zone of Inhibition (mm in diameter)		
		Control	Standard*	INPs
1	<i>Escherichia coli</i>	-	17	19
2	<i>Klebsiella pneumoniae</i>	-	16	17
3	<i>Staphylococcus aureus</i>	-	21	24
4	<i>Bacillus subtilis</i>	-	19	21
NIT-Nitrofurantoin (300µg).				

MIC values were achieved over a period of 24 hrs. Results exhibited *S.aureus* have a strong susceptibility to the INPs whereas other bacterial pathogens have lower

vulnerability as reported in the previous investigation [43, 44]. In fact, the mechanism of action of antibacterial activity remains unclear. However, the zone of inhibition indicated *S.aureus* exerted is susceptibility with INPs. When compared to the control and other pathogens.

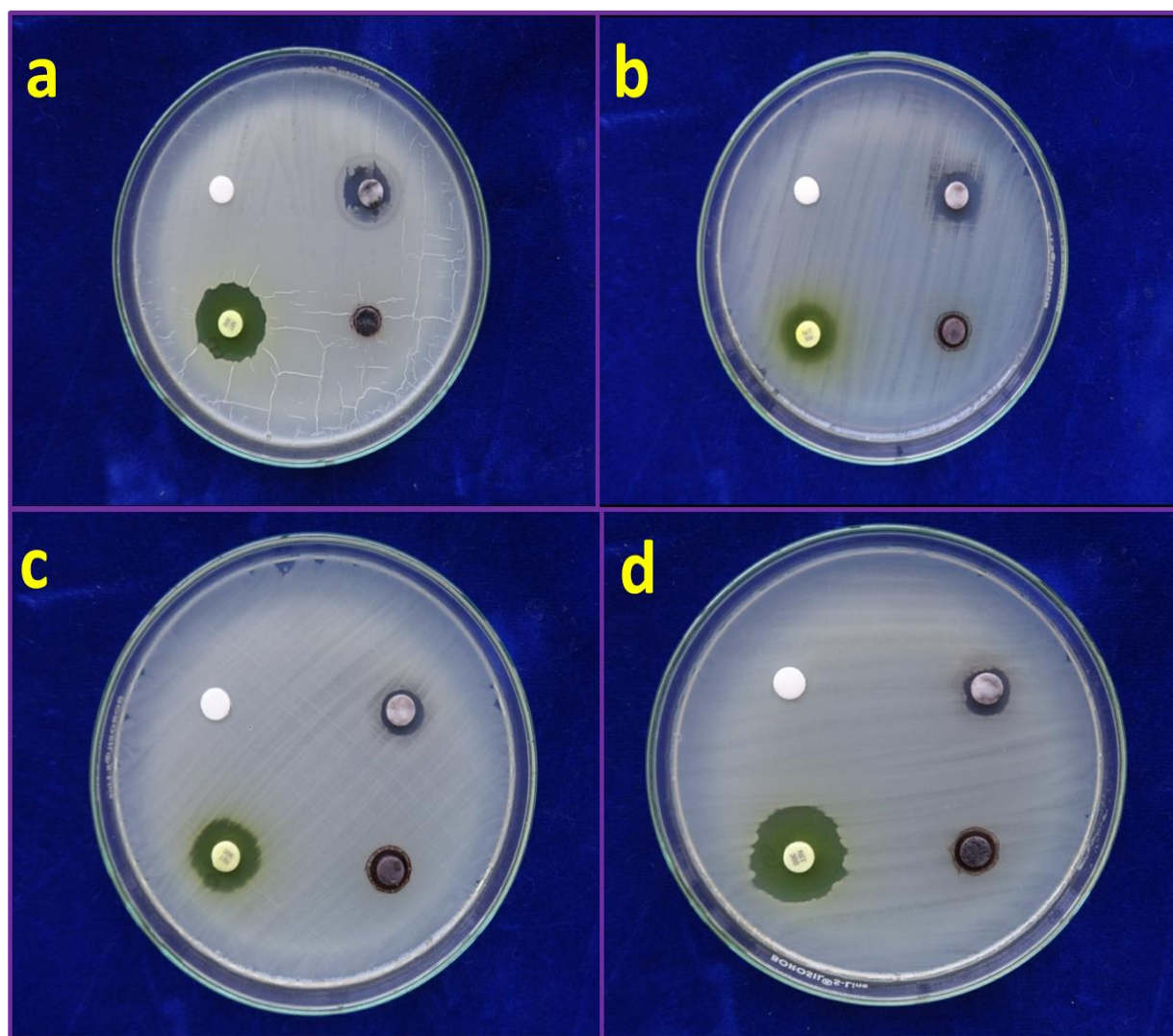


Fig.6.8 Antibacterial activity of iron nanoparticle a) *Bacillus subtilis* b) *Escherichia coli* c) *Klebsiella pneumoniae* d) *Staphylococcus aureus*

This indicated the potential of INPs to fight against harmful pathogens [45, 46]. It has been believed that INPs adhere to the cell wall of the pathogen due to the interaction of protein containing sulfur residue [47,48]. The activity leads to the permeability distraction

of intercellular content, DNA injury, accelerating ROS production and ultimately ends with death of bacteria (Fig.6.8) [49-51]. Graphical representation of zone of inhibition of INPs versus standard value was also shown in figure (Fig.6.9).

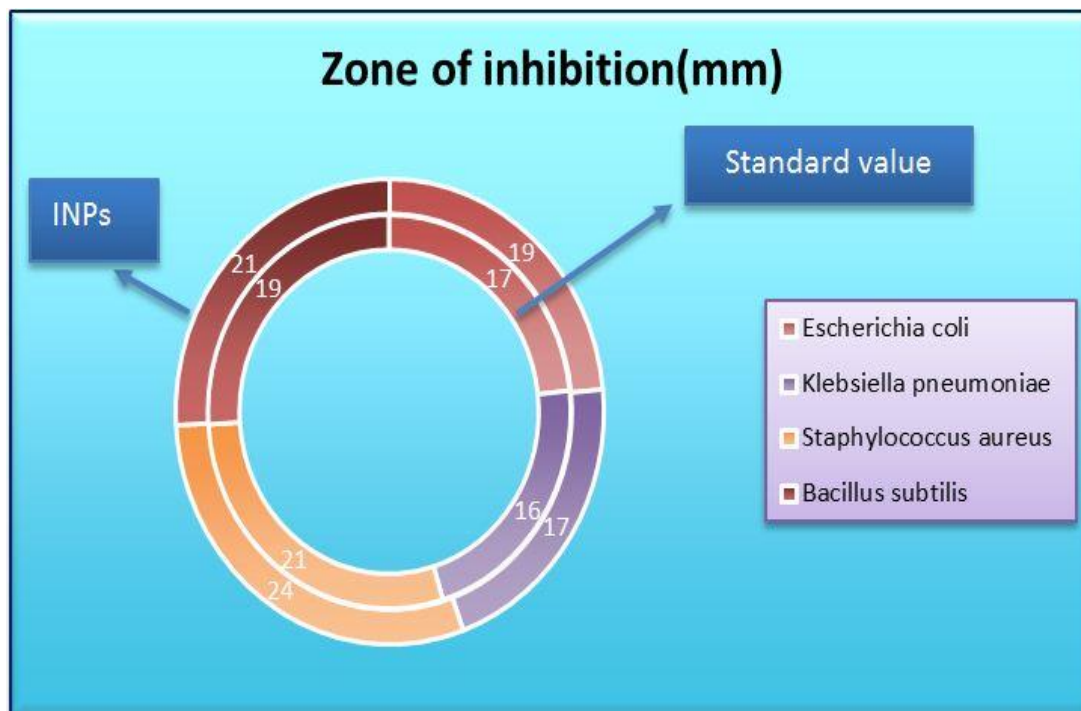


Fig.6.9 Graphical representation of zone of inhibition of INPs versus standard value

6.4 Conclusion

In summary, the iron nanoparticles were synthesized using *Camellia sinensis* as a reducer and stabilizer. The green approach on iron nanoparticles was treated with *Camellia sinensis* leaf extract was the most rapid, easy, cost effective method and it has a wide scope in opting as an outstanding drug delivery system. The morphological study of biosynthesized iron nanoparticles has been revealed the size was around 27nm with amorphous morphology. The antibacterial activity results of biosynthesized iron nanoparticles showed the higher inhibition zone upon bacterial pathogens treated with leaf extract. It has summarized that the further studies on this area are much importance in elaborating bio synthesized iron nanoparticles and is highly recommended for pharmaceutical and biomedical applications.

References

- [1] E. Sánchez-López, D. Gomes, G. Esteruelas, L. Bonilla, A.L. Lopez-Machado, R. Galindo, A. Cano, M. Espina, M. Ettcheto, A. Camins, A.M. Silva, *Nanomaterials*, 10(2) (2020) 292.
- [2] Y.N. Slavin, J. Asnis, U.O. Häfeli, H. Bach, *Journal of Nanobiotechnology*, 15 (2017) 1–20.
- [3] L. Wang, C. Hu, L. Shao, *International Journal of Nanomedicine*, 12 (2017) 1227–1249.
- [4] M. Martínez-Cabanas, M. López-García, P. Rodríguez-Barro, T. Vilariño, P. Lodeiro, R. Herrero, J.L. Barriada, M.E. Sastre de Vicente, *Nanomaterials*, 11(7) (2021) 1679.
- [5] B. Khanzada, N. Akthar, M.Z. Bhatti, H. Ismail, M. Alqarni, B. Mirza, G. Mostafa-Hedeab, G.E.S. Batiha, *Journal of Chemistry*, (2021).
- [6] Y. Wang, Y. Xia, *Nano Letters*, 4 (2004) 2047–2050.
- [7] A. Akbarzadeh, H. Mikaeili, N. Zarghami, R. Mohammad, A. Barkhordari, S. Davaran, *International Journal of Nanomedicine*, 12 (2012) 511–526.
- [8] A.K. Gupta, M. Gupta, *Biomaterials*, 26 (2005) 3995–4021.
- [9] S. Laurent, D. Forge, M. Port, A. Roch, C. Robic, L. Vander Elst, R.N. Muller, *Chemical Reviews*, 108 (2008) 2064–2110.
- [10] P. Li, D.E. Miser, S. Rabiei, R.T. Yadav, M.R. Hajaligol, *Applied Catalysis B*, 43 (2003) 151–162.
- [11] S. Yu, G.M. Chow, *Journal of Material Chemistry*, 14 (2004) 2781–2786.
- [12] X. Zhou, W. Xu, G. Liu, D. Panda, P. Chen, *Journal of the American Chemical Society*, 132 (2009) 138–146.
- [13] S.Y. Mak, D.H. Chen, *Dyes and pigments*, 61(1) (2004) 93-98.
- [14] B. Zargar, H. Parham, A. Hatamie, *Chemosphere*, 76 (2009) 554–557.
- [15] P. Xu, G.M. Zeng, D.L. Huang, C.L. Feng, S. Hu, M.H. Zhao, C. Lai, Z. Wei, C. Huang, G.X. Xie, Z.F. Liu, *Science of the Total Environment*, 424 (2012) 1–10.

- [16] L.S. Zhong, J.S. Hu, H.P. Liang, A.M. Cao, W.G. Song, L.J. Wan, *Advance Materials*, 18 (2006) 2426–2431.
- [17] T. Hyeon, *Chemical Communications*, 8 (2003) 927–934.
- [18] R.R. Chavan, S.D. Bhinge, M.A. Bhutkar, D.S. Randive, G.H. Wadkar, S.S. Todkar, M.N. Urade, *Materials Today Communications*, 24 (2020) 101320.
- [19] A.S.Y. Ting, J.E. Chin, *Water Air and Soil Pollution*, 231 (2020) 1-10.
- [20] A. Ebrahiminezhad, Y. Ghasemi, S. Rasoul-Amini, J. Barar, S. Davaran, *Colloids and Surfaces B*, 102 (2013) 534–539.
- [21] H. Jan, M. Shah, A. Andleeb, S. Faisal, A. Khattak, M. Rizwan, S. Drouet, C. Hano, B.H. Abbasi, *Oxidative medicine and cellular longevity*, 2021 (2021).
- [22] L. Katata-Seru, T. Moremedi, O.S. Aremu, I. Bahadur, *Journal of Molecular Liquids*, 256 (2018) 296-304.
- [23] P. Singh, Y.J. Kim, D. Zhang, D.C. Yang, *Trends Biotechnology*, 34 (2016) 588–599.
- [24] K.S.V. Gottimukkala, *Journal of Nanomedicine & Biotherapeutic Discovery*, 7 (2017) 151.
- [25] M. Flores-González, M. Talavera-Rojas, E. Soriano-Vargas, V. Rodríguez-González, *New Journal of Chemistry*, 42 (2018) 2133–2139.
- [26] Y. Vitta, C. Ciangherotti, *Materials Science for Energy Technologies*, 3 (2020) 97-103.
- [27] D. Ramdani, A.S. Chaudhry, C.J. Seal, *Chemical composition*, *Journal of Agriculture and Food Chemistry*, 61 (2013) 4961–4967.
- [28] L. Huang, X. Weng, Z. Chen, M. Megharaj, R. Naidu, *Spectrochimica Acta Molecular and Biomolecular*, 130 (2014) 295–301.
- [29] V.V. Makarov, S.S. Makarova, A.J. Love, O.V. Sinitsyna, A.O. Dudnik, I.V. Yaminsky, M.E. Taliany, N.O. Kalinina, *Langmuir*, 30 (2014) 5982–5988.
- [30] Y. Cai, Y. Shen, A. Xie, S. Li, X. Wang, *Journal of Magnetism and Magnetic Materials*, 322 (2010) 2938–2943.

-
- [31] A. Soliemanzadeh, M. Fekri, S. Bakhtiary, M.H. Mehrizi, *Chemical Ecology*, 32 (2016) 286–300.
- [32] M. Pattanayak, P.L. Nayak, *World Journal of Nano Science & Technology*, 2(1) (2013) 06-09.
- [33] T. Wang, X. Jin, Z. Chen, M. Megharaj, R. Naidu, *Science of the Total Environment*, 466 (2014) 210–213.
- [34] N. Beheshtkhoo, M.A.J. Kouhbanani, A. Savardashtaki, A.M. Amani, S. Taghizadeh, *Applied Physics A*, 124(5) (2018) 1-7.
- [35] X. Weng, L. Huang, Z. Chen, M. Megharaj, R. Naidu, *Industrial Crops and Products*, 51 (2013) 342-347.
- [36] H. Jan, M. Shah, A. Andleeb, S. Faisal, A. Khattak, M. Rizwan, S. Drouet, C. Hano, B.H. Abbasi, *Oxidative medicine and cellular longevity*, 2021 (2021).
- [37] M. Sivakami, K. Renuka Devi, R. Renuka, T. Thilagavathi, *Journal of Environmental Chemical Engineering*, 8(5) (2020) 104420.
- [38] A. Ebrahimezhad, M. Bagheri, S. Taghizadeh, A. Berenjian, Y. Ghasemi, *Advances in Natural Sciences*, 7 (2016) 015018.
- [39] T. Wang, X. Jin, Z. Chen, M. Megharaj, R. Naidu, *Science of the Total Environment*, 466 (2014) 210–213.
- [40] C.P. Devatha, K. Jagadeesh, M. Patil, *Environmental Nanotechnology, Monitoring & Management*, 9 (2018) 85-94.
- [41] E.C. Njagi, H. Huang, L. Stafford, H. Genuino, H.M. Galindo, J.B. Collins, G.E. Hoag, S.L. Suib, *Langmuir*, 27 (2010) 264–271.
- [42] Z. Xiao, M. Yuan, B. Yang, Z. Liu, J. Huang, D. Sun, *Chemosphere*, 150 (2016) 357–364.
- [43] H.K. Farshchi, M. Azizi, M.R. Jaafari, S.H. Nemat, A. Fotovat, *Biocatalysis and agricultural biotechnology*, 16 (2018) 54-62.
- [44] J.K. Patra, K. Hun Beak, *Green Chemistry letters and Reviews*, 9(2) (2016) 132-142.
- [45] Y. Orooji, R. Mohassel, O. Amiri, A. Sobhani, M. Salavati-Niasari, *Journal of Alloys and Compound*, 835 (2020) 155240.

- [46] M. Nasrollahzadeh, S.M. Sajadi, A. Rostami-Vartooni, *Journal of Colloid Interface Science*, 459 (2015) 183-188.
- [47] B. Khodadadi, M. Bordbar, M. Nasrollahzadeh, L. *Achillea millefolium*, *Journal of Colloid and Interface Science*, 493 (2017) 85-93.
- [48] S. Venkateswarlu, Y.S. Rao, T. Balaji, B. Prathima, N.V.V. Jyothi, *Material Letters*, 100 (2013) 241-244.
- [49] M. Jamzad, M.K.J. Bidkorpeh, *Nanostructure in Chemistry*, 10(3) (2020) 193-201.
- [50] H.K. Handral, A. Pandith, S.D. Shruthi, *Asian Journal of Pharmaceutical and Clinical Research*, 5(4) (2012) 5-14.
- [51] M. Sivakami, K. Renuka Devi, R. Renuka, *Applied Physics A*, 128(4) (2022).1-13.
- [52] K. Velsankar, V. Vinothini, S. Sudhahar, M. Krishna Kumar, S. Mohandoss, *Applied Nanoscience*, 10(10) (2020) 3953-3971.

Chapter VII

A Comparative Study of Antibacterial Activities of Plant Mediated Iron Nanoparticles

7.1. Highlights

- A comparison of four different leaf extracts with good anti-oxidant capacity was made to find out the best available leaf extract for green synthesis for iron nanoparticles for its biomedical applications.
- The *Cinnamomum verum* barks were used for the first time for the synthesis of iron nanoparticles, and they showed promising results in the form of high antibacterial capacity.
- These green-synthesized nanoparticles were characterized using EDS, XRD, FTIR, SEM, TEM, DLS, VSM, UV and antibacterial studies.
- The iron nanoparticles which are having best anti-oxidant, reducing and capping properties were fabricated from *Green tea to Cinnamomum verum* bark extracts.

7.2. Introduction

In recent years, biosynthesis of nanoparticles has been acquired growing attention and developed as a promising alternative for chemical and physical methods, due to its advantages of a simple, rapid and inexpensive synthesis, biodegradable materials instead of hazardous reagents and less agglomeration of nanoparticles. In this synthesis, a variety of materials from bio-renewable natural sources can be employed, which are even considered as wastes or do not have any added value in some cases. And the extracts of biomaterials can also act as a nutrient source to improve complementary biodegradation.

Nowadays, nanoparticles have potential effects in sciences and human health care applications. Among the nanoparticles, iron nanoparticles are playing a pivotal role in the field of biomedical fields. Iron is a naturally occurring precious metal, most often as a mineral ore in association with other elements. Iron nanoparticles have a natural antimicrobial effect against many pathogens such as bacteria, fungus, viruses, and yeast. The biosynthesis of iron nanoparticles has several advantages such as cost-effectiveness and compatibility for biomedical and pharmaceutical applications as well as for large-scale commercial productions.

Iron nanoparticles were traditionally synthesized by chemical synthesis techniques that used chemicals used which were quite often toxic and flammable. So, a reliable and eco-friendly process for the synthesis of iron nanoparticles has become an important step in the field of nanotechnology. Plant extracts are eco-friendly and are economic and efficient alternatives for the large-scale synthesis of iron nanoparticles.

The present study has planned to compare the biosynthesis of iron nanoparticles using the fresh plant extracts of four potential plants with high medicinal value such as *Camellia sinensis*, *Murraya koenigii*, *Rosa Gallica*, *Cinnamomum verum barks*. A rapid reduction of iron ions leading to the formation of stable iron nanoparticles in the solution immediately at room temperature as compared to that on heating was studied. The UV-Visible spectrum of iron nanoparticles in an aqueous solution has shown an absorbance peak of around 265 nm due to surface plasmon resonance. Transmission electron microscope images have shown the particle size as around 30 nm. This is the first attempt to perform ecofriendly synthesis of iron nanoparticles using fresh plants of *Murraya koenigii*, *Cinnamomum verum barks* and produced the maximum yield which may benefit various industries with wide a range of applications. These biologically synthesized iron

nanoparticles were tested for antibacterial activity against four human pathogens such as *Escherichia coli*, *Klebsiella pneumonia*, *Bacillus subtilis*, and *Staphylococcus aureus*.

Plenty of microorganisms and plant extracts have been applied to synthesize inorganic nanostructures either intracellularly or extracellularly. It can be revealed by electrostatic interaction between Fe⁺ and negatively charged carboxylate groups on the cell surface. In the reduction of metal ions process using microorganism occurs on their cell surface by enzymes present in the cell wall. The development of bioprocesses for the synthesis of nanoparticles is develop gradually into an important branch of nanotechnology. Several plant biomass or plant extracts have been successfully used for the extracellular biosynthesis of iron nanoparticles. The metal ions reduction occurs very rapidly, and the reduction of Fe ions will be achieved within hours. Rapid synthesis and excellent yield of iron nanoparticles through this plant-mediated biosynthesis have a time-related (~2h) advantage in comparison with microbial synthesis (~24h).

7.3. Plants chosen for the comparative analysis

Plant extracts have been used as stabilizing agents for the synthesis of numerous nanoparticles because of their high antioxidant magnitude and environmentally benign reducing properties. Four different plant species were chosen among several plants (Tomato, Murungai Leaves and so on) for this comparative study of the synthesis of iron nanoparticles. Based on the amazing reducing properties from the analysis, the following plants were selected for this study:

- Green tea leaves (*Camellia sinensis*)
- Curry Leaves (*Murraya koenigii*)
- Rose Petals (*Rosa Gallica*)
- Pattai (*Cinnamomum verum* bark)

Iron nanoparticles were synthesized by using the green synthesis method with the above mentioned plants.



Fig. 7.1. Pictorial representation of *Camellia sinensis*, *Cinnamomum verum*, *Murraya koenigii* and *Rosa Gallica*

7.4. Nomenclature

S. No	Abbreviation	Description
1	GT-INPs	<i>Camellia sinensis</i> (Green tea) extract -based iron nanoparticles
2	CL-INPs	<i>Murraya koenigii</i> (Curry leaves) extract -based iron nanoparticles
3	RP-INPs	<i>Rosa Gallica</i> (Rose petals) extract -based iron nanoparticles
4	PT-INPs	<i>Cinnamomum verum</i> (Pattai) bark extract-based iron nanoparticles

The objective of this comparative study was to investigate the use of four different selected locally available plants that showed excellent antioxidant capacities (Machado et al. 2013) for the synthesis of iron nanoparticles. The four iron nanoparticles, thus synthesized, were compared for the antibacterial activities against selected pathogens. The biosynthesized iron nanoparticles act as the best reducing agent was determined. Characterization techniques such as SEM combined EDS, TEM, VSM, DLS, FTIR, UV visible spectroscopy and XRD were used to analyze the nanoparticles in terms of size, morphology, and structure.

The employ of plant extracts for the synthesis of nanoparticles has been of much interest in recent years (Parsons et al. 2007; Shahwan et al. 2011; Kuang et al. 2013; Mahdavi

et al. 2013; Huang et al. 2014; Wang et al. 2014). These extracts are inexpensive, non-toxic, and biodegradable. Because of these reasons, biosynthesized iron nanoparticles can have applications in medical and biomedical fields (Shiv Shankar et al. 2004). The polyphenols in plants also act as capping agents; thus, there is no need for an extra stabilization agent. Multiple researchers have applied green synthesis of nanoparticles using different plant extracts (Shahwan et al. 2011; Machado et al. 2013; Nethaji et al. 2013; Huang et al. 2014; Wang et al. 2014). Different plant extracts have different organic compounds that can make changes to the behaviour of the iron nanoparticles by using them.

7.5. Comparison of antibacterial activities

Cinnamomum Verum and *Murraya koenigii* functionalized iron NPs have displayed higher inhibition activity compared to other plant species against *Klebsiella pneumonia*, *Staphylococcus aureus* and *Bacillus subtilis* bacterial strains. Therefore, the biosynthesized iron NPs were shown efficient antibacterial properties because of *Cinnamomum Verum* and *Murraya koenigii* extracts when compared to *Rosa Gallica* and *Camellia sinensis* mediated iron nanoparticles. The comparison of inhibition values of all plant species was also shown in the figure (fig.7.2).

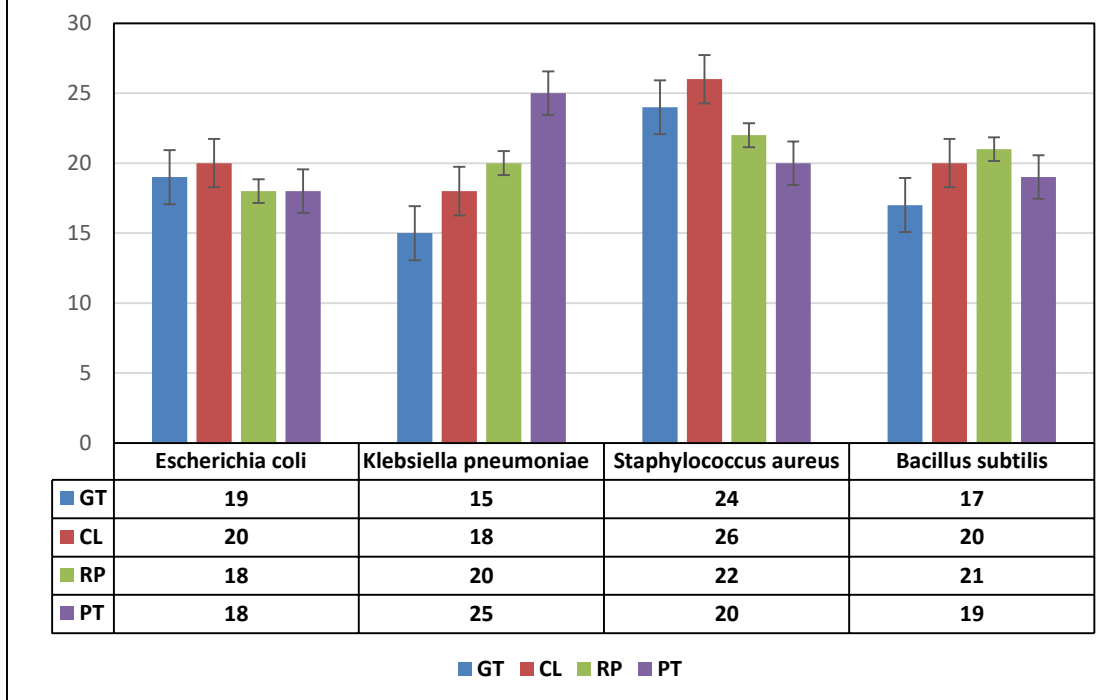
Fig.7.2. Comparison of antibacterial capacity of biosynthesized iron nanoparticles

Table 7.1 Summarized Characterization results of Biosynthesized iron nanoparticles

Nanoparticles	Extracting Agent	Particle Size (nm)	Magnetic Behaviour	Reducing & Stabilizing Capacity	Color Change	Morphology	Applications
GT-INPs	<i>Camellia sinensis</i> Leaves	21	Paramagnetic	High	Black	Irregular	Anti-bacterial
CL-INPs	<i>Murraya koenigii</i> Leaves	14	Ferromagnetic	Very High	Black (Immediately)	Spherical	Anti-bacterial, Anti-diabetic, Anti-inflammatory, Anti-oxidant.
RP-INPs	<i>Rosa gallica</i> Petals	24	Ferromagnetic	High	Black	Spherical	Anti-bacterial
PT-INPs	<i>Cinnamomum verum</i> barks	36	Paramagnetic	Very High	Black (Immediately)	Spherical	Anti-bacterial, Anti-oxidant, Anti-diabetic, Anti-inflammatory.

7.6. Conclusion

The current study gives a comparison between the biosynthesis of Fe NPs by using the aqueous extracts of the fresh leaves of *Camellia sinensis*, *Murraya Koenigii*, *Rosa Gallica*, *Cinnamomum verum barks* (Table 7.1). The plant extract of *Murraya Koenigii* leaves and *Cinnamomum verum barks* had the higher reducing and stabilizing capacity, giving rise to spherical iron nanoparticles. *Rosa gallica* mediated iron nanoparticles had the strong ferromagnetic behavior when compared to *Cinnamomum verum barks*. Fe NPs were crystalline in nature; the average size of the iron nanoparticles was in the range of around 30 nm. The biosynthesized Fe NPs can be used for medical applications, especially in the drug delivery process because of their higher antibacterial activity.

SUMMARY

Green synthesis of iron nanoparticles using plants, fungus and bacterial extracts has gained a lot of attraction in the research community during the last decade. The basic premise for this attention includes economic viability, non-toxicity and environment friendly nature of iron NPs. Chemical synthesis of NPs requires the use of expensive and non-biodegradable capping agents which are highly toxic to both the environment and human. Synthesis of NPs from commonly available plants can overcome all these limitations and provide a basis for utilizing the untapped potential of nanotechnology.

In this research work, iron nanoparticles were synthesized by using plants the extracts such as *Cinnamomum Verum*, *Murraya Koenigii*, *Rosa Gallica* and *Camellia Sinensis* by a biological method. In this work, results and discussion were split up into four chapters. All the chapters were clearly discussed through effective microscopic and spectroscopic techniques. The antibacterial, anti-inflammatory, antioxidant and antidiabetic assays were also investigated. From this entire works, the summary was given below;

The iron nanoparticles were successfully synthesized by *Cinnamomum verum* bark extract by a greener method. From the XRD, UV, FTIR, EDS, VSM and spectral analyses, the formation of iron nanoparticles was confirmed. SEM and HR-TEM analyses were depicted the spherical iron nanoparticles formation. The plant has improved the surface morphology synthesized of iron nanoparticles. The antibacterial assay showed the better inhibition by plant assisted iron nanoparticles. The antioxidant and anti-inflammatory assays have depicted better inhibition by plant-derived iron nanoparticles. In the antidiabetic assay, better inhibition was illustrated by plant-assisted iron nanoparticles.

The study has compiled the impact of iron NPs and *Cinnamomum Verum* extract played an essential role in the reduction and stabilization of iron NPs. The synthesized

magnetic Fe NPs have confirmed by UV-Vis analysis with SPR band at 288 nm. XRD analysis has revealed the mean crystallite size of iron NPs was at 36 nm. SEM and HR-TEM images revealed that iron NPs were compatible, stable in circular and spherical shaped with size at 20-50 nm. The EDAX and mapping analysis validated the formation of Fe NPs. The VSM analysis has explicated the paramagnetic behavior of prepared NPs. The inhibition zones that appeared in the antibacterial assay designated the synthesized Fe NPs has an efficient higher inhibition of antibacterial effect against human pathogenic bacteria. The antioxidant, anti-inflammatory and anti-diabetic assay have showed the efficient behavior of Fe NPs with low concentration value in biomedical applications. These studies have revealed that green synthesis of iron NPs has potential as an easy, economical and beneficial process for most scientific and technical applications in the future, including treatment of wastewater, pesticides in agriculture and screening of drugs to hasten the natural drug discovery against promising chemicals.

In the present research work, the eco-friendly green synthesis of iron NPs was efficiently performed by using *Murraya koenigii* leaves extract. The synthesized iron oxide NPs were characterized by various analytical techniques such as UV, XRD, FT-IR, DLS, TEM, and EDS analyses. UV analysis has confirmed the formation of iron NPs with SPR band at 240 nm. XRD pattern proved that the high crystalline formation of iron NPs with strong and intense peaks. FT-IR analysis has confirmed the functional groups of iron nanoparticles. DLS spectrum has identified the formed particles was in nano meter range. TEM graphs were illustrated that the formed NPs were in spherical shape with size from 10-25 nm. EDS spectrum with its mapping proved that the iron, oxygen presence in formed NPs. VSM analysis has revealed the paramagnetic behavior of nanoparticles. The biomedical applications based characterizations such as antimicrobial, antioxidant, anti-inflammatory and anti-diabetic assays were performed. The antimicrobial assay has proved the potency inhibition of iron NPs on various human pathogens. The antioxidant, anti-

inflammatory and anti-diabetic assays proved the iron NPs have biomedical behavior. With these results, the prepared iron NPs by using *Murraya koenigii* leaves extract will be utilized as antibiotic, anti-diabetic, anti-inflammatory anti-cancer drugs and pesticides in biomedical and agricultural fields in future.

The study has figure out the *Rosa Gallica* petals extract was more compatible for the biosynthesis of iron nanoparticles. The formation of iron nanoparticles has been confirmed primarily by changing of immediate black colour. It has been further confirmed by UV-vis spectroscopic analysis. From X-ray diffraction analysis, the average crystalline size of iron nanoparticles was calculated by using Debye Scherrer equation and was found to be in the range of 24nm. Moreover, iron nanoparticles offered potential antimicrobial activity against harmful bacteria strains. Interestingly, fabricated FeNPs exhibited effective antibacterial actions against *K.pneumoniae* strain. The results of this study were suggested the synthesis of iron nanoparticles from green route is an easy, effective and can be used for various biomedical and biotechnological applications such as Multi Drug Resistance (MDR) pathogens in clinical settings due to its highly potent antibacterial actions.

In this study, the iron nanoparticles were synthesized using *Camellia sinensis* as a reducer and stabilizer. The green approach on iron nanoparticles treated with *Camellia sinensis* leaf extract is the most rapid, easy, cost effective method and it has a wide scope in opting as an outstanding drug delivery system. The morphological study of biosynthesized iron nanoparticles has been revealed the size was around 27nm with amorphous morphology. The antibacterial activity results of biosynthesized iron nanoparticles showed a higher inhibition zone upon bacterial pathogens treated with leaf extract. It was summarized that the further studies on this area are much importance in elaborating bio synthesized iron nanoparticles and was highly recommended for pharmaceutical and biomedical applications.

Tremendous efforts have been made to composite the bio-methodologies in order to fabricate new sustainable nanoparticles. This research confers about different investigations in which microorganisms, and biomolecules are being used to produce iron nanoparticles. Biosynthesis method has been used because of an inexpensive, environmentally friendly and an alternative approach to fabricate nanoparticles for multiple applications. This work deals with different characterization techniques to examine the properties of the fabricated nanoparticles, such as morphology, size, surface, crystallinity, and so on. The green method has been used for the synthesis of iron nanoparticles using the aqueous extract of plants, which are believed to be responsible for the reduction of Fe ions. The comprehensive study has also compared the extracts of four plants for the synthesis of iron nanoparticles and their efficacy in various fields. The overall analysis has revealed that the biosynthesized iron nanoparticles can be made for biomedical applications due to their anti-oxidant, anti-bacterial, anti-diabetic and anti-cancer properties. Though all of the synthesized iron nanoparticles showed a high affinity toward reduction and stabilization, the *Cinnamomum verum* FeNPs and curry leaf FeNPs showed particularly higher reducing capacity than green tea, Rose petals FeNPs. *Cinnamomum verum* bark and *curry leaf* extracts have found particularly compatible for the fabrication of such nanoparticles. The greater reducing capacities of biosynthesized iron nanoparticles have recommended that the plant-based iron nanoparticles can be applied for both biomedical and industrial applications.

Future work

In future, the nanoparticles based on iron and copper were synthesized by diverse medicinal green extracts like *Vitis vinifera*, *Punica granatum*, *Beta vulgaris*, *Solanum lycopersicum*, and *Musa extracts*. Moreover, the morphology can be improved by incorporating other metals like zinc in to the nanoparticles to improve the biological activities. The synthesized nanoparticles will be tested for structural, vibrational, optical, morphological, and elemental analyses using XED, FTIR, UV, PL, SEM, HR-TEM, EDX and XPS analyses. Furthermore, the synthesized iron nanoparticles will be tested for antibacterial activity, anti-oxidant activity, anti-inflammatory activity and anticancer activity to ensure its potential over diverse biological activities.

LIST OF PUBLICATIONS

Papers published in International Journals

1. **M. Sivakami**, K. Renuka Devi, R, Renuka, T, Thilagavathi, Green synthesis of magnetic nanoparticles via Cinnamomum verum bark extract for biological application, Journal of Environmental Chemical Engineering, 8(5) (2020) 104420. **IF-5.909**. <https://doi.org/10.1016/j.jece.2020.104420>.
2. **M. Sivakami**, K. Renuka Devi, R, Renuka, Phytomediated synthesis of magnetic nanoparticles by Murraya Koenigii leaves extract and its biomedical applications, Applied Physics A: Materials Science and Processing, 128(4) (2022) 1-13. **IF-2.584**. <https://doi.org/10.1007/s00339-022-05437-9>.
3. **M. Sivakami**, K. Renuka Devi, Antimicrobial efficacy of iron nanoparticles (INPs) using Camellia sinensis Leaves Extract-An Alternate Approach, Inorganic Chemistry Communications, (2022).Communicated. **IF-2.495**.
4. **M. Sivakami**, K. Renuka Devi, Biosynthesized magnetic nanoparticles using Rosa Gallica petals extract and its antibacterial activities against selected pathogens for biomedical applications, South African Journal of Botany, (2022). Communicated. **IF-2.315**.

Papers presented in National and International Conferences

1. “Biosynthesis of Iron nanoparticles using Rosa Gallica (Rose Petals) and its antibacterial activity”, National Conference on Recent Trends in Nanomaterials and Thin Films Research (RTNMTR-2018), organized by PG & Research Department of physics, A.V.V.M. Sri Pushpam College, Thanjavur, held from 9th to 11th February 2018.
2. “Synthesis and characterization of Iron nanoparticles using Curry leaves (Murraya Koenigii) Extract”, National Conference on Recent Trends in Nano and Bulk Superconducting and Magnetic materials, organized by PG & Research Department of physics, Srimad Andavan Arts and Science College, Tiruchirappalli, held from 20th to 21th December 2018.
3. “Biosynthesis of iron nanoparticles using Tomato (Solanum lycopersicum) extract and its antibacterial activity”, International Virtual Conference on Recent Innovation of Bio-Materials in Current Scenario (RICBCS), D.G Government Arts College (W), Mayiladuthurai, during 7th to 8th April 2022.

Participated in National and International Seminars & Conferences

1. India-UK Second International Conference on Advanced Nanomaterials for Energy, Environment and Health (ANEH-2019), held from 4th to 6th February 2019, organized by PG & Research Department of Physics, Bishop Heber College, Tiruchirappalli, India.
2. International e-Conference on “Advanced functional Nanomaterials and Their Device Applications”, held on 10th August 2020, organized by Department of Physics and IQAC, Shetkari Shikshan Prasarak Mandal’s Krishna Mahavidyalaya, Rethare Bk, Satara, Maharashtra, India.
3. International Webinar on Opto-Electrical Applications of Semiconducting, held on 26th June 2021, organized by PG & Research Department of Physics, Government Arts College for Women, Pudukkottai, India.

Participated in National and International Workshops & Training Programme

1. One Day Workshop on “XRD Techniques” Organized by National College Instrumentation Facility (NCIF), National College, Tiruchirappalli, held on 16th December 2017.
2. National Workshop on “Institutional Assessment and Accreditation” Organized by Internal Quality Assurance Cell (IQAC), H.H. The Rajah’s College, Pudukkottai, held on 12th February 2019.
3. National Workshop on “Materials Modelling using Quantum Espresso-Theory and Practice for Beginners(QE19)” Organized by PG & Department of Physics, Government Arts College for Women, Kumbakonam, during 29th to 30th July 2019.
4. One Week e-Workshop on “Innovation & Intellectual Property Rights (IPR 2021)” Organized by Innovative Technology Enabling Centre (InTEC), CSIR-IMMT, Bhubaneswar, during 14th to 19th June 2021.

Best Awards

1. **Best Oral Presentation Award:** “Biosynthesis of iron nanoparticles using Tomato (*Solanum lycopersicum*) extract and its antibacterial activity”, International Virtual Conference on Recent Innovation of Bio-Materials in Current Scenario (RICBCS), D.G Government Arts College (W), Mayiladuthurai, during 7th to 8th April 2022.

Source details

Feedback > Compare sources >

Journal of Environmental Chemical Engineering

Scopus coverage years: from 2013 to Present

Publisher: Elsevier

ISSN: 2213-3437

Subject area: [Environmental Science: Pollution](#) [Chemical Engineering: Process Chemistry and Technology](#)
[Environmental Science: Waste Management and Disposal](#) [Chemical Engineering: Chemical Engineering \(miscellaneous\)](#)

Source type: Journal

[View all documents >](#) [Set document alert](#) [Save to source list](#) [Source Homepage](#)

CiteScore 2021 [?](#)
7.7

SJR 2021 [?](#)
1.042

SNIP 2021 [?](#)
1.378

[CiteScore](#) [CiteScore rank & trend](#) [Scopus content coverage](#)

i Improved CiteScore methodology ×
CiteScore 2021 counts the citations received in 2018-2021 to articles, reviews, conference papers, book chapters and data papers published in 2018-2021, and divides this by the number of publications published in 2018-2021. [Learn more >](#)

CiteScore [2021](#) [?](#)
7.7 = $\frac{36,399 \text{ Citations 2018 - 2021}}{4,697 \text{ Documents 2018 - 2021}}$
Calculated on 05 May, 2022

CiteScoreTracker 2022 [?](#)
7.1 = $\frac{33,578 \text{ Citations to date}}{4,722 \text{ Documents to date}}$
Last updated on 05 May, 2022 • Updated monthly

CiteScore rank 2021 [?](#)



Green synthesis of magnetic nanoparticles via *Cinnamomum verum* bark extract for biological application

M. Sivakami^{a,*}, K. Renuka Devi^b, R. Renuka^b, T. Thilagavathi^c

^a H.H. The Rajah's College, Pudukkottai, 622001, India

^b Government Arts College for Women, Pudukkottai, 622001, India

^c Government Arts College for Women, Kumbakonam, 612001, India

ARTICLE INFO

Editor: GL Dotto

Keywords:

Biosynthesis
Nanoparticles
Cinnamomum verum bark
Antibacterial activity
Scanning electron micrographs
Vibrating sample magnetometer analysis

ABSTRACT

The green synthesis of magnetic Fe nanoparticles (NPs) was prepared via *Cinnamomum Verum* bark extract. The UV–vis analysis explained the formation of Fe NPs with SPR band at 288 nm. The powder X-ray diffraction analysis (XRD) explicated the mean crystallite size was at 36 nm. The Fourier Transform Infra-Red analysis (FTIR) revealed the functional groups in the prepared Fe NPs. The Scanning Electron Microscope (SEM) and High-Resolution Transmission Electron Microscope (HR-TEM) analyses notified the circular and spherical shaped Fe NPs with the size at 20–50 nm. The Energy dispersive X-ray spectroscopy (EDS) and mapping analyses validated the formation of Fe NPs with purity. The Vibrating Sample Magnetometer (VSM) revealed the paramagnetic behavior of prepared Fe NPs. The phytochemical analysis described the phytochemicals compounds which present in *Cinnamomum Verum* bark extract. The Antibacterial assay described the much higher inhibition zone of prepared Fe NPs upon human pathogenic bacteria. The Antioxidant (DPPH) assay described the efficient scavenging behavior of Fe NPs with 89 % at 80 µg/mL concentration. The Anti-inflammatory assay explicated the potential protein denaturation behavior of Fe NPs with 87 % at 500 µg/mL concentration. The Anti-diabetic assay reported the much higher potential efficiency of prepared Fe NPs with 84 % at 500 µg/mL concentration.

1. Introduction

In recent decades, nanotechnology has gained more recognition due to its unique properties associated with the size distribution and morphology of nanoparticles. Nanotechnology was an umbrella term that covers many research areas dealing with objects that are covered in nanometers such as chemistry, physics, biology, engineering and other scientific aspects of nanotechnology [1,2]. Nanoparticles having 1–100 nm possess great impact in the field of chemistry, optics, batteries, physics, environmental remediation, drug delivery and medicine. Nanoparticles exhibit enormous structures which create a different approach in catalytic, physical, chemical and medicinal properties of materials than bulk [3–5].

Nowadays, the researchers concentrate on the metal nanoparticles due to the large surface area, low melting point, and good optical, catalytic, electrical and thermal properties. These distinctive properties of metal nanoparticles create exploitation in the industrial area such as food, agriculture, space, cosmetics, medical and chemical aspects of use

in day-to-day life [6–9].

Recent research in the synthesis of nanoparticles opened a new era in the fast-growing method for the production of nanoparticles. Physical and chemical methods were usually used for the synthesis of nanoparticles, however, based on the toxicity of these methods; the objective of the research has latterly moved towards the biosynthetic method [10–12].

Nanoparticles of magnetic materials have attracted much consideration due to their properties deviate from those of bulk materials and they can be used to make materials and devices with new properties [1]. Magnetic Nanoparticles have important applications in magnetic storage devices, in ferrofluids, i.e. stable suspensions of magnetic nanoparticles, in magnetic beads that are applied in biotechnology, for contrast enhancement in magnetic resonance imaging (MRI), and targeted drug delivery, bioelectrochemical sensing, environmental remediation and as an electrode for supercapacitors and lithium-ion batteries [2]. The magnetic nanoparticles received from the green synthesis method using plants applied in many fields such as semiconductors [13], catalysts [14], optics, chemistry [15] and medicine [16].

* Corresponding author at: Department of Physics, H.H. The Rajah's College, Pudukkottai, 622001, India.

E-mail address: Siva_hhrc@yahoo.in (S. M.).

<https://doi.org/10.1016/j.jece.2020.104420>

Received 11 July 2020; Received in revised form 16 August 2020; Accepted 20 August 2020

Available online 5 September 2020

2213-3437/© 2020 Elsevier Ltd. All rights reserved.

Metal nanoparticles can be synthesized by adopting several methods such as physical, chemical or photochemical reactions, thermal decomposition, electrochemical and sonication. However, most of the methods are related to certain disadvantages such as using hazardous chemicals and high energy requirements which extended the environmental toxicity and cost ineffectiveness [17–20]. The biosynthetic method has recognized as an environment-friendly, low-cost, and safer alternative to chemical and physical methods. Nanoparticles can be synthesized from a variety of biological entities such as actinomycetes, algae, bacteria, fungi, plants, viruses, and yeast. Mainly, Fe nanoparticles were used in industrial sites. More focussly, iron nanoparticles used in textile industry [21], plastic industry [22] with nanowire and nanofibre structure for coatings. In medical field, Fe nanoparticles are used in tissue repair, drug delivery and detoxification of biological fluids, hyperthermia, and immunoassay in cell separation. Iron nanoparticles contribution extended in sunscreen products [23], leather industry [24] and food industry [25]. The antibacterial effect of Fe nanoparticles creates distinctive position for it among other metal nanoparticles. The magnetic property of Fe nanoparticles exhibited a specific approach in drug delivery on targeted cancer cells [26–30].

Plants are particularly assuring for bioreduction since they are easily available, inexpensive and scalable [31–33]. Plant extracts containing bioactive alkaloids, phenolic acids, polyphenols, proteins, sugars, and terpenoids which can reduce the metal ions and then stabilizing them.

Medicinal plants are of most importance in traditional medicine, in which in most part, the antioxidant activity of the plant-derived compounds deemed responsible for curing numerous diseases. Cinnamomum Verum consists of many polyphenolic compounds with antioxidant activity. The purpose of this research was to reduce iron III chlorides to iron nanoparticles by biosynthesis method using Cinnamomum Verum extracts which contain phenolic compounds that act as reducing and capping agents. Cinnamomum Verum plant was used as a spice to flavor cooking, stewed fruit, and tea. Traditionally, it was used as one of the Ayurvedic medicinal herbs in Asia. It required warm climate. Cinnamomum Verum was native to Sri Lanka and favors free-draining soils in a humid position. Cinnamomum Verum was rich in polyphenols and its biomolecules act as reducing and capping agents during the synthesis of iron nanoparticles. Cinnamomum Verum was a spice that has ancient origins and popularly used as flavorings, condiment in cooking. Cinnamomum Verum was also known to provide various medicinal benefits that include lowering of blood cholesterol, for diabetes. Cinnamomum Verum was widely believed to be high in anti-oxidants. Regular drinking of Cinnamomum Verum tea could be beneficial to oxidative stress-related illness in humans. Cinnamomum Verum barks received from the Cinnamomum Verum tree. It has a polyphenolic compound which diminished the iron chloride to iron nanoparticles [34,35].

There are many plants based reports to synthesize silver and gold nanoparticles. A few pieces of literature were available on the

biosynthesis of metals like iron and palladium. The present study of biosynthesized nanoparticles was the first report which narrated the synthesis of iron nanoparticles using Cinnamomum Verum extracts. Comparing with recent literatures, we prepared iron nanoparticles with cost effectiveness and high antibacterial effect. The phytochemicals in Cinnamomum Verum bark extract provide much higher rapid capping and stabilizing action for Fe nanoparticles. Therefore, the present work was carried out to synthesize and characterize the iron nanoparticles using Cinnamomum Verum extract.

2. Materials and methods

2.1. Chemicals

Ferric III chloride (FeCl_3) ($\geq 98.97\%$), ethanol ($\text{C}_2\text{H}_5\text{OH}$) ($\geq 98.02\%$), acetone ($\text{C}_3\text{H}_6\text{O}$) ($\geq 99.20\%$) and Deionized water ($\geq 99.58\%$) were obtained from Sigma-Aldrich chemicals. All glass wares were cleaned with distilled water and acetone as well as dried well before use. The raw Cinnamomum Verum barks were used.

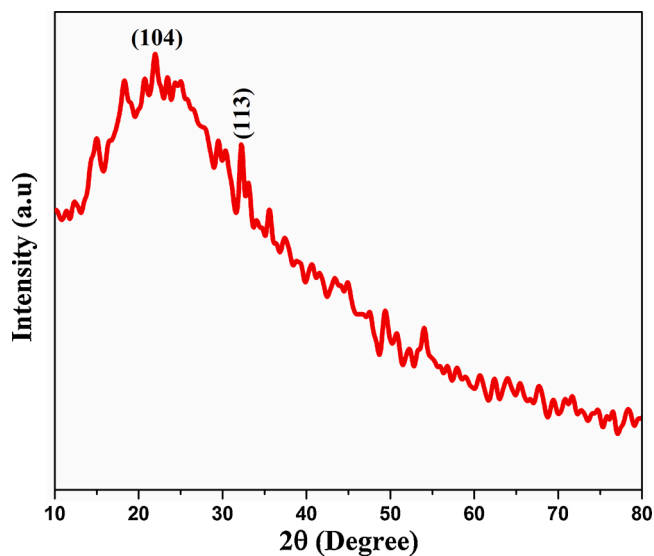


Fig. 2. XRD pattern of Fe NPs synthesized using Cinnamomum Verum extract.

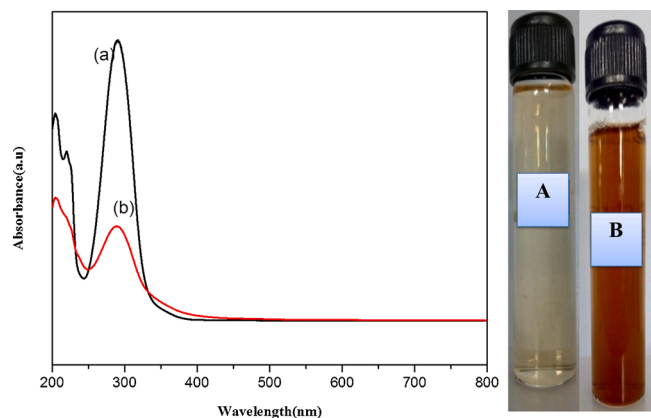


Fig. 1. UV Spectra of (a) Extract and (b) Synthesized Iron NPs.

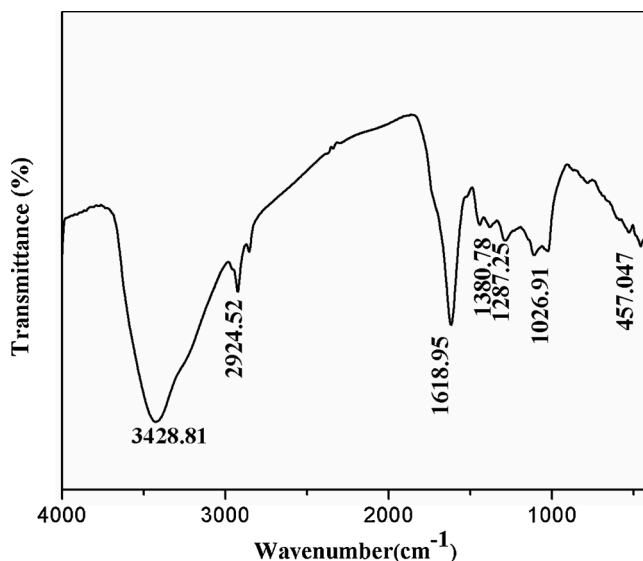


Fig. 3. FT-IR spectrum of Fe NPs synthesized using Cinnamomum Verum extract.

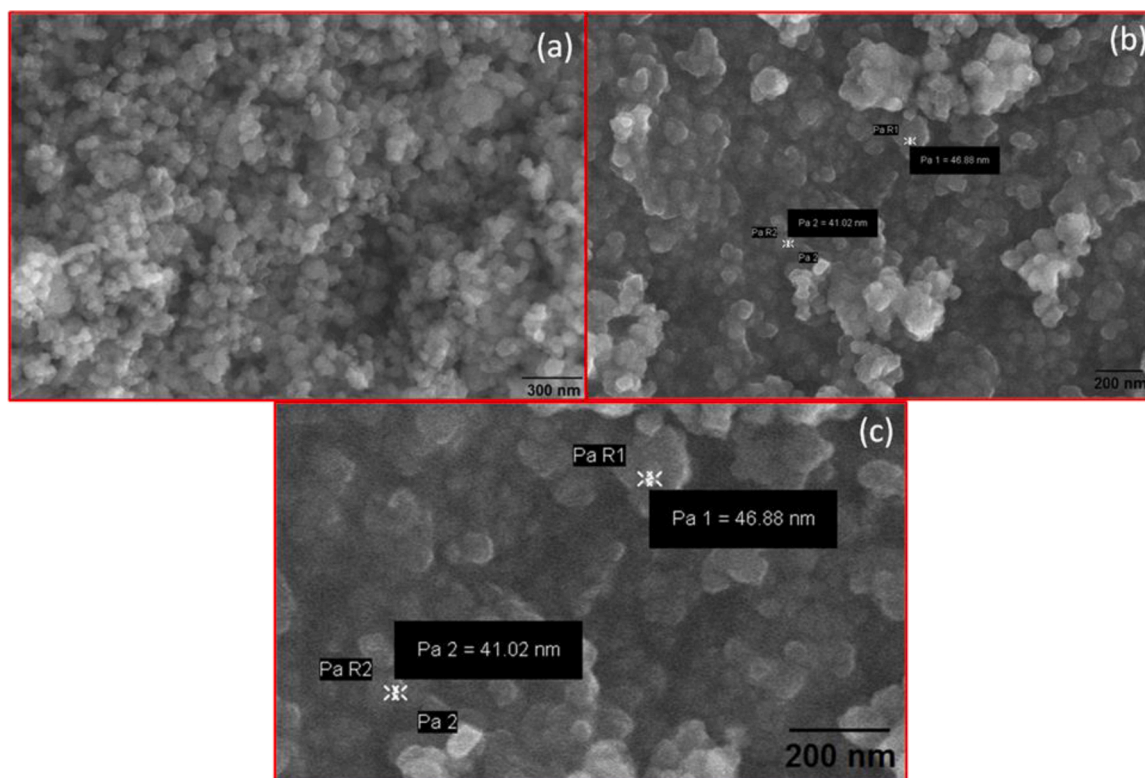


Fig. 4. SEM images of synthesized iron NPs using Cinnamomum Verum extract at 300 nm, and 200 nm magnification.

2.2. Preparation of Cinnamomum Verum bark extract

The barks of Cinnamomum Verum were purified with deionized water for three times to eliminate mud and dust. After, it was dehydrated at room temperature for three weeks. 5 g of Cinnamomum Verum strands were put in 100 mL of distilled water and the solution heated up to 70 °C for 20 min in a heater mantle under reflux. This mixture was put in an undisturbed condition to attain room temperature and then it was filtered through a Whatman No. 1 paper. The extract solution was stored at 4 °C for further use.

2.3. Synthesis of iron nanoparticles

0.01 M of FeCl₃ solution and Cinnamomum Verum bark extract was taken as precursor in 1:1 proportion for synthesizing iron nanoparticles.

In the 0.01 M of FeCl₃ solution, the extract solution was added dropwise by a burette. The reaction mixture solution was converted into black color instantly. It indicated the formation of iron nanoparticles, which absorb radiation in the visible region. After 24 h, the reaction mixture was centrifuged at 10,000 rpm for 15 min. The resultant black pellet was purified with deionized water and ethanol. Then, it was dehydrated at 60 °C in a hot air oven for removing residual impurities and moisture. The attained black powder of iron nanoparticles was deposited in a dried dark place for further analyses.

3. Characterization of iron nanoparticles

The synthesized iron NPs were characterized with the help of a UV–vis Spectrophotometer. X-ray powder diffraction (XRD) data was taken with

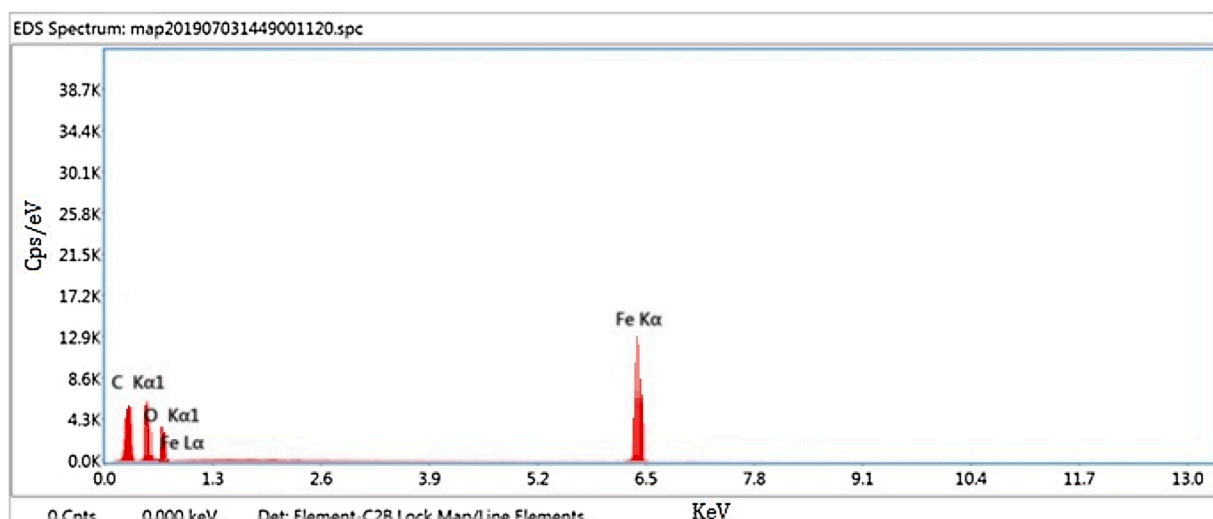


Fig. 5. EDS Spectrum of synthesized iron NPs using Cinnamomum Verum extract.

Table 1

Elemental composition of synthesized iron NPs using Cinnamomum Verum extract.

Elements	Weight (%)
C K	3
O K	3
Fe K	93

a Ni filter and Cu K α radiation ($\lambda = 0.15406$ nm), on the PANalytical X'pert PRO powder X-Ray diffractometer. The FTIR spectra of extracts were taken before and after synthesis of iron NPs by using Thermo Nicolet 380 FTIR spectrometer in attenuated total reflection mode and using a spectral range of 4000–400 cm^{-1} . To identify the average particle size and morphology of iron NPs, SEM and HR-TEM analyses have performed using CARL ZEISS, EVO 18 SEM machine and JEOL-2100+ High-Resolution Transmission Electron Microscope. The presence of the elemental composition of magnetic NPs was determined employing EDX analysis. The magnetic measurements were taken utilizing vibrating sample magnetometer (VSM) at room temperature with a magnetic field up to 2.2 T using Microsense, Model ADE – EV9.

3.1. Antibacterial assay

3.1.1. Disc preparation

The 6 mm (diameter) discs were made from Whatman No. 1 filter paper. The discs were sterilized by autoclave at 121 °C. After the sterilization, the moisture discs were dried on a hot air oven at 50 °C. Then various solvent extract discs and control discs have prepared [36].

3.1.2. Collection of test bacterial species

The Bacterial strains of *Bacillus subtilis*, *Escherichia coli*, *Klebsiella pneumonia* and *Staphylococcus aureus* were obtained from Microbial Type Culture Collection Centre (MTCC), Chandigarh.

3.1.3. Assay of antibacterial activity

The antibacterial activity test was carried out following the modification of the method originally defined by Bauer et al. (1966). Muller Hinton agar was ready and autoclaved at 15 fifteen lbs pressure for twenty minutes and cooled to 45 °C. The medium was permitted to cool and poured on to sterile Petri plates and left for solidification. The plates with media were seeded with their corresponding microbial suspension by utilizing a sterile swab. The various solvents extract were made as discs individually set on each Petri plates and also placed control and standard (*Nitrofurantoin* (300 μg) for Bacteria) discs. The plates were incubated at 37 °C for one day. After the incubation period, the diameter of the zone formed around the paper disc was measured and expressed in mm [36].

3.2. Antioxidant assay

Aliquot of DPPH methanol solution (2 mL) was added with a sample solution in various concentrations. For a few min, this solution was stirred. After this, it was allowed to stand in dark at room temperature for 30 min. After, the inhibition percentage was viewed with the help of spectrophotometer [37]. The inhibition percentage by,

$$\text{Scavenging behavior (\%)} = 100 - [(A_c - A_s)/A_c] \times 100 \quad (1)$$

Where A_c = Control Absorbance, A_s = Sample Absorbance.

3.3. Anti-inflammatory assay

0.2 mL of egg albumin, 2.8 mL Phosphate-buffered saline at pH 6.4 and 2 mL of analyzed sample with different concentrations were mixed. Then, this solution was put in an incubator at 37 ± 2 °C for 15 min. After, the reaction mixture was dehydrated at 70 °C for 5 min. After, the inhibition percentage was viewed with the help of spectrophotometer [37]. The inhibition percentage by,

$$\% \text{ inhibition} = 100 - [(V_c - V_t)/V_c] \times 100 \quad (2)$$

Where,

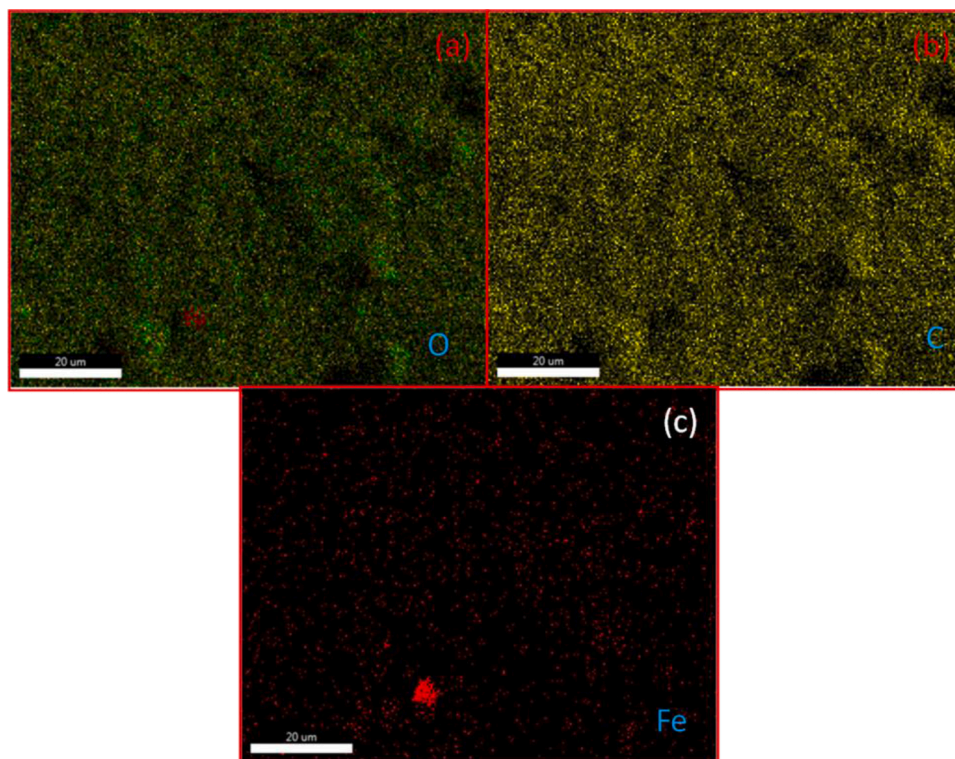


Fig. 6. Mapping of a) Oxygen b) Carbon c) Fe elements in synthesized iron NPs using Cinnamomum Verum extract at 20 μm magnification.

V_t = Sample Absorbance, V_c = Control Absorbance.

3.4. Anti-diabetic assay

For 10 min, 0.5 mg/mL of α -Amylase was placed at 25 °C. After, it was mixed with the starch solution, 20 mM of sodium phosphate buffer at pH 6.9 and 6 mM of sodium chloride. Then, this solution was placed at 25 °C for 30 min. For 5 min, the medium was dehydrated at 70 °C. After, the inhibition percentage was viewed with the help of spectrophotometer [37]. The inhibition percentage by,

$$\% \text{ inhibition} = 100 - \left\{ \frac{V_c - V_t}{V_c} \right\} \times 100 \quad (3)$$

Where,

V_t = Sample Absorbance, V_c = Control Absorbance.

4. Results and discussion

4.1. UV-vis spectroscopy analysis

The UV-vis spectrum of synthesized iron NPs showed (Fig. 1) a maximum absorbance at about 288 nm which may be assigned to the surface plasmon absorption of iron NPs [35]. The peak at 220 nm in UV-vis Spectra for the extract assigned to $\pi \pi^*$ or $n \pi^*$ transitions confined in the polyphenolic compounds. After the addition of the FeCl_3 solution to an aqueous Cinnamomum Verum extract, the brown color solution was transferred into black color which intimated the form of Fe^0 from Fe^+ [20].

4.2. XRD analysis

The structure and formation of iron NPs was further supported by X-ray diffraction (XRD) analysis. The sample was scanned from 5° to 80° 2 θ at a scanning rate of 3° 2 θ per minute. It was observed that the pattern has deficient in distinctive diffraction peaks and suggested that iron NPs exist in amorphous. The reflections in the Fig. 2 realized to iron (Fe). The characteristics peak at 32.23° corresponded to iron NPs, (JCPDS no.89-7047) [20]. In the XRD pattern of iron NPs, another peak appeared at 2 θ = 22° which could be enclosed to organic materials adsorbed from extract as a capping or stabilizing agent [19,20]. The average crystallite size determined with Scherer's formula was at 36 nm. This pattern coincides with a similar type of XRD pattern for iron NPs synthesized using T. Chebula extract [20].

4.3. FTIR analysis

The FTIR of synthesized iron NPs was carried out to demonstrate the presence of polyphenols as antioxidant sources for green synthesis of iron NPs. The FT-IR spectrum of Cinnamomum Verum (Fig. 3) revealed the peaks at 3428, 2924 and 1026 cm^{-1} which was related to C—H and C—OH stretching vibrations due to hydroxyl groups [38]. The strong absorption band at 1618 cm^{-1} was due to C=O stretching of the carbonyl group and the peak at about 1442 cm^{-1} which intimated C=C stretching vibrations because of aromatic hydrocarbon groups. The FT-IR of synthesized iron NPs by Cinnamomum Verum peaks which were slightly modified from the FT-IR spectrum of Cinnamomum Verum extract. This observation confirmed that the organic compounds in the

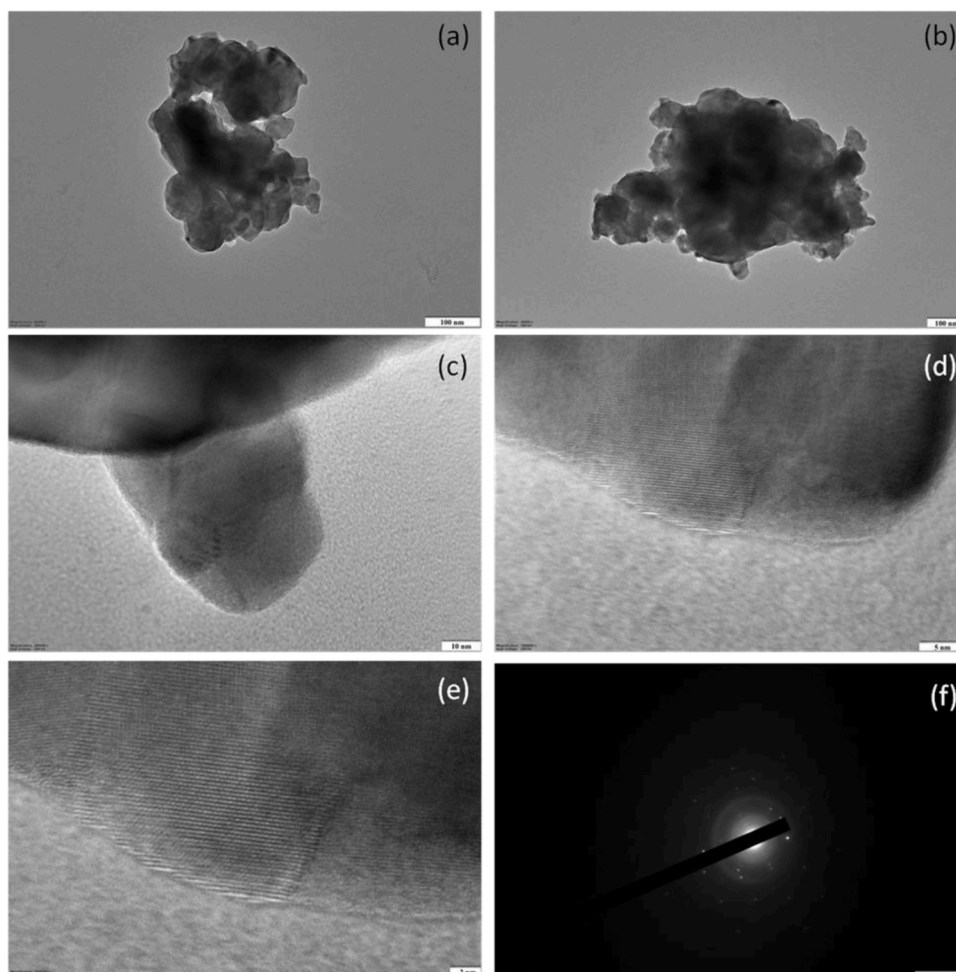


Fig. 7. (a–e) HR-TEM images in the magnification of 100 nm, 100 nm, 10 nm, 5 nm and 2 nm respectively and (f) SAED pattern of synthesized Fe NPs.

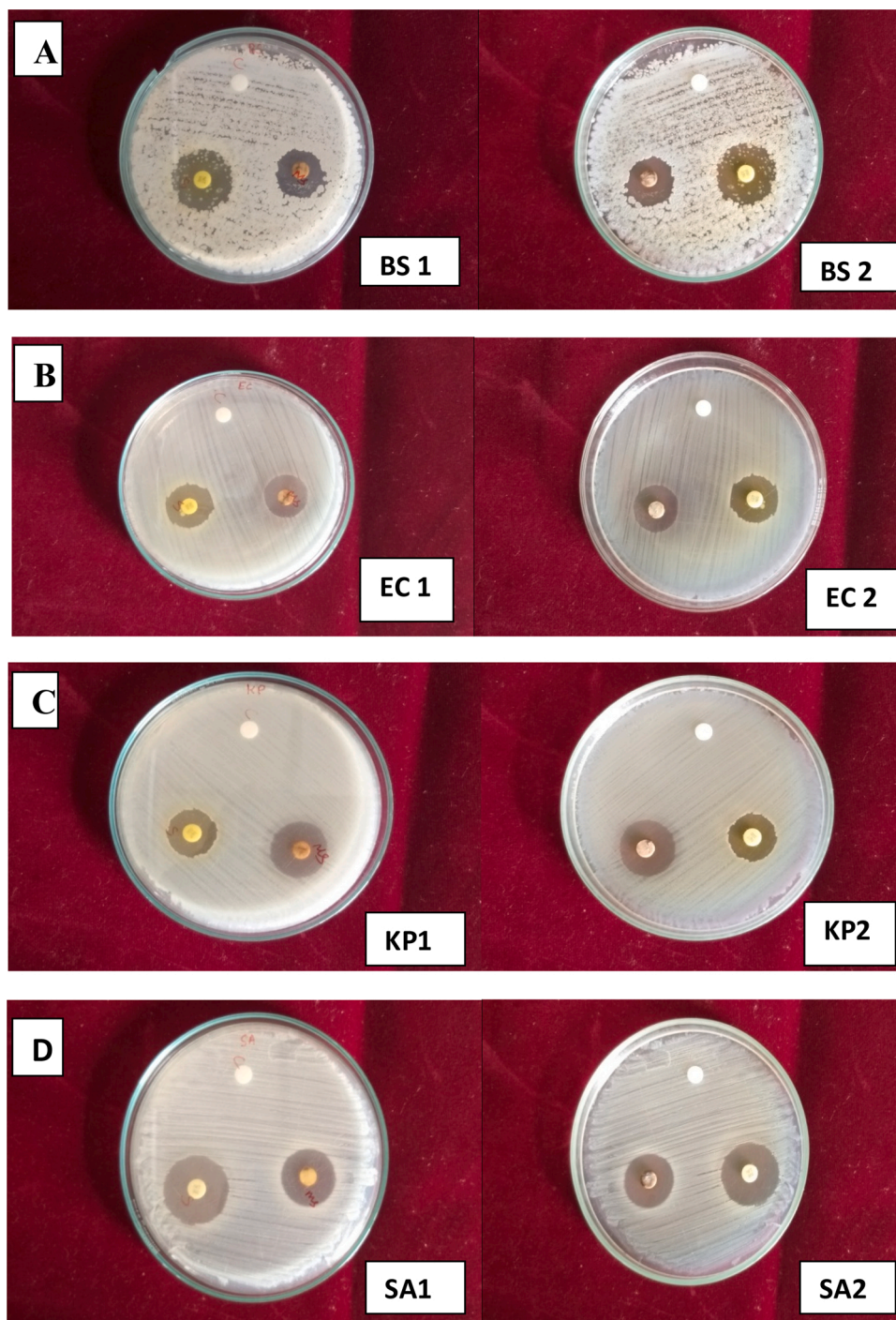


Fig. 8. Antibacterial assay of synthesized iron NPs using *Cinnamomum Verum* extract against a) *Bacillus subtilis* b) *Staphylococcus aureus* c) *Escherichia coli* d) *Klebsiella pneumoniae*.

Table 2

Inhibition zone of biosynthesized iron NPs against various human pathogenic bacteria.

Bacterial Species	Zone of Inhibition (mm) against human pathogenic bacteria	
	Standard ^a	Fe
<i>Escherichia coli</i>	18	18
<i>Klebsiella pneumoniae</i>	17	25
<i>Staphylococcus aureus</i>	16	20
<i>Bacillus subtilis</i>	18	19

^a Nitrofurantoin (300µg).

extract which absorbed on the surface of magnetic NPs by π -electrons interaction. Hence, the constituents of extract not only act as reducing agents but also played the role of capping agents for the stabilization on the surface of prepared iron NPs [39].

4.4. SEM and EDS analysis

The SEM images (Fig. 4) of iron NPs exposed that the synthesis of nano-sized particles. It is simply revealed that the particles varied from 20 to 80 nm with spherical morphology. It varied from those iron NPs synthesized using chemicals as reducing agents, which tend to have a

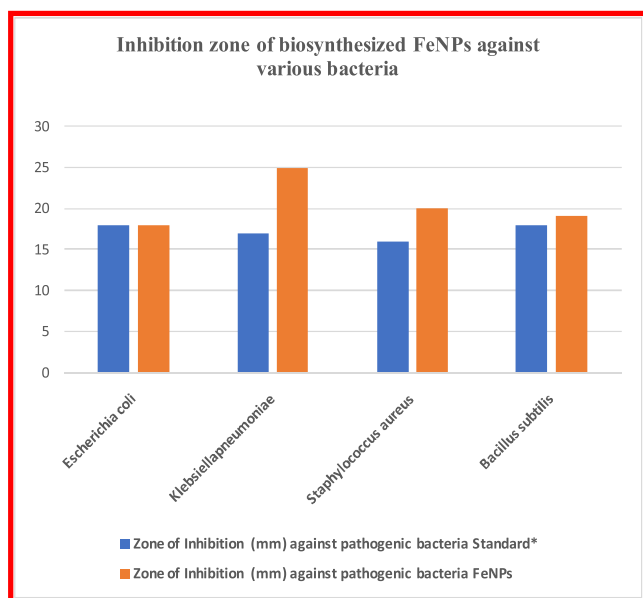


Fig. 9. Inhibition zone of biosynthesized FeNPs against various bacteria.

more homogeneous size distribution [40]. The different shapes of NPs lead to the different distinctive application [39]. The spherical shaped NPs were mainly contributing its efficient application in biomedical field. The hexagonal and rectangular shaped NPs contributed its tendency mainly in biomedical imaging application [39]. The circular shaped NPs contributed its potential in electrical, optical and biomedical application [37]. It was most surely since the Cinnamomum Verum extract was a combination of various naturally occurred compounds with different reducing properties [41]. Polyphenols or antioxidants in the Cinnamomum Verum bark played an indispensable role in controlling the agglomeration of the NPs and developed their dispersion by operating as a capping agent [42]. To furthermore understanding the elements in the synthesized NPs, the elemental composition of biosynthesized NPs was determined with EDS analysis which was given in Fig. 5. From that, a strong intense peak of C, O, and Fe in the spectrum was observed. This spectrum established the existence of Fe in NPs. The C and O peaks were attributed mainly to the polyphenol groups and other C, O-containing molecules in the Cinnamomum Verum [43,44]. The weight percentage of molecules present in Fe NPs was registered in Table 1. This weight percentage was 27 % weight of O, 71 % weight of C and 2% weight of Fe. The EDS spectrum could further be signified with EDS mapping. EDS mapping designed in different colors (Green, yellow

and Red) showed the Oxygen, Carbon and Iron elements in the Fe NPs which bestowed in Fig. 6. Fe was originated from FeCl_3 as a precursor in the synthesis of iron NPs. O_2 may be from high flavonoids content in Cinnamomum Verum extract. The mentioned values would be useful in atomic content on the surface regions of iron NPs [45,46].

4.5. HR-TEM analysis

The HR-TEM analysis (Fig. 7) of prepared Fe NPs explicated the circular, spherical shaped NPs with size at 20–50 nm. The large agglomeration of NPs was eliminated by extract usage in synthesis. Some agglomeration of NPs was viewed with the high surface energy of Fe NPs. Further, it was reasoned by the Fe NPs synthesis was carried out in water medium. The hydrophilic and hydrophobic behavior of prepared Fe NPs was understood by the black and white regions viewed in the images. The fringes viewed denoted the regular arrangement of lattice planes in prepared Fe NPs [37,39]. The fringes and SAED pattern was merged with the XRD d-spacings of (113) plane.

4.6. Phytochemical analysis

The phytochemical analysis listed the phytochemicals in Cinnamomum Verum bark extract which were responsible for capping and stabilizing action of prepared Fe NPs [39]. In the aqueous extractive value, Polyphenols, Alkaloids, Tannin, Steroids, Terpenoids, and Glycoside were present in high concentration. These phytochemicals were the reason for the reduction of iron chloride to iron NPs. Further, it reasoned for the capping and stabilizing action of prepared Fe NPs. This phytochemicals diminished the size of NPs. It represented the Cinnamomum Verum bark were rich in antioxidants agents. This further improved the biomedical application of prepared Fe NPs.

4.7. Antibacterial assay

The antibacterial activity of synthesized iron NPs from Cinnamomum Verum extract was investigated against various pathogenic organisms such as *Escherichia coli*, *Klebsiella pneumonia*, *Staphylococcus aureus* and *Bacillus subtilis* using disc diffusion method was shown in Fig. 8. The diameter of inhibition zones (mm) of iron NPs was reported in Table 2. Cinnamomum Verum functionalized iron NPs displayed higher inhibition activity against *Klebsiella pneumonia* (25 mm), *Staphylococcus aureus* (20 mm) and *Bacillus subtilis* (19 mm) bacterial strains. Therefore, we can conclude that the biosynthesized iron NPs were shown efficient antibacterial property because of plant extract when compared to a standard value. This inhibition values were also shown in Fig. 9.

The inhibition of applied bacteria with synthesized iron NPs was

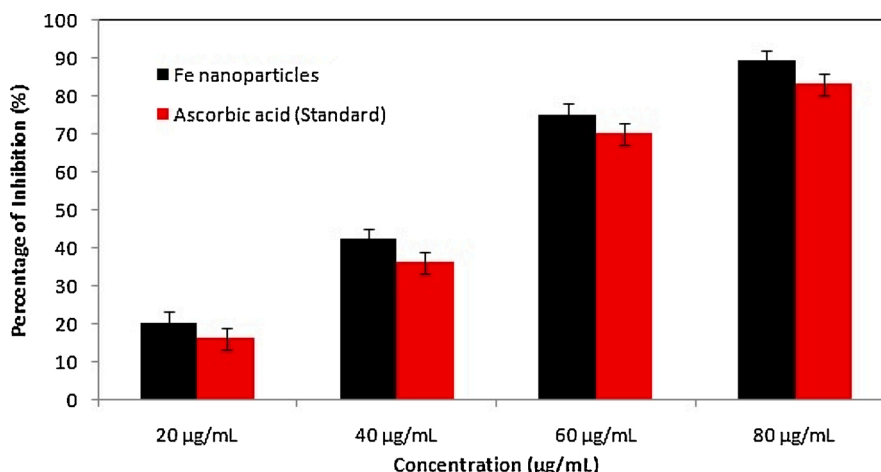


Fig. 10. Antioxidant assay of synthesized Fe NPs using Cinnamomum verum extract.

Table 3
Antioxidant assay of synthesized Fe NPs via *Cinnamomum Verum* bark extract.

Samples	% of inhibitions (%)				IC ₅₀ value
	Concentration (µg/mL)				
	20	40	60	80	
Fe	20.19 ± 0.70	42.07 ± 0.14	75.43 ± 1.10	89.24 ± 0.18	47.50
Ascorbic acid (Standard)	16.73 ± 0.32	36.45 ± 0.71	70.81 ± 1.01	83.18 ± 0.10	50.02

± indicated the triplicate experimental results.

demonstrated in the following ways.

- The release of reactive oxygen species such as H₂O₂, Fe²⁺ ions, O₂⁻ ions bind with the cell wall of bacteria.
- These species penetrate and perforated the cell membrane. This leads to cell wall damage.
- This action released the interior components of the cell and attacks the DNA of bacteria.
- Moreover, all actions lead to cell damage and death [47].

This result has comparable with the earlier literatures [37,47].

4.8. Antioxidant assay

The DPPH antioxidant assay analyzed the scavenging behavior of Fe NPs and which was showed in Fig. 10. The (Table 3) provided the percentage of inhibition values and which showed the high concentration of Fe NPs applied have high inhibition. The concentrations used for analyzing the scavenging behavior of Fe NPs were 20, 40, 60 and 80 µg/mL. Moreover the positive control of ascorbic acid as standard was used in analysis.

The inhibition values of Fe NPs were 20 %, 42 %, 75 % and 89 % and for ascorbic acid were 16 %, 36 %, 70 % and 83 % with 20, 40, 60 and 80 µg/mL concentrations respectively.

Further, the IC₅₀ value measurement described the 50 % of inhibition. The low value of IC₅₀ value expressed the efficient inhibition. The IC₅₀ value measured for Fe NPs was at 47.50 µg/mL and for ascorbic acid measured was at 50.02 µg/mL. The phytochemicals in *Cinnamomum Verum* bark extract may also reasoned for the high scavenging behavior of prepared Fe NPs [37]. Overall, the synthesized Fe NPs expressed the efficient scavenging assay than ascorbic acid. This result has comparable with earlier reports [37,48].

4.9. Anti-inflammatory assay

The usual process of breaking the proteins as secondary and tertiary structures provided the loss of biological function. It was an interesting assay for analyzing the protective action than destroying action as antibacterial assay. With this, the anti-inflammatory assay was evaluated for synthesized Fe NPs and which was showed in Fig. 11. The Table 4 showed the values of inhibition percentage measured in the analysis. These values expressed the high concentration applied in analysis have high inhibition percentage value. The concentrations used in analysis were 100, 200, 300, 400 and 500 µg/mL and the positive control of Diclofenac sodium as standard have also deployed.

The inhibition percentage of Fe NPs were at 21 %, 44 %, 70 %, 79 % and 87 % and for Diclofenac sodium were at 17 %, 38 %, 63 %, 73 % and 83 % with 100, 200, 300, 400 and 500 µg/mL concentrations respectively.

The IC₅₀ value measured for Fe NPs was at 212 µg/mL and for Diclofenac sodium was at 250 µg/mL. These values reported the synthesized Fe NPs have efficient action than Diclofenac sodium. This result has comparable with the earlier reports [37,49].

4.10. Anti-diabetic assay

The biomedical behavior of synthesized Fe NPs was understood via analyzing it in anti-diabetic assay. The Fig. 12 described the anti-diabetic assay and the measured values of inhibition percentages were grouped in Table 5. The concentrations used in analysis were 100, 200, 300, 400 and 500 µg/mL and the positive control of Acarbose as standard have also deployed.

The inhibition percentage for Fe NPs were at 15 %, 26 %, 45 %, 70 %, 84 % and for acarbose were at 11 %, 19 %, 37 %, 63 %, 73 % with 100, 200, 300, 400 and 500 µg/mL concentrations respectively. These values described the high concentration applied in analysis have high inhibition percentage value.

The IC₅₀ value measured for Fe NPs was at 312 µg/mL and for acarbose was at 370 µg/mL. These values proved the effective behavior of Fe NPs than acarbose. This result has comparable with earlier reports [48,49].

4.11. Vibrating sample magnetometer (VSM) analysis J1-2

To investigate the magnetic behavior of biosynthesized iron NPs, magnetization measurements filed using a vibrating sample magnetometer (VSM) at room temperature. Fig. 13 showed magnetization curve of synthesized Fe NPs. A linear Magnetization-Applied magnetic field ((M-H) graph with no hysteresis loop was achieved, which

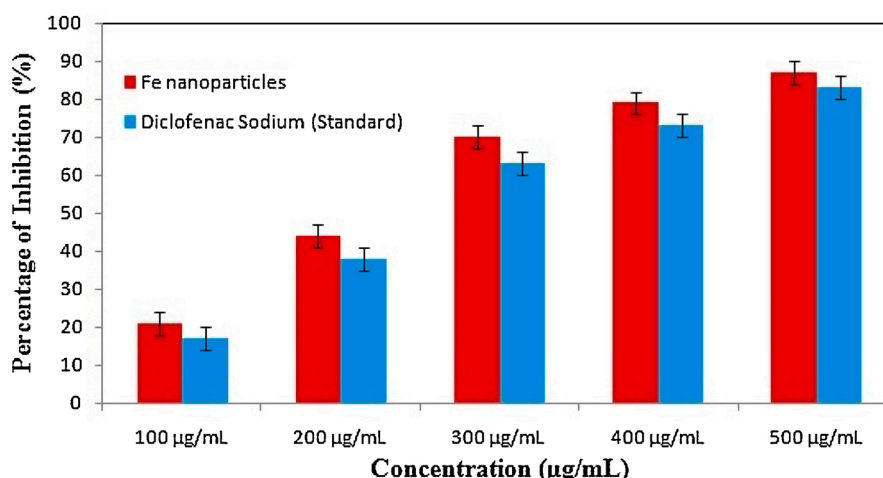


Fig. 11. Anti-inflammatory assay of synthesized Fe NPs using *Cinnamomum verum* extract.

Table 4Anti-inflammatory assay of synthesized Fe NPs via *Cinnamomum Verum* bark extract.

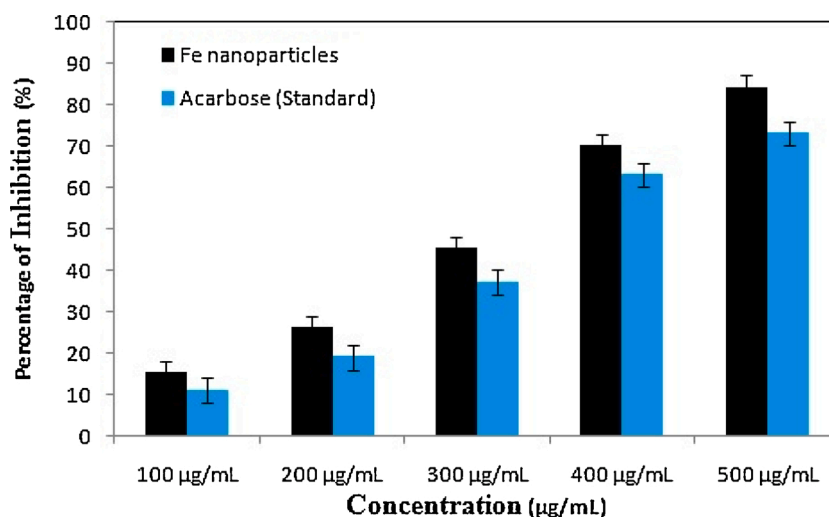
Samples	% of inhibitions (%)					IC ₅₀ value
	Concentration (µg/mL)					
	100	200	300	400	500	
Fe	21.10 ± 0.15	44.10 ± 0.13	70.19 ± 1.05	79.45 ± 0.90	87.35 ± 0.10	212.10
Diclofenac sodium (Standard)	17.20 ± 0.40	38.15 ± 0.12	63.15 ± 0.20	73.06 ± 0.70	83.03 ± 0.81	250.06

± indicated the triplicate experimental results.

Table 5Anti-diabetic assay of synthesized Fe NPs via *Cinnamomum Verum* bark extract.

Samples	% of inhibitions (%)					IC ₅₀ value
	Concentration (µg/mL)					
	100	200	300	400	500	
Fe	15.19 ± 0.15	26.20 ± 0.13	45.09 ± 0.45	70.19 ± 1.17	84.15 ± 0.17	312.17
Acarbose (Standard)	11.19 ± 0.19	19.17 ± 0.05	37.26 ± 0.15	63.15 ± 0.17	73.15 ± 0.19	370.13

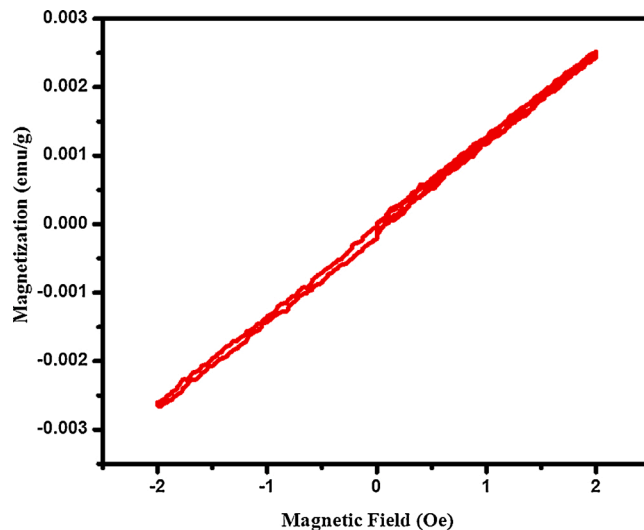
± indicated the triplicate experimental results.

**Fig. 12.** Anti-diabetic assay of synthesized Fe NPs using Cinnamomum verum extract.

intimated that the synthesized iron NPs have paramagnetic properties. Therefore, the biosynthesized iron NPs were weakly attracted by a strong externally applied magnetic field, and form internal induced magnetic fields in the direction of the applied magnetic field [50].

5. Conclusion

The present study compiled the impact of iron NPs and *Cinnamomum Verum* extract plays an essential role in the reduction and stabilization of iron NPs. The synthesized magnetic Fe NPs have confirmed by UV–vis analysis with SPR band at 288 nm. XRD analysis revealed the mean crystallite size of iron NPs was at 36 nm. SEM and HRTEM images revealed that iron NPs were compatible, stable in circular and spherical shaped with size at 20–50 nm. The EDAX and mapping analysis validated the formation of Fe NPs. The VSM analysis explicated the paramagnetic behavior of prepared NPs. The inhibition zones that appeared

**Fig. 13.** Magnetization curve of synthesized Fe NPs using Cinnamomum verum extract.

in the antibacterial assay designated the synthesized Fe NPs has an efficient higher inhibition of antibacterial effect against human pathogenic bacteria. The antioxidant, anti-inflammatory and anti-diabetic assay showed the efficient behavior of Fe NPs with low concentration value in biomedical applications. These studies revealed that green synthesis of iron NPs has potential as an easy, economical and beneficial process for most scientific and technical applications in the future, including treatment of wastewater, pesticides in agriculture and screening of drugs to hasten the natural drug discovery against promising chemicals.

CRedit authorship contribution statement

M. Sivakami: Conceptualization, Methodology, Writing - original draft. **K. Renuka Devi:** Funding acquisition, Resources, Project administration, Supervision, Validation, Writing - review & editing. **R.**

Renuka: Software, Visualization. **T. Thilagavathi:** Investigation, Data curation, Formal analysis.

Declaration of Competing Interest

The authors report no declarations of interest.

References

- [1] S.P. Dubey, M. Lahtinen, M. Sillanpää, Green synthesis and characterizations of silver and gold nanoparticles using leaf extract of *Rosa rugosa*, *Colloids Surf. A Physicochem. Eng. Asp.* 364 (1–3) (2010) 34–41.
- [2] N. Beheshtkhou, M.A.J. Kouhbanani, A. Savardashtaki, A.M. Amani, S. Taghizadeh, Green synthesis of iron oxide nanoparticles by aqueous leaf extract of *Daphne mezereum* as a novel dye removing material, *Appl. Phys. A-Matter.* 124 (5) (2018) 363.
- [3] M. Sabet, M. Salavati-Niasari, O. Amiri, Using different chemical methods for deposition of CdS on TiO₂ surface and investigation of their influences on the dye-sensitized solar cell performance, *Electrochim. Acta* 117 (2014) 504–520.
- [4] M. Salavati-Niasari, Synthesis and characterization of host (nanodimensional pores of zeolite-Y)-guest [unsaturated 16-membered octaaza-macrocyclic manganese (II), cobalt (II), nickel (II), copper (II), and zinc (II) complexes] nanocomposite materials, *Chem. Lett.* 34 (10) (2005) 1444–1445.
- [5] M. Salavati-Niasari, D. Ghanbari, M.R. Loghman-Estarki, Star-shaped PbS nanocrystals prepared by hydrothermal process in the presence of thioglycolic acid, *Polyhedron* 35 (1) (2012) 149–153.
- [6] F. Davar, M. Salavati-Niasari, Synthesis and characterization of spinel-type zinc aluminate nanoparticles by a modified sol-gel method using new precursor, *J. Alloys Compd.* 509 (5) (2011) 2487–2492.
- [7] F. Mohandes, F. Davar, M. Salavati-Niasari, Magnesium oxide nanocrystals via thermal decomposition of magnesium oxalate, *J. Phys. Chem. Solids* 71 (12) (2010) 1623–1628.
- [8] M. Salavati-Niasari, M.R. Loghman-Estarki, F. Davar, Controllable synthesis of nanocrystalline CdS with different morphologies by hydrothermal process in the presence of thioglycolic acid, *Chem. Eng. J.* 145 (2) (2008) 346–350.
- [9] M. Salavati-Niasari, Ship-in-a-bottle synthesis, characterization and catalytic oxidation of styrene by host (nanopores of zeolite-Y)/guest ([bis (2-hydroxyanil) acetylacetonato manganese (III)]) nanocomposite materials (HGNN), *Microporous Mesoporous Mater.* 95 (1–3) (2006) 248–256.
- [10] M. Salavati-Niasari, Nanoscale microreactor-encapsulation of 18-membered decaaza macrocycle nickel (II) complexes, *Inorg. Chem. Commun.* 8 (2) (2005) 174–177.
- [11] E. Esmaeili, M. Salavati-Niasari, F. Mohandes, F. Davar, H. Seyghalkar, Modified single-phase hematite nanoparticles via a facile approach for large-scale synthesis, *Chem. Eng. J.* 170 (1) (2011) 278–285.
- [12] M. Salavati-Niasari, A. Sobhani, F. Davar, Synthesis of star-shaped PbS nanocrystals using single-source precursor, *J. Alloys Compd.* 507 (1) (2010) 77–83.
- [13] S. Mortazavi-Derazkola, S. Zinatloo-Ajabshir, M. Salavati-Niasari, Novel simple solvent-less preparation, characterization and degradation of the cationic dye over holmium oxide ceramic nanostructures, *Ceram. Int.* 41 (8) (2015) 9593–9601.
- [14] M. Yousefi, F. Gholamian, D. Ghanbari, M. Salavati-Niasari, Polymeric nanocomposite materials: preparation and characterization of star-shaped PbS nanocrystals and their influence on the thermal stability of acrylonitrile-butadiene-styrene (ABS) copolymer, *Polyhedron* 30 (6) (2011) 1055–1060.
- [15] M. Masjedi-Arani, M. Salavati-Niasari, A simple sonochemical approach for synthesis and characterization of Zn₂SiO₄ nanostructures, *Ultrason. Sonochem.* 29 (2016) 226–235.
- [16] S. Zinatloo-Ajabshir, M.S. Morasaei, O. Amiri, M. Salavati-Niasari, Green synthesis of dysprosium stannate nanoparticles using *Ficus carica* extract as photocatalyst for the degradation of organic pollutants under visible irradiation, *Ceram. Int.* 46 (5) (2020) 6095–6107.
- [17] T. Meenatchi, A. Palanimurugan, A. Dhanalakshmi, V. Maheshkumar, B. Natarajan, Green synthesis of *Cynodon Dactylon* capped concentrations on ZnO nanoparticles for antibacterial activity, ROS/ML-DNA treatment and compilation of best controlling microbes by mathematical comparisons, *Chem. Phys. Lett.* (2020), 137429.
- [18] V.V. Makarov, S.S. Makarova, A.J. Love, O.V. Sinityn, A.O. Dudnik, I. V. Yaminsky, N.O. Kalinina, Biosynthesis of stable iron oxide nanoparticles in aqueous extracts of *Hordeum vulgare* and *Rumex acetosa* plants, *Langmuir* 30 (20) (2014) 5982–5988.
- [19] S. Arokiyaraj, M. Saravanan, N.U. Prakash, M.V. Arasu, B. Vijayakumar, S. Vincent, Enhanced antibacterial activity of iron oxide magnetic nanoparticles treated with *Argemone mexicana* L. leaf extract: an in vitro study, *Mater. Res.* 48 (9) (2013) 3323–3327.
- [20] K.M. Kumar, B.K. Mandal, K.S. Kumar, P.S. Reddy, B. Sreedhar, Biobased green method to synthesize palladium and iron nanoparticles using *Terminalia chebula* aqueous extract, *Spectrochim. Acta A* 102 (2013) 128–133.
- [21] P. Mehdizadeh, Y. Orooji, O. Amiri, M. Salavati-Niasari, H. Moayedi, Green synthesis using cherry and orange juice and characterization of TbFeO₃ ceramic nanostructures and their application as photocatalysts under UV light for removal of organic dyes in water, *J. Clean. Prod.* 252 (2020), 119765.
- [22] Y. Orooji, R. Mohassel, O. Amiri, A. Sobhani, M. Salavati-Niasari, Gd₂ZnMnO₆/ZnO nanocomposites: green sol-gel auto-combustion synthesis, characterization and photocatalytic degradation of different dye pollutants in water, *J. Alloys Compd.* 835 (2020), 155240.
- [23] Y. Orooji, A.A. Alizadeh, E. Ghasali, M.R. Derakhshandeh, M. Alizadeh, M.S. Asl, T. Ebadzadeh, Co-reinforcing of mullite-TiN-CNT composites with ZrB₂ and TiB₂ compounds, *Ceram. Int.* 45 (16) (2019) 20844–20854.
- [24] M. Ghasemi, A. Khataee, P. Gholami, R.D.C. Soltani, A. Hassani, Y. Orooji, In-situ electro-generation and activation of hydrogen peroxide using a CuFe/NLDH-CNTs modified graphite cathode for degradation of cefazolin, *J. Environ. Manage.* 267 (2020), 110629.
- [25] A.J. Sisi, M. Fathinia, A. Khataee, Y. Orooji, Systematic activation of potassium peroxydisulfate with ZIF-8 via sono-assisted catalytic process: mechanism and ecotoxicological analysis, *J. Mol. Liq.* 308 (2020), 113018.
- [26] Y. Orooji, M. Ghanbari, O. Amiri, M. Salavati-Niasari, Facile fabrication of silver iodide/graphitic carbon nitride nanocomposites by notable photo-catalytic performance through sunlight and antimicrobial activity, *J. Hazard. Mater.* 389 (2020), 122079.
- [27] M. Bordbar, N. Negahdar, M. Nasrollahzadeh, Melissa officinalis L. leaf extract assisted green synthesis of CuO/ZnO nanocomposite for the reduction of 4-nitrophenol and Rhodamine B, *Sep. Purif. Technol.* 191 (2018) 295–300.
- [28] M. Nasrollahzadeh, S.M. Sajadi, Preparation of Au nanoparticles by *Anthemis xylipoda* flowers aqueous extract and their application for alkyne/aldehyde/amine A 3-type coupling reactions, *RSC Adv.* 5 (57) (2015) 46240–46246.
- [29] M. Nasrollahzadeh, S.M. Sajadi, A. Rostami-Vartooni, Green synthesis of CuO nanoparticles by aqueous extract of *Anthemis nobilis* flowers and their catalytic activity for the A3 coupling reaction, *J. Colloid Interface Sci.* 459 (2015) 183–188.
- [30] B. Khodadadi, M. Bordbar, M. Nasrollahzadeh, *Achillea millefolium* L. extract mediated green synthesis of waste peach kernel shell supported silver nanoparticles: application of the nanoparticles for catalytic reduction of a variety of dyes in water, *J. Colloid Interface Sci.* 493 (2017) 85–93.
- [31] A. Rostami-Vartooni, M. Nasrollahzadeh, M. Alizadeh, Green synthesis of seashell supported silver nanoparticles using *Bunium persicum* seeds extract: application of the particles for catalytic reduction of organic dyes, *J. Colloid Interface Sci.* 470 (2016) 268–275.
- [32] M. Nasrollahzadeh, S.M. Sajadi, A. Rostami-Vartooni, S.M. Hussin, Green synthesis of CuO nanoparticles using aqueous extract of *Thymus vulgaris* L. leaves and their catalytic performance for N-arylation of indoles and amines, *J. Colloid Interface Sci.* 466 (2016) 113–119.
- [33] S. Mathew, T.E. Abraham, Studies on the antioxidant activities of cinnamon (*Cinnamomum verum*) bark extracts through various in vitro models, *Food Chem.* 94 (4) (2006) 520–528.
- [34] P.S. Yap, T. Krishnan, K.G. Chan, S.H. Lim, Antibacterial mode of action of *Cinnamomum verum* bark essential oil, alone and in combination with piperacillin against a multi-drug-resistant *Escherichia coli* strain, *J. Microbiol. Biotechnol.* 25 (8) (2015) 1299–1306.
- [35] L. Huang, X. Weng, Z. Chen, M. Megharaj, Synthesis of iron-based nanoparticles using oolong tea extract for the degradation of malachite green, *Spectrochim. Acta A* 117 (2014) 801–804.
- [36] D. Li, T. Yang, Y. Li, Z. Liu, W. Jiao, Facile and green synthesis of highly dispersed tar-based heterogeneous Fenton catalytic nanoparticles for the degradation of methylene blue, *J. Clean. Prod.* 246 (2020), 119033.
- [37] K. Velsankar, R. Preethi, P.S. Jeevan Ram, M. Ramesh, S. Sudhakar, Evaluations of biosynthesized Ag nanoparticles using *Allium Sativum* flower extract in biological applications, *Appl. Nanosci.* (2020), <https://doi.org/10.1007/s13204-020-01463-2>.
- [38] A. Rostami-Vartooni, M. Alizadeh, M. Bagherzadeh, Green synthesis, characterization and catalytic activity of natural bentonite-supported copper nanoparticles for the solvent-free synthesis of 1-substituted 1H-1, 2, 3, 4-tetraazoles and reduction of 4-nitrophenol, *Beilstein J. Nanotechnol.* 6 (1) (2015) 2300–2309.
- [39] K. Velsankar, S. Sudhakar, G. Parvathy, R. Kalliammal, Effect of cytotoxicity and Antibacterial activity of biosynthesis of ZnO hexagonal shaped nanoparticles by *Echinochloa frumentacea* grains extract as a reducing agent, *Mater. Chem. Phys.* 239 (2020) 121976, <https://doi.org/10.1016/j.matchemphys.2019.121976>.
- [40] M. Mahdavi, F. Namvar, M. Ahmad, R. Mohamad, Green biosynthesis and characterization of magnetic iron oxide (Fe₃O₄) nanoparticles using seaweed (*Sargassum muticum*) aqueous extract, *Molecules* 18 (5) (2013) 5954–5964.
- [41] T. Wang, X. Jin, Z. Chen, M. Megharaj, R. Naidu, Green synthesis of Fe nanoparticles using eucalyptus leaf extracts for treatment of eutrophic wastewater, *Sci. Total Environ.* 466 (2014) 210–213.
- [42] S. Venkateswarlu, Y.S. Rao, T. Balaji, B. Prathima, N.V.V. Jyothi, Biogenic synthesis of Fe₃O₄ magnetic nanoparticles using plantain peel extract, *Mater. Lett.* 100 (2013) 241–244.
- [43] B. Kumar, K. Smita, L. Cumbal, A. Debut, Biogenic synthesis of iron oxide nanoparticles for 2-arylbenzimidazole fabrication, *J. Saudi Chem. Soc.* 18 (4) (2014) 364–369.
- [44] M. Senthil, C. Ramesh, Biogenic synthesis of Fe₃O₄ nanoparticles using tridax procumbens leaf extract and its antibacterial activity on *Pseudomonas aeruginosa*, *Digit. J. Nanomater. Biostruct.* 4 (2012) 7.
- [45] E.C. Njagi, H. Huang, L. Stafford, H. Genuino, H.M. Galindo, J.B. Collins, S.L. Suib, Biosynthesis of iron and silver nanoparticles at room temperature using aqueous sorghum bran extracts, *Langmuir* 27 (1) (2010) 264–271.
- [46] H. Muthukumar, M. Matheswaran, *Amaranthus spinosus* leaf extract mediated FeO nanoparticles: physicochemical traits, photocatalytic and antioxidant activity, *ACS Sustain. Chem. Eng.* 3 (12) (2015) 3149–3156.

- [47] K. Velsankar, S. Sudhahar, G. Maheswaran, M. Krishna Kumar, Effect of biosynthesis of ZnO nanoparticles via Cucurbita seed extract on *Culex tritaeniorhynchus* mosquito larvae with its biological applications, *J. Photochem. Photobiol. B* 200 (2019), 111650.
- [48] K. Velsankar, R.M. Aswin Kumar, R. Preethi, V. Muthulakshmi, S. Sudhahar, Green synthesis of CuO nanoparticles via *Allium sativum* extract and its characterizations on antimicrobial, antioxidant, antilarvicidal activities, *J. Environ. Chem. Eng.* (2020), <https://doi.org/10.1016/j.jece.2020.104123>.
- [49] K. Velsankar, V. Vinothini, S. Sudhahar, M. Krishna Kumar, S. Mohandoss, Green Synthesis of CuO nanoparticles via *Plectranthus amboinicus* leaves extract with its characterization on structural, morphological, and biological properties, *Appl. Nanosci.* (2020), <https://doi.org/10.1007/s13204-020-01504-w>.
- [50] B. Desalegn, M. Megharaj, Z. Chen, R. Naidu, Green synthesis of zero valent iron nanoparticle using mango peel extract and surface characterization using XPS and GC-MS, *Heliyon* 5 (2019), e01750.

Source details

Feedback > Compare sources >

Applied Physics A: Materials Science and Processing

Formerly known as: [Applied Physics A: Solids and Surfaces](#)

Scopus coverage years: from 1995 to Present

Publisher: Springer Nature

ISSN: 0947-8396 E-ISSN: 1432-0630

Subject area: [Chemistry: General Chemistry](#) [Materials Science: General Materials Science](#)

Source type: Journal

[View all documents >](#) [Set document alert](#) [Save to source list](#) [Source Homepage](#)

CiteScore 2021
4.2

SJR 2021
0.444

SNIP 2021
0.759

[CiteScore](#) [CiteScore rank & trend](#) [Scopus content coverage](#)

i Improved CiteScore methodology ×
CiteScore 2021 counts the citations received in 2018-2021 to articles, reviews, conference papers, book chapters and data papers published in 2018-2021, and divides this by the number of publications published in 2018-2021. [Learn more >](#)

CiteScore 2021 ▼
4.2 = $\frac{15,059 \text{ Citations 2018 - 2021}}{3,624 \text{ Documents 2018 - 2021}}$
Calculated on 05 May, 2022

CiteScoreTracker 2022 ⓘ
3.7 = $\frac{11,763 \text{ Citations to date}}{3,175 \text{ Documents to date}}$
Last updated on 05 May, 2022 • Updated monthly

CiteScore rank 2021 ⓘ



Phytomediated synthesis of magnetic nanoparticles by *Murraya koenigii* leaves extract and its biomedical applications

M. Sivakami¹ · K. Renuka Devi² · R. Renuka²

Received: 7 October 2021 / Accepted: 25 February 2022

© The Author(s), under exclusive licence to Springer-Verlag GmbH, DE part of Springer Nature 2022

Abstract

Green synthesis of nanoparticles is a facile method as they are eco-friendly and cost-effective and also the resources are easily available. Nowadays, the demand for magnetic nanoparticles has increased around 13% and they are used in magnetic sensing, medical imaging, wastewater treatment and antibiotic drugs. In this report, the eco-friendly green synthesis of magnetic iron nanoparticles was efficiently synthesized by using *Murraya koenigii* leaves extract. The UV–visible spectrum revealed the presence of a surface Plasmon resonance band at 240 nm and analyzed the formation of iron nanoparticles. X-ray diffraction pattern determined the crystallinity of nanoparticles. Fourier-transform infrared spectrum illustrated the functional groups of iron nanoparticles. The particle size distribution graph showed that the formed particles were in the range of nanometer. High-resolution transmission electron microscopy spectrum realized the spherical-shaped iron nanoparticles were ranging between 4 and 9 nm in size. The energy-dispersive X-ray spectrum and mapping revealed the iron, oxygen and carbon elements in the prepared nanoparticles. The vibrating sample magnetometer analysis showed the paramagnetic behavior of the prepared magnetic iron nanoparticles. The inhibition potent of magnetic nanoparticles on various human pathogens was revealed through antimicrobial assay. The antioxidant, anti-inflammatory and anti-diabetic assays revealed the biomedical behavior of the iron nanoparticles.

Keywords Iron nanoparticles · Spherical shape · Antimicrobial · Anti-inflammatory · Anti-diabetic

1 Introduction

Nanoparticles (NPs) with a dimension of 1–100 nm have specific physical, chemical, magnetic and biological properties. Nanotechnology has shown tremendous growth in all the fields such as optical, electronic, textile, agricultural, environmental and biomedical [1–5]. Nanoparticles have enormous applications with a particularly large surface-to-volume ratio property and enhanced efficiency in all the fields in the form of catalysts, batteries, solar cells, gas sensors, LEDs, semiconductors, glasses, sunscreen products, cosmetics, building materials, leathers, food packaging, batteries, clothes and drugs [6–10]. The manipulation of nanoparticles is one of the interesting research areas for

researchers as it creates a demand for the existence of living organisms in the world, because it solves the simple and difficult issues which are imperative in materials science [11, 12]. Nowadays, treating nutrition deficiency diseases and bacterial infections has become a challenge to clinical field. The infectious strains are easily spread and cause huge health crisis problems to humans and animals. Some pathogenic strains are not responding to antimicrobial agents and create huge damage to the human health system [13]. Bio-nanotechnology involves the production, operation and implementation process of drugs to several human and animal diseases, and hence, it aids. It can able to create antibiotic drugs against human pathogens without producing any side effects. In clinical fields, bio-nanotechnology plays a vital role in finding drugs to cure life-threatening diseases [13–17].

In nanotechnology, particles were synthesized by various physical, chemical and biological methods [6, 7, 15–19]. The synthesis of nanoparticles in some chemical methods requires toxic reducing agents which may produce harmful by-products, that pollute the environment and affect

✉ M. Sivakami
Siva_hhrc@yahoo.in; sivahhrc2020@gmail.com

¹ H.H. The Rajah's College, Pudukkottai 622001, India

² Government Arts College for Women, Pudukkottai 622001, India

the living organisms [13, 15, 16]. But, in green synthesis method, it can be reduced by substituting the chemicals with plant materials, bacteria or fungi, yeasts and agricultural wastes. Also, it is inexpensive comparatively and does not require high energy, pressure and hazardous chemicals. It does not produce any hazards to the environment [15, 16]. Furthermore, green synthesis of nanoparticles using plant extracts is an easy large productive approach compared to other biological methods and is a cost-effective method, which utilizes easily available resources. The chemicals and by-products in green synthesis of NPs are comparably low hazardous to environment than other methods [13, 16]. The eco-friendly synthesis of nanoparticles has practical applications in clinical, biomedical, agricultural and drug delivery fields as drugs without producing any side effects [20, 21].

Among the green synthesized nanoparticles, researchers have a specific interest in inorganic nanoparticles since they are easily available and necessary [11] as they have many practical applications, viz. sunscreen glasses and products [22], cosmetics [23], sensors [24], catalysts [25], food packaging [26], paints [27], ceramics [28], batteries [29] and drugs [30]. The magnetic NPs attain interest in research with their high catalytic, intrinsic and versatile properties. It is used in vast fields, viz. food, bio-sensing, medical and magnetic separation, degradation of organic pollutants and wastewater treatment [31]. Iron NPs are mostly used as dye removers for conserving a pollution-free environment [12]. Mostly, iron NPs are clinically used as biosensors in a magnetic field-assisted drug delivery therapy [32]. Reports of green synthesis of magnetic NPs using different plant extracts have gained attention, and some of them are: *Cymbopogon citratus* [33], *Carica papaya* [34], *Laurus nobilis* [35], *Platanus orientalis* [36], *Amaranthus spinosus* [37], *Pinus pinaster* [38], *Moringa oleifera* [39], *Eucalyptus* [40], *Rosemary* [41], *Mangifera indica* [42], *Camellia sinensis* [43], *Daphne mezereum* [12], *Vitex negundo* [44], *Terminalia bellirica* [39] and *Psoralea corylifolia* [45].

Murraya koenigii is native to India, and they are used in both medicinal and culinary applications. They are highly aromatic and have a unique citrus flavor. Aside from being a versatile culinary herb, they offer an abundance of health benefits due to the presence of powerful phytochemicals. Curry leaves are rich in alkaloids, glycosides and phenolic compounds that give potent health benefits and most of them possess antioxidant properties. Antioxidants play an indispensable role in maintaining our body healthy also; they help us to stay away from diseases. Curry leaves are good sources of iron and calcium, and hence, they are used to treat calcium deficiency. Also, it reduces blood glucose levels effectively. They shield the insulin-producing cells and protect them from the harms caused by free radicals [46]. Traditionally, curry leaves are assumed to have favorable effect for good-eyesight, so they can be used to prevent

the early onset of cataract problems. Most of the illnesses caused in our body are initiated by infections or oxidative damage in the body. Curry leaves can be used as an alternative to treat certain infections. Curry leaves contains the carbazole alkaloids that are present in the curry leaves possess antibacterial, anti-inflammatory, antioxidant and anticancer properties [46, 47].

We are reporting about the eco-friendly synthesis of iron NPs by *Murraya koenigii* leaves extract from the literature survey for the first time. The prepared magnetic NPs were studied using various analytical techniques for realizing their spectral, optical, morphological, electrical, magnetic and biological properties.

2 Materials and methods

2.1 Chemicals used

Ferric chloride (FeCl_3 ($\geq 98.99\%$)), ethanol ($\geq 99.92\%$), deionized water and *Murraya koenigii* leaves collected from Pudukkottai were used. All the chemicals used were purchased from Sigma-Aldrich, India.

2.2 *Murraya koenigii* leaves extract preparation

5 g of fresh healthy *Murraya koenigii* leaves was taken and thoroughly cleaned with tap water and deionized water. The leaves were immersed in 100 mL of deionized water and heated on a magnetic stirrer to 80 °C for 30 min. The solution was allowed to cool once it reaches room temperature, and the solution was filtered with Whatman No.1 filter paper to remove the residual impurities. The filtered *Murraya koenigii* leaves extract solution was preserved at 4 °C in a refrigerator for further use.

2.3 Synthesis of iron NPs by *Murraya koenigii* leaves extract

About 0.1 M of FeCl_3 was dissolved in 90 mL of deionized water by continuous stirring on a magnetic stirrer. Then, a 10 mL of *Murraya koenigii* leaves extract was taken in a burette and mixed with ferric chloride solution which was added drop by drop. The solution was heated to 70 °C for 2 h and stirred continuously. The brown color solution turned black immediately, which indicated the formation of iron NPs. The dark brownish-black precipitate was washed with deionized water and dried at 80 °C in a hot air oven. Then, the magnetic NPs were preserved and analyzed by various analytical techniques. The synthesis scheme is revealed in Fig. 1.

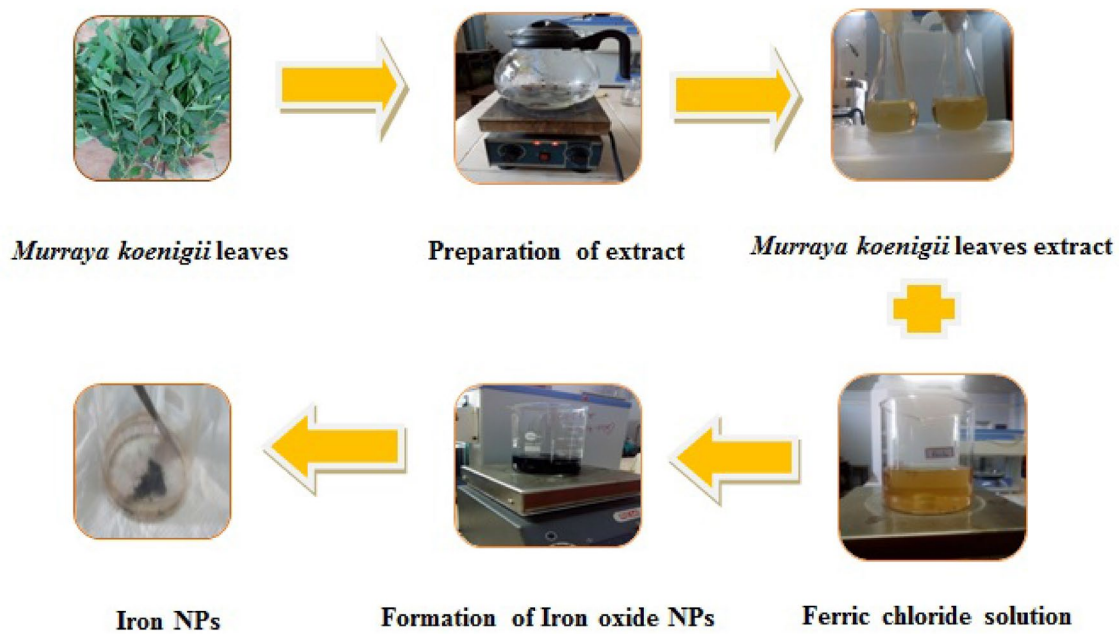


Fig. 1 Synthesis scheme of iron NPs green synthesized by *Murraya koenigii* leaf extract

2.4 Characterization of magnetic NPs

The prepared NPs were characterized by using various analytical techniques. UV–visible analysis was completed by UV-DRS spectrophotometer Thermofisher Evaluation 220. X-ray powder diffraction (XRD) analysis was recorded with the help of PANalytical X'Pert PRO powder X-ray diffractometer at 10° – 80° scan rate using Cu K α radiation ($\lambda = 1.5406 \text{ \AA}$). Fourier-transform infrared spectrum was recorded using Thermo Nicolet 380 FT-IR spectrometer at 4000 – 400 cm^{-1} . The particle size distribution analysis (dynamic light scattering—DLS) was studied by a particle size analyzer. The morphology of the prepared sample was analyzed using JEOL-2100+ High-Resolution Transmission Electron Microscope. The elemental and mapping analyses were taken from Energy-Dispersive X-ray Spectrometer Quantax 200 with X Flash® 6130. The phytochemical analysis was carried out by the procedure described as in the earlier reports [30, 48–50]. The magnetic property of the prepared sample was studied by Microsense model ADE-EV9 vibrating sample magnetometer at room temperature in -2 – 2 T magnetic fields.

2.5 Antimicrobial assay

The antimicrobial assay was completed through well plate method using microtiter plate [48]. LB broth and the chosen microbial cells such as *Pseudomonas aeruginosa*, *Acinetobacter baumannii*, *Serratia marcescens*, *Chromobacterium violaceum*, *Enterobacter aerogenes*, *Klebsiella*

pneumonia (Gram-negative bacterial cells), *Enterococcus faecalis*, *Staphylococcus aureus* (Gram-positive bacterial cells), *Candida albicans*, *Candida tropicalis*, *Aspergillus niger* and *Aspergillus flavus* (fungus cells) were utilized as a growth medium. The analysis was performed by 96 microtiter plates containing fully grown microbial cells in the medium and microbial inoculums with the prepared sample in varied concentrations, viz. 5, 10, 25, 50, 100 and 150 $\mu\text{g}/\text{mL}$. Similarly, positive control chloramphenicol was treated. Then, the plates were put at 37°C for 24 h. The analysis was performed and studied in triplicates. Later, it was analyzed with UV spectrophotometer. The changes in absorbance were noted for calculating percentage of inhibition by,

$$\text{Antimicrobial assay (\%)} = [(A_c - A_s) / A_c] \times 100 \quad (1)$$

where A_c = Control absorbance, and A_s = Sample absorbance.

2.6 Antioxidant assay

The antioxidant assay was completed as stated in the earlier report [49]. 0.5 mL of prepared NPs solution was taken and separated into varied concentrations, viz. 20, 40, 60, 80 and 100 $\mu\text{g}/\text{mL}$. It was then mixed with 2 mL of DPPH methanol solution. The reaction mixture solution was continuously stirred for 30 min. Then, it was kept in a dark place at room temperature. After 30 min, it was analyzed by UV–visible spectrophotometer and the absorbance was recorded.

Similarly, the positive control ascorbic acid was treated. The assay was performed thrice.

$$\text{Antioxidant assay (\%)} = 100 - [(A_c - A_s) / A_c] \times 100 \quad (2)$$

where A_c = Control absorbance, and A_s = Sample absorbance.

2.7 Anti-inflammatory assay

The anti-inflammatory assay was investigated by the method stated and followed as in the previous report [49]. At first, 2.8 mL of phosphate-buffered saline (PBS) (pH 6.4) and 0.2 mL of bovine serum albumin were taken and mixed with prepared NPs sample solution of 2 mL in varied concentration, viz. 100, 200, 300, 400 and 500 $\mu\text{g/mL}$. After that, the reaction mixture solution was incubated at 37 ± 2 °C. The procedure was completed in 15 min, and after completing it, it was heated to 70 °C. The solution was allowed to attain room temperature, and then, the absorbance was recorded from a UV–visible spectrophotometer. Similarly, positive control diclofenac sodium was treated. The assay was performed in triplicates.

$$\text{Anti-inflammatory assay (\%)} = 100 - [\{V_c - V_t\} / V_c] \times 100 \quad (3)$$

where V_c = Control absorbance, and V_t = Sample absorbance.

2.8 Anti-diabetic assay

The anti-diabetic assay was investigated by the method as stated in the earlier report [49]. At first, 0.5 mg/mL of α -Amylase was maintained at 25 °C for 10 min. The prepared NPs solution of 2 mL was taken in varied concentrations, viz. 100, 200, 300, 400 and 500 $\mu\text{g/mL}$, and was added to the starch solution. 20 mM of sodium phosphate (pH 6.9) and 6 mM of sodium chloride were also added to the sample solution, and then, it was mixed with the α -Amylase solution. The reaction mixture solution was maintained at 25 °C for 30 min. In this solution, di-nitrosalicylic acid was blended to view the color change. Further, the reaction mixture solution was heated to 70 °C for 5 min. Then, the absorbance was recorded from a UV–visible spectrophotometer to calculate the percentage of inhibition. Similarly, positive control acarbose was treated. The assay was performed thrice.

$$\text{Anti-diabetic assay (\%)} = 100 - [\{V_c - V_t\} / V_c] \times 100 \quad (4)$$

where V_c = Control absorbance, and V_t = Sample absorbance.

3 Results and discussion

In this report, the iron NPs were green synthesized with *Murraya koenigii* leaves extract. Green synthesis is a method that is eco-friendly and cost-effective and also avoids the production of hazardous by-products. The formation of iron NPs was confirmed when the solution turns to brownish-black color change during the synthesis. The phytochemicals in *Murraya koenigii* leaves extract played the role of capping and stabilizing agents in the formation of iron NPs [15, 16]. The phytochemicals are the most important agents in capping and stabilizing action of NPs. They interacted and attached to the precursor ions, which stabilized the NPs [13, 15, 16]. The phytochemicals in *Murraya koenigii* leaves extract were analyzed via two ways, viz. alcoholic and aqueous extractive method; among these, aqueous extracts provided favorable phytochemicals. Then, the synthesis was done in an aqueous extractive method. The phytochemicals in *Murraya koenigii* leaves extract are listed in Table 1. The *Murraya koenigii* aqueous leaf extract contains flavonoids, alkaloids and triterpenoids in high concentration, whereas tannin, terpenoids, steroids and polyphenol are in low concentration. The greener way mediated iron NPs were characterized by various analytical techniques for perceiving their properties.

3.1 Characterization of NPs

The UV–visible spectrum of prepared iron NPs is exposed in Fig. 2a. The surface Plasmon resonance band was observed at 240 nm. It confirms the formation of iron NPs, and it was compared with the inference recorded in the earlier report

Table 1 Phytochemical analysis of *Murraya koenigii* leaf extract

Phytochemicals analysis		
Phytochemicals	Aqueous extract	Ethanollic extract
Tannin	+	+
Flavonoids	++	+
Steroids	+	–
Saponin	–	–
Alkaloids	++	+
Terpenoids	+	+
Triterpenoids	++	+
Polyphenol	+	++
Anthraquinone	–	–
Glycoside	–	+
Coumarins	–	–

(–) Absent, (+) present, (++) high concentration

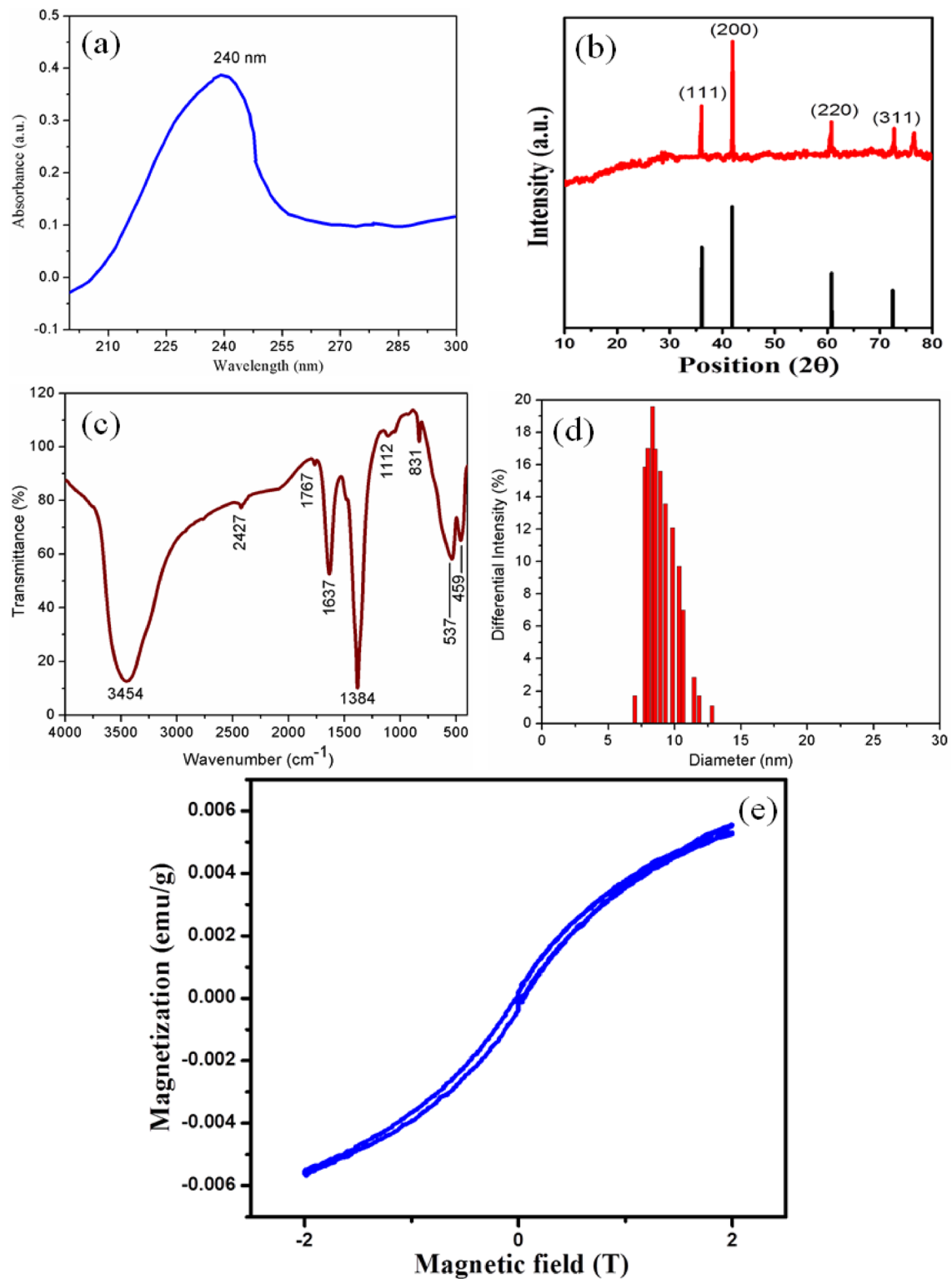


Fig. 2 a UV-visible, b X-ray diffraction (XRD) pattern, c Fourier-transform infrared spectrum (FT-IR), d particle size distribution (dynamic light scattering—DLS) graph and e magnetization curve

(vibrating sample magnetometer—VSM) of green synthesized iron NPs by *Murraya koenigii* leaf extract

[51]. Rajendran et al. [51] reported that the magnetic NPs synthesized using *Sesbania grandiflora* leaf extract had its SPR band at 220 nm.

XRD pattern of prepared iron NPs is shown in Fig. 2b. The strong and intense peaks at 36.09°, 41.87°, 60.72°, 72.74° and 76.54° and their corresponding planes (111), (200), (220), (311) and (222) represent the high crystalline formation of iron NPs. The pattern was matched with JCPDS no. 654150 and indicated the face-centered cubic phase formation of iron NPs. Certain amorphous behavior of noise signal is observed due to the use of leaf extract in synthesis of NPs [13, 16]. The extra peaks are witnessed due to the oxidation of iron NPs [52]. The average crystallite size was calculated at 14 nm from Scherer's formula,

$$D = K\lambda/\beta \cos \theta \quad (5)$$

where K is the constant (0.94), $\lambda=1.5406 \text{ \AA}$, β is the full width half maximum (FWHM), θ is the Bragg angle. Here, $\beta=0.635$ and $\theta=41.87^\circ$.

Kanagasubbulakshmi et al. reported that the magnetic NPs synthesized using *Lagenaria Siceraria* had its crystallite size between 14 and 18 nm [53]. The lattice strain was calculated at 0.0039 by [54],

$$\Delta L = L - L_0 \quad (6)$$

The dislocation density was calculated at $7.815 \times 10^{15} \text{ m}^{-2}$ by [55],

$$\delta = 1/D^2 \quad (7)$$

The microstrain was found at 5.030×10^{-3} by [54],

$$\epsilon = \beta \cos q/4 \quad (8)$$

The high crystalline and small size of iron NPs were attained by using *Murraya koenigii* leaves extract.

FT-IR spectrum of the prepared iron NPs is revealed in Fig. 2c. The bands were recorded at 3454, 2427, 1767, 1637, 1384, 1112, 831, 537 and 459 cm^{-1} . The band at 3454 cm^{-1} may be due to the OH stretching vibration of hydroxyl or phenolic group [55]. The band at 2427 cm^{-1} corresponds to the aromatic aldehyde group of C-H stretching vibration, whereas the band at 1767 cm^{-1} may be due to the ester group of C=O stretching vibration [56]. The band at 1637 cm^{-1} denotes the amino acid stretching vibration, whereas the band at 1384 cm^{-1} represents the germinal methyl group stretching vibration [48]. The band at 1112 cm^{-1} corresponds to carboxylic group stretching vibration [49, 54]. The bands at 831, 537 and 459 cm^{-1} represent the metal and oxygen stretching vibration. The appearance of oxygen functional group is mainly due to the oxidation of iron NPs [30]. It was clearly understood from the presence of various vibrations than oxygen functional groups, and they were due to the use of leaf extract in synthesis of NPs [13, 16].

DLS analysis was carried out to observe the particle size distribution, and it is shown in Fig. 2d. The particle size of the prepared iron NPs was at 7–15 nm. It was further confirmed by TEM particle size measurement. Compared with TEM analysis, the particle size observed in DLS was greater; it appeared to be greater due to the measurement in hydrodynamic size. The polydispersity index (PDI) was obtained at 0.298 which indicates the potential application of NPs in drug delivery and biomedical fields [55].

The magnetization curve of prepared iron NPs is revealed in Fig. 2e. The paramagnetic behavior of the prepared iron NPs was found to have no hysteresis loop that contains magnetization versus applied magnetic field (M-H) curve. The green synthesized magnetic NPs were weakly attracted by the strong magnetic field (B) and formed an internal induced magnetic field in that applied direction [42, 57].

HR-TEM analysis was carried out to view the morphology of the prepared iron NPs, and its graphs are displayed in Fig. 3a, b. The spherical-shaped [36] iron NPs were observed, and their size ranged from 4 to 9 nm. Some regions seem to be agglomerated due to the usage of *Murraya koenigii* leaves extract in synthesis (plant extract). Arsalani et al. synthesized magnetic NPs using natural rubber latex and reported that the size ranged from 7 to 15 nm and they were spherical in shape [58]. Jamzad et al. [35] prepared magnetic NPs using *Laurus nobilis* leaf extract and mentioned that they were spherical in shape and the sizes ranged from 8 to 10 nm. Figure 3c illustrates the selected area electron diffraction (SAED) pattern of NPs. The polycrystalline formation of NPs was understood from the white spots in the black area (SAED pattern). The d-spacing of (200) lattice plane in XRD was well matched with SAED d-spacings measurement.

The EDS spectrum of iron NPs is shown in Fig. 4. It confirmed the presence of iron (Fe) and oxygen (O) in the synthesized NPs. The low carbon (C) signal was present due to the use of leaf extract in synthesis of iron NPs [48, 54]. The presence of O represents the oxidation of prepared NPs [30]. The atomic and weight percentages of Fe, O and C are displayed in Fig. 4. The EDS spectrum was further analyzed with mapping analysis which is revealed in Fig. 5. It also shows the presence of iron, oxygen and carbon in NPs with red, green and blue spots.

3.2 Biomedical applications

3.2.1 Antimicrobial assay

The antimicrobial analysis is a preliminary investigation in the biomedical field to understand the antibiotic behavior against human pathogens as the microbial pathogens cause huge health crisis in the world. In this analysis, the prepared

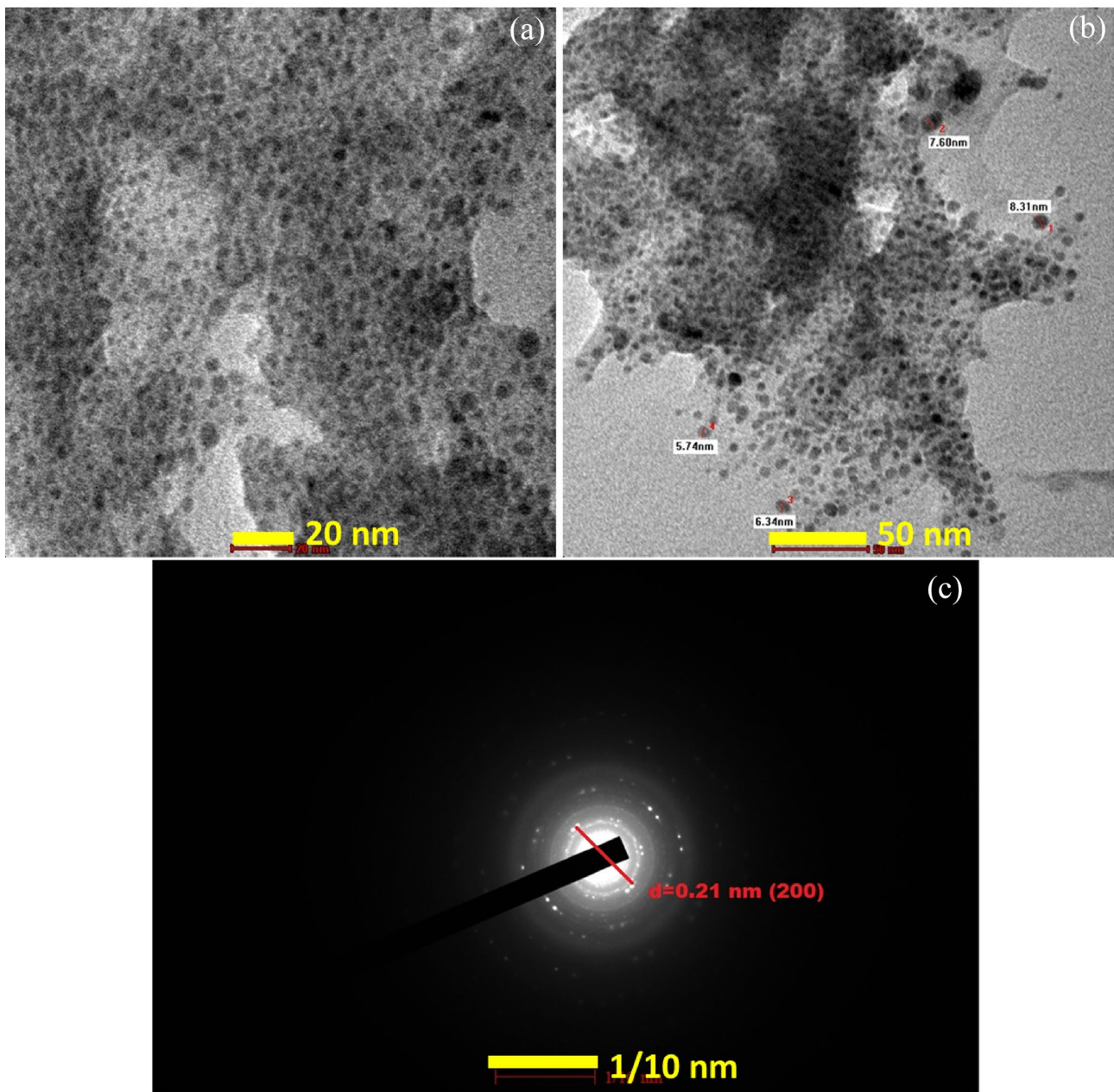


Fig. 3 **a-b** High-resolution transmission electron micrographs (HR-TEM) at 20 nm, 50 nm scale and **c** selected area electron diffraction pattern at 1/10 nm scale of green synthesized iron NPs by *Murraya koenigii* leaf extract

NPs were tested on various human pathogens such as *Pseudomonas aeruginosa*, *Acinetobacter baumannii*, *Serratia marcescens*, *Chromobacterium violaceum*, *Enterobacter aerogenes*, *Klebsiella pneumonia* (Gram-negative bacterial cells), *Enterococcus faecalis*, *Staphylococcus aureus* (Gram-positive bacterial cells), *Candida albicans*, *Candida tropicalis*, *Aspergillus niger* and *Aspergillus flavus* (fungus cells). The analysis was studied through Agar well diffusion method. The various concentrations such as 5, 10, 25, 50, 100 and 150 $\mu\text{g/mL}$ were applied for finding antibacterial

potency of prepared NPs. Chloramphenicol was set as a positive control. The Gram-negative bacterium was more pathogenic than the Gram-positive bacterium [59]. Then, the analysis was studied mostly on Gram-negative bacterial cells. Further, the fungi cell has much stronger cell wall structure than bacteria. Therefore, analysis was also investigated in fungi cells to know the NPs potency. The tested microbes which were present in the soil, water and air medium produced many dreadful infections. The microbes that produced the dreadful disease are the habitats of dirt,

Fig. 4 Energy-dispersive X-ray spectrum (EDX) of green synthesized iron NPs by *Murraya koenigii* leaf extract

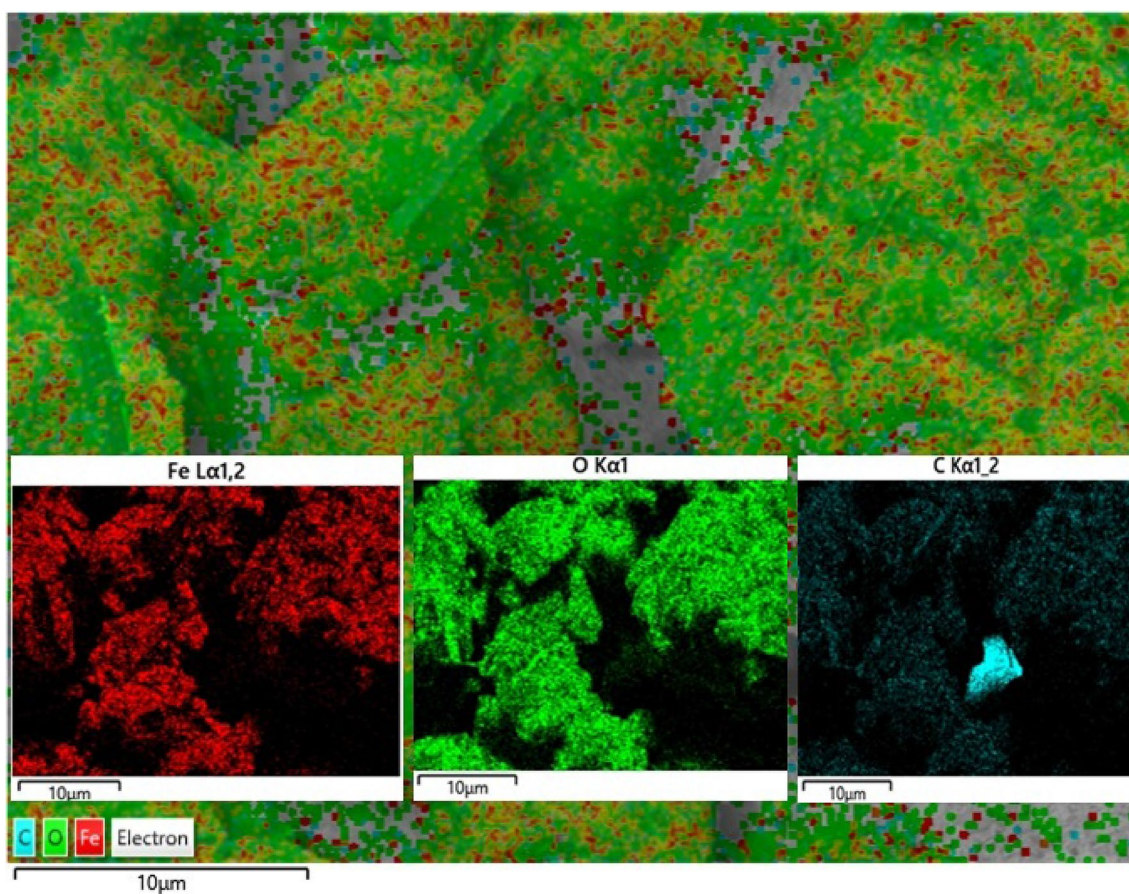
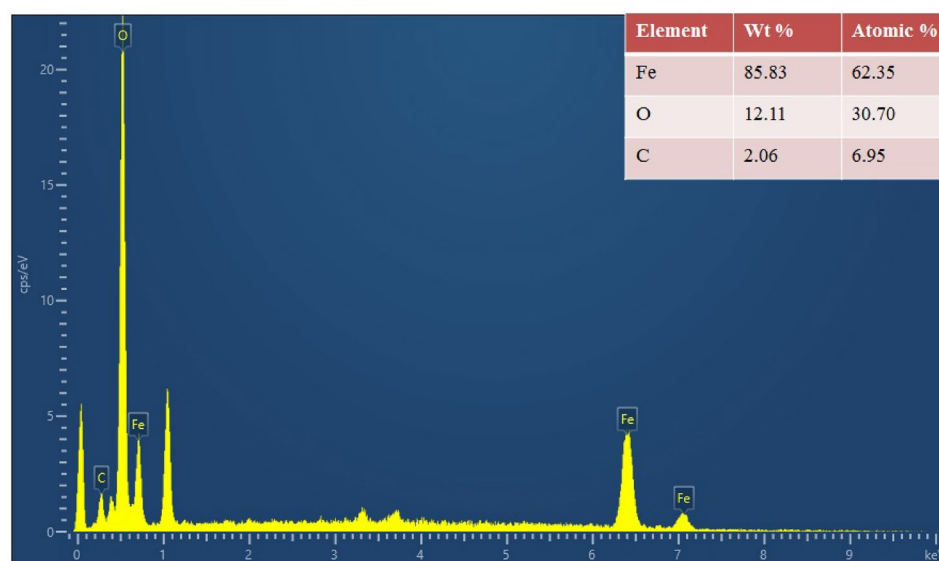


Fig. 5 Energy-dispersive X-ray spectrum (EDX) mapping of green synthesized iron NPs by *Murraya koenigii* leaf extract

hospital, drainage and unhygienic zones [49]. The inhibition of microbial cells by NPs was expressed as a percentage in Fig. 6 and taken in triplicate times.

Among the tested microorganisms, *Pseudomonas aeruginosa*, *Enterobacter aerogenes*, *Klebsiella pneumonia*, *Chromobacterium violaceum* were more susceptible at 100 $\mu\text{g/l}$

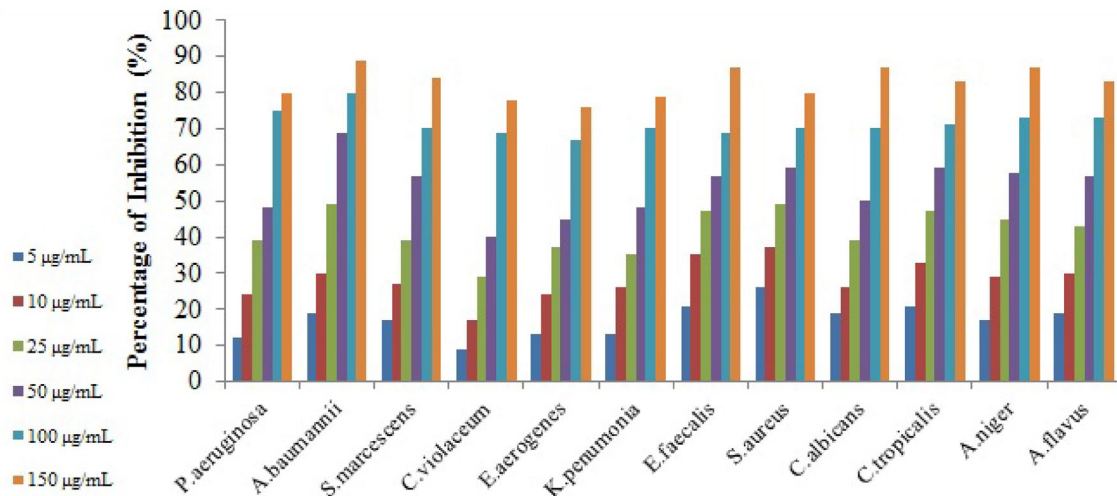


Fig. 6 Antimicrobial assay of green synthesized iron NPs by *Murraya koenigii* leaf extract on *Pseudomonas aeruginosa*, *Acinetobacter baumannii*, *Serratia marcescens*, *Chromobacterium violaceum*, *Enterobacter aerogenes*, *Klebsiella pneumonia* (Gram-negative bacterial

cells), *Enterococcus faecalis*, *Staphylococcus aureus* (Gram-positive bacterial cells), *Candida albicans*, *Candida tropicalis*, *Aspergillus niger* and *Aspergillus flavus* (fungi cells)

mL. *Acinetobacter baumannii*, *Serratia marcescens*, *Enterococcus faecalis*, *Staphylococcus aureus*, *Candida albicans*, *Candida tropicalis*, *Aspergillus niger* and *Aspergillus flavus* were susceptible at 25 µg/mL. Gram-positive bacteria were more inhibited than Gram-negative comparatively Premathan et al. [60]. The high concentration of NPs used in the analysis has higher inhibition on microbial cells, and it harmonized with Sangeetha et al. [61]. These results proved the synthesized NPs have antibiotic behavior on various human pathogens.

The process of inhibition of microbial cells by prepared NPs was as follows:

The generation of reactive oxygen species such as hydrogen peroxide (H_2O_2), superoxide ions (O_2^{2-} ions), free radicals, Fe^{2+} ions and its attachment on microbial cell wall leads to rupturing of the cell wall structure. Also, the electrostatic attraction between NPs and microbial cells prompts the cell wall damage; it led to the release of cytoplasmic ingredients from the cell, and then, the ROS easily penetrated it and inhibits the DNA nuclei of the cell. Finally, it leads to cell decay and it prompts the cell damage and death of the microbes [49, 54, 59].

3.2.2 Antioxidant assay

The antioxidant assay of the prepared NPs is displayed in Fig. 7a. Antioxidants are the essential agents for the human to attain stable functioning of the health system. Antioxidants are enormously present in fruits, nuts and vegetables. Free radicals contain unpaired electrons, and they are easily bound to the nearest molecules for attaining stability. They are produced in the human body to systemize immune

function, chemical signaling, energy supply and detoxification [37]. An assay was carried out with various concentrations such as 20, 40, 60, 80 and 100 µg/mL. Ascorbic acid was set as a positive control. The results were expressed as a percentage in Fig. 7a and taken in triplicate times, and the values are listed in Table 2.

The percentage of inhibition by magnetic NPs and ascorbic acid were 24.04, 45.17, 67.19, 80.06, 91.17% and 20.06, 40.15, 59.12, 75.27, 85.19% with 20, 40, 60, 80 and 100 µg/mL concentrations, respectively. The high concentration of NPs was directly proportional to the inhibition percentage. In all concentrations, the NPs had a higher inhibition percentage than the positive control.

IC_{50} value represents the quantity of sample needed to attain 50% inhibition; it denotes the potency of the sample. Low IC_{50} value symbolizes the efficient behavior of the sample. The IC_{50} value for NPs and ascorbic acid was at 42 and 49 µg/mL, respectively. The results proved the potential behavior of prepared NPs and were compared with earlier reports [37, 48].

3.2.3 Anti-inflammatory assay

The anti-inflammatory assay of synthesized NPs is illustrated in Fig. 7b. It is an interesting analysis to show the protective behavior of the sample than other destroying analyses. The fragmentation of secondary and tertiary protein structures caused loss of biological function [50]. The assay was carried out with assorted concentrations such as 100, 200, 300, 400 and 500 µg/mL. Diclofenac sodium was set as a positive control. The results were expressed as a

percentage in Fig. 7b and taken in triplicate times, and the values are listed in Table 3.

The percentage of inhibition by magnetic NPs and diclofenac sodium were 24.04, 45.27, 57.30, 70.04., 89.12%

and 19.04, 39.47, 51.02., 64.17, 79.99% with 100, 200, 300, 400 and 500 µg/mL concentrations, respectively. The high concentration of NPs is directly proportional to the inhibition percentage. In all the concentrations, NPs have a

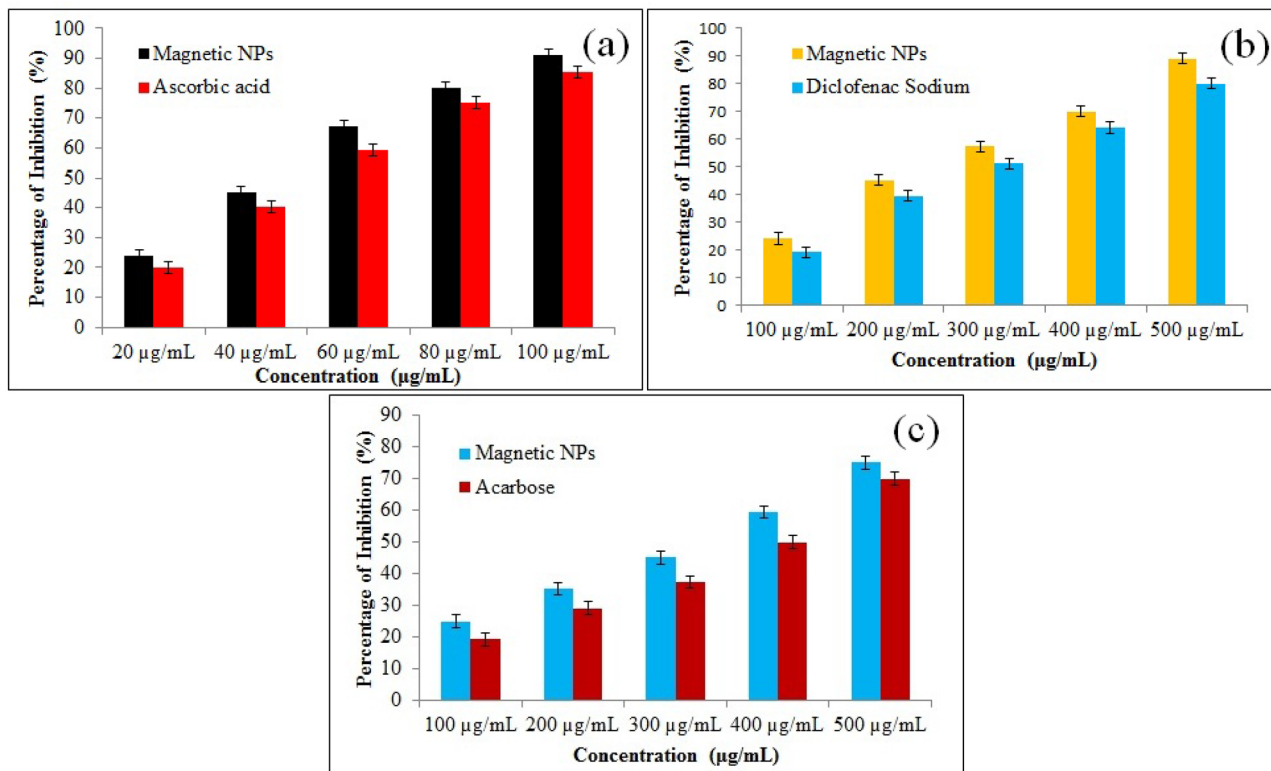


Fig. 7 a Antioxidant, b anti-inflammatory and c anti-diabetic assays of green synthesized iron NPs by *Murraya koenigii* leaf extract

Table 2 Percentage of inhibition in antioxidant assay of green synthesized iron NPs by *Murraya koenigii* leaf extract

Samples	Percentage of Inhibition (%)				
	Concentration (µg/mL)				
	20	40	60	80	100
Magnetic NPs	24.04 ± 0.19	45.17 ± 0.97	67.19 ± 0.93	80.06 ± 0.06	91.17 ± 0.04
Ascorbic acid	20.06 ± 0.17	40.15 ± 0.12	59.12 ± 0.27	75.27 ± 0.12	85.19 ± 0.06

± performed in triplicate times

Table 3 Percentage of inhibition in anti-inflammatory and anti-diabetic assays of green synthesized iron NPs by *Murraya koenigii* leaf extract

Samples	Percentage of Inhibition (%)				
	Concentration (µg/mL)				
	100	200	300	400	500
Magnetic NPs	24.04 ± 0.12	45.27 ± 0.93	57.30 ± 0.47	70.04 ± 0.19	89.12 ± 1.06
Diclofenac sodium	19.04 ± 0.19	39.47 ± 0.27	51.02 ± 0.93	64.17 ± 0.33	79.99 ± 1.04
Magnetic NPs	24.93 ± 0.33	35.19 ± 0.35	45.06 ± 1.12	59.37 ± 0.39	75.06 ± 0.99
Acarbose	19.12 ± 0.19	29.04 ± 0.37	37.17 ± 0.17	49.93 ± 0.93	69.99 ± 0.97

± performed in triplicate times

higher inhibition percentage than the positive control. The IC_{50} value for NPs and diclofenac sodium was at 247 and 293 $\mu\text{g/mL}$, respectively. The results proved the potential behavior of prepared NPs and were compared with earlier reports [49, 50].

3.2.4 Anti-diabetic assay

The anti-diabetic assay of prepared NPs is revealed in Fig. 7c. It is a preliminary analysis to show the sample has anti-diabetic potency. Free radical causes the oxidative damage and resists enzyme such as α -Amylase and α -Glucosidase. These enzymes cause diabetes. In this analysis, α -Amylase was used. It is an enzyme; it is present in saliva and the pancreas. α -Amylase played a vital role in the conversion of carbohydrates, glycogen and starch. Further, it rehabilitated into oligosaccharides from α -D(1,4) glycosidic bonds [48]. Earlier reports [62] stated that diabetes can be efficiently healed by plant-based material. Green synthesized NPs have more efficient results in curing diabetes than chemically prepared NPs without any side effects. The assay was carried out with various concentrations such as 100, 200, 300, 400 and 500 $\mu\text{g/mL}$ where acarbose was set as a positive control. The results were expressed as a percentage in Fig. 7c and taken in triplicate times in which values are listed in Table 3.

The percentage of inhibition on α -Amylase by NPs and acarbose were 24.93, 35.19, 45.06, 59.37, 75.06% and 19.12, 29.04, 37.17, 49.93, 69.99% with 100, 200, 300, 400 and 500 $\mu\text{g/mL}$ concentrations, respectively. The high concentration of NPs has a higher inhibition percentage. In all concentrations, NPs have a higher inhibition percentage than the positive control. The IC_{50} value for NPs and diclofenac sodium was at 330 and 397 $\mu\text{g/mL}$, respectively. The results proved the potency of prepared NPs and compared with earlier reports [48, 62].

4 Conclusion

In this study, the eco-friendly green synthesis of iron NPs was efficiently performed by using *Murraya koenigii* leaves extract. The synthesized NPs were characterized by various analytical techniques such as UV, XRD, FT-IR, DLS, TEM and EDS analyses. UV analysis confirmed the formation of iron NPs with SPR band at 240 nm. XRD pattern proved the high crystalline formation of iron NPs with strong and intense peaks. FT-IR analysis confirmed the functional groups of iron nanoparticles. DLS spectrum confirmed that the formed particles were in nanometer range. HR-TEM graphs illustrated that the formed NPs were spherical, and the size ranged from 4 to 9 nm. EDS spectrum with its mapping proved the presence of iron in the formed NPs. VSM

analysis revealed the paramagnetic behavior of nanoparticles. The biomedical applications-based characterizations such as antimicrobial, antioxidant, anti-inflammatory and anti-diabetic assays were performed. The antimicrobial assay proved the potency inhibition of iron NPs on various human pathogens. The antioxidant, anti-inflammatory and anti-diabetic assays proved the iron NPs have biomedical behavior. With these results, the prepared iron NPs will be employed as antibiotic, anti-diabetic and anti-inflammatory drugs in biomedical field in future.

Declarations

Conflict of interest The authors have no conflict of interest to declare.

References

1. S. Arokiyaraj, M. Saravanan, N.U. Prakash, M.V. Arasu, B. Vijayakumar, S. Vincent, Enhanced antibacterial activity of iron oxide magnetic nanoparticles treated with *Argemone mexicana* L. leaf extract: an in vitro study. *Mater. Res.* **48**(9), 3323–3327 (2013)
2. S. Li, M. Meng Lin, M.S. Toprak, D.K. Kim, M. Muhammed, Nanocomposites of polymer and inorganic nanoparticles for optical and magnetic applications. *Nano Rev.* **1**(1), 5214 (2010)
3. A. Fouda, E.L. Saad, S.S. Salem, T.I. Shaheen, In-Vitro cytotoxicity, antibacterial, and UV protection properties of the biosynthesized Zinc oxide nanoparticles for medical textile applications. *Microb. Pathog.* **125**, 252–261 (2018)
4. B. Mughal, S.Z.J. Zaidi, X. Zhang, S.U. Hassan, Biogenic nanoparticles: Synthesis, characterisation and applications. *Appl. Sci.* **11**(6), 2598 (2021)
5. R. Canaparo, F. Foglietta, T. Limongi, L. Serpe, Biomedical applications of reactive oxygen species generation by metal nanoparticles. *Mater.* **14**(1), 53 (2021)
6. K. Mathiyalagan, A. Ponnaiah, K. Karupiah, S. Rengapillai, S. Marimuthu, Enhanced performance on layered $\text{O}_3\text{-Na}_{0.95}\text{CrO}_2$ cathode material for emerging sodium-ion batteries. *Ionics* **26**(8), 3929–3936 (2020)
7. M. Kouthaman, K. Kannan, P. Arjunan, T. Meenatchi, R. Subadevi, M. Sivakumar, Novel layered $\text{O}_3\text{-NaFe}_{0.45}\text{Co}_{0.45}\text{Ti}_{0.1}\text{O}_2$ cathode material for sodium batteries. *Mater. Lett.* **276**, 128181 (2020)
8. S. Sahani, Y.C. Sharma, Advancements in applications of nanotechnology in global food industry. *Food Chem.* **342**, 128318 (2021)
9. L. Salvioni, L. Morelli, E. Ochoa, M. Labra, L. Fiandra, L. Palugan, M. Colombo, The emerging role of nanotechnology in skin-care. *Adv. Colloid Interface Sci.* **293**, 102437 (2021)
10. S. Prabha, D. Durgalakshmi, S. Rajendran, E. Lichtfouse, Plant-derived silica nanoparticles and composites for biosensors, bioimaging, drug delivery and supercapacitors: a review. *Environ. Chem. Lett.* **19**(2), 1667–1691 (2021)
11. K.M. Kumar, B.K. Mandal, K.S. Kumar, P.S. Reddy, B. Sreedhar, Biobased green method to synthesise palladium and iron nanoparticles using *Terminalia chebula* aqueous extract. *Spectrochim. Acta A.* **102**, 128–133 (2013)
12. N. Beheshtkhoo, M.A.J. Kouhbanani, A. Savardashtaki, A.M. Amani, S. Taghizadeh, Green synthesis of iron oxide

- nanoparticles by aqueous leaf extract of *Daphne mezereum* as a novel dye removing material. *Appl. Phys. A* **124**(5), 1–7 (2018)
13. K. Velsankar, G. Parvathy, S. Mohandoss, M. Krishna Kumar, S. Sudhahar, *Celosia argentea* leaf extract-mediated green synthesized iron oxide nanoparticles for bio-applications. *J. Nanostruct. Chem.* (2021). <https://doi.org/10.1007/s40097-021-00434-5>
 14. V.V. Makarov, S.S. Makarova, A.J. Love, O.V. Sinityna, A.O. Dudnik, I.V. Yaminsky, N.O. Kalinina, Biosynthesis of stable iron oxide nanoparticles in aqueous extracts of *Hordeum vulgare* and *Rumex acetosa* plants. *Langmuir* **30**(20), 5982–5988 (2014)
 15. K. Velsankar, S. Suganya, P. Muthumari, S. Mohandoss, S. Sudhahar, Ecofriendly green synthesis, characterization and biomedical applications of CuO nanoparticles synthesized using leaf extract of *Capsicum frutescens*. *J. Environ. Chem. Eng.* **9**(5), 106299 (2021)
 16. K. Velsankar, A. Venkatesan, P. Muthumari, S. Suganya, S. Mohandoss, S. Sudhahar, Green inspired synthesis of ZnO nanoparticles and its characterizations with biofilm, antioxidant, anti-inflammatory, and anti-diabetic activities. *J. Mol. Struct.* **1255**, 132420 (2022)
 17. R. Kaliammal, G. Parvathy, G. Maheshwaran, K. Velsankar, V.K. Devi, M. Krishnakumar, S. Sudhahar, *Zephyranthes candida* flower extract mediated green synthesis of silver nanoparticles for biological applications. *Adv. Powder Technol.* **32**(11), 4408–4419 (2021)
 18. Y. Orooji, R. Mohassel, O. Amiri, A. Sobhani, M. Salavati-Niasari, Gd₂ZnMnO₆/ZnO nanocomposites: Green sol-gel auto-combustion synthesis, characterization and photocatalytic degradation of different dye pollutants in water. *J. Alloys Compd.* **835**, 155240 (2020)
 19. M. Nasrollahzadeh, S.M. Sajadi, A. Rostami-Vartooni, Green synthesis of CuO nanoparticles by aqueous extract of *Anthemis nobilis* flowers and their catalytic activity for the A3 coupling reaction. *J. Colloid Inter. Sci.* **459**, 183–188 (2015)
 20. B. Khodadadi, M. Bordbar, M. Nasrollahzadeh, *Achillea millefolium* L. extract mediated green synthesis of waste peach kernel shell supported silver nanoparticles: application of the nanoparticles for catalytic reduction of a variety of dyes in water. *J. Colloid Inter. Sci.* **493**, 85–93 (2017)
 21. M. Nasrollahzadeh, S.M. Sajadi, A. Rostami-Vartooni, S.M. Hussein, Green synthesis of CuO nanoparticles using aqueous extract of *Thymus vulgaris* L. leaves and their catalytic performance for N-arylation of indoles and amines. *J. Colloid Inter. Sci.* **466**, 113–119 (2016)
 22. W.D.H. Schneider, A.J.P. Dillon, M. Camassola, Lignin nanoparticles enter the scene: a promising versatile green tool for multiple applications. *Biotechnol. Adv.* **47**, 107685 (2021)
 23. A.C. Paiva-Santos, A.M. Herdade, C. Guerra, D. Peixoto, M. Pereira-Silva, M. Zeinali, F. Veiga, Plant-mediated green synthesis of metal-based nanoparticles for dermatopharmaceutical and cosmetic applications. *Int. J. Pharm.* **597**, 120311 (2021)
 24. K.S. Kumar, T. Ramakrishnappa, Green synthesized uncapped Ag colloidal nanoparticles for selective colorimetric sensing of divalent Hg and H₂O₂. *J. Environ. Chem. Eng.* **9**(4), 105365 (2021)
 25. S.N. Naidi, M.H. Harunsani, A.L. Tan, M.M. Khan, Green-synthesized CeO₂ nanoparticles for photocatalytic, antimicrobial, antioxidant and cytotoxicity activities. *J. Mater. Chem. B* **9**(28), 5599–5620 (2021)
 26. N. Omerović, M. Džisalo, K. Živojević, M. Mladenović, J. Vunduk, I. Milenković, J. Vidić, Antimicrobial nanoparticles and biodegradable polymer composites for active food packaging applications. *Compr. Rev. Food Sci. Food Saf.* **20**(3), 2428–2454 (2021)
 27. A. Roy, A. Elzaki, V. Tirth, S. Kajoak, H. Osman, A. Algahtani, M. Bilal, Biological synthesis of nanocatalysts and their applications. *Catalysts* **11**(12), 1494 (2021)
 28. F. Elmusa, A. Aygun, F. Gulbagca, A. Seyrankaya, F. Göl, C. Yenikaya, F. Sen, Investigation of the antibacterial properties of silver nanoparticles synthesized using *Abelmoschus esculentus* extract and their ceramic applications. *Int. J. Environ. Sci. Technol.* **18**(4), 849–860 (2021)
 29. M. Kheradmandfard, H. Minouei, N. Tsvetkov, A.K. Vayghan, S.F. Kashani-Bozorg, G. Kim, D.E. Kim, Ultrafast green microwave-assisted synthesis of high-entropy oxide nanoparticles for Li-ion battery applications. *Mater. Chem. Phys.* **262**, 124265 (2021)
 30. M. Sivakami, R. Renuka, T. Thilagavathi, Green synthesis of magnetic nanoparticles via *Cinnamomum verum* bark extract for biological application. *J. Environ. Chem. Eng.* **8**(5), 104420 (2020)
 31. S. Venkateswarlu, Y.S. Rao, T. Balaji, B. Prathima, N.V.V. Jyothi, Biogenic synthesis of Fe₃O₄ magnetic nanoparticles using *plantain* peel extract. *Mater. Lett.* **100**, 241–244 (2013)
 32. L. Gu, V. Vardarajan, A.R. Koymen, S.K. Mohanty, Magnetic-field-assisted photothermal therapy of cancer cells using Fe-doped carbon nanoparticles. *J. Biomed. Opt.* **17**(1), 018003 (2012)
 33. D. Patiño-Ruiz, L. Sánchez-Botero, L. Tejada-Benitez, J. Hinestroza, A. Herrera, Green synthesis of iron oxide nanoparticles using *Cymbopogon citratus* extract and sodium carbonate salt: Nanotoxicological considerations for potential environmental applications. *Environ. Nanotechnol. Monit. Manag.* **14**, 100377 (2020)
 34. M.S.H. Bhuiyan, M.Y. Miah, S.C. Paul, T.D. Aka, O. Saha, M.M. Rahaman, M. Ashaduzzaman, Green synthesis of iron oxide nanoparticle using *Carica papaya* leaf extract: application for photocatalytic degradation of remazol yellow RR dye and antibacterial activity. *Heliyon* **6**(8), e04603 (2020)
 35. M. Jamzad, M.K. Bidkorpeh, Green synthesis of iron oxide nanoparticles by the aqueous extract of *Laurus nobilis* L. leaves and evaluation of the antimicrobial activity. *J. Nanostruct. Chem.* **10**(3), 193–201 (2020)
 36. H.S. Devi, M.A. Boda, M.A. Shah, S. Parveen, A.H. Wani, Green synthesis of iron oxide nanoparticles using *Platanus orientalis* leaf extract for antifungal activity. *Green Process. Synth.* **8**(1), 38–45 (2019)
 37. H. Muthukumar, M. Matheswaran, *Amaranthus spinosus* leaf extract mediated FeO nanoparticles: physicochemical traits, photocatalytic and antioxidant activity. *ACS Sustain. Chem. Eng.* **3**(12), 3149–3156 (2015)
 38. M. Martínez-Cabanas, M. López-García, J.L. Barriada, R. Herrero, M.E.S. de Vicente, Green synthesis of iron oxide nanoparticles, Development of magnetic hybrid materials for efficient As (V) removal. *Chem. Eng. J.* **301**, 83–91 (2016)
 39. G.B. Jegadeesan, K. Srimathi, N.S. Srinivas, S. Manishkanna, D. Vignesh, Green synthesis of iron oxide nanoparticles using *Terminalia bellirica* and *Moringa oleifera* fruit and leaf extracts: antioxidant, antibacterial and thermoacoustic properties. *Biocatal. Agric. Biotechnol.* **21**, 101354 (2019)
 40. T. Wang, X. Jin, Z. Chen, M. Megharaj, R. Naidu, Green synthesis of Fe nanoparticles using *eucalyptus* leaf extracts for treatment of eutrophic wastewater. *Sci. Total Environ.* **466**, 210–213 (2014)
 41. H.K. Farshchi, M. Azizi, M.R. Jaafari, S.H. Nemati, A. Fotovat, Green synthesis of iron nanoparticles by *Rosemary* extract and cytotoxicity effect evaluation on cancer cell lines. *Biocatal. Agric. Biotechnol.* **16**, 54–62 (2018)
 42. B. Desalegn, M. Megharaj, Z. Chen, R. Naidu, Green synthesis of zero valent iron nanoparticle using mango peel extract and surface characterization using XPS and GC-MS. *Heliyon* **5**(5), e01750 (2019)
 43. K.S.V. Gottimukkala, R.P. Harika, D. Zamare, Green synthesis of iron nanoparticles using green tea leaves extract. *J. Nanomed. Biother. Discov.* **7**, 151 (2017)

44. P. Karnan, A. Anbarasu, N. Deepa, R. Usha, Green biosynthesis of magnetic iron oxide nanoparticles of *vitex negundo* aqueous extract. *Int. J. Curr. Pharm. Res.* **10**(3), 11–14 (2018)
45. P.C. Nagajyothi, M. Pandurangan, D.H. Kim, T.V.M. Sreekanth, J. Shim, Green synthesis of iron oxide nanoparticles and their catalytic and in vitro anticancer activities. *J. Clust. Sci.* **28**(1), 245–257 (2017)
46. H.K. Handral, A. Pandith, S.D. Shruthi, A review on *Murraya koenigii*: multipotential medicinal plant. *Asian J. Pharm. Clin. Res.* **5**(4), 5–14 (2012)
47. Y. Tachibana, H. Kikuzaki, N.H. Lajis, N. Nakatani, Antioxidative activity of carbazoles from *Murraya koenigii* leaves. *J. Agric. Food Chem.* **49**(11), 5589–5594 (2001)
48. K. Velsankar, R. Preethi, P.S. Jeevan Ram, M. Ramesh, S. Sudhahar, Evaluations of biosynthesized Ag nanoparticles via *Allium Sativum* flower extract in biological applications. *Appl. Nanosci.* **10**, 3675–3691 (2020)
49. K. Velsankar, V. Vinothini, S. Sudhahar, M. Krishna Kumar, S. Mohandoss, Green synthesis of CuO nanoparticles via *Plectranthus amboinicus* leaves extract with its characterization on structural, morphological, and biological properties. *Appl. Nanosci.* **10**(10), 3953–3971 (2020)
50. K. Velsankar, R.M. Aswin Kumar, R. Preethi, V. Muthulakshmi, S. Sudhahar, Green synthesis of CuO nanoparticles via *Allium sativum* extract and its characterizations on antimicrobial, antioxidant, antilarvicidal activities. *J. Environ. Chem. Eng.* **8**(5), 104123 (2020)
51. S.P. Rajendran, K. Sengodan, Synthesis and characterization of zinc oxide and iron oxide nanoparticles using *Sesbania grandiflora* leaf extract as reducing agent. *J. Nanosci.* (2017) Article ID, 8348507 pp, 7
52. R. Renuka, K.R. Devi, M. Sivakami, T. Thilagavathi, R. Uthrakumar, K. Kaviyarasu, Biosynthesis of silver nanoparticles using *Phyllanthus emblica* fruit extract for antimicrobial application. *Biocatal. Agric. Biotechnol.* **24**, 101567 (2020)
53. S. Kanagasubbulakshmi, K. Kadirvelu, Green synthesis of iron oxide nanoparticles using *Lagenaria siceraria* and evaluation of its antimicrobial activity. *Def. Life Sci. J.* **2**(4), 422–427 (2017)
54. K. Velsankar, S. Sudhahar, G. Parvathy, R. Kaliammal, Effect of cytotoxicity and Antibacterial activity of biosynthesis of ZnO hexagonal shaped nanoparticles by *Echinochloa frumentacea* grains extract as a reducing agent. *Mater. Chem. Phys.* **239**, 121976 (2020)
55. K. Velsankar, S. Sudhahar, G. Maheshwaran, M. Krishna Kumar, Effect of biosynthesis of ZnO nanoparticles via *Cucurbita* seed extract on *Culex tritaeniorhynchus* mosquito larvae with its biological applications. *J. Photoch. Photobio. B.* **200**, 111650 (2019)
56. J. Suresh, G. Pradheesh, V. Alexramani, M. Sundrarajan, S.I. Hong, Green synthesis and characterization of zinc oxide nanoparticle using insulin plant (*Costus pictus* D. Don) and investigation of its antimicrobial as well as anticancer activities. *Adv. Nat. Sci. Nanosci. Nanotechnol.* **9**(1), 015008 (2018)
57. D.W. Park, K.S. Kim, Seed-mediated synthesis of iron oxide and gold/iron oxide nanoparticles. *J. Nanosci. Nanotechnol.* **11**(8), 7214–7217 (2011)
58. S. Arsalani, E.J. Guidelli, J.F. Araujo, A.C. Bruno, O. Baffa, Green synthesis and surface modification of iron oxide nanoparticles with enhanced magnetization using natural rubber latex. *ACS Sustain. Chem. Eng.* **6**(11), 13756–13765 (2018)
59. L. Panawala, Difference between gram positive and gram negative bacteria. *Epediaa* **3**, 1–13 (2017)
60. M. Premanathan, K. Karthikeyan, K. Jeyasubramanian, G. Manivannan, Selective toxicity of ZnO nanoparticles toward Gram-positive bacteria and cancer cells by apoptosis through lipid peroxidation. *Nanomedicine* **7**(2), 184–192 (2011)
61. G. Sangeetha, S. Rajeshwari, R. Venkatesh, Green synthesis of zinc oxide nanoparticles by *aloe barbadensis miller* leaf extract: Structure and optical properties. *Mater. Res. Bull.* **46**(12), 2560–2566 (2011)
62. M. Thiruvengadam, I.M. Chung, T. Gomathi, M.A. Ansari, V.G. Khanna, V. Babu, G. Rajakumar, Synthesis, characterization and pharmacological potential of green synthesized copper nanoparticles. *Bioprocess. Biosyst. Eng.* **42**(11), 1769–1777 (2019)

Publisher's Note Springer Nature remains neutral with regard to jurisdictional claims in published maps and institutional affiliations.